

**Extended Duration Simulation and Testing of Cellular and  
Decellularised Heart Valve Roots**

Amisha Desai

Submitted in accordance with the requirements for a degree of  
Doctor of Philosophy

The University of Leeds  
School of Mechanical Engineering  
February 2019

The candidate confirms that the work submitted is her own, except where work which has formed part of jointly authored publications has been included. The contribution of the candidate and the other authors to this work has been explicitly indicated below. The candidate confirms that appropriate credit has been given within the thesis where reference has been made to the work of others.

Chapters 4 and 5 of this thesis contain material published in a jointly authored publications:

*In vitro* biomechanical and hydrodynamic characterisation of decellularised human pulmonary and aortic roots (2018) Amisha Desai, Tayyebah Vafae, Paul Rooney, John Kearney, Helen Berry, Eileen Ingham, John Fisher, Louise M Jennings; *Journal of the Mechanical Behavior of Biomedical Materials*, 79. pp. 53-63. ISSN 1751

As the lead author the candidate was responsible for the research and writing of the paper. The contributions of the co-authors included critique, guidance and proof reading of the manuscript.

Decellularization of human donor aortic and pulmonary valved conduits using low concentration sodium dodecyl sulfate (2018) Tayyebah Vafae, Daniel Thomas, Amisha Desai, Louise M Jennings, Helen Berry, Paul Rooney, John Kearney, John Fisher, and Eileen Ingham; *Journal of Tissue Engineering Regenerative Medicine* Feb; 12(2): e841–e853.

The candidate was responsible for conducting the uniaxial tensile tests on cellular and decellularised human cryopreserved aortic and pulmonary heart valve root tissue specimens.

This copy has been supplied on the understanding that it is copyright material and that no quotation from the thesis may be published without proper acknowledgement.

© 2019 The University of Leeds and Amisha Samip Desai

The right of Amisha Samip Desai to be identified as the Author of this work has been asserted by her in accordance with the Copyright, Designs and Patents Act 1988.

## Acknowledgements

First and foremost, I'd like to express my sincere gratitude to my primary supervisor, Dr Louise Jennings. Over the last six years, Louise has shown patience and kindness towards me, continuously encouraging me to realise my full potential. I'd like to thank my co-supervisors Professors John Fisher and Eileen Ingham for their invaluable suggestions, comments and guidance throughout my PhD. I dedicate the following mantra in honour of all my Gurus (PhD supervisors and my mum) who guided me on my PhD journey.

***“Guru (the source of all knowledge) Brahma, Guru Vishnu, Guru Devo Maheshwara (Shiva), Guru Saakshat, Parabrahma (Supreme God), Tasmai Shri Guravay Namah (Salutations to such Guru)!”.***

I would like to thank Institute of Medical and Biological Engineering (iMBE) for providing a scholarship for my PhD; and WELMEC and Innovation and Knowledge Centre (IKC) for their support during my PhD. This research would not have been possible without the support and collaboration with NHS Blood and Transplant Tissue and Eye Services, who provided human heart valve roots for carrying out a major part of this research. I would like to thank the generosity of all the donors and their families for donating hearts towards this study and I would like thanks to Tay, Helen and Tim for decellularising the heart valves. Many thanks to the technical support team...Phil, Irvin, Jane, Lee, Rhys and Keith. In my daily life, I have been blessed with amazing friends and colleagues. Special regards and thanks to my best friend and mentor Mr Billy Ghost for literally everything from presentation practice to thesis writing, just chatting away about life in England and India or making big plans to make things right!

My mum is an outstanding inspiration to me, getting to this stage in my life has taken a lot of work, but it is nothing compared to how you (mummy) worked and sacrificed for me. Motakaka (uncle), your encouragement and constant motivation pushed me to heights I never thought possible. I'd like to take this opportunity to thank Kaka (dad), Sarakaka (uncle), Motikaki (auntie), the late Vahala (uncle), Gitaben (auntie), sister, brother in-law, all my brothers, and bhabhis (sister-in-laws) for

unconditional love, continuous support and looking after me as the youngest in the family. Thanks to my in-laws for understanding my dedication to my PhD.

Finally, I must express my very profound gratitude to my husband Samip for believing in my PhD dream and his patience throughout my years of study. Finally, Aarush, my smart son, who inspires me more and more as each day goes by, and I will continue to work harder to make you proud my chikli. Your innocent smile, hugs and questions are the biggest motivation in my life.



## Abstract

Heart valve disease can affect people of all ages, and can be treated by either valve repair or valve replacement surgery. Currently available replacement heart valves, including mechanical prostheses, bioprostheses, autografts and allografts improve patient survival and quality of life, but have limitations. Key limitations include the risk of immunological reaction and the lack of growth potential and regeneration, which is of particular importance in young patients. To address these limitations, low concentration sodium dodecyl sulphate (SDS) decellularised human aortic, human pulmonary, porcine aortic and porcine pulmonary heart valve roots have been developed. Decellularisation of allografts would potentially reduce the risk of immunological reaction, and the development of a decellularised porcine pulmonary heart valve root would potentially provide an option for right ventricular outflow reconstruction in younger patients who have undergone the Ross Procedure. Before moving to clinical trials, the functional performance of decellularised heart valve roots needs to be pre-clinically assessed appropriately to determine mechanical safety. Whilst there are recommended test methods in place for the *in vitro* functional performance assessment of newly manufactured and modified surgical replacement heart valves, they need to be optimised or replaced with novel methods suitable for decellularised heart valve roots, due to their time dependent viscoelastic properties.

The main aim of this research was to optimise *in vitro* hydrodynamic and biomechanical performance test methods and develop a novel real time fatigue test method for biological heart valve roots. The secondary aim was to apply the developed *in vitro* test methods to cellular and decellularised (human and porcine) heart valve roots to evaluate the effect of decellularisation, prior to the decellularised heart valve roots being implanted in patients for clinical trials.

In collaboration with NHS Blood and Transplant, Tissue and Eye Services, *in vitro* biomechanical and hydrodynamic performance of decellularised human aortic and pulmonary heart valve roots was evaluated for the first time in this research. This research determined that the hydrodynamic and functional biomechanical

performance of human aortic and pulmonary heart valve roots was not affected by decellularisation treatment. Decellularisation, however, significantly altered some of the directional material properties of pulmonary and aortic heart valve root leaflets.

To support clinical translation of decellularised porcine pulmonary heart valve roots, material properties of pulmonary heart valve roots was evaluated following 12 months implantation in sheep. In addition, the effect of the processing steps of cryopreservation and decellularisation on the material properties of porcine pulmonary heart valve roots was investigated. Cryopreservation was shown not to alter the material properties of cellular porcine pulmonary heart valve roots, however, decellularisation did have an effect on the material properties of the porcine pulmonary heart valve root wall. Following 12 months implantation in sheep, the decellularised porcine pulmonary heart valve root wall and leaflets showed a trend for decreasing stiffness and strength; becoming more like the cellular ovine, potentially indicating constructive remodelling.

A novel method was developed to investigate the real time fatigue of biological heart valve roots, which was then applied to porcine cellular aortic heart valve roots and porcine decellularised aortic heart valve roots at 120 bpm under physiological cyclic pressures for a maximum of 1.2 million cycles. The results showed no fatigue difference between the cellular and decellularised heart valve roots.

Overall, a portfolio of *in vitro* pre-clinical test methods were developed, optimised and applied to assess the hydrodynamic, biomechanical and fatigue performance of biological heart valve roots including decellularised human and porcine heart valve roots. The *in vitro* pre-clinical test methods developed in this study will lead to the refinement of *in vivo* large animal studies and revision of international standards; and the data will help in the development of the next generation of replacement biological heart valve roots, such as decellularised heart valve roots.

## Table of Contents

<b>Acknowledgements</b> .....	<b>iii</b>
<b>Abstract</b> .....	<b>v</b>
<b>Table of Contents</b> .....	<b>vii</b>
<b>Figures</b> .....	<b>xix</b>
<b>Tables</b> .....	<b>xxviii</b>
<b>Abbreviations</b> .....	<b>xxxii</b>
<b>1 Introduction and Literature Review</b> .....	<b>1</b>
1.1 Introduction .....	1
1.2 The Heart.....	3
1.3 Cardiac Cycle .....	4
1.3.1 Ventricular Systole .....	5
1.3.2 Ventricular Diastole.....	6
1.4 Characteristics of Semilunar (Aortic and Pulmonary) Heart Valve Roots....	6
1.5 Function of Semilunar (Aortic and Pulmonary) Heart Valve Roots .....	11
1.6 Valvular Disease .....	12
1.7 Replacement Heart Valves .....	13
1.7.1 Mechanical Heart Valves.....	13
1.7.2 Bioprosthetic Heart Valves.....	13
1.7.3 Allografts (Homograft) Heart Valve Roots .....	14
1.7.4 Autograft Heart Valves.....	14
1.7.5 Tissue Engineered Heart Valves .....	15
1.7.5.1 Synthetic Scaffolds .....	16
1.7.5.2 Allogenic and Xenogenic Scaffolds.....	17

1.7.5.3	Clinical Experience with Decellularised Heart Valve Roots .....	20
1.8	<i>In vitro</i> Pre - Clinical Assessment of Functional Performance .....	24
1.8.1	Biomechanical Performance .....	28
1.8.2	Hydrodynamic Performance .....	35
1.8.3	Fatigue/Durability Performance .....	39
1.9	Project Rationale .....	44
1.10	Aims and Objectives .....	46
<b>2</b>	<b>Materials and Methods.....</b>	<b>50</b>
2.1	Introduction .....	50
2.2	Aim and Objectives .....	52
2.3	Materials .....	52
2.3.1	Chemicals and General Stock Solutions .....	52
2.3.2	Porcine and Human Cellular Heart Valve Roots .....	53
2.3.3	Björk-Shiley mono leaflet valve (BSM; Shiley Corporation Incorporated, USA).....	54
2.3.4	Imaging System .....	54
2.4	Methods .....	55
2.4.1	Decellularisation.....	55
2.4.2	Glutaraldehyde Fixation.....	55
2.4.3	Antibiotic and Antifungal Treatment .....	56
2.4.4	Heart Valve Root Storage and Defrosting Procedure .....	57
2.4.5	Dimensional Measurement.....	57
2.4.5.1	Data Analysis of Dimensional Measurements .....	58
2.4.5.2	Dimension Measurement Technique Validation .....	59

2.4.6 Hydrodynamic Performance I: Competency under Static Back Pressure.....	60
2.4.6.1 Static Leakage Rig.....	60
2.4.6.1.1 Modification of Static Leakage Rig.....	61
2.4.6.1.2 Validation of Static Leakage Rig.....	62
2.4.6.1.3 Test Procedure – Biological Heart Valve Roots.....	63
2.4.6.1.4 Data Analysis.....	64
2.4.7 Hydrodynamic Performance II: Pulsatile Flow Testing.....	65
2.4.7.1 Optimisation of Pulsatile Flow Simulator.....	65
2.4.7.1.1 SuperPump and Viscoelastic Impedance Adapter (VIA).....	68
2.4.7.1.2 Aortic Test Section.....	70
2.4.7.1.3 Compliance Chamber.....	71
2.4.7.1.4 Mitral Valve Test Section.....	71
2.4.7.1.5 Measuring Instruments.....	71
2.4.7.1.6 Data Acquisition.....	72
2.4.7.2 Calibration and Verification of Pulsatile Flow Simulator Components.....	73
2.4.7.3 Heart Valve Root Mounting in Pulsatile Flow Simulator.....	74
2.4.7.4 Test Procedure.....	76
2.4.7.5 Data Processing.....	77
2.4.7.5.1 Statistical Analysis.....	81
2.4.7.5.2 Validation of Pulsatile Flow Simulator.....	81
2.4.8 Biomechanical Performance.....	81
2.4.8.1 Biomechanical Performance I: Expansion Characteristics (Dilation Testing).....	81
2.4.8.1.1 Dilation Tester.....	82

2.4.8.1.2	Test Procedure .....	84
2.4.8.1.3	Data Analysis .....	86
2.4.8.1.4	Statistical Analysis .....	87
2.4.8.2	Biomechanical Performance II: Uniaxial Tensile Test and Suture Pull-Out Test .....	87
2.4.8.2.1	Uniaxial Tensile Tester: Instron 3365 (Instron® Corporation) .	87
2.4.8.2.2	Thickness Measurement .....	88
2.4.8.2.3	Uniaxial Tensile Test.....	90
2.4.8.2.4	Suture Pull-out Test.....	98
2.4.9	Tissue Behavior .....	100
2.4.10	Statistical Analysis for Uniaxial Tensile Test and Suture Pull-Out Test.....	102
2.5	Summary .....	102
<b>3</b>	<b><i>In vitro</i> Hydrodynamic and Biomechanical Performance of Cellular Porcine Aortic and Pulmonary Heart Valve Roots.....</b>	<b>103</b>
3.1	Introduction .....	103
3.2	Aim and Objectives .....	103
3.3	Materials .....	104
3.4	Methods .....	104
3.4.1	Hydrodynamic Performance of Cellular Porcine Aortic and Pulmonary Heart Valve Roots.....	104
3.4.1.1	Hydrodynamic Performance I: Competency.....	104
3.4.1.2	Hydrodynamic Performance II: Pulsatile Flow.....	105
3.4.2	Biomechanical Performance of Cellular Porcine Aortic and Pulmonary Heart Valve Roots.....	105

3.4.2.1	Biomechanical Performance I: Dilation (Expansion Characteristics).....	105
3.4.2.2	Biomechanical Performance II: Uniaxial Tensile and Suture Pull-Out.....	106
3.5	Results .....	106
3.5.1	Hydrodynamic Performance of Cellular Porcine Aortic and Pulmonary Heart Valve Roots.....	106
3.5.1.1	Hydrodynamic Performance I: Competency.....	106
3.5.1.2	Hydrodynamic Performance II: Pulsatile Flow.....	107
3.5.2	Biomechanical Performance of the Cellular Porcine Aortic and Pulmonary Heart Valve Roots .....	110
3.5.2.1	Dilation (Expansion Characteristics) .....	110
3.5.2.2	Uniaxial Tensile and Suture Pull – Out Characteristics .....	110
3.6	Discussion.....	113
3.7	Conclusion.....	118
<b>4</b>	<b>Effect of Decellularisation on Hydrodynamic and Biomechanical Performance of Human Aortic Heart Valve Roots .....</b>	<b>120</b>
4.1	Introduction .....	120
4.2	Aim and Objectives .....	120
4.3	Study Experimental Design .....	120
4.4	Materials .....	121
4.5	Methods .....	123
4.5.1	Hydrodynamic Performance I: Competency.....	123
4.5.2	Hydrodynamic Performance II: Pulsatile Flow.....	123
4.5.3	Biomechanical Performance I: Dilation (Expansion Characteristics)...	124
4.5.4	Biomechanical Performance II: Uniaxial Tensile and Suture Pull-Out.	125

4.5.5	Statistics .....	125
4.6	Results .....	125
4.6.1	Hydrodynamic Performance of Human Cellular and Decellularised Aortic Heart Valve Roots .....	125
4.6.1.1	Competency .....	125
4.6.1.2	Pulsatile Flow .....	127
4.6.2	Biomechanical Performance of Human Cellular and Decellularised Aortic Heart Valve Roots .....	131
4.6.2.1	Dilation .....	131
4.6.2.2	Tensile Properties.....	132
4.6.2.3	Suture Pull – Out Properties .....	135
4.7	Discussion.....	136
4.7.1	Effect of Decellularisation on Hydrodynamic Performance of Human Cellular Aortic Heart Valve Roots.....	136
4.7.2	Effect of Decellularisation on Biomechanical Performance of Human Cellular Aortic Heart Valve Roots.....	137
4.7.3	Limitations.....	139
4.8	Conclusion .....	140
<b>5</b>	<b>Effect of Decellularisation on Hydrodynamic and Biomechanical Performance of Human Pulmonary Heart Valve Roots .....</b>	<b>141</b>
5.1	Introduction .....	141
5.2	Aim and Objectives .....	141
5.3	Study Experimental Design .....	142
5.3.1	Materials (Study I and Study II).....	143
5.4	Methods .....	145
5.4.1	Methods Used in Study I .....	145



5.4.1.1	Hydrodynamic Performance .....	145
5.4.1.1.1	Competency .....	145
5.4.1.1.2	Pulsatile Flow .....	145
5.4.1.2	Biomechanical Performance .....	146
5.4.1.2.1	Dilation (Expansion Characteristics).....	146
5.4.1.2.2	Uniaxial Tensile and Suture Pull-Out.....	146
5.4.2	Statistics .....	147
5.4.3	Methods Used in Study II .....	147
5.4.3.1	Dimensional Measurements .....	147
5.4.3.2	Functional Biomechanical Performance .....	147
5.4.3.2.1	Competency with Annulus Support .....	147
5.4.3.2.2	Dilation (Expansion Characteristics).....	149
5.5	Results .....	149
5.5.1	Study I.....	149
5.5.1.1	Hydrodynamic Performance of Human Cellular and Decellularised Pulmonary Heart Valve Roots .....	149
5.5.1.1.1	Competency .....	149
5.5.1.1.2	Pulsatile Flow .....	150
5.5.1.2	Biomechanical Performance of Human Cellular and Decellularised Pulmonary Heart Valve Roots .....	154
5.5.1.2.1	Dilation (Expansion Characteristics).....	154
5.5.1.2.2	Tensile Properties.....	155
5.5.1.2.3	Suture Pull-Out Properties .....	158
5.5.2	Study II.....	159

5.5.2.1	Dimensions of Human Pulmonary Heart Valve Roots (Cellular Un scraped, Cellular Scraped, Decellularised Un-Scraped and Decellularised Scraped Heart Valve Roots) .....	159
5.5.2.2	Functional Biomechanical Performance of Human Pulmonary Heart valve roots (Cellular Un scraped, Cellular Scraped, Decellularised Un-Scraped and Decellularised Scraped Heart Valve Roots).....	161
5.5.2.2.1	Competency with and without Annulus Support.....	161
5.5.2.2.2	Dilation (Expansion Characteristics).....	163
5.6	Discussion.....	164
5.6.1	Effect of Decellularisation on Hydrodynamic Performance of Human Cellular Pulmonary Heart Valve Roots.....	164
5.6.2	Effect of Decellularisation on Biomechanical Performance of Human Cellular Pulmonary Heart Valve Roots.....	167
5.7	Conclusion .....	170
<b>6</b>	<b><i>In vitro</i> Material Properties of Non- and Post-Implanted Decellularised Porcine Pulmonary Heart Valve Roots .....</b>	<b>171</b>
6.1	Introduction .....	171
6.2	Aim .....	172
6.3	Materials .....	173
6.4	Methods .....	174
6.4.1	Preparation, Shipment and Storage of Heart Valve Roots for Material properties Assessment.....	174
6.4.2	Material properties Assessment of Heart Valve Roots.....	175
6.5	Results .....	176
6.6	Discussion.....	181
6.6.1	Effect of Cryopreservation on Material Properties of the Porcine Pulmonary Heart Valve Roots .....	181

6.6.2	Effect of Decellularisation on Material Properties of the Porcine Pulmonary Heart Valve Roots .....	181
6.6.3	Effect of 12 Months Implantation in Sheep on Material Properties of the Decellularised Porcine Pulmonary Heart Valve Roots.....	182
6.6.4	Study Limitations.....	183
6.7	Conclusion .....	183
<b>7</b>	<b>Development of a Pre-Clinical Method for Assessment of Real Time Fatigue and Durability of Biological Heart Valve Roots .....</b>	<b>185</b>
7.1	Introduction .....	185
7.2	Aim and Objectives .....	189
7.3	Materials and Methods.....	190
7.3.1	Mechanical Valves.....	190
7.3.2	Cellular and Glutaraldehyde Fixed Porcine Aortic Heart Valve Roots.	190
7.4	Real Time Wear Tester (RWT).....	191
7.4.1.1	SuperPump and Pump Controller .....	193
7.4.1.2	Tank Assembly.....	194
7.4.1.3	Valve Holder .....	196
7.4.1.4	Pressure Measurement Instruments and Data Acquisition.....	197
7.4.1.5	Data Analysis .....	200
7.5	Terminology and Conditions Used During Characterisation, Validation and Method Development.....	200
7.6	Approach to Characterisation and Validation of the RWT .....	201
7.6.1	Mounting of Tilting Disc Mechanical Heart Valves in the RWT .....	201
7.6.2	Pressure Transducers Calibration .....	202
7.6.3	Pressure Tuning.....	203

7.6.4	Discussion and Conclusions Following Characterisation and Validation of the RWT .....	208
7.6.5	Summary .....	211
7.7	Method Development Approach for Testing Biological Heart Valve Roots.....	211
7.8	Method Development: Real Time Fatigue Testing of Biological Heart Valve Roots.....	212
7.8.1	Design Specification for Heart Valve Root Holder .....	213
7.8.1.1	Conceptual Designs for the Heart Valve Root Holder.....	215
7.8.1.1.1	Design 1 .....	216
7.8.1.1.2	Design 2 .....	216
7.8.1.1.3	Design 3 .....	216
7.8.1.1.4	Concept Screening.....	216
7.8.1.2	Detailed Heart Valve Root Holder Design .....	217
7.8.1.3	Heart Valve Root Holder Feasibility Test .....	218
7.8.1.4	Modified Heart Valve Root Holder Design.....	221
7.8.2	Modification of RWT to Control Physiological Pressure of the Aorta during Fatigue Testing of Biological Heart Valve Roots.....	222
7.8.2.1	Validation of Modified RWT.....	223
7.8.2.2	Modification of Blanking Plates .....	225
7.8.3	Summary of the Test Method: Fatigue and Durability Testing of Biological Heart Valve Roots in the RWT .....	226
7.9	Discussion and Conclusion Following Method Development for Biological Heart Valve Roots.....	227
<b>8</b>	<b><i>In vitro</i> Real Time Fatigue Assessment of Cellular and Decellularised Porcine Aortic Heart Valve Roots .....</b>	<b>229</b>
8.1	Introduction .....	229

8.2	Aim and Objectives .....	229
8.3	Study Experimental Design .....	230
8.4	Materials .....	233
8.4.1	Feasibility Study .....	233
8.4.2	Primary Study .....	233
8.5	Methods .....	234
8.5.1	Methods used in Feasibility Study .....	234
8.5.1.1	Real Time Fatigue .....	234
8.5.1.2	Hydrodynamic Performance under Pulsatile Flow .....	236
8.5.1.3	Uniaxial Tensile Properties of the Heart Valve Root Leaflets .....	237
8.5.2	Methods used in Primary Study .....	237
8.5.2.1	Real Time Fatigue .....	237
8.5.2.2	Hydrodynamic Performance I: Competency (Pre-test, Mid-test, Post-test).....	239
8.5.2.3	Hydrodynamic Performance II: Pulsatile Flow (Post-test).....	240
8.5.2.4	Uniaxial Tensile Properties of the Leaflets (Post-Test) .....	241
8.5.3	Statistical Analysis .....	242
8.6	Results .....	242
8.6.1	Feasibility Study .....	242
8.6.1.1	Real Time Fatigue .....	242
8.6.1.2	Hydrodynamic Performance under Pulsatile Flow .....	243
8.6.1.3	Uniaxial Tensile Properties of the Cellular Aortic Leaflets.....	244
8.6.1.4	Discussion.....	245
8.6.2	Primary Study .....	249

8.6.2.1	Real Time Fatigue of Cellular and Decellularised Porcine Aortic Heart Valve Roots.....	249
8.6.2.2	Hydrodynamic Performance of Cellular and Decellularised Porcine Aortic Heart Valve Roots .....	253
8.6.2.2.1	Hydrodynamic Performance I: Competency .....	253
8.6.2.2.2	Hydrodynamic Performance II: Pulsatile Flow .....	254
8.6.2.3	Uniaxial Tensile Properties of the Cellular and Decellularised Aortic Leaflets.....	258
8.6.3	Discussion.....	259
8.6.3.1	Limitations and Recommendations .....	266
8.7	Conclusion .....	266
<b>9</b>	<b>Discussion, Conclusions and Future Work .....</b>	<b>268</b>
9.1	General Discussion .....	268
9.2	Limitations and Future Work .....	276
9.3	Conclusion .....	280
<b>10</b>	<b>References .....</b>	<b>282</b>
<b>11</b>	<b>Appendix A: Journal Publications.....</b>	<b>307</b>
<b>12</b>	<b>Appendix B: Engineering Drawings for Tissue Specimen Holder and Adaptors for the Uniaxial Tensile Tester .....</b>	<b>308</b>
<b>13</b>	<b>Appendix C: Engineering Drawing for Heart Valve Root Holder for the RWT.....</b>	<b>315</b>

## Figures

1.	Figure 1.1 Schematic Diagram of the Structure of the Heart (figure derived from <a href="http://www.sorin.com/anatomy">http://www.sorin.com/anatomy</a> ) .....	4
2.	Figure 1.2 The Cardiac Cycle. Adapted from (Stehle and Iorga, 2010) .....	5
3.	Figure 1.3 Defined Terminology for the (a) Aortic and (b) Pulmonary Heart Valve Root Components .....	7
4.	Figure 1.4 Semilunar Heart Valve Leaflet Region (Dawidowska, 2016).....	8
5.	Figure 1.5 Schematic Diagram of the Multi-Layered Structure of Heart Valve Root Leaflet (Rippel et al., 2012).....	8
6.	Figure 1.6 Schematic Diagram of the Multi-Layered Structure of Heart Valve Root Wall (McCloskey et al., 2014) .....	10
7.	Figure 1.7 Typical Stress-Strain Behaviour Curve for Heart Valve Tissue .....	29
8.	Figure 1.8 Representative Flow Waveform for Cardiac Cycle where (a) Forward Flow Volume (b) Closing Volume and (c) Leakage Volume (ISO 5840, 2015) .....	37
9.	Figure 1.9 Outline of Objective 1 .....	46
10.	Figure 1.10 Outline of Objective 2 .....	47
11.	Figure 1.11 Outline of Objective 3 .....	48
12.	Figure 1.12 Outline of Objective 4 (a) and (b) .....	48
13.	Figure 1.13 Outline of Objective 5 .....	49
14.	Figure 1.14 Outline of Objective 6 .....	49
15.	Figure 2.1 Valve Sizing Obturator Set .....	54
16.	Figure 2.2 Schematic Drawing of Glutaraldehyde Fixation of Porcine Aortic Heart Valve Roots .....	56
17.	Figure 2.3 Dimension Measurement Set Up.....	58
18.	Figure 2.4 Dimension Measurement with ImageJ .....	59
19.	Figure 2.5 Static Leakage Rig (not drawn to scale) .....	61
20.	Figure 2.6 Test Set-up to Derive Leakage Flow Rate under Static Back Pressure for Mechanical Valve.....	62

21.	Figure 2.7 Test Set-up for Static Leakage Testing of Heart Valve Roots.....	64
22.	Figure 2.8 Pulsatile Flow Simulator Schematic Diagram used to assess Hydrodynamic Performance of the Heart Valve Roots .....	67
23.	Figure 2.9 Pulsatile Flow Simulator Showing the Test Chambers with Supporting Tables .....	68
24.	Figure 2.10 SuperPump System used for Pulsatile Flow Simulator .....	69
25.	Figure 2.11 A Viscoelastic Impedance Adapter.....	70
26.	Figure 2.12 Flow Probe Mounting Arrangements .....	72
27.	Figure 2.13 Stroke Volume Verification Setup.....	73
28.	Figure 2.14 Schematic Diagram of Heart Valve Root Position and Mounting in Pulsatile Flow Simulator .....	75
29.	Figure 2.15 Heart Valve Root Mounting in Pulsatile Flow Simulator .....	75
30.	Figure 2.16 Cable Tie Gun .....	76
31.	Figure 2.17 Example of Acquired Pressure and Flow Curve (a) Minimum (b) Maximum Compliance.....	79
32.	Figure 2.18 Perspex Tube for Dilation Test Setup.....	83
33.	Figure 2.19 Schematic Diagram of Dilation Test Setup.....	83
34.	Figure 2.20 Dilation Testing Setup for Pulmonary Heart Valve Root with Annulus Ring.....	84
35.	Figure 2.21 Static Pressure Calculation during Dilation Testing .....	85
36.	Figure 2.22 Representative images taken during dilation test at (a) 0 mmHg and (b) 35 mmHg.....	86
37.	Figure 2.23 Uniaxial Tensile Tester 3365 with Biobath.....	88
38.	Figure 2.24 Mitutoyo Digital Thickness Gauge 700-122 .....	89
39.	Figure 2.25 Digital Thickness Gauge J-40 V (James H. Heal and Company Limited) .....	90
40.	Figure 2.26 Tissue Specimen Holder for the Uniaxial Tensile Tester.....	92
41.	Figure 2.27 (a) Bottom Adaptor with Plunger Assembly – Connect to Bio Bath (b) Spring Loaded Plunger Assembly Automatically Adjusts Holder Slack (c) Top Adaptor –Connect to 50 N Load Cell.....	93



42.	Figure 2.28 Clamping of the Wall Tissue Specimen (a) with Polypropylene Suture to hold the wall specimen in the middle of the grips (b) Top View (C) Side View .....	94
43.	Figure 2.29 Specimen Cutter.....	95
44.	Figure 2.30 Specimen Preparation.....	96
45.	Figure 2.31 Typical Stress-Strain Graph of Heart Valve Tissue Specimen Subjected to Uniaxial Tensile Loading to Failure. ....	98
46.	Figure 2.32 Specimen Preparation for Suture Pull-Out Testing.....	99
47.	Figure 2.33 Tissue Specimen Holder for the Suture Pull-Out Testing .....	99
48.	Figure 2.34 A Sample Specimen Showing the Position of Suture through Material.....	100
49.	Figure 2.35 Representative Images of Tissue Specimens Undergoing Uniaxial Tensile Testing.....	101
50.	Figure 2.36 Circumferential Wedge Propagation in the Wall Specimen due to a Suture Pull-Out Load in the Axial Axis. ....	101
51.	Figure 3.1 Mean Transvalvular Pressure Difference versus RMS Flow for Cellular Porcine (a) Aortic (b) Pulmonary Heart Valve Roots – Data fitted with second order polynomial trend line - The error bars indicate 95 % confidence limits .....	108
52.	Figure 3.2 Valve Opening, Valve Fully Opened, Valve Closing and Valve Fully Closed Images of a Typical Cellular Porcine (a) Aortic and (b) Pulmonary Heart Valve Root at Heart Rate 72 bpm, Captured from the Front View by a High-Speed Camera .....	109
53.	Figure 3.3 Percentage Dilation as a Function of Applied Pressure of all Cellular Porcine (a) Aortic and (b) Pulmonary Heart Valve Roots - Data fitted with a second order polynomial trend line.....	110
54.	Figure 3.4 Stress-Strain Graphs for the Cellular Porcine (a) Aortic Wall, (b) Aortic Leaflets, (c) Pulmonary Wall and (d) Pulmonary Leaflets Specimens [Wall Specimens: Axial (Solid Lines) and Circumferential (Dotted lines)] and Leaflet Specimens [Radial (Solid Lines) and Circumferential (Dotted lines)] .....	112
55.	Figure 4.1 Flow Chart Indicating Cellular and Decellularised Aortic Heart Valve Root Hydrodynamic and Biomechanical Performance Assessment Sequence .....	121
56.	Figure 4.2 Representative Image of Human Aortic Heart Valve Root .....	122

57.	Figure 4.3 Decellularised Aortic Heart Valve HA050 Showing Central Regurgitant Jet .....	126
58.	Figure 4.4 Mean Transvalvular Pressure versus Mean RMS Flow for Human Cellular and Decellularised Aortic Heart Valve Roots - Data fitted with a second order polynomial trend line - The error bars indicate 95 % confidence limits .....	127
59.	Figure 4.5 (a) Valve Opening, (b) Valve Fully Opened, (c) Valve closing and (d) Valve Fully Closed Images of Human Cellular Aortic Heart Valve Roots at Heart Rate 72 bpm, captured from the Front View by a High-Speed Camera .....	129
60.	Figure 4.6 (a) Valve Opening, (b) Valve Fully Opened, (c) Valve closing and (d) Valve Fully Closed Images of Human Decellularised Aortic Heart Valve Roots at Heart Rate 72 bpm, captured from the Front View by a High-Speed Camera.....	130
61.	Figure 4.7 Percentage Dilation as a Function of Applied Pressure of all Cellular (Solid line, n=4) and Decellularised (Dotted line, n=3) Aortic Heart Valve Roots - Data fitted with a third order polynomial trend line...	131
62.	Figure 4.8 Load versus Extension Graph with Two Peaks for the Leaflet Specimen Undergoing Uniaxial Tensile Testing .....	132
63.	Figure 4.9 Stress-Strain Graphs for the Cellular (solid line, n=8) and Decellularised (dotted line, n=4) (a) Circumferential Aortic Wall (b) Axial Aortic Wall (c) Circumferential Aortic Leaflet (d) Radial Aortic Leaflet Specimens .....	133
64.	Figure 5.1 Flow Chart Indicating Pulmonary Heart Valve Roots Performance Assessment Sequence used in (a) Study I and (b) Study II.....	143
65.	Figure 5.2 Representative Image of Cellular Human Pulmonary Heart Valve Root .....	145
66.	Figure 5.3 Pulmonary Heart valve root with Annulus Ring Mounted in Static Leakage Tester .....	148
67.	Figure 5.4 Mean Transvalvular Pressure versus Mean RMS Flow for Human Cellular and Decellularised Pulmonary Heart Valve Roots - Data fitted with second order polynomial trend line - The error bars indicate 95 % confidence limits .....	151
68.	Figure 5.5 (a) Valve Opening, (b) Valve Fully Opened, (c) Valve closing and (d) Valve Fully Closed Images of Human Cellular Pulmonary Heart Valve Roots at Heart Rate 72 bpm, captured from the Front View by a High-Speed Camera.....	152

69.	Figure 5.6 (a) Valve Opening, (b) Valve Fully Opened, (c) Valve closing and (d) Valve Fully Closed Images of Human Decellularised Pulmonary Heart Valve Roots at Heart Rate 72 bpm, captured from the Front View by a High-Speed Camera .....	153
70.	Figure 5.7 Human Decellularised Pulmonary Heart Valve HP042 with Fenestrations Visible .....	154
71.	Figure 5.8 Percentage Dilation as a Function of Applied Pressure of Cellular (Solid Line, n=4) and Decellularised (Dotted Line, n=3) Porcine Heart Valve Roots- Data fitted with a third order polynomial trend line....	155
72.	Figure 5.9 Stress-Strain Graphs for the Cellular (solid line, n=4) and Decellularised (dotted line, n=4) (a) Circumferential Pulmonary Wall (b) Axial Pulmonary Wall (c) Circumferential Pulmonary Leaflet (d) Radial Pulmonary Leaflet Specimens .....	156
73.	Figure 5.10 Percentage Dilation as a Function of Applied Pressure of Cellular Un-scraped (Group 1, n=7) and Cellular Scraped (Group 2, n=4), Decellularised Un- Scraped (Group 3, n=3) and Decellularised Scraped (Group 4, n=4) Heart valve roots .....	163
74.	Figure 5.11 Mean Percentage Dilation at Approximately 20 mmHg For All the Pulmonary Cellular (Group 1, n=6), Cellular Scraped (Group 2, n=3), Decellularised Un-Scraped (Group 3, n=3) and Decellularised Scraped (Group 4, n=3) Heart Valve Roots. - The error bars indicate 95 % confidence limits. ....	164
75.	Figure 6.1 Pulmonary Heart Valve Root Experimental Groups .....	173
76.	Figure 6.2 Mean Valve Size (Internal Diameter) for Pulmonary Heart Valve Root Groups - The error bars indicate 95 % confidence limits. * - Denotes significant difference ( $p < 0.05$ ).....	176
77.	Figure 6.3 Mean Pulmonary Heart Valve Root Wall Groups Thickness in the Axial and Circumferential Directions - The error bars indicated 95 % confidence limits. * - Denotes significant difference ( $p < 0.05$ ) .....	176
78.	Figure 6.4 Mean Collagen Phase Slope for the Pulmonary Heart Valve Root Wall Groups in the Axial and Circumferential Directions - The error bars indicate 95 % confidence limits. * - Denotes significant difference ( $p < 0.05$ ) .....	177
79.	Figure 6.5 Mean Elastin Phase Slope for the Pulmonary Heart Valve Root Wall Groups in the Axial and Circumferential Directions - The error bars indicate 95 % confidence limits. *- Denotes significant difference ( $p < 0.05$ ) .....	177

80.	Figure 6.6 Mean Ultimate Tensile Stress (UTS) for the Pulmonary Heart Valve Root Wall Groups in the Axial and Circumferential Directions. The error bars indicate 95 % confidence limits. * - Denotes significant difference ( $p < 0.05$ ).....	178
81.	Figure 6.7 Mean Thickness for the Pulmonary Heart Valve Root Leaflets in the Radial and Circumferential Directions - The error bars indicate 95 % confidence limits. * - Denotes significant difference ( $p < 0.05$ ) .....	179
82.	Figure 6.8 Mean Collagen Phase Slope for the Pulmonary Heart Valve Root Leaflets in the Radial and Circumferential Directions- The error bars indicate 95 % confidence limits.....	179
83.	Figure 6.9 Mean Elastin Phase Slope for the Pulmonary Heart Valve Root Leaflets in the Radial and Circumferential Directions - The error bars indicate 95 % confidence Limits. * - Denotes significant difference ( $p < 0.05$ ) .....	180
84.	Figure 6.10 Mean Ultimate Tensile Stress (UTS) for the Pulmonary Heart Valve Root Leaflets in the Radial and Circumferential Directions - The error bars indicate 95 % confidence limits. * - Denotes significant difference ( $p < 0.05$ ).....	180
85.	Figure 7.1 (a) Left Ventricle and Aortic Pressure Waveforms During a Cardiac Cycle at Heart Rate of 60 bpm (b) Transvalvular Pressure across Aortic Valve, Image Adapted from (Conti et al., 2010).....	187
86.	Figure 7.2 Inflow and Outflow Pressures in the Heart Valve Root .....	188
87.	Figure 7.3 Flowchart of the Method Development Process to Investigate the Fatigue and Durability of Biological Heart Valve Roots.....	189
88.	Figure 7.4 Tilting Disc Mechanical Heart Valve.....	190
89.	Figure 7.5 Real Time Wear Tester .....	191
90.	Figure 7.6 Basic Working Principle of the RWT (a) Backward Piston Stroke Closes the Test Valve (b) Forward Piston Stroke Opens the Test Valve.....	192
91.	Figure 7.7 Negative Pressure in the Inflow Chamber Measured by Inflow Pressure Transducer P1 at 60 bpm .....	193
92.	Figure 7.8 Real Time Wear Tester with (a) Side View (b) Front View with one Mechanical Valve in Station 4 and five Stations blanked off (C) Tank Assembly with one Mechanical Valve in Station 4 and five Stations blanked off and Bypass Valve Adjustment (Front View) .....	194
93.	Figure 7.9 Bypass Valve Assembly .....	195

94.	Figure 7.10 Working Principle of the Bypass Valve showing Movement of Rubber Diaphragms with Flow in (a) Reverse and (b) Forward Directions .....	196
95.	Figure 7.11 Standard Valve Holder (Side View), Image Adapted from Vivitro Systems Inc, Victoria BC, Canada Manual .....	197
96.	Figure 7.12 The HiTest Software Process Display .....	199
97.	Figure 7.13 Constant Amplitude Sine Wave (S50) with 50% Systolic and 50% Diastolic Phase.....	200
98.	Figure 7.14 Schematic showing Fluid Restriction Passageways of Bypass Valve Visually 50 % Closed Configuration .....	201
99.	Figure 7.15 (a) Blanking Plate Sealed in the Valve Holder (Top View) (b) Blanking Plate (c) A Tilting Disc Mechanical Heart Valve Mounted in the Valve Holder (Top View) (d) A Tilting Disc Mechanical Heart Valve Mounted in a Delrin Fixture (Looking from Inflow Side) .....	202
100.	Figure 7.16 Transvalvular Pressure across Tilting Disc Mechanical Heart Valve at Heart Rate (a) 60, (b)120 and (c)200 bpm .....	205
101.	Figure 7.17 Transvalvular Pressure across one Tilting Disc Mechanical Heart Valve for Different Bypass Valve Conditions .....	206
102.	Figure 7.18 Transvalvular Pressure Difference across one Tilting Disc Mechanical Heart Valve for Different Amplitude Conditions.....	207
103.	Figure 7.19 Transvalvular Pressures Difference across Tilting Disc Mechanical Heart Valve .....	207
104.	Figure 7.20 Transvalvular Pressure Waveforms Obtained for Different Bypass Valve Setting and Amplitude Values .....	210
105.	Figure 7.21 Conceptual Designs for the Heart Valve Root Holder (a) Design involved Sandwiching of Myocardium between the Two Flanges and Attaching Aorta to the Spigot with Cable Tie (b) Design involved Suturing of Myocardium and Aorta onto the Spigots (C) Design involved Attaching Myocardium and Aorta on to the Spigots with Cable Ties.....	215
106.	Figure 7.22 Heart Valve Root Holder for Biological Heart Valve Root with Pressure Measurement Assembly .....	218
107.	Figure 7.23 Representative Image of Heart Valve Root Mounting On the RWT .....	218
108.	Figure 7.24 (a) Schematic Diagram showing Inflow and Outflow Pressures during the Porcine Aortic Heart Valve Root Testing in the RWT	

	(b) Movement of the Aorta and the Valve Opening and Closing from the Outflow Side.....	220
109.	Figure 7.25 (a) First version of Heart Valve Holder (b) Modified Heart Valve Root Holder for Biological Heart Valve Root Mounted in the RWT with Pressure Measurement Assembly .....	221
110.	Figure 7.26 Physical Model Illustrating the Application of External Load (Pressure) on the Aorta by Attaching a Vertical Column.....	222
111.	Figure 7.27 Schematic Diagram of Modified RWT .....	223
112.	Figure 7.28 Representative Pressure Waveforms Measured for Cellular Porcine Aortic Heart Valve Roots during Real Time Fatigue and Durability Testing .....	224
113.	Figure 7.29 Blanking Plate Designs and Assemblies. Top: First Version of the Design. Bottom: Modified Design.....	225
114.	Figure 7.30 Modified RWT with Modified Blanking Plates .....	226
115.	Figure 8.1 Flow Chart Indicating Cellular Porcine Aortic Heart Valve Roots <i>In Vitro</i> Performance Assessment Sequence used in the Feasibility Study.....	230
116.	Figure 8.2 Flow Chart Indicating Cellular and Decellularised Porcine Aortic Heart Valve Roots Performance Assessment Sequence used in the Primary Study.....	232
117.	Figure 8.3 Aortic Heart Valve Root Mounting in the RWT (a) Front View (b) Side View .....	235
118.	Figure 8.4 Representative Pressure Waveforms of the Tuned RWT at Heart Rate 120 bpm during Real Time Fatigue Assessment of Cellular Porcine Aortic Heart Valve Roots.....	236
119.	Figure 8.5 Heart Valve Root Mounting (a) with Free Axial Movement of the Sliding Spigot (used in the Feasibility Study) (b) and Restricted Axial Movement of the Sliding Spigot (used in the Primary Study ) during the Fatigue Assessment in the RWT.....	238
120.	Figure 8.6 Front View of Valve Closed Phase Showing Belly Region (red), Commissure Region (green) and Free Edge (black) .....	239
121.	Figure 8.7 Aortic Heart Valve Root Mounting during Mid-test and Post-test Competency Assessment (Top View).....	239
122.	Figure 8.8 Heart Valve Root Mounting with Fixed Spigot attached in the Pulsatile Flow Simulator.....	241

123.	Figure 8.9 Infected Cellular Porcine Aortic Heart Valve Root during Fatigue Testing in the RWT .....	243
124.	Figure 8.10 Mean Transvalvular Pressure Difference versus Mean RMS Flow for Cellular (n=3) Porcine Aortic Heart Valve Roots - Data fitted with second order polynomial trend line - The error bars indicate 95 % confidence limits .....	244
125.	Figure 8.11 Leaflet Tear of the Cellular Porcine Aortic Heart Valve Root A5 .....	244
126.	Figure 8.12 Free Body Diagram of the Clamping of Myocardium of the Heart Valve Root on the Fixed Spigot .....	246
127.	Figure 8.13 Cellular Aortic Heart Valve Roots Mounting (a) Before Fatigue Assessment in the RWT showing Un-deformed Myocardium (b) During Fatigue Assessment in the RWT showing Loosened Myocardium (c) with Restricted Axial Movement of the Sliding Spigot .....	247
128.	Figure 8.14 Modification in the (a) Flange for the Aortic Test Section of the Pulsatile Flow Simulator (Front View) (b) Fixed Spigot from the Heart Valve Root Holder for the RWT (Back View) (C) Mounting of the Fixed Spigot on the Flange (Front View) .....	249
129.	Figure 8.15 Mean Transvalvular Pressure Difference versus Mean RMS Flow for Cellular (n=4) and Decellularised (n=6) Porcine Aortic Heart Valve Roots - Data fitted with second order polynomial trend line - The error bars indicate 95 % confidence limits .....	255
130.	Figure 8.16 (a) Valve Fully Opened and (b) Valve Fully Closed Images of Cellular Porcine Aortic Heart Valve Roots at Heart Rate 72 bpm, captured from the Front View by a High-Speed Camera with a Leaflet Tear in AC4 Highlighted.....	256
131.	Figure 8.17 (a) Valve Fully Opened and (b) Valve Fully Closed Images of Decellularised Porcine Aortic Heart Valve Roots at Heart Rate 72 bpm, captured from the Front View by a High-Speed Camera with a Leaflet Tears Highlighted in AD1 and AD5 .....	257
132.	Figure 8.18 Tear in Explanted Bovine Pericardial Trifecta Heart Valve (Piñón et al., 2015) .....	260
133.	Figure 8.19 The Structural Damage (indicated with arrow) in Porcine Bioprosthetic Heart Valve leaflet (a) Subjected to <i>in vitro</i> Accelerated Fatigue (b) Explanted from Patient.....	261
134.	Figure 9.1 <i>In Vitro</i> Test Methods Developed to Assess Performance of Biological (Decellularised) Heart Valve Roots .....	270

## Tables

1.	Table 1.1 Composition and Function of Each Leaflet Layer (Vesely and Noseworthy, 1992, Schoen and Levy, 1999).....	9
2.	Table 1.2 Composition and Function of Each Wall Layer (Tsamis et al., 2013, Pak et al., 2007).....	10
3.	Table 2.1 The Chemicals and General Stock Solutions used during this Study.....	53
4.	Table 2.2 Dimensions of the Cellular Porcine Pulmonary Heart Valve Root Measured On Two Consecutive Days.....	60
5.	Table 2.3 Static Leakage Results for the Mechanical Valve.....	63
6.	Table 2.4 The Major Performance Specifications required during optimisation of the Pulsatile Flow Simulator.....	65
7.	Table 2.5 Design Specification for Dilation Tester.....	82
8.	Table 2.6 Design Specification for the Holder to Test Heart Valve Specimens under Uniaxial Tensile Testing.....	91
9.	Table 3.1 Test Conditions Used in the Pulsatile Flow Performance of Cellular Porcine Aortic and Pulmonary Heart Valve Roots (Maximum Compliance Condition).....	105
10.	Table 3.2 Mean Leakage Flow Times ( $T_L$ ) and Mean Leakage Flow Rates ( $F_L$ ) for the Cellular Aortic and Pulmonary Heart Valve Roots.....	107
11.	Table 3.3 Mean Effective Orifice Areas for Cellular Porcine Pulmonary and Aortic Heart Valve Root.....	109
12.	Table 3.4 Mean Thickness $\pm$ 95 % Confidence Limits for the Cellular Porcine Aortic and Pulmonary Heart Valve Root Specimens (Wall and Leaflet).....	111
13.	Table 3.5 Mean Collagen Phase Slope ( $E_c$ ), Mean Elastin Phase Slope ( $E_e$ ), Mean Ultimate Tensile Stress (UTS) and Mean Failure Strain ( $\epsilon_f$ ) ( $\pm$ 95 % Confidence Limits) for the Cellular Porcine Aortic and Pulmonary Wall and Leaflet Specimens.....	113
14.	Table 4.1 Details of Cellular and Decellularised Aortic Heart Valve Roots Including Patient Age, Patient Sex and Valve Size Used for Hydrodynamic and Biomechanical Performance Testing.....	122



15.	Table 4.2 Details of the Four Additional Cellular Aortic Heart Valve Roots including Patient Age and Patient Sex Used for Uniaxial and Suture Pull-Out Testing .....	123
16.	Table 4.3 Test Conditions Used in the Pulsatile Flow Performance of Cellular and Decellularised Aortic Heart Valve Roots .....	124
17.	Table 4.4 Mean Leakage Flow Times ( $T_L$ ), Mean Leakage Flow Rates ( $F_L$ ), Competency and Arterial Diameters at 120 mmHg Pressure of Tested Human Cellular and Decellularised Aortic Heart Valve Roots .....	126
18.	Table 4.5 Effective Orifice Area for Each Human Cellular and Decellularised Aortic Heart Valve Root Averaged over 3 Heart Rate conditions.....	128
19.	Table 4.6 Mean Thickness for the Cellular and Decellularised Aortic Heart Valve Root Wall and Leaflet specimens – p values: statistical probability in the comparison between cellular and decellularised aortic heart valve roots .....	134
20.	Table 4.7 Tensile Parameters (Collagen Phase Slope $E_c$ , Elastin Phase Slope $E_e$ , Ultimate Tensile Stress $\sigma_{UTS}$ , Failure Strain $\epsilon_{failure}$ ) for Cellular and Decellularised Aortic Wall in the Axial (A) and Circumferential (C) Directions and Leaflet Specimens in the Radial (R) And Circumferential (C) Directions, Number of Specimens (n). *-Statistical significant difference ( $p < 0.05$ ; Student's t-test) for decellularised versus cellular heart valve roots. ....	134
21.	Table 4.8 Mean Maximum Suture Pull-Out Force and Mean Resistance to Tearing for the Cellular and Decellularised Aortic Heart Valve Root Wall and Myocardial specimens (Where n- Number Specimens) - p values: statistical probability in the comparison between cellular and decellularised aortic heart valve roots.....	135
22.	Table 5.1 Details of Pulmonary Heart Valve Roots Assessed in Study I, Including Patient Age, Sex and Valve Size.....	144
23.	Table 5.2 Test Conditions Used in the Pulsatile Flow Performance of Cellular and Decellularised Pulmonary Heart Valve Roots .....	146
24.	Table 5.3 Mean Leakage Flow Times ( $T_L$ ), Mean Leakage Flow Rates ( $F_L$ ), Competency and Arterial Diameters of Human Cellular and Decellularised Pulmonary Heart Valve Roots, assessed in Study I .....	150
25.	Table 5.4 Effective Orifice Area (EOA)for each Human Cellular and Decellularised Pulmonary Heart Valve Root averaged over the three Cycle Rates .....	151

26.	Table 5.5 Mean Thickness for the Cellular and Decellularised Pulmonary Heart Valve Root Wall and Leaflet Specimens - p values: statistical probability in the comparison between cellular and decellularised pulmonary heart valve roots.....	157
27.	Table 5.6 Tensile Parameters (collagen phase slope $E_c$ , elastin phase slope $E_e$ , ultimate tensile stress $\sigma_{UTS}$ , failure strain $\epsilon_{failure}$ ) based on the Engineering Stress versus Engineering Strain behaviour of the Cellular and Decellularised Pulmonary Heart Valve Root Wall Specimens [Axial (A) and Circumferential (C) Directions] and Leaflet Specimens [Radial (R) and Circumferential (C) Directions] *-Statistical significant difference ( $p < 0.05$ ) for decellularised versus cellular heart valve roots.....	157
28.	Table 5.7 Mean Maximum Suture Pull-Out Force and Mean Resistance to Tearing for the Cellular and Decellularised Pulmonary Heart Valve Root Wall and Myocardial specimens - p values: statistical probability in the comparison between cellular and decellularised pulmonary heart valve roots.....	158
29.	Table 5.8 Wall Widths ( $W_1$ and $W_2$ ) of each Human Pulmonary Heart Valve Root for all the Groups [Cellular Un- Scraped (Group 1), Cellular Scraped (Group 2), Decellularised Un-Scraped (Group 3), Decellularised Scraped (Group 4)] and Percentage Change in Widths $W_1$ ( $\Delta W_{13}$ and $\Delta W_{14}$ ) and $W_2$ ( $\Delta W_{23}$ and $\Delta W_{24}$ ) for Decellularised Un-Scraped (Group 3) and Decellularised Scraped (Group 4) Human Pulmonary Heart Valve Roots.....	160
30.	Table 5.9 Mean Leakage Flow Rates ( $F_L \text{ mL}\cdot\text{s}^{-1}$ ) and Competency ( $C_p$ ) for each Human Pulmonary Heart Valve Root for all the Groups [Cellular Un- Scraped (Group 1), Cellular Scraped (Group 2), Decellularised Un-Scraped (Group 3), Decellularised Scraped (Group 4)].....	162
31.	Table 5.10 Diameters $D_1$ of each Human Pulmonary Heart Valve Root for all the Groups [Cellular Un- Scraped (Group 1), Cellular Scraped (Group 2), Decellularised Un-Scraped (Group 3), Decellularised Scraped (Group 4)] at 60 mmHg Static Pressure and Change in Diameter $\Delta D_1$ .....	163
32.	Table 6.1 Details of Pulmonary Heart Valve Roots Groups Assessed Including Abbreviation, Age of the Animal and Number of Specimens in Each Group.....	174
33.	Table 7.1 Test Plan for the Evaluation of Pressure Controlling Mechanism in the RWT.....	203
34.	Table 7.2 Specifications for Initial Method Development.....	212
35.	Table 7.3 Heart Valve Root Holder Design Specification.....	214
36.	Table 7.4 Concept Screening and Ranking.....	217

37.	Table 8.1 Details of Cellular and Decellularised Porcine Aortic Heart Valve Roots Assessed Including Identification Number and Valve Size .....	234
38.	Table 8.2 Test Conditions Used in the Pulsatile Flow Performance of Cellular Porcine Aortic Heart Valve Roots (Maximum Compliance Condition).....	237
39.	Table 8.3 Test Conditions Used in the Pulsatile Flow Performance of Cellular and Decellularised Porcine Aortic Heart Valve Roots (Maximum Compliance Condition).....	241
40.	Table 8.4 Mean Thickness and Mean Tensile Parameters (Collagen Phase Slope $E_c$ , Elastin Phase Slope $E_e$ , Ultimate Tensile Stress (UTS), Failure Strain $\epsilon_f$ ) $\pm$ 95 Confidence Limits for the Cellular Porcine Aortic Heart Valve Root Leaflet specimens .....	245
41.	Table 8.5 Valve Fully Closed Images (where LC: left coronary leaflet, RC: right coronary leaflet and NC: non-coronary leaflet) and Visual Examinations of the Cellular Porcine Aortic Heart Valve Roots at Maximum 1.2 Million cycles .....	250
42.	Table 8.6 Valve Fully Closed Images (where LC: left coronary leaflet, RC: right coronary leaflet and NC: non-coronary leaflet) and Visual Examinations of the Decellularised Porcine Aortic Heart Valve Roots at Maximum 1.2 Million cycles .....	252
43.	Table 8.7 Pre, Mid and Post- Test Mean Leakage Flow Rates ( $F_L$ ) of Each Cellular and Decellularised Porcine Aortic Heart Valve Roots.....	254
44.	Table 8.8 Effective Orifice Area for Each Cellular and Decellularised Porcine Aortic Heart Valve Root Averaged over 4 Heart Rate conditions...	255
45.	Table 8.9 Mean Thickness $\pm$ 95 % confidence limits for the Cellular and Decellularised Porcine Aortic Heart Valve Root Leaflet Radial and Circumferential specimens – p (<0.05) value shows significant difference between cellular and decellularised aortic heart valve roots ....	258
46.	Table 8.10 Tensile Parameters (Collagen Phase Slope $E_c$ , Elastin Phase Slope $E_e$ , Ultimate Tensile Stress $\sigma_{UTS}$ , Failure Strain $\epsilon_{failure}$ ) $\pm$ 95 % Confidence Limits for Cellular and Decellularised Radial (R) and Circumferential (C) Aortic Leaflet Specimens and Number of Test Specimens (N) *-Statistical significant difference (p<0.05) for decellularised versus cellular aortic heart valve roots. ....	259
47.	Table 8.11 Tensile Parameters (Collagen Phase Slope $E_c$ , Elastin Phase Slope $E_e$ , Ultimate Tensile Stress $\sigma_{UTS}$ ) $\pm$ 95 % Confidence Limits for the Cellular Aortic Leaflets Following Cyclic Testing in the RWT and for the Fresh Cellular Aortic Leaflets (Chapter 3) .....	265

## Abbreviations

ANOVA	Analysis of Variance
bpm	Beats per minute
cm	Centimeter
Ec	Collagen phase slope
ECM	Extracellular matrix
Ee	Elastin phase slope
EOA	Effective orifice area
GAGs	Glycosaminoglycans
Hz	Hertz
ISO	International standards organisation
L	Litre
mL	Millilitre
mL.s <sup>-1</sup>	Millilitre/second
mm	Millimetre
mmHg	millimeter of mercury
MPa	Mega pascals
PBS	Phosphate buffered saline
Q <sub>RMS</sub>	Root mean square forward flow
RVOT	Right ventricular outflow tract
RWT	Real time wear tester
SDS	Sodium dodecyl sulphate
UTS	Ultimate tensile strength
ΔP	Transvalvular pressure difference

# 1 Introduction and Literature Review

## 1.1 Introduction

Heart valve disease affects all population ages as a result of rheumatic fever in young adults, atherosclerosis in elderly patients, or by congenital malformation of the heart valve in children (Boudoulas et al., 2013). In severe heart valve disease, replacement of the native heart valve is the most effective solution and is currently performed over 300,000 times each year worldwide (Lei et al., 2018). The available options for heart valve replacement include mechanical heart valves (Gott et al., 2003), bioprosthetic heart valves (Starr et al., 2002), allograft heart valves (Fukushima et al., 2014), and the pulmonary autograft for the diseased aortic valve (Ross procedure) (Yacoub et al., 2006, Ross et al., 1991).

The choice of heart valve replacement in older patients (age  $\geq 70$  years) is less critical than the choice in young patients, because bioprosthetic heart valves are durable in this age group (Bourguignon et al., 2015, David et al., 2010, Pupello et al., 1992). However, the choice of replacement heart valve is complex in young patients due to longer life expectancy and patient growth (Alsoufi et al., 2009). Despite more than 55 years of development and use of replacement heart valves, no ideal heart valve replacement option is available for young patients. Bioprosthetic heart valves are an option due to superior haemodynamic performance but at the cost of accelerated valvular degeneration (Gao et al., 2004). Mechanical heart valves are durable but carry the risk of thromboembolism and require lifetime anticoagulation therapy (Gott et al., 2003). Regeneration and growth is a major problem with both heart valve replacements. Allograft and autograft heart valves do not require anticoagulation therapy and have good hemodynamic performance, but allograft, in contrast to autograft heart valves do not increase in size with child growth. Root dilation (David et al., 2000, Carr-White et al., 2001) and regurgitation (Sampath Kumar et al., 2006) have been reported with the use of autograft heart valves. In addition, the Ross procedure is a surgically demanding operation, and both the autograft in the aortic position and the valve replacement in the right ventricular

outflow tract (RVOT) suffer structural degeneration over time (da Costa et al., 2005, Dignan et al., 2003).

In order to minimise the immune response to allograft heart valves and hence overcome the limitations of degeneration over time, decellularised allograft heart valve roots have been developed (Elkins et al., 2001, da Costa et al., 2005, Cebotari et al., 2011, Vafaei et al., 2016). Decellularised allograft heart valve roots have shown remarkable favourable initial *in vivo* results (Elkins et al., 2001, Lichtenberg et al., 2006, da Costa et al., 2010, Dohmen, 2012). Decellularised allograft heart valve roots, however, suffer from limitations of availability in sizes adequate for young patients. To address this problem, “off the shelf” decellularised porcine heart valve roots in a range of sizes have been investigated by several groups (Luo, 2011, Knight et al., 2005, Choe et al., 2018). Initial clinical translation of decellularised porcine heart valve roots however proved disastrous (Simon et al., 2003, Cicha et al., 2011), and subsequent findings reported that incomplete decellularisation was one of the main reasons for failure of decellularised porcine heart valves.

In addition to complete decellularisation, the success of the replacement heart valve roots relies heavily on an understanding of the biomechanics, hydrodynamics and fatigue performance of the heart valve roots before implanting them in a human body. Such *in vitro* performance evaluation is one of the approval criteria specified by ISO 5840 (2015) and FDA (2010) for the newly manufactured and modified surgical replacement heart valves. However, the *in vitro* performance assessment methods described by the ISO 5840 (2015) standard were developed on the basis of existing mechanical and chemically fixed bioprosthetic heart valves (excluding allografts which are not classified as a manufactured valve) and need to be optimised or replaced with novel methods suitable for decellularised heart valve roots. In particular, the accelerated fatigue assessment method is not suitable for decellularised heart valve roots as the decellularised heart valve roots have time dependent viscoelastic properties and fatigue performance must be assessed in real time. The real time fatigue assessment under physiologic conditions (e.g. heart rates <200 bpm), to cycle counts less than 200 million cycles is recommended by ISO 5840 (2015) for replacement heart valves which have components manufactured from

viscoelastic materials. However, the ISO 5840 (2015) standard does not define either the test equipment or detail the test method for real time fatigue assessment.

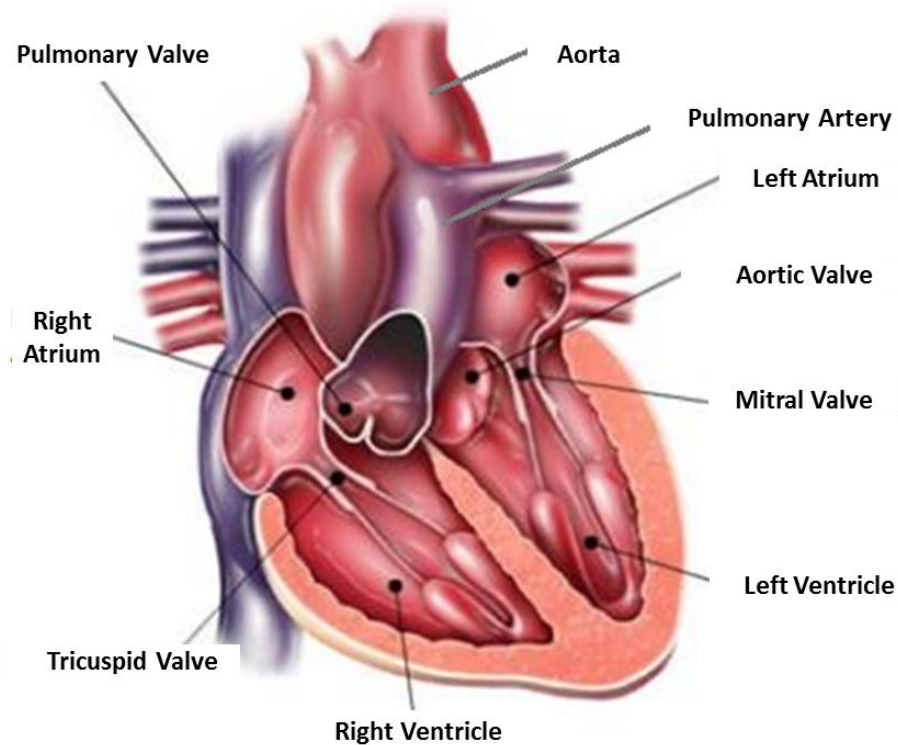
This chapter will examine: the function of semilunar human cellular heart valve roots; the current heart valve replacement options, their advantages and disadvantages; next generation tissue engineered heart valves for heart valve replacement; *in vitro* biomechanical, hydrodynamic and fatigue performance assessment methods for current replacement heart valves and decellularised heart valve roots and the limitations of each; *in vitro* performance of replacement heart valves with the emphasis on *in vitro* performance of decellularised heart valve roots. The aim of this thesis was to develop, optimise and apply *in vitro* pre-clinical test methods to determine the hydrodynamic, biomechanical and fatigue performance of biological heart valve roots (including decellularised heart valve roots), to predict their safety and reliability before they can be used in clinical studies.

## **1.2 The Heart**

The human heart is a pump circulating blood in the body. The pumping system of the heart is coordinated by a series of synchronised contractions. A contraction is generated by electrical activation, spread by a wave of bioelectricity that propagates throughout the heart in a coordinated manner. The human heart contracts 70 times per minute on average, equating to 100,800 cycles per day, and 36 million cycles per year (Roberts and Mitchelmore, 1985).

The heart is composed of four chambers (right atrium, right ventricle, left atrium and left ventricle) and four valves (tricuspid, pulmonary, mitral and aortic valves) (Klabunde, 2005). The anatomy of the human heart is shown in Figure 1.1.

The atrioventricular valves (tricuspid and mitral valve) are located between the atria and ventricles; the tricuspid valve resides between the right atrium and the right ventricle, and the mitral valve is between the left atrium and the left ventricle. The semilunar valves (pulmonary and aortic valve) are located between the ventricles and arteries; the pulmonary valve resides between the right ventricle and pulmonary artery, and the aortic valve is between the left ventricle and aorta (Bateman et al., 2013).



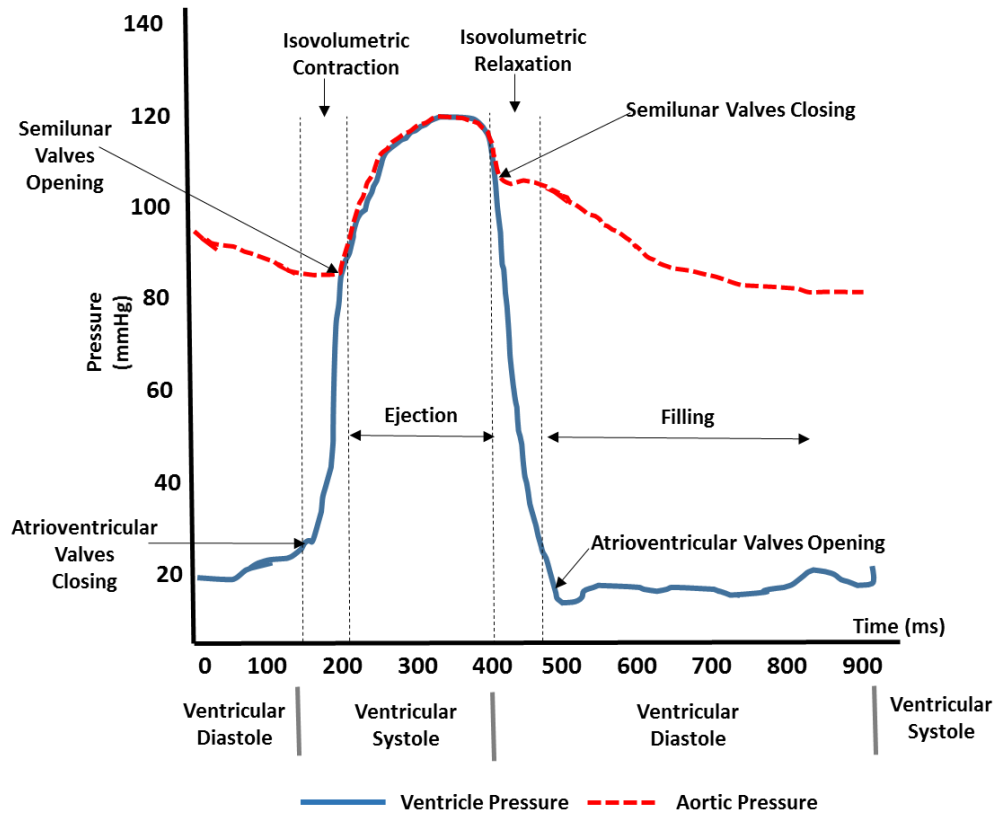
**Figure 1.1 Schematic Diagram of the Structure of the Heart (figure derived from <http://www.sorin.com/anatomy> )**

All the heart valves, except for the mitral valve, consist of three leaflets. The mitral valve has two leaflets and tendinous chords. The right atrium receives deoxygenated blood from the systemic circulation. The right ventricle pumps deoxygenated blood to the pulmonary network where the lungs replenish the oxygen in the blood. The left atrium receives oxygenated blood from the pulmonary network and the left ventricle then pumps oxygenated blood through the rest of the body.

### 1.3 Cardiac Cycle

A cardiac cycle consists of two phases named ventricle systole and ventricle diastole (Figure 1.2). The ventricle systole phase consists of ventricular contraction and blood outflow, whereas the ventricle diastole phase comprises ventricular relaxation and blood inflow.





**Figure 1.2 The Cardiac Cycle. Adapted from (Stehle and Iorga, 2010)**

### 1.3.1 Ventricular Systole

The ventricular systole phase, also known as isovolumetric contraction (Klabunde, 2011), is divided into two stages. Firstly, the ventricles of the heart undergo contraction. During this stage, the blood pressure inside the ventricles is not high enough to open the semilunar (aortic and pulmonary) valves. The second stage of systole is when the blood flows out. As the pressure in the ventricles increases, the semilunar valves are forced open, and blood is expelled from the ventricles very rapidly. The ejection of blood from the ventricle gradually decreases. The decrease in strength from the ejection of blood is directly correlated to the reduction in strength of the ventricular contraction near the end of systole. As the ejection weakens, the rate of blood leaving the ventricles and the heart is less than the rate of blood leaving the aorta, thus decreasing the pressure in the aorta. The amount of blood in a single cycle/beat ejected from the heart is called the stroke volume (Milnor, 1990). The stroke volume multiplied by the number of beats per minute (heart rate) is the cardiac output (Klabunde, 2005).

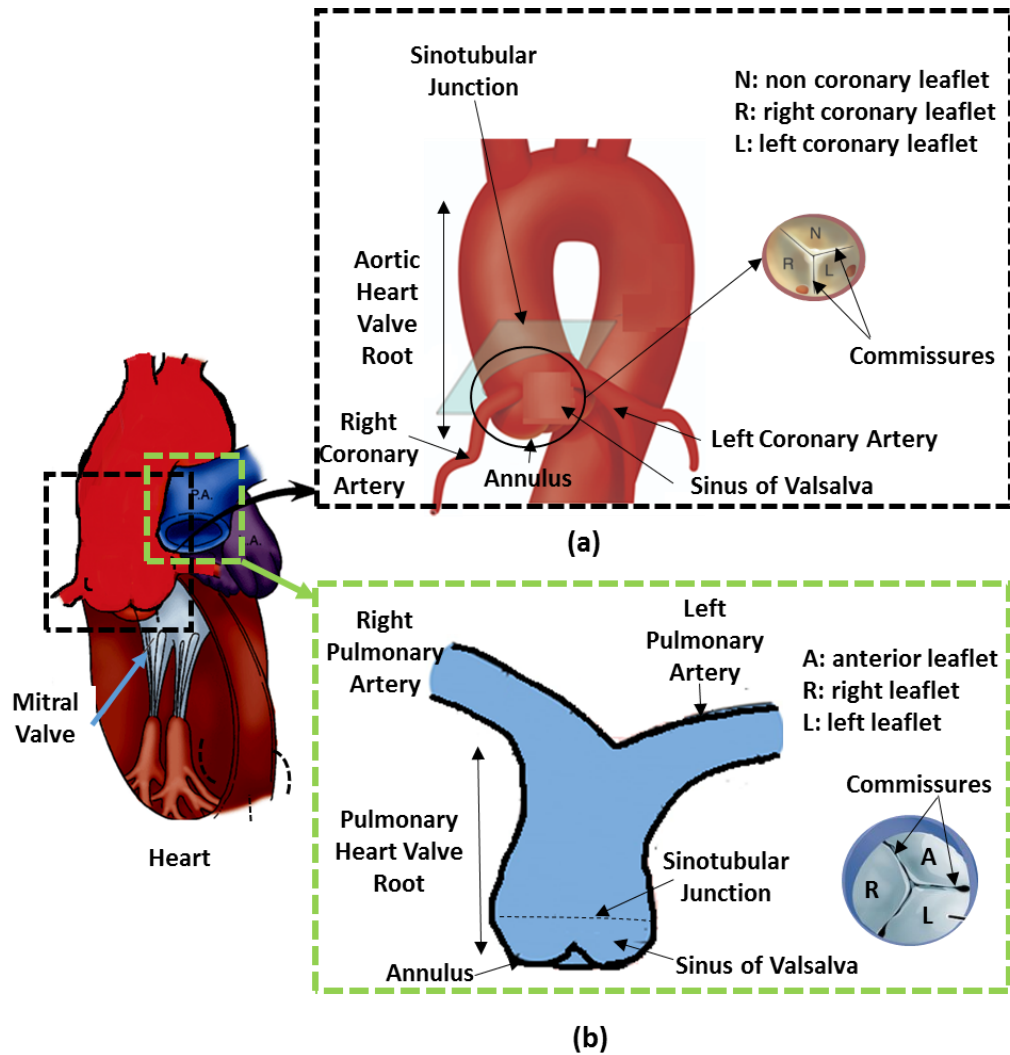
### **1.3.2 Ventricular Diastole**

Ventricular diastole begins with a period of ventricular relaxation. In this period, the outflow of blood is prevented by the closure of semilunar valves, and the influx of blood is stopped by the closed atrioventricular (mitral and tricuspid) valves. Once the ventricles have relaxed even further, the atrioventricular valves open. Diastole ends when the atria contracts to assist in the timely filling of the ventricles (Milnor, 1990).

### **1.4 Characteristics of Semilunar (Aortic and Pulmonary) Heart Valve Roots**

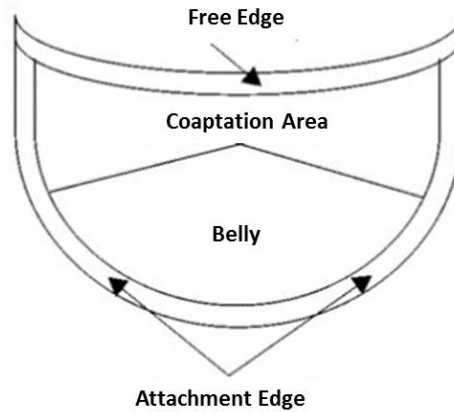
The term 'aortic heart valve root' refers to the aortic valve from its position at the left ventricular outlet to its junction with the ascending portion of the aorta (Ho, 2009). Anatomically, this whole structure is the aortic heart valve root. The aortic heart valve has four anatomic components: the aortic annulus, the aortic leaflets, the aortic sinuses or sinuses of Valsalva, and the sinotubular junction [Figure 1.3 (a)] (Bateman et al., 2013).

The aortic annulus is the attachment between the aortic heart valve root and the left ventricle. The aortic heart valve root is attached to the ventricular myocardium throughout 45% of its circumference and to the anterior leaflet of the mitral valve and the membranous septum in the remaining 55%. The aortic annulus forms a superior border of the left ventricular outflow tract. The three leaflets (left, right and non-coronary leaflets) of the aortic heart valve root are named after their coronary arteries that branch from the sinus of Valsalva, which supply blood to the left and right side of the heart. The sinotubular junction is above the commissures and is functionally important for the aortic heart valve root as the sinotubular junction on the commissure suspends the aortic leaflets. The aortic sinuses are described as the arterial walls contained between the aortic annulus and sinotubular junction. The aortic sinuses facilitate coronary artery blood flow during the cardiac cycle while maintaining eddies and currents to facilitate closure of the aortic leaflets during diastole.



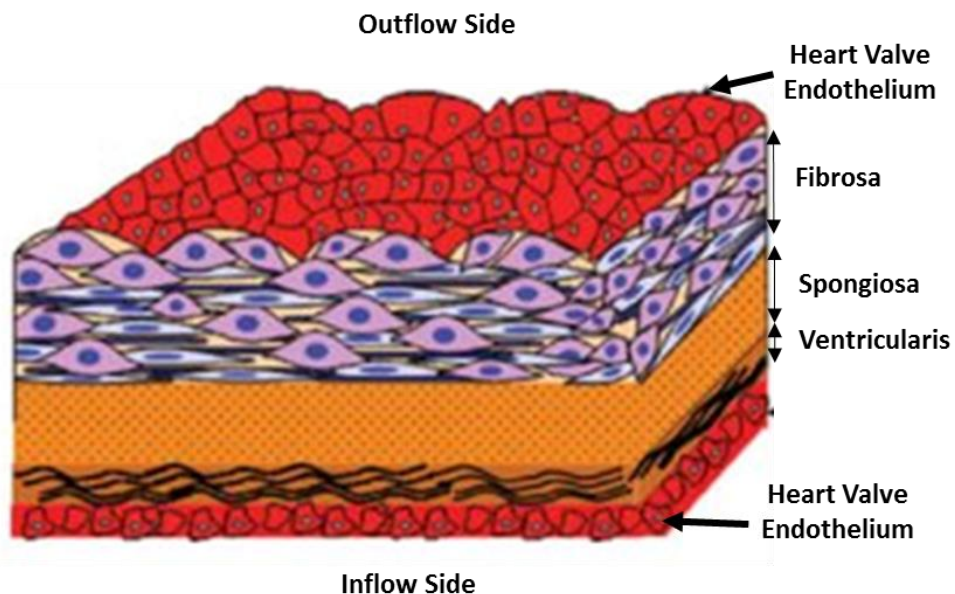
**Figure 1.3 Defined Terminology for the (a) Aortic and (b) Pulmonary Heart Valve Root Components**

The structural components of the pulmonary heart valve root are similar to the aortic heart valve root. The pulmonary heart valve root also consists of a valve with three leaflets, three sinuses of Valsalva, a crown-shaped annulus and commissures [Figure 1.3(b)]. The pulmonary valve leaflets are named according to their position with respect to the aortic valve. Two leaflets face towards the right coronary and left coronary aortic leaflets are known as right and left leaflets respectively. The third leaflet (the non-facing leaflet), being the most anterior is known as the anterior leaflet (Bateman et al., 2013).



**Figure 1.4 Semilunar Heart Valve Leaflet Region (Dawidowska, 2016)**

*In vitro* studies have shown that native aortic and pulmonary heart valve roots undergo rapid, complex conformational changes during opening/closing. The valve opens from the belly region to the free edge (Figure 1.4) while during closing both the free edge and circumferential section close together indicating important differences between the opening and closing phases.



**Figure 1.5 Schematic Diagram of the Multi-Layered Structure of Heart Valve Root Leaflet (Rippel et al., 2012)**

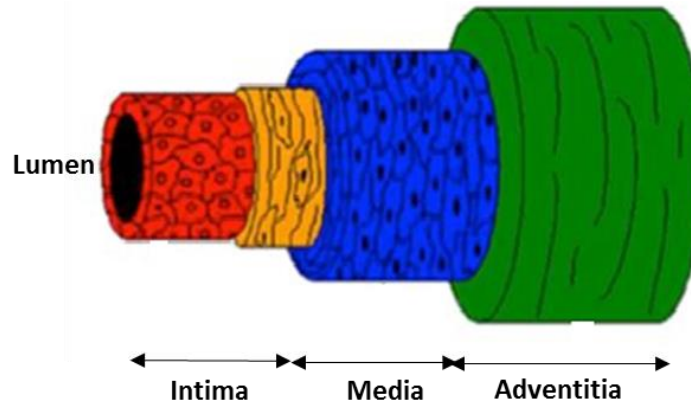
Heart valve leaflets are multi-layered structures with complex architecture. They have functionally adapted cells and an anisotropic arrangement of extracellular matrix (ECM) (Ho, 2009). Heart valve leaflets have three major layers, which together have the necessary material properties to withstand cyclic loading (Figure 1.5). Each layer's composition and function is displayed in Table 1.1.

**Table 1.1 Composition and Function of Each Leaflet Layer (Vesely and Noseworthy, 1992, Schoen and Levy, 1999).**

Layer	Matrix Composition	Function
<b>Fibrosa</b> – on the outflow/backward flow side,	Consists of macroscopic collagen bundles arranged in a circumferential manner where the collagen fibers run parallel to the leaflet free edge ; elastin	Maintain durability and stiffness to withstand pressure gradient (Chester et al., 2014)
<b>Spongiosa</b> – the centrally arranged layer between fibrosa and ventricularis	Consists of loosely arranged collagen fibers along with abundant glycosaminoglycans (GAGs).	Allows shearing between the ventricularis and fibrosa during cardiac valve cycle (Chester et al., 2014)
<b>Ventricularis</b> - on the inflow side	Consists of densely packed collagen; radially aligned elastin fibers	Maintains valve resilience, allows stretch in response to pressure change (Chester et al., 2014)

The leaflets of the heart valve root exhibit highly nonlinear stress-strain relationships, are anisotropic, and have significant time dependent viscoelastic features exhibiting behaviours that combine features of elastic solids and viscous fluids. The viscoelastic response of the leaflets has often been attributed to the glycosaminoglycan (GAG) component of the ECM (Tseng et al., 2013). Indeed, there is evidence that the GAG rich spongiosa layer acts as a damper, to reduce the impact created by sudden changes in pressure gradient (Luo, 2011).

The aortic and pulmonary heart valve root wall consists of three separate layers (Figure 1.6) as described in Table 1.2.



**Figure 1.6 Schematic Diagram of the Multi-Layered Structure of Heart Valve Root Wall (McCloskey et al., 2014)**

**Table 1.2 Composition and Function of Each Wall Layer (Tsamis et al., 2013, Pak et al., 2007)**

Layer	Matrix Composition	Function
<b>Intima</b> – inner layer, in contact with blood	A single layer of endothelial cells which create a lining along the wall	Becomes mechanically significant with ageing and the associated onset of arteriosclerosis (Holzapfel et al., 2005)
<b>Media</b> – middle thickest layer	Made up of a complex network of both elastin and collagen fiber bundles	Allows wall to resist loads in both the circumferential and longitudinal directions. (Tsamis et al., 2013, Pak et al., 2007)
<b>Adventitia</b> – external thinnest layer of connective tissues	Consists of fibroblasts and fibrocytes, which are cells that produce collagen and elastin respectively	Under high pressures, the collagen fibers are engaged creating an extremely stiff structure in order to help resist rupture (Tsamis et al., 2013, Pak et al., 2007)

The elastic property of heart valve root walls is mediated by elastin, whereas the stiffer collagen contributes to wall strength (van Soldt et al., 2015). The dynamic circumferential movement (dilation) of the heart valve root wall enhances leaflet closure at the end of systole and protects the leaflets from wall impact during systole.

In addition, movement of the annulus changes the tension/length relationships of the leaflets to enhance function (Hopkins, 2003).

### **1.5 Function of Semilunar (Aortic and Pulmonary) Heart Valve Roots**

The aortic and pulmonary heart valve roots are compliant biological structures experiencing dynamic cyclic loading and permit the blood flow in one direction only. When the ventricles contract (ventricular systole), the aortic and pulmonary valve leaflets are pushed open by the blood flow from the ventricles to the aorta and pulmonary artery respectively. When the ventricles are at rest (ventricular diastole) the aortic and pulmonary valve leaflets are pushed closed by blood rebounding off the walls of the aorta and pulmonary artery respectively, effectively preventing the blood flowing back into the ventricles (Bateman et al., 2013). Although the leaflets are the most dynamic parts of the aortic and pulmonary heart valve root, the motion of other associated structures such as the heart valve root wall and the expansion of the entire valve root structure itself also play important role (Thubrikar, 2018).

Moreover, the aortic heart valve root wall dilation is assumed to prevent the leaflets from sticking to the wall of the aorta (Hopkins, 2003) and to transmit the stress from the leaflets to the wall (Thubrikar, 2018). The dynamic aortic heart valve root wall anatomy has been described as designed to reduce leaflet stresses and thereby fatigue and eventual structural failure of the valve leaflets (Sutton et al., 1995). During diastole, when the aortic valve is closed, a part of each leaflet coapts against the other two leaflets. The coaptation surface serves two important functions; it provides a safety margin for the valve to close without regurgitation or leakage, and it transfers the load on the leaflets to the commissures (Thubrikar, 2018). During the closed phase, the aortic valve leaflets experience a tensile stretch, which stretches the elastin within the ventricularis layer, while the crimp and un-crimp action of the collagen heavy fibrosa layer enables opening and closing of the leaflet.

The action of the heart valve root may be explained on the basis of local pressure gradients in the regions of the aortic heart valve root. The transvalvular pressure difference across the open aortic heart valve is less than 10 mmHg in a healthy aortic heart valve root, typical closing pressures are 80 - 100 mmHg

(Chandran et al., 2012). The aortic heart valve is highly affected by diseases more than the pulmonary heart valve due to the fact that the aortic valve (100 mmHg) carries higher pressure than the pulmonary valve (30 mmHg) (Yoganathan et al., 2004).

The pulmonary heart valve leaflets respond in the same manner in response to relaxation and contraction of the right ventricle in moving de-oxygenated blood into the pulmonary artery and hence to the lungs for re-oxygenation.

## **1.6 Valvular Disease**

Heart valve disease is defined as the improper function of one or more heart valves (Boudoulas et al., 2013). Heart valve disease affects more than 100 million people worldwide and is a growing problem because of the high incidence of rheumatic heart disease in developing countries (Carapetis et al., 2005). Almost 500,000 people die every year from rheumatic heart disease, with most deaths occurring during childhood or early adulthood (Carapetis et al., 2005). The other main causes of valvular disease include calcification of the valve as people age (Kodali et al., 2018), congenital defects (a malformation during pregnancy)(Lincoln and Yutzey, 2011) and valvular infections (called endocarditis) (Torpy et al., 2007). In some instances the valve does not function properly due to deterioration of valvular supportive tissue (loose valve sealing) or due to aortic aneurysm (the dilated aorta). Deficit in the function of any heart valve reduces the effectiveness of the heart, and can eventually lead to heart failure and death. In adults, the prevalence of valvular heart disease increases dramatically with age reaching 13% of patients who are 75 years old and older (Nkomo et al., 2006, Roger et al., 2012). The most common treatment option for a severely damaged heart valve is heart valve replacement, comprising of approximately 300,000 surgeries per year (Lei et al., 2018). It is also expected for the number of patients requiring heart valve replacement to triple from approximately 290,000 in 2003 to over 850,000 by 2050 (Cheung et al., 2015).



## **1.7 Replacement Heart Valves**

### **1.7.1 Mechanical Heart Valves**

Mechanical heart valves are made totally of mechanical parts and have evolved through several design changes since 1952 (Gott et al., 2003). There have been numerous repetitions of these valves with multiple designs, including mono leaflet, bileaflet, and ball-in-cage models. The bileaflet valve is the most common type of mechanical valve used today. The bileaflet valve has two semicircular leaflets attached to the ring on pivots (Suh et al., 2015). The advantage of mechanical valves is their excellent long-term durability. However, patients require lifelong anticoagulation treatment to manage risks of thromboembolism (due to foreign body response) and haemorrhage (from too much anticoagulation) (Schoen and Levy, 1999). Another disadvantage with the mechanical valve is the mechanical clicking sound resulting from the opening and closing of the valve leaflets, which can be disturbing for some patients. Moreover, pregnancy in patients with mechanical valves may present a high risk due to the need for anticoagulation (Ashour et al., 2000).

### **1.7.2 Bioprosthetic Heart Valves**

The term “bioprosthetic” commonly denotes an organic valve which is a chemically treated stented or stentless valve (Meuris and Flameng, 2008). Bioprosthetic heart valves have leaflets produced of animal tissue (Pibarot and Dumesnil, 2009) and were first commercialised in the 1970’s but continue to face durability issues resulting from a variety of causes. Bioprosthetic heart valves do have an advantage of lower thrombogenicity compared to mechanical valves, and do not subject the recipient to a lifetime of anticoagulant therapy (Yadava, 2013). Another advantage in comparison with mechanical valves is the absence of the mechanical clicking sound. The major disadvantage of biological alternatives is the risk of structural deterioration and malfunction of the valve, which is accelerated in younger patients (Gao et al., 2004, Applegate et al., 2017). Tears and calcification of the leaflets can occur and the risk of failure (stenosis or regurgitation) and limited durability increases with time. Recent models of these types of bioprosthetic heart

valves have demonstrated good durability and last for 10–15 years in elderly patients over 70 years of age (Siddiqui et al., 2009, Gao et al., 2004).

### **1.7.3 Allografts (Homograft) Heart Valve Roots**

Allograft heart valve roots are aseptically recovered from cadavers and treated with antibiotics before cryopreservation (Shaddy and Hawkins, 2002, O'Brien et al., 2001). The allografts are implanted as a freehand subcoronary implantation or as a full heart valve root replacement in place of a diseased heart valve (Koolbergen et al., 2002). The advantages of using allografts in heart valve replacement surgery include the excellent hemodynamic performance, low risk of thromboembolism, and possibly a reduction in the risk of prosthetic valve infection (O'Brien et al., 2001, Staab et al., 1998, Park et al., 2012, Elkins et al., 2001, Fukushima et al., 2014). In addition, these heart valve roots do not have any rigid stent mounting like most prosthetic heart valves, which is helpful for good haemodynamic characteristics of these heart valves. However, allograft heart valve roots fail due to progressive degenerative changes resulting from immunologically mediated inflammation and calcification (Hoekstra et al., 1996, Oei et al., 2002, Homann et al., 2000, Penta et al., 1984, da Costa et al., 2005). In addition, the limited availability of allograft heart valve roots due to donor shortages, especially for small sized heart valve roots for young patients, is a significant disadvantage (Delmo Walter et al., 2012). In addition, donor human heart valve roots of consistent quality are often limited.

### **1.7.4 Autograft Heart Valves**

The autograft heart valve is the pulmonary heart valve translocated within the same patient to the aortic position. The autograft valve replacement procedure requires the pulmonary heart valve to be replaced with a pulmonary allograft, and this surgical procedure is referred to as the “Ross operation” or the “Ross procedure” (Ross et al., 1991). The Ross procedure has proven a good option for younger patients due to its ability to grow with the child, and can result in long term complication free survival for patients with aortic heart valve disease (Yacoub et al., 2006, Ross et al., 1991). The Ross procedure has shown higher survival rates in comparison with mechanical heart valves, largely due to improved hemodynamic performance and lack of anticoagulation therapy (Alsoufi et al., 2009, Mazine et al., 2018, Nagy and

Watterson, 2008). However, a progressive dilation of the pulmonary autograft has been observed after aortic heart valve root replacement (Hokken et al., 1997, David et al., 2000, Takkenberg et al., 2006). In addition, the heart valve substitute in the pulmonary position often fails, compounding the problem of reoperations in patients with failed Ross procedure (Mokhles et al., 2012, Luciani et al., 2012). The use of autograft valves requires longer operation times and a requirement of very high levels of surgical skill.

### **1.7.5 Tissue Engineered Heart Valves**

In spite of all the existing heart valve replacement options (Section 1.7.1, 1.7.2, 1.7.3, 1.7.4), there is still a need for a better living replacement heart valve with the capacity to grow, repair and integrate in a biological environment. Most importantly, none of the current replacement heart valve options available are adequate for young patients, as most heart valve replacement options cannot grow with patients and patients may need to go through multiple revision surgeries during their life. The goal of heart valve tissue engineering requires the design of a scaffold that essentially acts as an artificial extracellular matrix (ECM) to support cell migration, attachment, proliferation, differentiation and tissue regeneration (Mooradian, 2016, Sacks et al., 2009, Mendelson and Schoen, 2006). Two main types of scaffolds have been developed:

- Biodegradable synthetic scaffolds (Hoerstrup et al., 2000, Sodian et al., 2000, Robinson et al., 2008, Syedain et al., 2015)
- Decellularised heart valve scaffolds from allogeneic (a genetically non-identical donor of the same species) or xenogeneic (animal) sources (Luo et al., 2014, da Costa et al., 2005, Vafaei et al., 2016, Paniagua Gutierrez et al., 2015, Elkins et al., 2001, Ozawa et al., 2018).

Besides choosing the appropriate scaffold material, the choice of a right cell source is essential for the creation of a functional tissue engineered heart valve. The approaches to tissue-engineered heart valves can be divided into the *in vitro* and the *in vivo* tissue engineering approach (Kluin et al., 2017). The *in vivo* tissue engineering approach is, also known as '*in situ* tissue engineering' or 'guided tissue regeneration' approach.

The *in vitro* heart valve tissue engineering approach aims to create a new viable three-dimensional heart valve *in vitro*. In this approach cells from individual cellular components are isolated, expanded and subsequently seeded on an appropriate (biodegradable) scaffold. The seeded scaffold is exposed to stimulation transmitted via a culture medium (biochemical stimuli) or via 'mechanical conditioning' of the tissue (mechanical stimuli) (Bader et al., 1998, Lichtenberg et al., 2006, Cicha et al., 2011, Rippel et al., 2012, Roosens et al., 2017) prior to *in vivo* implantation. Different cell types have been investigated for the ability to synthesize extracellular matrix (ECM) for tissue engineered heart valves. Myofibroblasts are an interesting cell source because of their capacity for fast proliferation and collagen synthesis (Maish et al., 2003). These cells can be isolated from the vasculature of the patient, involving surgical intervention to obtain a tissue sample. To prevent multiple surgical interventions, alternative cell sources have been investigated, such as bone marrow stem cells (Hoerstrup et al., 2000), adipose tissue derived stem cells (Roosens et al., 2017), amniotic fluid stem cells (Schmidt et al., 2007), endothelial progenitor cells from peripheral blood (Lichtenberg et al., 2006) and umbilical cord blood (Sodian et al., 2000).

The *in vivo* heart valve tissue engineering approach is based on the use of the natural regenerative potential of the body for tissue maturation. In this approach, decellularised (xenografts, allografts) and synthetic scaffold (either with or without autologous cells) are directly implanted into the patient. This *in vivo* tissue engineering approach could be attractive for clinical application due to off-the-shelf availability, lack of the *in vitro* maturation phase (*in vitro* conditioning phase) and the regulatory process prior to implantation is likely to be more straightforward (especially if cells do not have to be expanded).

#### **1.7.5.1 Synthetic Scaffolds**

To increase the potential for growth and remodelling biodegradable synthetic polymers [polyglycolic acid (PGA), polylactic acid (PLA), *poly-4-hydroxybutyrate* (P4HB) and polycaprolactone (PCL)] are being widely investigated as scaffold materials to fabricate tissue engineered heart valves (Stock and Mayer, 2001, Hong et al., 2009, Santoro et al., 2017, Kluin et al., 2017, Mayer et al., 1997, Cascone et al.,

2001). All the biodegradable synthetic polymer materials have characteristics such as a large surface to volume ratio, high porosity with small pore size, biocompatible, adequate mechanical properties, low cost of production, consistency, and long shelf life (Hutmacher, 2001). However, biodegradable synthetic scaffolds face cell adhesion and tissue reorganisation challenges since such materials are usually isotropic and ECM proteins are not usual constituents of synthetic scaffolds. Some limitations are encountered due to degradation of the scaffolding material being faster than the ECM production, leading to early structural incompetency. PGA degrades at the fastest rate, in weeks, while PCL degrades over years. Slow or incomplete polymer degradation, in contrast, may result in excessive chronic local tissue inflammation, possibly leading to fibrosis (scar) and hampered valve function (Cheung et al., 2015).

#### **1.7.5.2 Allogenic and Xenogenic Scaffolds**

Scaffolds derived from allogenic and xenogenic heart valves can be used as in tissue engineered heart valves because they have a geometry and structure that is closer to native human heart valves, with similar material constituents and functional properties and there are no potentially toxic by-products from polymer biodegradation. However, both xenogenic and allogenic heart valve replacements increase the risk of immunogenic reactions. Moreover, using native (unfixed) biological material, particularly xenogenic scaffolds, exposes the recipient to the risk of disease transmissions. These risks can be mitigated by chemical crosslinking or decellularisation of the tissue. Chemically crosslinked xenograft and allograft heart valves inhibit cellular deterioration, enhance mechanical stability, and makes it possible to carry an inventory of different sized heart valves (Mooradian, 2016). As crosslinked valves are fixed, inanimate and non-degrading scaffolds, they cannot grow and remodel, and thus are not suitable for heart valve tissue engineering. On the other hand, decellularisation of biological tissues decreases adverse immunological response without limiting the remodelling capacity (Luo et al., 2014, Wilcox et al., 2005). Several decellularisation methods have been developed to produce decellularised heart valves using enzymatic digestion and detergent cell extraction techniques. None of the currently used decellularisation techniques are

capable of removing 100% of cellular material. However, it has been suggested that the decellularisation technique has to satisfy a set minimal criteria; double-stranded DNA content below 50 ng/mg ECM (dry weight), DNA fragments less than a maximum length of 200 bp, and no nuclear material visible with 6-diamidino-2-phenylindole (DAPI) or haematoxylin and eosin (HE) staining (Crapo et al., 2011).

Enzymatic techniques for heart valve decellularisation include the use of protease digestion and nucleases. Trypsin is a highly specific enzyme that breaks the peptide bonds or cell matrix attachments and washes the cells from the native tissue (Grauss et al., 2005). Steinhoff et al. (2000), demonstrated that a 48-hour trypsin/ethylene diamine tetra-acetic acid (EDTA) treatment resulted in a decellularised ovine pulmonary heart valve root. The procedure revealed an almost complete removal of cells while the static reseeding of the upper surface with autologous myofibroblasts and endothelial cells showed a limited and patchy coverage. This protocol was later applied to human aortic and pulmonary allograft valves, resulting in decellularisation (Cebotari et al., 2002). However, incomplete decellularisation of porcine aortic and pulmonary heart valve roots was reported even though the same trypsin/EDTA protocol was used (Kasimir et al., 2003, Rieder et al., 2004).

Detergents are amphipathic molecules, consisting of a polar head group and a hydrophobic chain (or tail), which can solubilize amphiphilic cell membranes and separate DNA from proteins by disrupting lipid-lipid and lipid-DNA interactions. For heart valve decellularisation, the most commonly used non-ionic detergent is Triton X-100 (tert-octylphenylpolyoxyethylen) and ionic detergents are sodium dodecyl sulphate (SDS) and sodium deoxycholate (SDC). Non-ionic detergents are relatively mild detergents as they break lipid-lipid and lipid-protein interactions, but leave protein-protein interactions intact (Seddon et al., 2004). The ionic detergents are known to solubilize cell and nucleic membranes, but tend to denature proteins (Gilbert, 2012). Bader et al. (1998) was the first to use non-ionic detergent Triton X-100 for the decellularisation of porcine aortic valves. Numata et al. (2004) showed successful decellularisation of porcine pulmonary heart valve roots with Triton X-100 treatment. However, Booth et al. (2002) did not achieve complete decellularisation of porcine aortic valve roots after Triton X-100 treatment.

Several authors have demonstrated complete decellularisation of porcine pulmonary (Luo et al., 2014, Tudorache et al., 2007) and aortic (Paniagua Gutierrez et al., 2015, Korossis et al., 2002) heart valve roots using the ionic detergent, SDS. Booth et al. (2002) used 0.03 – 1% (w/v) SDS and 0.5 – 2% (w/v) deoxycholic acid to decellularise porcine aortic heart valve root leaflets. Concentrations of SDS of 0.1% (w/v) facilitated the removal of cellular material without causing substantial damage to the ECM (Booth et al., 2002) and this concentration was subsequently adopted in the Leeds proprietary decellularisation treatment protocol. Concentrations of SDS of 1% (w/v) and higher have been found to change the biomechanical properties of tissues in some studies (Nakayama et al., 2010, Wollmann et al., 2011). Korossis et al. (2002) used the Leeds proprietary decellularisation treatment to decellularise porcine aortic heart valve leaflets and reported that the 0.1 % SDS decellularised porcine aortic leaflet retained its natural structure, biochemical composition, mechanical strength and function but decellularisation altered leaflet stiffness. These changes may have been due to the significant reduction of GAGs and removal of cells (Vafae et al., 2016, Luo, 2011). The loss of GAGs in the decellularised leaflets, may have led to loosening of the fibrous structure, and uncrimping of the circumferentially aligned collagen fibers. Although the SDS treatment was successful in the decellularisation of aortic valve leaflets, it was not effective alone for decellularisation of the aortic wall component of whole aortic heart valve roots and, a modified protocol was developed by including a 1.25% (w/v) trypsin digestion step, applied only to the surfaces of the aortic root wall. Again, in this protocol, SDS was used at a concentration of 0.1% (w/v) (Wilcox et al., 2005, Luo et al., 2014).

Porcine pulmonary heart valve roots have also been decellularised using SDS 0.1% (w/v) with trypsin. No significant difference in the tensile properties of the decellularised wall and leaflet specimens compared with cellular specimens were found, except for a significant decrease in the elastin phase slope in both the circumferential and axial directions of the decellularised heart valve root wall specimens (Luo et al., 2014).

Subsequently the Leeds proprietary decellularisation process comprising washes in hypotonic buffer, 0.1% (w/v) SDS and nuclease digestion was applied to

human donor aortic and pulmonary heart valve roots and this has been reported to remove 97% of the DNA (Vafaei et al., 2016). DNA levels are a good indicator of the degree of cell removal (Crapo et al., 2011). However, although the process described by da Costa et al. (2010) also used 0.1% (w/v) SDS, the use of nuclease was not described. The decellularisation technology used by da Costa et al. (2010) was developed at Pontificia Universidade Católica do Paraná (PUCPR), in conjunction with the research team from the University of Leeds, United Kingdom. The Haverich group (Lichtenberg et al., 2006, Neumann et al., 2014) used harsher detergent treatment [0.5% (w/v) SDC plus 0.5 % (w/v) SDS] to decellularise human donor pulmonary heart valve roots but again did not appear to incorporate a nuclease treatment (Cebotari et al., 2011).

### **1.7.5.3 Clinical Experience with Decellularised Heart Valve Roots**

Clinical implantation of decellularised allograft heart valve roots has shown promising success in recent years. SynerGraft® (CryoLife, Kennesaw, GA) decellularised cryopreserved aortic and pulmonary allograft heart valve roots were introduced in 2000. The allograft heart valve roots were decellularised using a SynerGraft proprietary decellularisation process involving incubation of the tissue in sterile water to promote cell lysis. The allografts are then exposed to deoxyribonuclease and are repeatedly washed in an isotonic solution prior to cryopreservation. Clinical studies of the CryoValve SG™ pulmonary allograft heart valve roots in young patients and adults undergoing Ross procedures and RVOT reconstructions have reported comparable or improved performance relative to cryopreserved pulmonary allograft heart valve roots in the short to medium-term (Bechtel et al., 2008, Brown et al., 2010, Burch et al., 2010, Brown et al., 2011, Elkins et al., 2001, Zehr et al., 2005). Most of the studies reported either no valve related or operative death (Sievers et al., 2003, Brown et al., 2011, Burch et al., 2010, Elkins et al., 2001) and no significant difference in death or survival (Bechtel et al., 2008, Tavakkol et al., 2005). However, some of these studies reported evidence of structural deterioration, although Dohmen et al. (2007) reported no structural deterioration at a mean of 4 years post-implantation. In addition, most of these clinical studies are focused solely on heart valve function and do not have clear



information about inclusion and exclusion criteria in their clinical outcome assessment methods. For example, the dysfunction or failure of the decellularised heart valve root was not specified to be structural or non-structural. Brown et al. (2010) stated that no significant differences were found between CryoValve SG™ decellularised pulmonary heart valve roots and the control group of heart valve roots in terms of non-structural valve dysfunction.

Despite these promising reports on the benefits of using decellularised allograft heart valve roots, some studies (Bechtel et al., 2005, Bechtel et al., 2008) which have compared CryoValve SG™ pulmonary allograft heart valve roots with conventional cryopreserved pulmonary allograft heart valve roots have found no significant difference in heart valve root longevity, with only slight trends toward improved peak pressure gradients in smaller CryoValve SG™ pulmonary allograft heart valve roots in maximum 5 years follow up time. The results showed freedom from heart valve root dysfunction was significantly worse at 10 years in the cryopreserved allograft heart valve roots (58%) than in the CryoValve SG™ pulmonary heart valve roots (83%,  $p < 0.001$ ). Adventitial fibrosis, degeneration, and calcification have been reported for most explanted decellularised heart valve roots (Helder et al., 2016). Other noticeable studies on decellularised allograft heart valve roots have been performed by the Hannover group (Cebotari et al., 2011, Tudorache et al., 2016) and the da Costa group (da Costa et al., 2010, da Costa et al., 2018) from Brazil using 0.5% (w/v) SDS plus 0.5% (w/v) SDC and 0.1% (w/v) SDS respectively to achieve decellularisation. They reported short to medium term success with decellularised pulmonary allograft heart valve roots (Cebotari et al., 2011, da Costa et al., 2005, da Costa et al., 2014, da Costa et al., 2018) and decellularised aortic allograft heart valve roots (da Costa et al., 2010, Kneib et al., 2012). da Costa et al. (2009) reported good results in RVOT in the Ross procedure (up to 4 years) in patients with a mean age of  $30 \pm 11$  years using decellularised pulmonary allograft heart valve roots. Clinical studies of decellularised aortic valve allograft heart valve roots implanted in patients with a median age of 34 years (range, 0.1 to 71) showed stable structural integrity, low rate of calcification and adequate haemodynamics in a mean follow-up of 19 months (range, 1 to 53) (da Costa et al., 2010).

Tudorache et al. (2016) analysed results of 69 decellularised aortic allograft implants in children and young patients. Hemodynamic performance of these decellularised allografts was excellent up to 7.6 years of follow up. Most importantly, this study showed clinical data of decellularised aortic allograft implanted in 16 patients younger than 10 years (Tudorache et al., 2016). Cebotari et al. (2006) reported normal physiological growth of decellularised human pulmonary heart valve roots in the pulmonary position in two paediatric patients (aged 11 and 13 years old) in a 3.5 years follow up. The human pulmonary heart valve roots were decellularised using trypsin/EDTA and seeded with endothelial progenitor cells (Cebotari et al., 2006). In another study by same the research group (Cebotari et al., 2011), the *in vivo* performance of decellularised pulmonary allografts was investigated in 38 patients (mean age at implantation  $16.4 \pm 11.4$  years) and compared with glutaraldehyde-fixed bovine jugular vein and cryopreserved allografts in children and young adults. The heart valves were decellularised using the harsher detergent treatment (0.5% SDC plus 0.5% SDS). The decellularised pulmonary allograft heart valves showed very promising early results (no development of high pressure gradients, rare insufficiency observations, no revision surgery) in a maximum of 5 years follow up (Cebotari et al., 2011). In a more recent study Sarikouch et al. (2016) reported 100 % freedom from surgical replacement after ten years of follow-up with decellularised pulmonary allograft heart valve roots using the same harsher detergent treatment (0.5% SDC plus 0.5% SDS) in young patients ( $n=93$ ) with mean age  $15.8 \pm 10.2$  years at implantation. However, the mean short term follow up, small number of patients and complex surgical procedure in these young patients, limit the discussion of the results. Despite the fact that these decellularised allograft heart valves have been implanted into patients, details of DNA levels in these decellularised human donor valve allografts is lacking. Overall the results from these studies in young patients (Sarikouch et al., 2016, Cebotari et al., 2011, Tudorache et al., 2016, Lichtenberg et al., 2006) are promising; even though the decellularisation protocols were different.

These studies (Tudorache et al., 2016, Cebotari et al., 2011, da Costa et al., 2005, da Costa et al., 2014, da Costa et al., 2018) suggested that the short-term and mid-term performance of decellularised allograft heart valve roots was superior or similar to that of cryopreserved allograft heart valve roots which usually last 8-12

years without issues (Fukushima et al., 2014, Homann et al., 2000). Hence, studies comparing decellularised heart valve roots with cryopreserved allograft heart valve roots which are less than 10 years would not be expected to show any differences. Further long-term follow-up is needed to see whether this decellularisation process improves long-term durability of allograft heart valve roots.

Although clinical performance of the decellularised allograft heart valve roots is satisfactory, only four decellularised allograft heart valve roots [Espoir PV (decellularised human pulmonary) by CorLife GbH (Hannover, Germany), Arise AV (decellularised human aortic) by CorLife GbH (Hannover, Germany), CryoValve SG™ (decellularised pulmonary) by CryoLife (CryoLife Inc), CryoValve Aortic (decellularised aortic) by CryoLife (CryoLife Inc)] are commercially available.

Although decellularised heart valve roots are commercially available and have been in clinical use in some countries for more than 10 years, they are not yet routinely available in the UK. However, the decellularised human heart valve roots were used in the UK and as a part of the European Commission funded clinical trial studies [European clinical study for the application of regenerative heart valves (ESPOIR) (<http://www.espoir-clinicaltrial.eu>) and Aortic Valve Replacement using Individualised Regenerative Allografts (ARISE) (<http://www.arise-clinicaltrial.eu>)] which was started in 2012 to evaluate performance of the decellularised pulmonary and aortic allograft heart valve roots in young patients. These studies are conducted in collaboration with seven leading European clinics (London, Leiden, Padua, Zürich, Leuven, Chisinau and Hannover), four European tissue banks (European Homograft Bank, Deutsche Gesellschaft für Gewebetransplantation, Fondazione Banca dei Tessuti di Treviso and Euro Heart Valve Bank), and a bio-tech company, Corlife GbH, Germany). Heart valve roots were supplied by the tissue banks, decellularised by Corlife oHG, and subsequently transplanted at one of the clinical centres. Currently, 240 patients are documented within this registry with the aim of a 10 year follow-up for all patients.

The lack of availability of decellularised allograft heart valve roots, particularly in smaller sizes suitable for young patients, led to the proposal of decellularised xenogenic “off the shelf” aortic and pulmonary heart valves in a range of sizes.

However, to date clinical performance of these decellularised xenogenic heart valve roots has been disappointing (Cicha et al., 2011, Simon et al., 2003). Simon et al. (2003) reported failures of the FDA-approved SynerGraft® (Model 500 and 700; Cryolife Inc., USA) decellularised porcine pulmonary heart valve roots, leading to the death of three out of four male children (age 2.5-11 years). Post-implant examination of failed heart valve roots revealed incomplete decellularisation, lack of cell repopulation, lack of endothelialization with severe inflammation, fibrous sheath creation inside and outside the graft, foreign body reaction, calcification, and severe degeneration of leaflets and wall.

Dohmen et al. (2002) reported the first successful implantation of a 1 % deoxycholic acid decellularised cryopreserved pulmonary allograft (AutoTissue Ltd™ process) seeded with autologous vascular endothelial cells in the RVOT of a 43 year old patient that underwent the Ross procedure. The results showed good clinical outcome at one year of follow-up. Subsequently, porcine heart valve roots were decellularised using a modification of the AutoTissue Ltd™ decellularisation method (with the addition of ethanol 70 % to the protocol). The decellularised porcine heart valve roots (Matrix P™ and Matrix P Plus™ valves; AutoTissue GmbH, Berlin, Germany) were implanted in 93 patients that underwent the Ross operation. A total of 33 patients (35.5%) experienced conduit failure, and conduit dysfunction occurred in 27 (29%) of the patients. The most common reason for conduit failure was stenosis in 20 cases (60%). Histological examination showed inflammatory giant-type cells and poor autologous recellularisation in all explanted valves (Cicha et al., 2011, Perri et al., 2012).

### **1.8 *In vitro* Pre - Clinical Assessment of Functional Performance**

Decellularised heart valve roots have demonstrated promising results in both pre-clinical (Berry et al., 2017, Baraki et al., 2009, Syedain et al., 2015, Goecke et al., 2018) and clinical (da Costa et al., 2005, da Costa et al., 2014, Bechtel et al., 2008, Bibevski et al., 2017) trials, however their clinical approval is limited as many primary challenges remain. These include key scientific questions to enable the safe clinical translation and logistical, technical, and infrastructural challenges for the production and commercialisation of such decellularised heart valve roots. Although the studies

outlined above have indicated that decellularisation processes do not affect the *in vivo* short or mid-term performance of allogeneic heart valve roots; the longer-term outcome may differ depending upon the specific decellularisation process. Therefore it is important to understand the effects of specific decellularisation processes on the functional characteristics of allogeneic heart valves. The newly manufactured and modified surgical replacement heart valve roots should be performed in accordance to the appropriate international standards [e.g., ISO 13485 (2016): Medical Devices - Quality Management System - Requirements for Regulatory Purposes; ISO 10993-13 (2009): Biological Evaluation of Medical Devices, ISO 5840 (2015): Cardiovascular Implants - Cardiac Valve Prosthesis (part 1 and part 2)] and the product should be evaluated by an accredited notified body. These standards are helpful to achieve the quality and effectiveness of replacement heart valves for use in patients and worldwide commercialisation.

The United States Food and Drug Administration (FDA) classification of medical devices is based upon the level of control required to assure safety and effectiveness of a device (Zuckerman et al., 2011). Device classification in the European Union is similar to that of the United States FDA system. There are three regulatory classes for devices. Class I devices are defined as non-life sustaining. These products are the least complicated of the three classes, and their failure poses little risk to patients. Class II devices are more complicated than Class I devices, and present increased, but non-life sustaining, risk to users. Class III devices sustain or support life, hence their failure is life threatening. The majority of heart valve replacements (mechanical and bioprosthetic heart valves) are considered to be Class III medical devices. However, classification of a tissue engineered heart valve is complex. In particular, and importantly, medical devices containing living cells are usually classified by the FDA as biological or pharmaceutical products due to their pharmacological, immunological, or metabolic function upon implantation. The CryoValve SynerGraft® allograft heart valve roots are marketed as an unclassified medical device but in October 2014 the FDA recommendation is to reclassify them to a class III medical device and the requirements will not fully apply until 26<sup>th</sup> May 2020 for Medical Devices. Similar discrepancies also exist in the European classification for tissue engineered products. According to the medical device regulation (MDR) (Regulation, Chapter 1

2017/745), all non-living (i.e., decellularised and fixed) products, such as decellularised allograft or xenograft heart valve roots, will be categorised as medical devices from 26<sup>th</sup> May 2020.

Decellularised heart valve roots are expected to undergo remodelling and regeneration *in vivo*. For this reason, *in vitro* investigations alone are not sufficient to provide information about the clinical safety and efficacy of the device because of the modifications that will occur upon *in vivo* implantation. The remodelling potential of decellularised heart valve roots should be investigated in animal models for proof-of-concept, efficacy, and safety evaluation. In addition, *in vitro* investigations can be used to assess the individual components of decellularised heart valve roots such as scaffold degradation rate, cytotoxicity and biocompatibility by following ISO 10993-13 (2009) (Biological Evaluation of Medical Devices). Also the scaffold of the decellularised heart valve roots is an essential part and, therefore, its chemical and physical properties (e.g., porosity, stiffness, topography, hydrophilicity, and biodegradation) should be characterised according to ISO 10993-13 (2009).

Subsequently, the performance and efficacy of decellularised heart valve roots should be evaluated as per the international standard ISO 5840 (2015) to ensure that the decellularised heart valve roots will be able to function upon implantation. ISO 5840 (2015) includes investigations of material property (biomechanical performance), function (hydrodynamic performance), as well as structural performance assurance, device durability and component fatigue assessments. However, application of this standard to decellularised heart valve roots may be challenging, as indeed the ISO 5840 (2015) standard was designed to assess the performance of mechanical and biological heart valve prostheses and therefore the extrapolation to decellularised heart valve roots may be difficult, especially as the decellularised heart valve root leaflets have time dependent viscoelastic properties (Wilczek et al., 2018).

Various studies have evaluated the pre-clinical functional performance of mechanical and bioprosthetic heart valves through the assessment of mechanical (Luo, 2011, Sauren et al., 1983, Zhang et al., 2015, Stella et al., 2007), hydrodynamic (Nagy et al., 2000, Jennings et al., 2002, Yoganathan, 1989) and fatigue (Iwasaki et

al., 2002, Butterfield and Fisher, 2000) performance. The ability of *in vitro* performance assessment methods to predict structural failure in the clinical setting is still questionable. There are some mechanical heart valve prostheses which showed post-market failure such as thromboembolism (Medtronic Parallel) (Bodnar, 1996) or strut fracture (Björk-Shiley) (Harrison et al., 2013) or chronic inflammatory reaction due to a toxic reaction to the silver-coated sewing cuff (St. Jude Medical Silzone) (Tozzi et al., 2001) even though *in vitro* performance was assessed. Clinical failures have been reported for both mono leaflet mechanical valves (Omnicarbon, Björk–Shiley) (Kornberg et al., 1999, Ericsson et al., 1992) and bileaflet mechanical valves (Edward –Duromedics, TRI technologies) (Hemmer et al., 2000, Bottio et al., 2003). The most striking example is the Björk-Shiley convexo-concave valve, which was implanted in 86,000 patients between 1978 and 1986 before being withdrawn from the market because of outlet strut fracture and embolisation of the disc. With the valve in the aortic position, the result was massive aortic regurgitation and often death (>90% of cases) (Blot William et al., 2005).

In the past, this kind of post-market failure has also been observed in bioprosthetic heart valves. The first generation bovine pericardial valves (Ionescu-Shiley bovine pericardial valve and Hancock pericardial xenografts) were withdrawn from the market, because of poor clinical results and a high rate of deterioration characterized by leaflet tears and valve incompetence (Gallo et al., 1985, Bortolotti et al., 1991). The limited durability of the Ionescu-Shiley bovine pericardial valve was due to factors related to its design, that is, abrasion-related damage at the alignment suture (Schoen et al., 1987). Much of this insight came from clinical outcomes. It is possible that this failure could have been identified in pre-clinical *in vitro* or *in vivo* animal studies if such studies had been performed.

Clinical implantation of the first decellularised porcine heart valve roots [SynerGraft®; Cryolife Inc., Kennesaw, GA, USA] resulted in patient mortality. The SynerGraft® heart valve roots were implanted into 4 children; two were homograft (donor organ) replacements and two as part of a Ross operation (Simon et al., 2003). Despite normal function of the heart valve roots after surgery, 3 of the 4 children died due to valve failure (Simon et al., 2003). Two children died suddenly at 6 weeks and

1 year after implantation due to severely degenerated SynerGraft® heart valve roots. The third child died at day 7 due to a SynerGraft® heart valve rupture. The fourth heart valve root was explanted 2 days after implantation. Histological analysis of the SynerGraft® heart valve roots showed incomplete decellularisation of the valves and calcified deposits (Simon et al., 2003).

These post market catastrophic failures of mechanical, bioprosthetic and decellularised porcine heart valve roots illustrate the importance of assessing heart valve reliability, verifying safety requirements, and identifying weak points in the design before introducing heart valve products into clinical practice. This leads to the requirement for robust pre-clinical *in vitro* investigations of the products.

### **1.8.1 Biomechanical Performance**

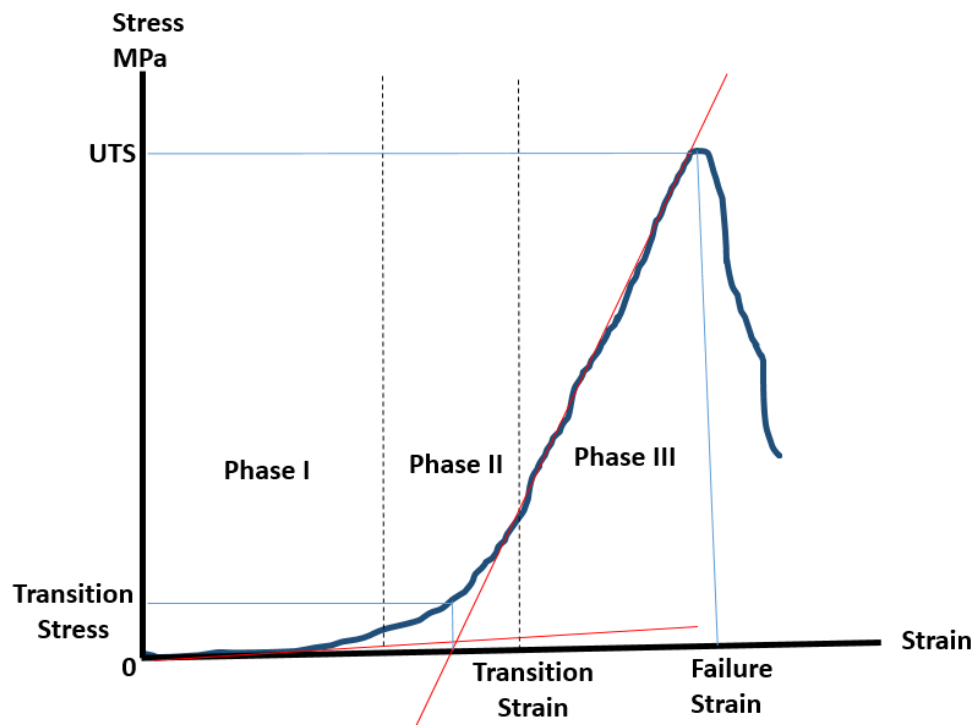
From a biomechanical perspective, replacement heart valve roots have to function under enormous dynamic *in vivo* loads immediately upon implantation in the patient. The *in vivo* loads are imposed cyclically on the heart valve leaflets as the valve opens (flexure), permits blood to pass (shear), closes (flexure), and prevents the reverse flow of blood (tension and compression). The dynamic movement (dilation) of the heart valve root wall enhances leaflet closure at the end of systole and protects leaflets from wall impact during systole (Hopkins, 2003). Therefore, successful development of these replacement heart valve roots will require that the whole heart valve root structure (wall and leaflets) exhibit and maintain mechanical properties similar to those of native heart valve roots (Hasan et al., 2014). Native heart valve tissue exhibits nonlinear and anisotropic behaviour under quasi-static and dynamic load due to its structure and specific morphology (Carew et al., 2000).

The material properties of the wall and leaflets of human aortic and pulmonary heart valve roots can be determined using quasi-static uniaxial or biaxial loading test methods. The material properties of human cellular heart valves have rarely been investigated in the literature due to the limited availability of fresh cellular human heart valves (Clark, 1973, Stradins et al., 2004), while a substantial number of studies have investigated the material properties of cellular xenogeneic heart valves (Anssari-Benam et al., 2011, Luo, 2011, Korossis et al., 2002, Sauren et al., 1983, Sacks, 2000, Hoerstrup et al., 2000). In addition, the ability to predict biomechanical



performance could be hampered by significant levels of biological variability present in human heart valve roots and quality of donor human heart valve roots.

Uniaxial tensile testing of the wall and leaflets of heart valve roots has proved a more common method to determine stress-strain characteristics and failure loads, due to it being relatively straightforward to perform. However, this information is not sufficient to fully understand heart valve tissue biomechanics, in that they rarely fail catastrophically. The main concern is that the leaflets must have adequate biomechanical properties to allow the leaflets to remain compliant and co-apted when closed during diastole, which are biaxial properties. Because of these considerations, the native leaflet response to diastolic pressure is often examined mechanically by biaxial tensile testing of the belly region of heart valve leaflets (Billiar and Sacks, 2000, Wells and Sacks, 2002). During biaxial tensile testing, the applied load and amount of strain in each direction (axial and circumferential) can be controlled, similar to the experience of the leaflets *in vivo*. However, there are several limitations with biaxial tensile testing including the difficulty in clamping the tissue specimen without damaging it, and the stress calculation requires the assumption of homogeneity whereas heart valve tissues are heterogeneous (Sacks and Sun, 2003).



**Figure 1.7 Typical Stress-Strain Behaviour Curve for Heart Valve Tissue**

The typical shape of the stress-strain behaviour curve of heart valve tissue (wall and leaflet) is shown in Figure 1.7 (Sauren et al., 1983). During the initial phase (Phase I, Figure 1.7), the bundle of collagen fibers are rearranged in the principal direction of loading and the elastin fibers are a significant determinant of the initial tissue stiffness. During the transitional phase (Phase II, Figure 1.7), the stiffness begins to rise rapidly, as the fiber recruitment concludes the high stiffness collagen bundles begin to bear load. At the end of the final phase (Phase III, Figure 1.7), the collagen network begins to slip and rupture, the slope of the stress curve falls until complete failure is observed (Natali et al., 2008).

There have been many reports of the tensile testing of heart valve tissue to determine mechanical properties, although there are many inconsistencies between methods. Several studies (Korossis et al., 2002, Fitzpatrick et al., 2010, David et al., 1994) have preconditioned heart valve tissue during uniaxial tensile testing when determining the material parameters (collagen and elastin phase stiffness, ultimate tensile stress and strain) as it is believed that this generates a consistent stress-stress response. Preconditioning typically involves the repeated loading and unloading cycles for a certain number of times prior to actual tests, to overcome history dependency of soft tissues (Quinn and Winkelstein, 2011). However, the exact mechanisms of preconditioning are unknown and it is the least studied area (Sacks, 2000). Carew et al. (2000) tested porcine aortic leaflets and suggested that preconditioning must be accompanied by an adequate period of viscoelastic material recovery in order to fully reset strain history as preconditioning without an adequate rest period may actually increase the complexity of the strain history and may be worse than a rest period without any preconditioning. However, no study has directly quantified the reorganisation of collagen fibers in heart valve tissue following preconditioning and assessed its correlation with any altered mechanical response of the tissue. Martin and Sun (2012) investigated biomechanical properties of human aortic heart valve leaflets and reported reduced hysteresis and a stable mechanical response after a 60 second rest period between two preconditioning cycles. In summary, while some studies explained that preconditioning is necessary, protocols for the determination of the mechanical properties of heart valve tissue have not yet been standardised.

In addition to preconditioning, it is also important to consider the strain rate while determining material properties of heart valve tissue using tensile testing. During tensile testing of heart valve leaflets, the majority of studies have used relatively slower strain rates [0.6 mm.min<sup>-1</sup> (Sokolis et al., 2002), 1 mm.min<sup>-1</sup> (Casado et al., 2012), 10 mm.min<sup>-1</sup> (Lee et al., 1984, Luo et al., 2014, Duprey et al., 2010, Seebacher et al., 2008), 300 mm.min<sup>-1</sup>(Tseng et al., 2013)] than physiological strain rates [1800 mm.min<sup>-1</sup> to 2400 mm.min<sup>-1</sup> (Duncan et al., 1997, Leeson-Dietrich et al., 1995)] often due to the constraints of tensile testing equipment. Additionally, Lendon et al. (1993) indicated that slow strain rate helped to capture the full characteristics of the material behaviour and it allows time for the biological tissue constituents to adapt, realign and fill spaces between the tissue structural components, therefore reducing the force at a given extension. However, it has been reported that stress-strain characteristics of heart valve leaflets are insensitive to strain rates (Sauren et al., 1983).

There are other factors such as, the clamping of heart valve tissue specimens and the test specimen geometry that may contribute to the variation in material properties of the heart valve tissue specimens, observed by different laboratories. Studies have used mainly either dog bone shaped (Helder et al., 2016, Garcia-Herrera et al., 2012, Seebacher et al., 2008) or rectangular shaped wall specimens (Sauren et al., 1983, Mavrilas and Missirlis, 1991, Luo et al., 2014, Korossis et al., 2002, Patwardhan and Vaideeswar, 2004, Kalejs et al., 2009). Dog bone shaped samples have been avoided for heart valve leaflet specimens as the tissue tends to distort under the cutting blade pressure of the punch, making it difficult to cut precise curves. The reason for using a dog bone shaped heart valve wall tissue specimen is to ensure that the highest stress concentrations do not build up at the grip ends. Whereas rectangular-shaped specimens are easier to cut from both wall and leaflet of the heart valve root and permit the calculation of the strain from the grip-to-grip displacement (gauge length), which is not possible using the dog-bone shaped specimen.

There are further reasons for treating the results of uniaxial tensile testing with caution, as there are several practical challenges such as specimen clamping and

gauge length measurement. Many efforts have been made to prevent grip-specimen slippage during testing, namely the use of specially designed hydraulic or pneumatic clamps (Elenes and Hunter, 2014), serrated jaws (Jennings et al., 2001), sandpaper (Warnock et al., 2010, Sokolis et al., 2002), tissue paper (Seebacher et al., 2008), etc. Also, it is very important to measure the cross-sectional area as accurately as possible, because the calculation of stress relies on it. Particularly with a soft biological tensile specimen, it is more difficult to determine thickness due to the compressive nature of specimen tissue (Lee and Langdon, 1996). Also heart valve leaflet thicknesses are non-uniform due to collagen fiber distributions and orientations (Clark and Finke, 1974, Li et al., 2001). Hence different studies (Vesely, 1998, Seebacher et al., 2008, Sacks and Yoganathan, 2007) have used “tension”, that is, force per unit width of tissue specimen and have expressed the results purely in terms of load to overcome the problem of measuring the thickness.

A final point to consider is the environmental conditions during tensile testing. In some studies specimens have been immersed in saline at 37 °C (Lee et al., 1984, David et al., 1994) whilst Sauren et al. (1983) dripped saline onto specimens to keep them hydrated to prevent mechanical artefacts due to tissue drying.

To add further insight to heart valve tissue material properties, flexural assessment of heart valve leaflets has been used in many studies (Vesely and Boughner, 1989, Mirnajafi et al., 2006, Thubrikar et al., 1982, Narine et al., 2006), particularly when subjected to different modes of deformation (bending and creep) that are not included in uniaxial and biaxial extension. Various methods have been used to derive flexure properties of heart valve leaflets such as three-point bending (Engelmayr et al., 2005, Williams et al., 2009), macro-indentation test (Narine et al., 2006) and cantilever bending (Mirnajafi et al., 2006). In the flexural macro-indentation test method, the excised valve tissue is clamped over a round opening and indented with a ball probe, resulting in a load versus depth of indentation curve (Narine et al., 2006). Whereas, a three-point bending test measures the flexural response of the entire leaflet, as opposed to cut-out strips from the leaflet, whose behaviour is dependent on the direction in which they are cut. Although the entire valve leaflets were used in the three point bending flexure test method, the flexural

behaviour of the belly region was evaluated, as the commissural region remained inside the clamped part (Engelmayr et al., 2005). Furthermore, flexural testing allows the determination of the effect of compressive forces on heart valve leaflets in a bending configuration. The compressive flexure stresses are believed to impact the degradation of bioprosthetic heart valve tissues (Thubrikar et al., 1982, Vesely and Boughner, 1989). The flexural deformation mode not only represents a major deformation mode of heart valve leaflets, but also allows direct examination of individual layer responses in tension and compression. Mirnajafi et al. (2006) used the flexural method to derive the layer specific mechanical properties of heart valve tissue in the low stress-strain region.

There is an alternative to testing excised tissue of simple geometry to derive the biomechanical response of the heart valve root wall under more physiological conditions, which is to test whole heart valve roots. For aortic and pulmonary heart valve roots, the circumferential expansion (dilation) can be measured with respect to different internal static pressures (Jennings et al., 2001, Nagy et al., 2000). The function of the replacement heart valve root leaflets is dependent on the dilation of the heart valve root and when the dilation was reduced to non-physiological levels, open leaflet bending strains were higher (Butterfield et al., 1991, Lockie et al., 1993).

In open heart valve surgery, replacement heart valves are typically sutured to the annulus which is left in situ when the native valve is removed; suture line breakdown can lead to paravalvular leakage or separation of the replacement heart valve from the annulus (valve dehiscence). Risk factors for replacement heart valve dehiscence include bacterial endocarditis, aneurysm of the ascending aorta, degenerative regurgitation, and severe calcification of the valve (Rizzoli et al., 1984). In order to determine whether the sutures and replacement heart valve tissue are strong enough to withstand *in vivo* load, studies (Pierce et al., 2016, Walraevens et al., 2008, Choe et al., 2018, McGregor et al., 2016) have reported upon *in vitro* suture pull out tests. These investigations were aimed at quantifying the suture retention strength, often referred to as anastomotic strength, which is “the force necessary to pull a suture from the replacement heart valve”. The test methods usually involve

pulling a suture loop until the suture pulled through the heart valve specimen (wall and/or myocardium) using a uniaxial tensile tester (Walraevens et al., 2008).

The chemical treatments used to treat animal and human heart valve tissue for producing bioprosthetic and decellularised heart valves have been shown to affect the biomechanical and viscoelastic properties of the tissue. Generally, viscoelasticity is manifested by a number of different features, including hysteresis, preconditioning, stress relaxation and creep. Glutaraldehyde fixation of bioprosthetic heart valves reduces the immune response and prevents leaflet degradation but can induce ECM cross-links and other structural changes (Vesely and Noseworthy, 1992, Golomb et al., 1987) that reduce radial stiffness and increase extensibility as well as reduce creep and stress relaxation (Lee et al., 1984, Vesely et al., 1995, Rousseau et al., 1983). The effects of decellularisation treatment on viscoelasticity have been reported in some studies (Jiao et al., 2011, Spina et al., 2003). Spina et al. (2003) reported no change in relaxation behaviour of porcine aortic valve leaflets following decellularisation using Triton X-100. Jiao et al. (2011) also reported no change in ovine pulmonary and aortic leaflet viscoelasticity under torsional loading following decellularisation using Triton X-100. Conversely, the decellularisation treatment using Triton X-100 resulted in significant changes to the stress relaxation behaviour of pulmonary heart valve leaflets, but, the creep behaviour remained unchanged (Converse et al., 2012). The difference seen in these studies (Quinn et al., 2012, Spina et al., 2003, Jiao et al., 2011) may be due to the use of different types of heart valve leaflets.

Several reports of the effects of decellularisation on the quasi-static material properties of heart valve tissues are available in the literature (Korossis et al., 2002, Seebacher et al., 2008, Liao et al., 2008, Tudorache et al., 2007). Korossis et al. (2002) and Luo et al. (2014) found no difference in the ultimate tensile strength of porcine aortic and pulmonary heart valve root leaflets respectively following 0.1% (w/v) SDS decellularisation treatment. However, Korossis et al. (2002) did report a significant decrease in elastin phase stiffness of porcine aortic leaflets following 0.1% (w/v) SDS decellularisation treatment. Seebacher et al. (2008) reported no change in the tensile strength and failure strain of porcine pulmonary heart valve roots in uniaxial tension

following detergent based decellularisation, though stiffness values were not reported. Liao et al. (2008) investigated the effects of multiple decellularisation protocols [SDS, trypsin, and a Triton X-100] on the biomechanical performance of porcine aortic valve leaflets and reported decreased flexural stiffness regardless of the decellularisation protocol used. Another study by Tudorache et al. (2007) *et al.* evaluated the effect of multiple decellularisation protocols [1% SDC, 1% SDS, or 0.05% trypsin/0.02% EDTA] under uniaxial loading conditions and found a decrease in tensile strength and stiffness in the elastin phase region for decellularised (1% SD, 1% SDS) pulmonary heart valve root wall axial specimens with the exception of trypsin/0.02% EDTA decellularised porcine pulmonary heart valve root wall specimens. However, the detergent/enzymatic decellularised ovine pulmonary heart valve root wall specimens Quinn et al. (2012) showed increased stiffness in the elastin phase region under biaxial loading conditions (Buse et al., 2016). The changes in material properties may have been due to different decellularisation protocols and heart valve root species.

Only one study (Elkins et al., 2001) investigated and compared biomechanical properties of cellular and decellularised human pulmonary heart valve roots to determine the effect of decellularisation. In this study, the heart valve roots were tested mechanically using uniaxial tensile (wall and leaflets) and suture retention (wall and myocardium) test protocols. No differences in biomechanical properties were detected between the cellular and decellularised human pulmonary heart valve roots.

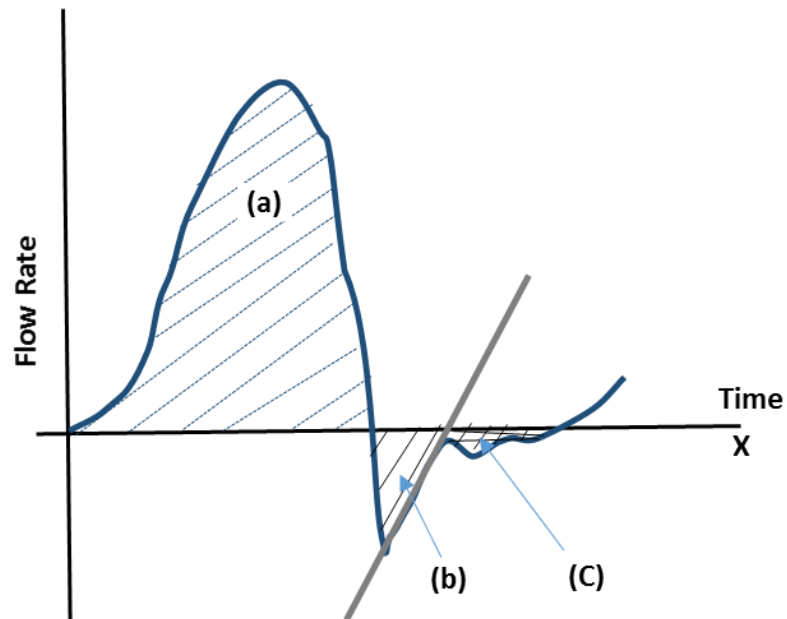
### **1.8.2 Hydrodynamic Performance**

The evaluation of the functional performance of heart valve replacements under pulsatile flow is a useful indicator of predicted clinical performance. The hydrodynamic performance of replacement heart valves can be assessed in terms of transvalvular pressure difference and forward flow performance, expressed as valve effective orifice area (EOA), and regurgitant volumes. Various designs of pulsatile flow simulators (or duplicators) have been used to gain information on the functional performance of replacement heart valves under physiological pulsatile flow conditions by many different laboratories (Jennings et al., 2001, Walker and

Yoganathan, 1992, Heiliger et al., 1987, Fisher et al., 1986). Commercial pulse duplicators include the Vivitro pulse duplicator (ViVitro Labs Inc., Victoria, BC), Dynatek Dalta MP3<sup>®</sup> (Dynatek Dalta<sup>®</sup>, Galena, MO, USA) hydrodynamic pulse duplicator and BDC Heart valve pulse duplicator system (Model: HDT-500 and HDTi-500; BDC laboratories, USA). All these pulse duplicator systems are designed with current prosthetic heart valve designs in mind. The pulsatile flow duplicator simulates and recreates the pressure and flow conditions that exist in the left or right side of the heart. The majority of pulse duplicator systems consist of aortic and mitral sections containing the valve under test, a compliance chamber, peripheral resistance and atrial reservoir, pulsatile pump and data collection instrumentation. These systems allow measurements of pressure and flow to assess hydrodynamic performance of the heart valve root under pulsatile flow in terms of the following key parameters:

- Mean transvalvular pressure difference ( $\Delta P$ ): the average value of the pressure difference (ventricle pressure – aortic pressure) across a valve during systolic ejection. This is a flow dependent quantity and is dependent on the internal diameter and orifice size.
- Effective orifice area (EOA): relates to pressure gradient and volumetric flow rate for an estimation of heart valve efficiency (Gorlin and Gorlin, 1951).  
EOA is also a standard measure of clinical assessment, measured using Doppler echocardiography to investigate the effectiveness of heart valve opening during the forward flow phase (Dasi et al., 2009).
- Regurgitation volume: the sum of the closing volume and the leakage (closed) volume. The closing volume is the volume of fluid flowing retrograde through the valve during closure. Any fluid accumulation after valve closure results from leakage and is referred to as the leakage volume (Figure 1.8).





**Figure 1.8 Representative Flow Waveform for Cardiac Cycle where (a) Forward Flow Volume (b) Closing Volume and (c) Leakage Volume (ISO 5840, 2015)**

The resistance to blood flow has a significant effect on the circulatory system. The body has the ability to change the resistance to flow by contracting or dilating the arteries. To adjust this resistance in the pulse duplicator system, a simple restrictor clamp has been used in many previous studies (Jennings et al., 2001, Korossis et al., 2002, Schichl and Affeld, 1993). Donovan (1975) used a bellows operated valve with a metal plate which rotated about a pivot to change the cross sectional area of the flow tube. This technique was useful for achieving lower resistance, especially for the testing of pulmonary heart valves. The method used by Liu et al. (2005) used a porous material which had appropriate permeability to represent compliance and peripheral resistance. The resistance value was achieved by moving a slide plate over porous material to block and unblock some of the pores.

One of the key factors to making the pulsatile flow simulator representative of the physiological system is to have variable arterial compliance so that the pressure and flow waveforms adequately simulate that of the human body. The most common design for producing compliance in the pulse duplicator system is to simply have a cylindrical chamber downstream filled with circulating test fluid and air (Jennings et al., 2001, Donovan, 1975, Korossis et al., 2002, Fisher et al., 1986). The compliance chamber and variable resistance in the pulsatile flow simulator reproduced the elastic characteristic of the heart valve root. Also, the type of test fluid to be used during

testing can be quite important, particularly when evaluating materials such as polyester and polyurethanes whose viscoelastic properties are affected by blood (Campo-Deaño et al., 2013). Bazan and Ortiz (2016) used a glycerol-water mixture with 47.6% by volume of glycerin solution in water (with normal saline solution to allow the electromagnetic flowmeter operation) to validate the pulsatile flow simulator design with a bileaflet mechanical valve. However, the disadvantage of using glycerol in the pulsatile flow simulator makes the system difficult to clean due to its viscous nature. Hence most studies (Rahmani et al., 2017, Jennings et al., 2001, Luo, 2011) have used saline to test replacement heart valves in the pulsatile flow simulator.

In addition to pulsatile flow studies, limited studies (Leo et al., 2006, Loger et al., 2014, Jennings, 2001) have used a static leakage flow test to assess valve competency in terms of leakage flow rate of the closed valve under static back pressure. The test set up consisted of a vertical column of test fluid which was able to apply back pressure on the heart valves (Loger et al., 2014, Jennings, 2001). Loger et al. (2014) and Leo et al. (2006) measured competency of a transcatheter mechanical heart valve with Nitinol leaflets and bileaflet mechanical heart valves (St. Jude Medical Inc) respectively. Whereas Jennings (2001) used static leakage flow test method to measure competency of cellular and glutaraldehyde fixed porcine aortic and pulmonary heart valve roots. The static leakage flow test did not give quantitative values regarding overall valve performance.

The hydrodynamic performance of decellularised xenogenic heart valve roots has been reported in some studies (Bottio et al., 2010, Dohmen et al., 2002, Luo et al., 2014), however, only one study (Elkins et al., 2001) investigated hydrodynamic performance of decellularised (CryoValve SG) human heart valve roots. Elkins et al. (2001) showed no difference in hydrodynamic performance between cellular and decellularised human pulmonary heart valve roots.

Dohmen et al. (2002) investigated the *in vitro* hydrodynamic performance of decellularised porcine pulmonary heart valves in the pulsatile flow simulator and compared it with glutaraldehyde fixed xenogenic and polyurethane heart valves. The decellularised pulmonary porcine heart valves showed the same performance as

polyurethane heart valves, which were superior to the glutaraldehyde fixed xenograft. Bottio et al. (2010) investigated the *in vitro* hydrodynamic performance of porcine aortic heart valve roots, before and after decellularisation with sodium cholate (TRI-COL), SDC, 0.03% SDS, and 0.1% SDS. The results showed that except for 0.03% SDS, the other three decellularisation protocols modified the hydrodynamic performance of porcine aortic heart valve roots. SDC and TRI-COL-treated porcine aortic heart valve roots exhibited decreased transvalvular pressure difference and an increased EOA. However, compared to SDC and TRI-COL, the SDS decellularisation treatments showed contrasting results. The decellularised porcine aortic heart valve roots treated with 0.1% SDS resulted in a significantly increased transvalvular gradient and a reduced EOA. However, Luo et al. (2014) reported that hydrodynamic performance and leaflet kinematics of the 0.1% (w/v) SDS decellularised porcine pulmonary heart roots were similar to cellular porcine pulmonary heart valve roots. No significant difference was observed for either EOA or leaflet dynamics between the decellularised and cellular porcine pulmonary heart valve roots.

### **1.8.3 Fatigue/Durability Performance**

During the cardiac cycle, native heart valve roots are subjected to relatively high mechanical stresses (Dasi et al., 2009, Sacks et al., 2009). For this reason, any heart valve replacement must be capable of resisting these stresses to prevent structural fatigue and failure.

The FDA (2010) and ISO 5840 (2015) standards prescribe guidelines for accelerated fatigue test methods applied to mechanical and bioprosthetic heart valves. These standards require that a targeted minimum peak transvalvular pressure must be established across the closed test heart valves for at least 5% of each cycle, and this should be maintained for 95 % or more of all test cycles. The ISO 5840 (2015) [clause 7.2.4.2 Device durability assessment; ISO 5840:2-Part 2] standard requires that mechanical heart valves must be tested for at least 400 million cycles (equivalent to 15 years *in vivo*), and due to short term clinical expectations, bioprosthetic heart valves must be tested at least for 200 million cycles (equivalent to 5 years *in vivo*) in pulsatile flow prior to clinical application. In addition to accelerated fatigue assessment, real time wear assessment under physiologic conditions (e.g. heart rates

<200 bpm), to cycle counts less than 200 million cycles is recommended for replacement heart valves which have components manufactured from viscoelastic materials. However, the ISO 5840 (2015) standard does not define the test equipment, test conditions or test method for real time wear assessment.

In order to predict structural fatigue, equivalent to its expectancy *in vivo*, it is not practical to perform *in vitro* fatigue tests for the same period of time. To reduce the *in vitro* testing time period, accelerated fatigue testing of replacement heart valves has been performed in numerous studies (Iwasaki et al., 2002, Butterfield and Fisher, 2000, Vesely, 1995, Bezuidenhout et al., 2015, Arokiaraj et al., 2016, Raghav et al., 2016). The assessment of durability by accelerated cycling has been widely accepted as a major component in the development stage of heart valve replacements. The typical duration of accelerated fatigue testing for an equivalent of 10 years *in vivo* is approximately 8 months at 15 Hz which is fifteen times faster than the normal heart rate producing dynamic loads different to those physiologically experienced. However, in the case of decellularised heart valve roots, the optimal protocol for predicting fatigue failure has yet to be established. Biologically derived products are not generally tested in an accelerated rate because the differences in physiological and accelerated rate environments influence the durability of the biological or decellularised heart valve roots due to viscoelastic properties of the heart valve tissue.

The viscoelastic behaviour of heart valve root leaflets, as determined by the strain rate sensitivity of the stress-strain curve or stress relaxation (Tseng et al., 2013), requires attention when accelerated fatigue testing is being considered. Broom (1977) and Stella et al. (2007) showed the stress-strain behaviour of such tissue to be insensitive to different non physiological and physiological strain rates. On the other hand, Vesely et al. (1995) has shown such tissue to be sensitive to strain rates. However, the strain rates investigated by Vesely et al. (1995) were lower than physiological strain rates. Vesely et al. (1995) further explained that due to the viscoelasticity of porcine heart valve leaflets, during durability testing in the accelerated fatigue tester, the heart valve leaflets may not have enough time to relax with reduced stress-relaxation, resulting in a higher preload for each subsequent

cycle. Accelerated fatigue testing would then under-estimate the valve durability. On the contrary, Vesely et al. (1995) explained that valve durability may be overestimated due to insufficient leaflet tissue relaxation between two consecutive cycles, since the valve would be under lower cyclic stresses than *in vivo*. When the viscoelastic material is exposed to cyclic loading, during each loading cycle the material undergoes a combination of the creep and relaxation process. At accelerated cyclic conditions the retardation process between two loading cycles cannot be fully completed. Consequently, strain starts to accumulate, which leads to hardening of the material and ultimately to failure of the material. The rate of this strain accumulation is dependent on the applied peak pressure and the period of time for which peak pressure is applied on the closed valve. This process has a greater effect on more compliant tissue, which has been demonstrated by the work of Butterfield and Fisher (2000) who investigated the fatigue of photo oxidised bovine pericardial heart valves (Butterfield and Fisher, 2000). This study showed that *in vitro* accelerated fatigue testing failed to replicate the *in vivo* failure of photo oxidised bovine pericardial heart valve, as the accelerated fatigue test did not replicate *in vivo* pressure and time per cycle. D'Souza et al. (2003) further explained that the leaflet kinematics, bending strains in the leaflet belly, the strain time integral and proportion of time that the valve fully closed or open were dependent on cycle rate. Iwasaki et al. (2002) tested a polymer valve (Jellyfish valve), in attempting to identify an ideal method to predict heart valve prosthesis durability and identified that the valve was less durable in accelerated fatigue testing than *in vivo*. The study also identified that there might be variation in dynamic pressures experienced by the heart valve leaflets between various designs of accelerated fatigue testers and that these factors may influence valve fatigue.

Frame mounted glutaraldehyde fixed pericardial and porcine xenograft bioprosthetic heart valves which failed mechanically in an accelerated fatigue tester have been shown to fail *in vivo* as well (Gabbay et al., 1984, Schuster and Wagner, 1989, Wheatley et al., 1987, Fisher, 1986, Ishihara et al., 1981). Mechanical degeneration was responsible for a large percentage of bioprosthetic heart valve failures. Bioprosthetic heart valve leaflets experience high transient stresses during valve closure, and cyclic flexural and compressive stresses during valve opening. It

was believed that tensile stresses induced during valve closure were responsible for leaflet tearing; studies have shown that tissue rupture is related to flexure fatigue (Ishihara et al., 1981, Vesely et al., 1988, Vesely et al., 2001) and the compressive stresses on the inner surface of the leaflets (Krucinski et al., 1993). In addition, Thubrikar et al. (1983) reported that the cyclic compressive stressing of the valve leaflets disrupted the collagen architecture. Studies (Christie, 1992, Wells and Sacks, 2002) indicated that accelerated fatigue testing underestimates the effects of long-term cycling on biomechanical performance of zero pressure-fixed bioprosthetic valves. Hence, studies (Sacks and Smith, 1998, Wells and Sacks, 2002) have determined the effects of *in vitro* accelerated cyclic loading on bioprosthetic valves by subsequent use of biaxial testing to quantify the changes in collagen fiber architecture.

Studies (Syedain et al., 2013, Costa et al., 2005, Lim et al., 2015) reported *in vitro* real time fatigue assessment of frame mounted tissue engineered heart valves under cyclic physiological test conditions. Syedain et al. (2013) and Lim et al. (2015) used custom made pulsatile flow simulators which were able to test one sample at a time, whereas Costa et al. (2005) tested four pericardial bioprostheses (three decellularised and one glutaraldehyde fixed) using a Shelhigh FTS 300 accelerated fatigue tester (Shelhigh Inc., Springfield, NJ, USA). Costa et al. (2005) fatigue tested three 0.3% EDTA decellularised pericardial bioprostheses and one glutaraldehyde bovine pericardial bioprostheses (control) at mean heart rate 80 bpm for 150 million cycles. The test was interrupted at every  $50 \times 10^6$  cycles to assess the hydrodynamic performance and showed that the decellularised bovine pericardial bioprostheses had similar hydrodynamic performance to the glutaraldehyde bovine pericardial bioprosthesis. However, fatigue of decellularised porcine pericardial bioprostheses was compared with only one control valve which limits critical analysis of this study. Syedain et al. (2013) performed a short term (maximum 2 million cycle) fatigue test at 120 bpm on two tissue engineered tubular heart valves under pulmonary heart conditions (average 8 mmHg end of diastolic pressure drop). To prevent bacterial contamination during testing antibiotics (penicillin and streptomycin) were added to the test fluid (PBS). The tissue engineered heart valves were made by moulding fibrin gel with fibroblasts into a tubular shape, culturing the tube within a bioreactor for 5

weeks, decellularising with 1 % SDS and then mounting on PEEK frame. No macroscopic tissue damage was observed in the end of test visual examination. However, there was evidence of leaflet thinning after 2 million cycles. Lim et al. (2015) tested frame mounted Triton X-100 decellularised and immunologically modified with  $\alpha$ -galactosidase porcine aortic heart valves with pulsatile pressure of 120/80 mmHg and heart rate of 60 bpm for 8 million cycles and no macroscopic leaflet failure was observed.

The fatigue test methods used in these studies (Syedain et al., 2013, Costa et al., 2005, Lim et al., 2015) were not suitable for decellularised heart valve roots as the studies investigated fatigue of frame mounted heart valves and hence elastic effects of the aorta were not included. More commonly, the fatigue of decellularised heart valve roots has been investigated in the *in vivo* juvenile sheep model (Dohmen et al., 2003, Quinn et al., 2011, Baraki et al., 2009, Goecke et al., 2018, Berry et al., 2017). Animal models are essential in the development of heart valve replacement to derive the effects (calcification, cytotoxicity, and biocompatibility) of the host environment, however, they are expensive and do not always represent the wide variation of size and morphology seen in the human population. In addition, sheep have normal blood pressure, but the majority of human patients suffering from heart valve disease have high blood pressure.

The clinical use of decellularised heart valve roots is increasing. Due to the lack of an *in vitro* real time fatigue method and corresponding lack of *in vitro* real time fatigue data for decellularised heart valve roots, there is an unmet need to develop a predictive *in vitro* real time cyclic fatigue method for decellularised heart valve roots. The decellularised heart valve root wall and leaflets are integral components and when implanted *in vivo*, both experience cyclic loading. Therefore it is appropriate to include wall dynamics in addition to leaflet dynamics for fatigue assessment. It is also important during the assessment to control transvalvular pressure across the closed valve to achieve radial expansion of the leaflets and dilation pressure within the heart valve root to maintain physiological function of the heart valve root (Lockie et al., 1993).

## 1.9 Project Rationale

Heart valve disease is a major health burden, treated by either valve repair or valve replacement, depending on the affected valve. Approximately, 290,000 heart valve replacements are performed worldwide and this number is expected to triple by the year 2050 (Cheung et al., 2015). Furthermore, an average of 10 out of every 1000 children are born with congenital cardiac defects (Hoffman, 2013) and every fifth of these needs a heart valve replacement (Yankah et al., 2010). Despite the life-saving benefits of available replacement heart valves, including mechanical prostheses, bioprosthetic valves, autografts (Ross Procedure) and allografts they have several disadvantages, such as calcification, the need for anticoagulation therapies, lack of any remodelling and regenerative capacity and inability to grow. Therefore, the quest for a better heart valve replacement goes on, particularly for young patients.

A review of the literature indicates that in the surgical treatment of heart valve disease, decellularised allograft and xenograft heart valve roots have the potential to offer good hemodynamic, and low thrombogenicity characteristics, with the potential for regeneration, remodelling and capacity to grow with the patient (Sarikouch et al., 2016, Cebotari et al., 2011, Tudorache et al., 2016, Lichtenberg et al., 2006, da Costa et al., 2010).

The production and pre-clinical assessment of the prosthetic heart valves (mechanical and bioprosthetic) must conform to international standards [e.g., ISO 13485 (2016): Medical Devices - Quality Management System - Requirements for Regulatory Purposes; ISO 10993-13 (2009): Biological Evaluation of Medical Devices, ISO 5840 (2015): Cardiovascular Implants - Cardiac Valve Prosthesis Part 1 and Part 2], evaluating *in vitro* mechanical and biological performance. The ISO 5840 (2015) standard was developed on the basis of existing mechanical and bioprosthetic heart valves and is not entirely appropriate to investigate the *in vitro* performance of decellularised heart valve roots, more specifically *in vitro* fatigue of decellularised heart valve roots. The literature review critically reviewed the test methods used to evaluate biomechanical, hydrodynamic and fatigue performance of native and replacement heart valves. The uniaxial tensile testing of biological heart valve roots



was criticised due to the technical challenges involved in clamping the specimens and cross sectional area measurement; and the hydrodynamic pulsatile performance assessment method due to heart valve root mounting in the pulsatile flow simulator. In addition, it was identified that there was no ideal physiological test method or test equipment which can be used to assess fatigue or durability of biological heart valve roots (including decellularised heart valve roots) which have viscoelastic properties. A lack of repeatable, robust and physiological *in vitro* biomechanical and hydrodynamic performance assessment test methods for biological heart valve roots, in addition to a lack of *in vitro* real time fatigue assessment test method for biological heart valve roots (including decellularised heart valve roots), has been identified as a target for study.

In addition, decellularised allograft heart valve roots (Sarikouch et al., 2016, Cebotari et al., 2011, Tudorache et al., 2016, Lichtenberg et al., 2006, da Costa et al., 2010) and decellularised xenogenic heart valve roots (Berry et al., 2017, Goecke et al., 2018) have shown promising results clinically and pre-clinically respectively; even though the decellularisation protocols are different. It is therefore essential to understand the effects of specific decellularisation processes on the *in vitro* fatigue in addition to hydrodynamic and biomechanical performance of allogeneic or xenogeneic heart valve roots. However, only a few studies have evaluated *in vitro* functional performance of decellularised allograft and xenogenic heart valve roots.

The University of Leeds have developed a decellularisation protocol using low concentration SDS and applied it to human and porcine aortic and pulmonary heart valve roots (Korossis et al., 2002, Vafaei et al., 2016, 2014). The decellularised human aortic and pulmonary heart valve roots were developed with a view to use clinically as heart valve replacements through a partnership with NHS BT TES, Speke, Liverpool. The decellularised human heart valve roots suffer from limitations of availability in sizes suitable for young patients. To address this problem, decellularised porcine pulmonary heart valve roots in a range of sizes were investigated and the biological, biomechanical and hydrodynamic performance of these heart valve roots has been evaluated (Luo, 2011). Subsequently, an *in vivo* proof of concept study of decellularised porcine pulmonary heart valve roots was conducted in collaboration

with Professor Francisco Da Costa, Pontificia Universidade Catolica do Parana, Curitiba, Brazil (Berry et al., 2017). The decellularised porcine heart valve roots were implanted in the orthotopic position (RVOT) of 3 months old juvenile sheep.

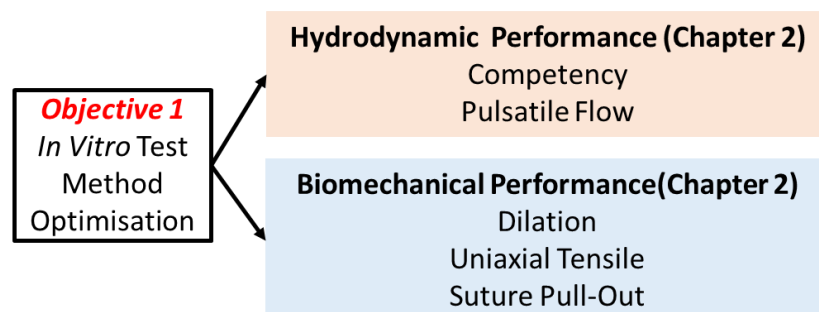
Before translating these decellularised human and porcine heart valve roots into clinical use it is important to understand the effects of decellularisation processes on the functional performance of the heart valves. Therefore, prior to *in vivo* clinical trials of the low concentration SDS decellularised human and porcine aortic and pulmonary heart valve roots, the effect of decellularisation on fatigue in addition to hydrodynamic and biomechanical performance will be investigated in this research.

### 1.10 Aims and Objectives

The primary aim of this research was to optimise *in vitro* hydrodynamic and biomechanical performance test methods and develop a novel real time fatigue test method using a real time wear tester (RWT) for biological heart valve roots. The secondary aim was to apply the developed *in vitro* test methods to decellularised human and porcine (aortic and pulmonary) heart valve roots to evaluate their *in vitro* functional performance and compare with cellular human and porcine heart valve roots.

The objectives for this research were as follows:

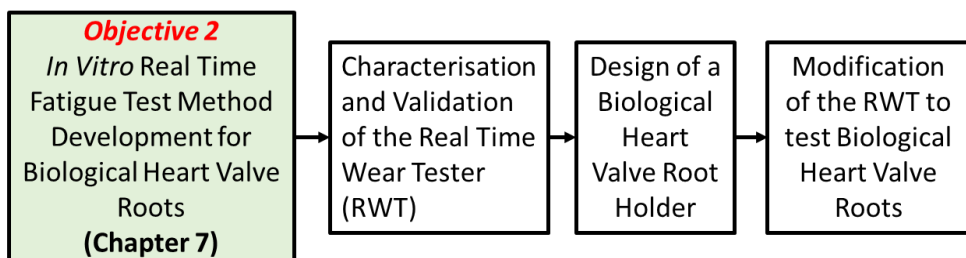
1. Optimise existing *in vitro* test methods to determine hydrodynamic and biomechanical performance of biological heart valve roots (Figure 1.9).



**Figure 1.9 Outline of Objective 1**

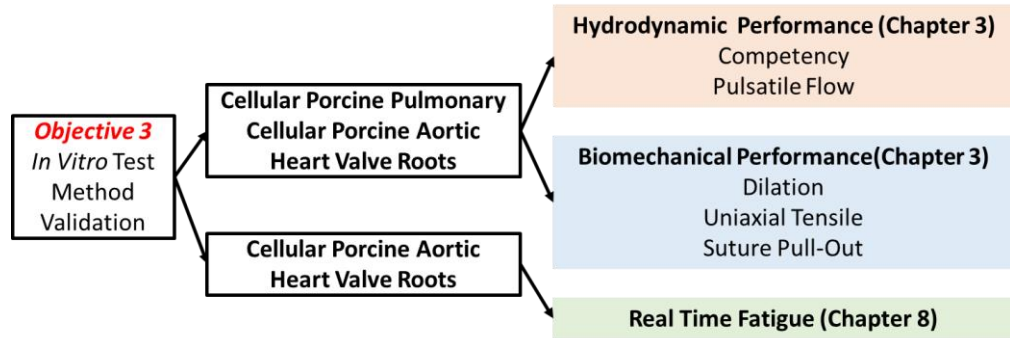
Key novel improvements to the test methods will be performed to optimise repeatability and robust *in vitro* functional performance assessment of biological heart valve roots.

- Competency test method: modification of static leakage rig will enable measurements of the leakage flow rate of a closed valve (aortic and pulmonary)
  - Pulsatile flow test method: optimisation of pulsatile flow simulator by replacing the existing instrumentation with the latest available instrumentation, the mounting technique of cellular and decellularised human heart valve roots in the pulsatile flow simulator and leakage free pulsatile flow simulation during functional performance assessment
  - Uniaxial tensile test method: a novel clamping technique of the heart valve root specimens (wall and leaflets) and cross sectional area measurement of the heart valve root specimens
  - Dilation test method: development of cylindrical Perspex tubes to accommodate different sizes of heart valve roots enabling the measurement of wall circumferential compliance
2. Develop a novel robust repeatable *in vitro* test method to determine the fatigue of biological heart valve roots (Figure 1.10).



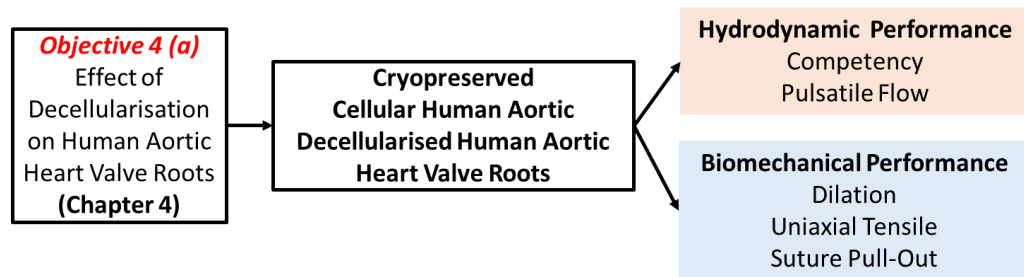
**Figure 1.10 Outline of Objective 2**

3. Evaluate the developed or optimised *in vitro* hydrodynamic, biomechanical and fatigue performance assessment test methods described in Objectives 1 and 2 using cellular porcine aortic and pulmonary heart valve roots to ensure the methods produced results that were consistent with existing data in the literature (Figure 1.11).

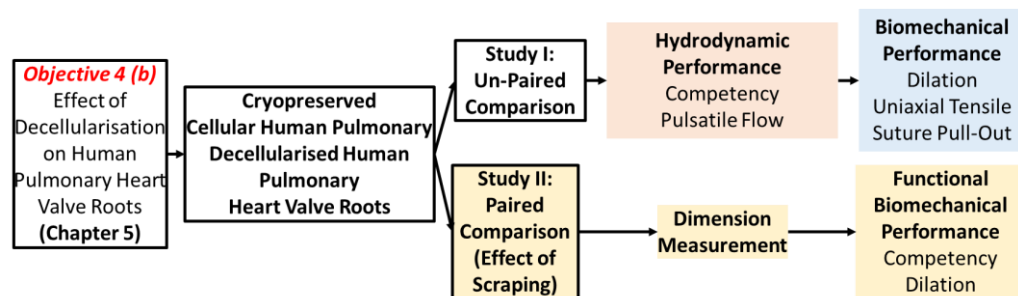


**Figure 1.11 Outline of Objective 3**

4. Apply the developed *in vitro* hydrodynamic (competency, pulsatile flow) and biomechanical (dilation, tensile, suture pull-out) performance assessment test methods described in Objective 1 to cellular and decellularised human aortic and pulmonary heart valve roots to investigate the effects of low concentration SDS decellularisation on human aortic heart valve roots [(Figure 1.12 (a)].



(a)



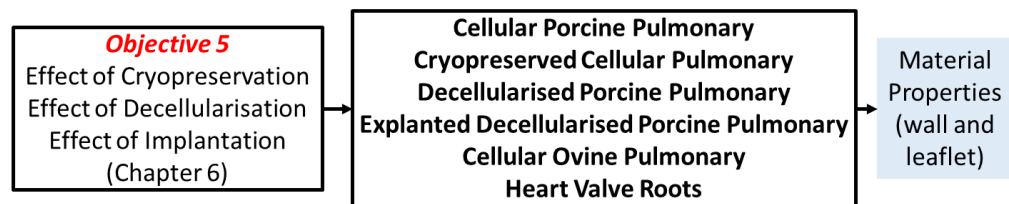
(b)

**Figure 1.12 Outline of Objective 4 (a) and (b)**

In addition, investigate the influence of a specific processing step (scraping) used during the decellularisation of human pulmonary heart valve roots on the functional biomechanical performance (competency, dilation) of cellular and

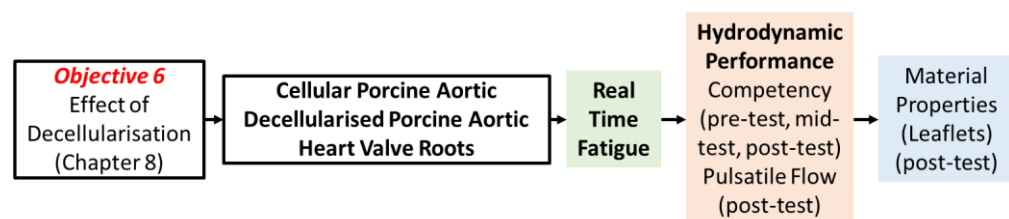
decellularised (scraped and un-scraped) pulmonary heart valve roots (in a paired comparison) [(Figure 1.12 (b)]. This will be the first full report comparing *in vitro* biomechanical and hydrodynamic performance of decellularised cryopreserved aortic and pulmonary human allograft heart valve roots with conventionally used cryopreserved human aortic and pulmonary allograft heart valve roots.

- Investigate the effects of low concentration SDS decellularisation and cryopreservation on the material properties of porcine pulmonary heart valve root wall and leaflet specimens and determine the material properties of decellularised porcine pulmonary heart valve root wall and leaflet specimens following 12 months implantation in 3 months old sheep (Figure 1.13).



**Figure 1.13 Outline of Objective 5**

- Investigate the effects of decellularisation on *in vitro* real time fatigue of porcine aortic heart valve roots under physiological cyclic pressures and heart rate conditions and determine the effect of cyclic loading conditions on competency, pulsatile flow performance and leaflet material properties of decellularised porcine aortic heart valve roots (Figure 1.14).



**Figure 1.14 Outline of Objective 6**

## 2 Materials and Methods

In this chapter the materials and methods used to characterise biological heart valve roots for hydrodynamic and biomechanical performance are described. First, the methodologies for the assessment of hydrodynamic performance of heart valve roots under static and pulsatile flow conditions are described. Secondly, the experimental methodologies for assessment of biomechanical performance of the heart valve roots in terms of circumferential expansion and material properties are described.

### 2.1 Introduction

Heart valves are complex structures consisting of cells and extracellular matrix (ECM) with a glycosaminoglycan content, collagen and elastin fibres (Chen and Simmons, 2011). The ECM plays a biomechanical role; it is responsible for the mechanical behaviour of the valve tissue and thus the overall valve function. Therefore, the development of decellularised heart valve roots for use in regenerative medicine requires the preservation of the valvular extracellular matrix (ECM). Hence, functional performance, safety and durability of these decellularised heart valve roots should be evaluated prior to their use in clinical studies. *In vitro* experimental test setups provide a way to test replacement heart valves in a controlled environment and minimised animal studies. Also, it is one of the main regulatory approval requirements to address key issues for safety and efficiency of the newly manufactured and modified surgical replacement heart valves.

The mechanical strength and elasticity of heart valve roots, which includes their ability to withstand physiological pressures and flow rates for the duration of usage, contributes significantly to the heart valve root's performance, safety and durability. During systole, the outward flexion of the heart valve root wall supports the opening of the leaflets. Therefore, mechanical function testing of each of the heart valve root components (wall and leaflets) is important and it is essential to assess how the component mechanical properties affect the function of the valve as a whole. Another important consideration is the efficiency of the whole heart valve root structure from the perspective of cardiovascular flow dynamics. Consequently, it is

important to derive *in vitro* performance of heart valve roots under steady and pulsatile flow conditions. These methods determine whether a valve is either stenotic or regurgitant. Various *in vitro* test methods have been used to assess both the mechanical properties of valve tissue such as flexural (Engelmayr et al., 2005, Sacks et al., 2009), local indentation (Cox et al., 2006), biaxial tensile (Fisher et al., 1986, Billiar and Sacks, 2000, Williams et al., 2009) uniaxial tensile (Korossis et al., 2002, Anssari-Benam et al., 2011, 2014), suture pull-out (Edwards et al., 2005, Walraevens et al., 2008), and dilation (Jennings et al., 2002, Wilcox et al., 2005) testing as well as hydrodynamic performance of the valves under physiological flow conditions (Fisher et al., 1986, Jennings et al., 2002, Syedain et al., 2013, Reimer et al., 2015). While biomechanical and hydrodynamic parameters may be estimated by a variety of methods, calculation of these parameters relies on test method reliability and test variables. The ideal test methods should be robust and reproducible. The most evident example of this scenario is uniaxial tensile testing. Uniaxial tensile testing of biological heart valve roots has however been criticised because of the technical challenges involving gripping the specimens, cross sectional area measurement of specimens and specimen hydration during testing. Another key issue is heart valve root mounting difficulty in the pulsatile flow simulator to derive hydrodynamic performance of the heart valve root. These issues have been examined and addressed in this Chapter. In addition, *in vitro* hydrodynamic properties of xenograft valves have been determined in various studies (Korossis et al., 2002, Schenke-Layland et al., 2003, Lichtenberg et al., 2006, Tudorache et al., 2007, 2014). Due to limited availability of fresh human hearts, repeatability of test methods and lack of physiological test conditions, there have been a limited number of studies investigating the hydrodynamic properties of human valves (Goldstein et al., 2000, Elkins et al., 2001). Even though the biomechanical and hydrodynamic properties of stented and stentless bioprosthetic xenograft valves are well defined, newer and upgraded measurement techniques can continuously improve the available data. Therefore, the approach was to take existing methods, critically review them and optimise certain processes, more specifically for biological heart valve roots. The developed hydrodynamic and biomechanical methods were then applied to different types of biological heart valve roots [cellular porcine aortic and pulmonary (Chapter

3), cryopreserved cellular and decellularised human aortic (Chapter 4) and pulmonary (Chapter 5), cellular ovine pulmonary (Chapter 6), explanted decellularised porcine pulmonary (Chapter 6), decellularised and cryopreserved porcine pulmonary (Chapter 6), cellular and decellularised porcine aortic (Chapter 8)], and the results are presented and discussed.

In addition to hydrodynamic and biomechanical performance, the durability or fatigue of the decellularised human and porcine heart valve roots will be critical to their success, and there is a need for this to be evaluated prior to being implanted in patients. A methodology for fatigue assessment of the heart valve roots is addressed in Chapter 7.

## **2.2 Aim and Objectives**

The aim of this chapter was to develop robust and repeatable methods to determine hydrodynamic and biomechanical performance of porcine and human (cellular and decellularised) aortic and pulmonary heart valve roots.

The specific objectives were:

1. Develop a test method to assess aortic and pulmonary heart valve root competency under static physiological back pressures.
2. Develop a method to determine the hydrodynamic performance of the aortic and pulmonary heart valve roots.
3. Develop a method to determine the circumferential compliance of the aortic and pulmonary heart valve root walls under static internal pressures.
4. Develop a uniaxial tensile test method to derive material parameters for the wall and leaflets of the aortic and pulmonary heart valve roots.
5. Develop a suture pull-out test method to derive suture pull-out properties of the wall and myocardium of the aortic and pulmonary heart valve roots.

## **2.3 Materials**

### **2.3.1 Chemicals and General Stock Solutions**

The chemicals and general stock solutions used during this project are listed in Table 2.1.



**Table 2.1 The Chemicals and General Stock Solutions used during this Study**

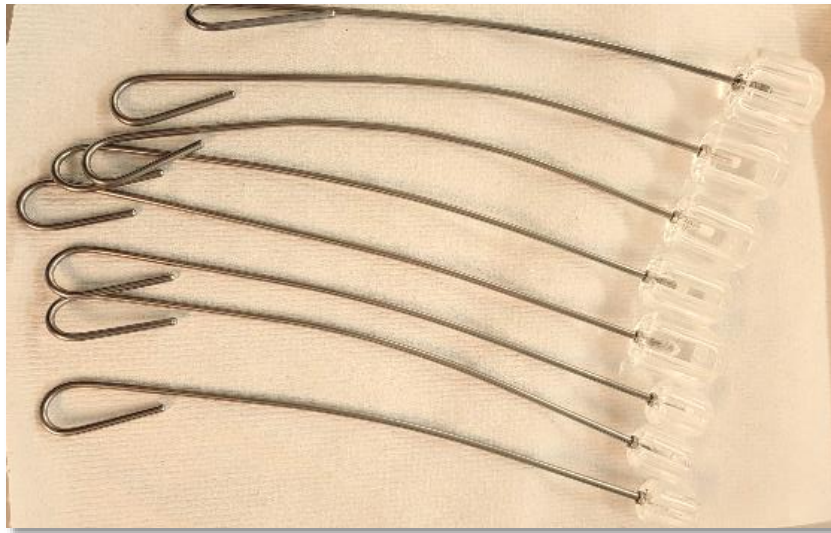
<b>Chemicals/ General stock solutions</b>	<b>Supplier</b>	<b>Product Code</b>
Saline (0.9%)	Leeds Pharmaceutical Ltd	31-58-736
Phosphate buffered saline (PBS): Ten PBS tablets were dissolved in 1L of distilled water	MP Biomedicals, LLC	092810305
Tissue marking dye	(Thermo Fisher Scientific, UK)	5000BL/ 5000R
Cambridge antibiotic solution with agitation 80 rpm	Source BioScience	04-301
Sodium azide 1 % (w/v) solution	Severn Biotech Ltd	40-2000-01
Amphotericin B	Sigma-Aldrich Company Ltd.	A2942
Aprotinin (10000 KIU.mr <sup>-1</sup> )	Mayfair house	AP012
Ethylenediaminetetraacetic acid	Thermo Fisher Scientific, UK)	E/P140/53
Glutaraldehyde Solution	Sigma-Aldrich Company Ltd, UK	49629-250 mL

### **2.3.2 Porcine and Human Cellular Heart Valve Roots**

Porcine heart valve roots were used to evaluate the test methods before applying said methods to human heart valve roots. The cellular porcine aortic and pulmonary heart valve roots used in this study were dissected from porcine hearts. The hearts were from approximately 24-28 week old pigs, slaughtered and supplied within 24 hours by M & C Meats, Crossgates, Leeds and John Penny & Sons, Rawdon, Leeds, UK.

The human aortic and pulmonary heart valve roots used in this study were provided by NHS Blood and Transplant Tissue and Eye Services (NHS BT TES), Liverpool, L24 8RB, UK. Ethics approval was obtained for the study from the Yorkshire and the Humber committee – Leeds West, UK under the REC reference 09/H1307/82. All the heart valve roots were visually examined and any roots with severe tissue

calcification were excluded from further processing. The size of the valves were measured with obturators (Figure 2.1).



**Figure 2.1 Valve Sizing Obturator Set**

### **2.3.3 Björk-Shiley mono leaflet valve (BSM; Shiley Corporation Incorporated, USA)**

A 23 mm Björk-Shiley mono leaflet mechanical valve (BSM; Shiley Corporation Incorporated, USA) was used as a control to validate static leakage rig and pulsatile flow simulator.

### **2.3.4 Imaging System**

The imaging system was used during pulsatile flow and real time fatigue testing to capture video of the heart valve root leaflets. It consisted of a high speed video camera (S-PRI Model, AOS Technologies, Inc), imaging software (AOS Imaging studio V3), Navitar high speed lens (50 mm focal length) and SCHOTT cold light lamp (model no: KL1500-T). The imaging software controlled the video capture speed and the quality of the videos. The high speed video camera was placed on a tripod. The cold light lamp was used to illuminate the leaflets of the test valves. A 2 second video clip was captured at rate of  $500 \text{ frames} \cdot \text{s}^{-1}$  to record high speed video of leaflets' motion.

## **2.4 Methods**

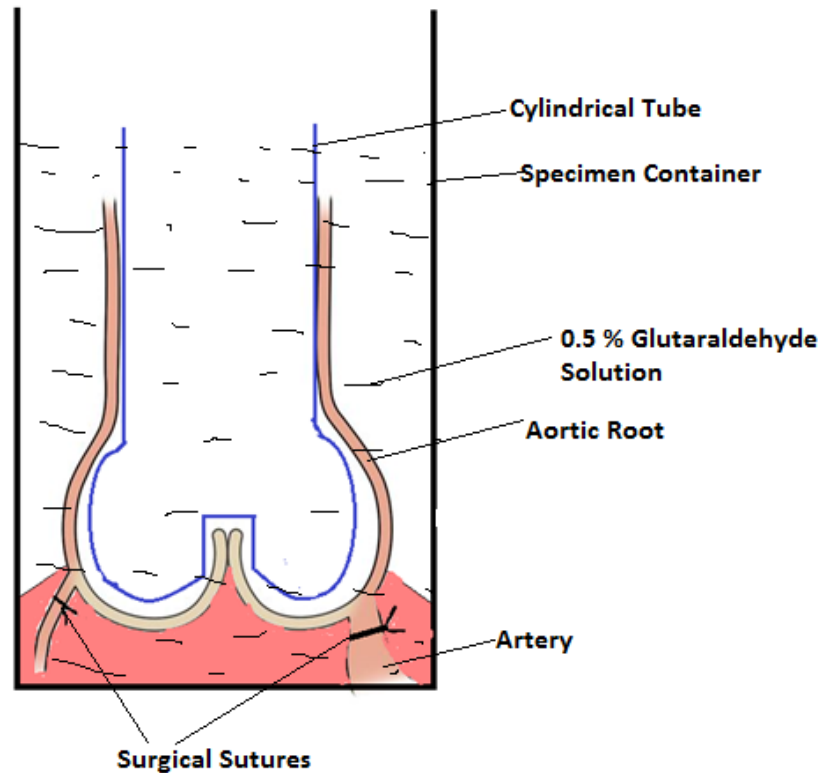
### **2.4.1 Decellularisation**

The porcine and human heart valve roots were decellularised using a proprietary low concentration sodium dodecyl sulphate (SDS) based protocol (Booth C, 2001). The details of decellularised protocol for porcine aortic and pulmonary heart valve roots are described in various studies (Korossis et al., 2002, 2014). The details of the optimised decellularisation protocol for human aortic and pulmonary heart valve roots are described by Vafaei et al. (2016). Both the cellular and decellularised human aortic and pulmonary heart valve roots were cryopreserved using the standard NHS BT TES process. Each root was placed in a nylon bag containing 100 mL heart valve cryopreservation medium [Hank's Balanced Salt Solution (HBSS); 16% v/v dimethyl sulfoxide (DMSO), 25 mM N-2-hydroxyethylpiperazine-N-2-ethane sulfonic acid (HEPES); product code 04-311, Inverclyde Biologicals]. The bag was then heat-sealed and placed into a second foil bag. The outer bag was also heat-sealed. The sealed foil bag was placed into a jiffy bag before storing at -80°C. The heart valve roots were removed from the bag 24 hours before testing, thawed, and stored at 4°C in Cambridge antibiotic solution.

### **2.4.2 Glutaraldehyde Fixation**

Glutaraldehyde fixed porcine aortic heart valve roots were used for both the initial real time fatigue test method development stage and as a control to understand any potential confounding factors caused during biological heart valve root testing. The aortic heart valve roots were used because they are well supported with thick myocardium, easy to handle and larger in size than pulmonary heart valve roots. Also pulmonary heart valve roots have an arch whereas aortic heart valve roots are a straight tubular shape, so it was more straightforward to use aortic heart valve roots for method development.

As described in Section 2.3.2, the cellular porcine aortic heart valve roots used in this study were harvested from porcine hearts, obtained from the local abattoir. The heart valve roots were stored in PBS at 4°C. The heart valve roots were then tested or fixed as necessary within 36 hours.



**Figure 2.2 Schematic Drawing of Glutaraldehyde Fixation of Porcine Aortic Heart Valve Roots**

Before the fixation process, the arteries of the aortic heart valve roots were ligated with surgical sutures. In the fixation process the aortic heart valve roots were treated with 0.5% glutaraldehyde solution (diluted in PBS). During the fixation process the valve was kept closed and a cylindrical tube was inserted from the wall side with 0.5% glutaraldehyde solution to keep aorta dilated to its original diameter (Figure 2.2). 150 mL of fixative was used for one heart valve root. Fixation was considered complete after 72 hours.

#### **2.4.3 Antibiotic and Antifungal Treatment**

All the cellular porcine aortic heart valve roots were treated with Cambridge antibiotic solution and amphotericin B to minimise growth of contaminating bacteria and fungi for real time fatigue testing in the real time wear tester (RWT). Before the antibiotic treatment, the arteries of the aortic heart valve roots were ligated with surgical sutures. The heart valve root was submersed in treatment solution (150 mL Cambridge antibiotic + 2.5 mL amphotericin B) for 3 hours at 37°C temperature. An Optima™ T 100 heated circulating bath was used to maintain 37°C temperature.

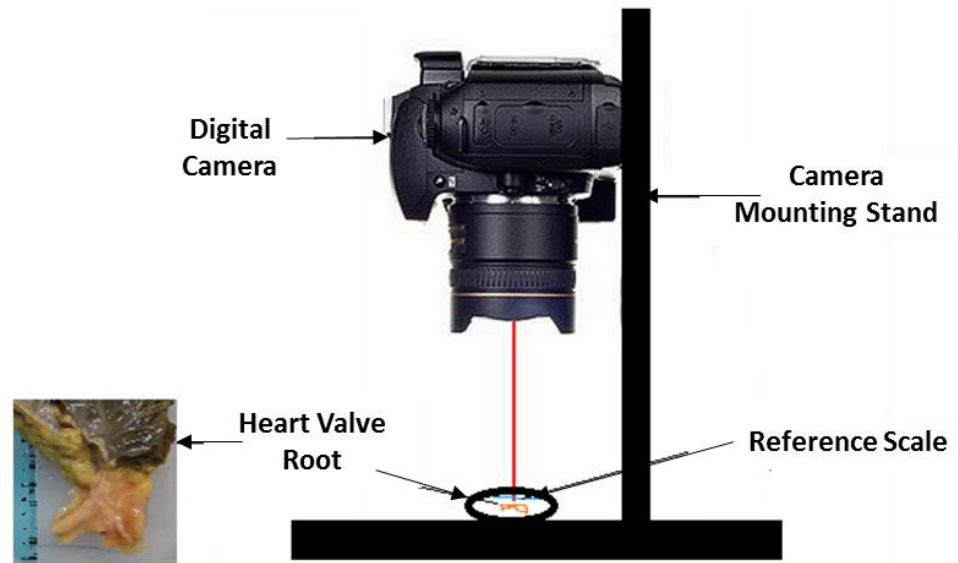
#### **2.4.4 Heart Valve Root Storage and Defrosting Procedure**

Following dissection, the cellular porcine heart valve roots were stored in 150 mL PBS and used straight away for testing or stored in 150 mL PBS individually at -20°C until required. A day before testing, the frozen roots were defrosted by leaving them at room temperature for maximum 12 hours.

All the human cellular and decellularised heart valve roots were cryopreserved using the standard NHS BT TES process and stored at -80°C prior to use. A day before testing, each heart valve root was thawed as per standard Leeds procedure. Briefly, the package containing the cryopreserved heart valve root was gently agitated in warm saline (37 °C) to dissolve ice crystals and soften the heart valve root. The outer and inner bags were cut open and the contents were placed into a sterile 2 L beaker. The cryopreservation solution was diluted by the successive addition of 200, 400, 800 mL PBS after 5, 10 and 15 minutes. The heart valve root was transferred to a sterile beaker containing 200 mL sterile PBS was solution (PBS plus 2.7 mM ethylenediaminetetraacetic acid disodium salt (EDTA) and 10 KIU.mL<sup>-1</sup> aprotinin). Then the thawed heart valve roots were disinfected in 200 mL Cambridge antibiotic solution with agitation at 80 rpm for 3 hours at 37°C in an incubator and stored at 4°C. Prior to testing. The heart valve root was washed with two changes of PBS solution (250 mL) for 5-15 min (twice).

#### **2.4.5 Dimensional Measurement**

All the cellular and decellularised human pulmonary heart valve roots were measured before and after decellularisation and also after the scraping procedure. The set up for measuring the dimensions of the heart valve roots is shown in Figure 2.3.

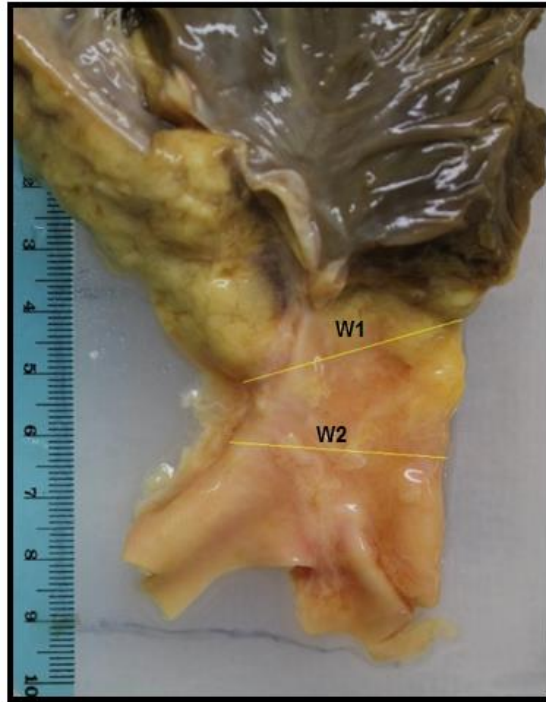


**Figure 2.3 Dimension Measurement Set Up**

Great care was taken during measurement and analysis when comparing the effect of decellularisation on tissue dimension. The camera (Canon digital SLR 550 D) was set up perpendicular to the heart valve root and a scale was kept in same plane as the heart valve root for calibration purposes. Images for all the pulmonary heart valve roots (cellular, cellular scraped, un-scraped decellularised and scraped decellularised) were captured.

#### **2.4.5.1 Data Analysis of Dimensional Measurements**

All the images were uploaded into ImageJ, a Java-based open source image processing software ImageJ (NIH, Bethesda, MD), for analysis. ImageJ line tool was used to take measurements  $W_1$  near annulus and  $W_2$  in the wall region as shown in Figure 2.4.



**Figure 2.4 Dimension Measurement with ImageJ**

The width W1 and W2 was measured for each heart valve root before and after the treatments (scraping and decellularisation). The formula shown below was used to measure percentage change in the widths W1 and W2 for un-scraped decellularised relative to un-scraped cellular and scraped decellularised relative to cellular scraped.

$$\% \text{ change in } W = \frac{W(\text{before treatment}) - W(\text{after treatment})}{W(\text{before treatment})} \times 100$$

#### **2.4.5.2 Dimension Measurement Technique Validation**

To validate the measurement approach the dimensions of a cellular porcine pulmonary heart valve root were measured over two consecutive days. An image of the porcine pulmonary heart valve root was taken three times at every two hours on each day. The heart valve root was stored in PBS at 4°C in between measurements. These images of porcine valves were captured and processed with ImageJ, keeping all the conditions and the procedures same as human pulmonary heart valve roots. The widths W1 near the annulus and W2 in the wall region (Figure 2.4) were measured and are displayed in Table 2.2.

**Table 2.2 Dimensions of the Cellular Porcine Pulmonary Heart Valve Root Measured On Two Consecutive Days**

	Width W1 mm		Width W2 mm	
	Day 1	Day 2	Day 1	Day 2
	2.62	2.76	2.48	2.62
	2.66	2.76	2.55	2.66
	2.60	2.74	2.47	2.61
<b>Mean <math>\pm</math> 95 % Confidence Limit</b>	2.63 $\pm$ 0.08	2.75 $\pm$ 0.03	2.50 $\pm$ 0.11	2.62 $\pm$ 0.01
<b>% Change in Width Between Two Days</b>	4.50%		4.80%	

From this experiment, the accuracy of the valve dimension measurement with ImageJ was estimated to be to 5 %.

#### **2.4.6 Hydrodynamic Performance I: Competency under Static Back Pressure**

Competency tests were performed to assess valve closure and quantify regurgitant flow rate under a range of physiological static back pressures. This section describes the modification of the static leakage rig, the use of the modified static leakage rig to conduct the tests, the process to validate the rig and the procedure for determining the competency of the heart valve roots.

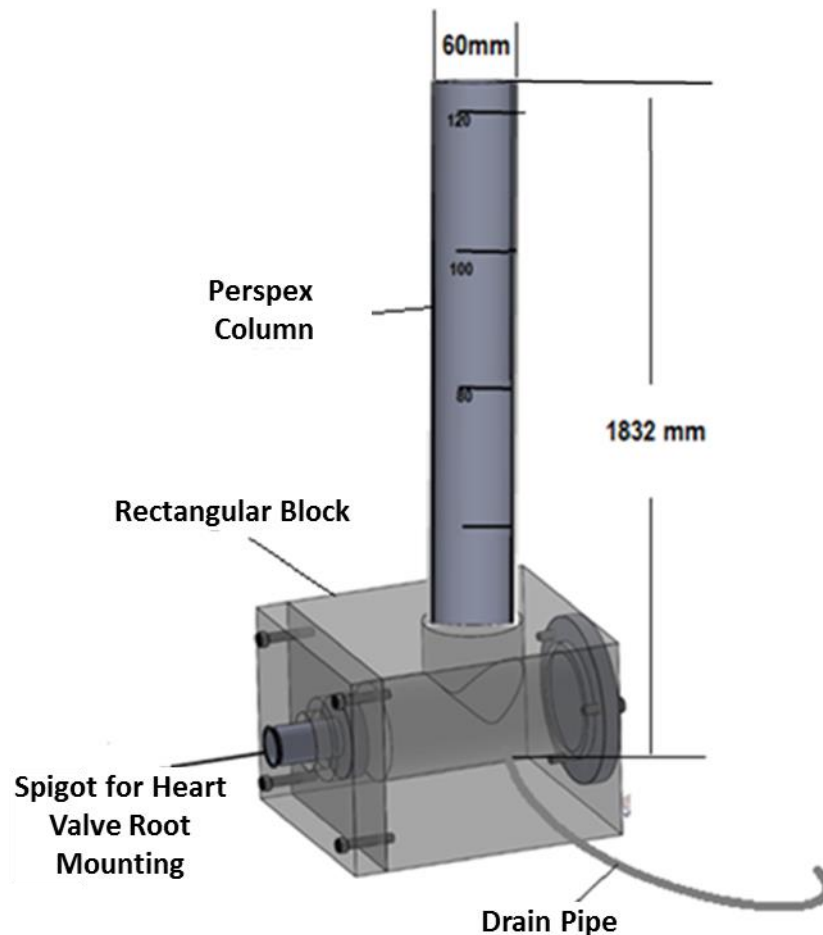
##### **2.4.6.1 Static Leakage Rig**

A static leakage rig was used to assess valve competency under static physiological back pressures. The rig enabled measurements of leakage flow rate of a closed valve. This information about valve behaviour during diastole, when the valve was closed, could expose the existence of regurgitation problems. A static leakage rig was used in previous study (Jennings, 2001) to measure leakage flow rates of porcine pulmonary heart valve roots. The rig consisted of a 1.56 meter high cylindrical Perspex column able to apply pressure of 100 mmHg when saline was used as a test fluid. However, this study also required testing of aortic heart valve roots with a pressure of 120 mmHg. Therefore, it was necessary to modify the static leakage rig.



#### 2.4.6.1.1 Modification of Static Leakage Rig

The static leakage test rig (Jennings, 2001) was modified to enable testing of aortic heart valve roots with a pressure 120 mmHg. The vertical cylindrical Perspex column was replaced with a longer vertical Perspex column which was applied a pressure of 120 mmHg.



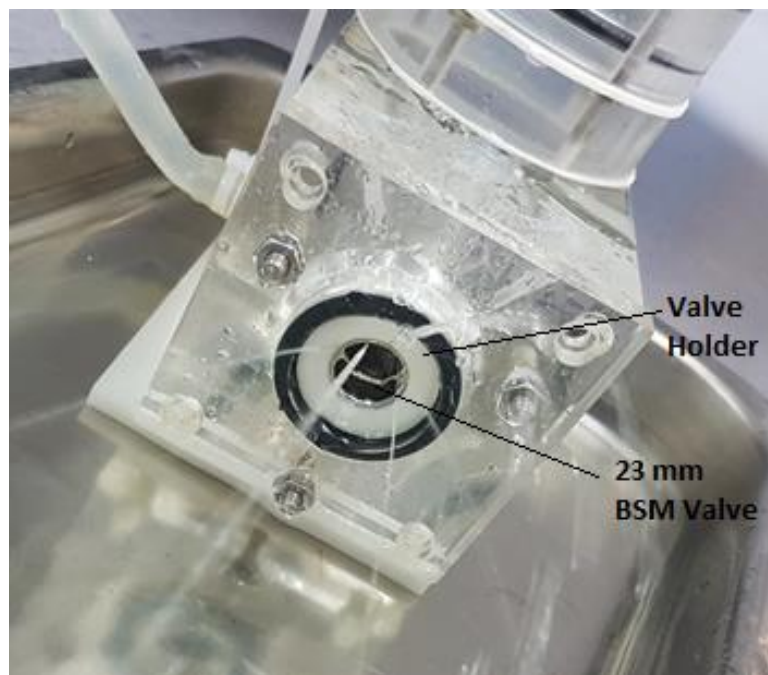
**Figure 2.5 Static Leakage Rig (not drawn to scale)**

The modified test rig (Figure 2.5) consisted of an 1832 mm tall cylindrical Perspex column with an internal diameter of 60 mm, housed vertically in a rectangular Perspex block. The column was marked at intervals of 20 mmHg up to 120 mmHg applicable for the test fluid of saline. It could be drained via an outlet drainage pipe at the base of the block (Figure 2.5). The rig was placed on the floor into a large stainless tray and the Perspex column secured vertically to a work bench with a G clamp.

#### 2.4.6.1.2 Validation of Static Leakage Rig

The static leakage rig was validated by recording the time taken for the pressure head to leak test fluid of 0.9 % (w/v) saline from 120 mmHg to 80 mmHg through a 1 mm diameter hole. The test was repeated 6 times, leakage times and leakage volumes were recorded for each iteration. An externally calibrated Hanhart Mesotron Quartz stop clock (serial number 6558CLK) was used to record leakage times. The mean volume of test fluid was calculated to be 1534 mL, which enabled the flow rate to be calculated, recorded leakage times and leakage volumes were within a range of  $\pm 5\%$  the mean values.

A baseline value (control data) for the static leakage rate of a heart valve was established using a 23 mm Björk-Shiley mono leaflet valve (BSM; Shiley Corporation Incorporated, USA) with the static leakage rig. A 23 mm BSM valve was placed in a closed position in a valve holder at the bottom of the leakage tester, as shown in Figure 2.6.



**Figure 2.6 Test Set-up to Derive Leakage Flow Rate under Static Back Pressure for Mechanical Valve**

The rig was filled with a 0.9 % (w/v) saline solution to the 120 mmHg pressure mark. The leakage time was measured for the pressure head to leak the test fluid from 120 mmHg to 80 mmHg. Five runs were performed to ensure repeatability. After

two runs, the valve holder was removed from the rig and the mechanical valve opened and closed again to allow possible leaflet alignment variation upon closure.

**Table 2.3 Static Leakage Results for the Mechanical Valve**

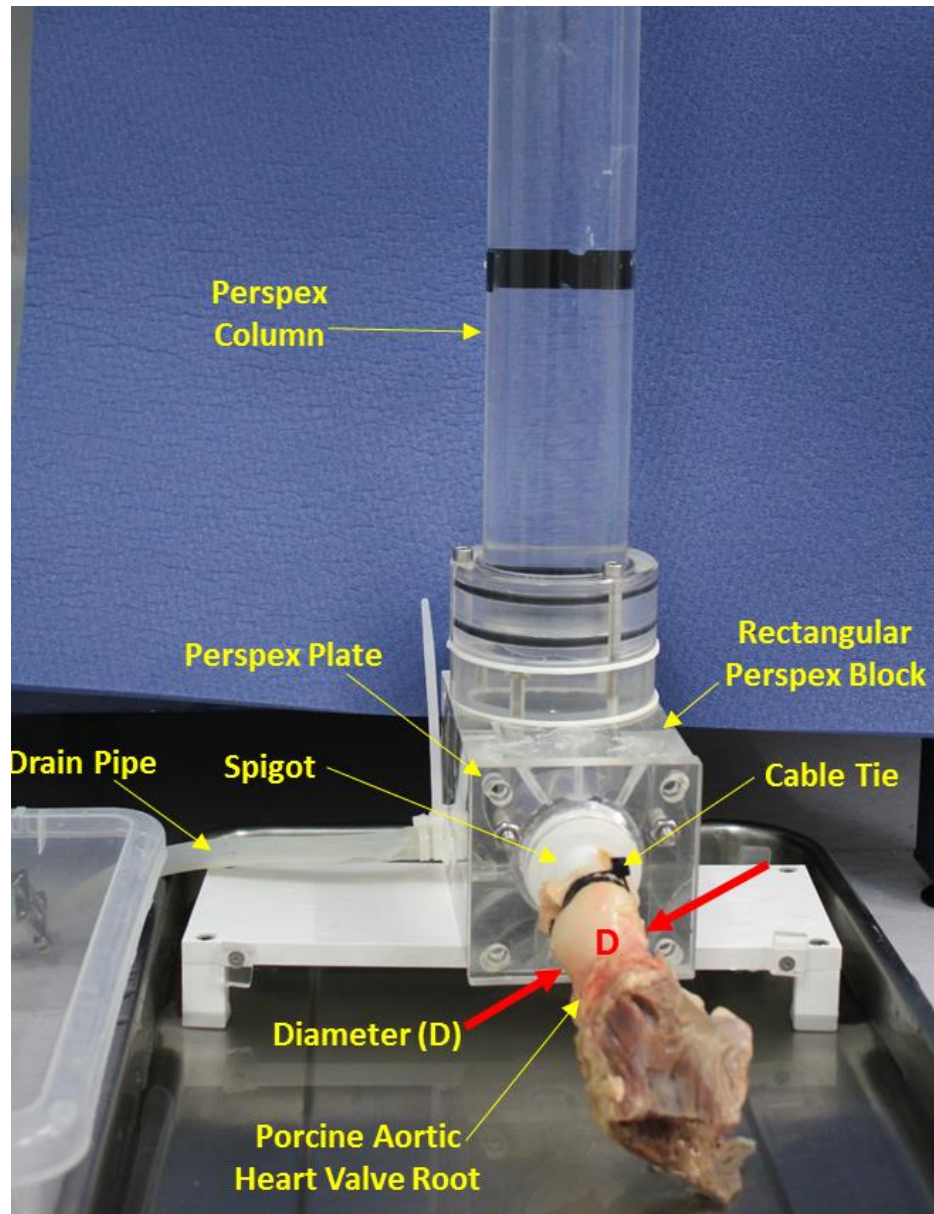
Test Run	Static Leakage Time (s)	Static Leakage Flow Rate (mL.s <sup>-1</sup> )
1	205	5.03
2	347	4.42
3	430	3.56
4	349	4.39
5	223	7.33

Table 2.3 shows the results of the static leakage tests. The mean leakage flow rate with 95% confidence limits of the 23 mm BSM valve was  $4.95 \pm 1.78$  mL.s<sup>-1</sup>.

#### **2.4.6.1.3 Test Procedure – Biological Heart Valve Roots**

The heart valve root was secured to the rig spigot with a cable tie, and mounted into the Perspex plate with gasket seal. The Perspex mounting plate and spigot assembly were attached to the rectangular Perspex block with 4 screws (Figure 2.7).

The desired maximum (systolic) pressure was achieved by filling the Perspex column with 0.9% (w/v) saline solution. The leakage time, i.e. time taken by the test fluid to drop from the systolic limit to the desired minimum (diastolic) pressure, was documented. The maximum applied pressure was 120 mmHg for all the aortic heart valve roots and 60 mmHg for all the pulmonary heart valve roots. The times taken for this test fluid to drop to 80 mmHg (for all aortic) and 20 mmHg (for all pulmonary) were recorded. An externally calibrated Hanhart Mesotron Quartz stop clock (serial number 6558CLK) was used to record leakage times.



**Figure 2.7 Test Set-up for Static Leakage Testing of Heart Valve Roots**

#### 2.4.6.1.4 Data Analysis

The mean flow rate was determined with the formula:  $Q = V/t$  [flow rate ( $Q$ ) = volume of test fluid ( $V$ ) /leakage time ( $t$ )]. This volume ( $V$ ) of test fluid was measured as 1534 mL in all iterations. A vernier caliper was used to measure heart valve root diameter  $D$  near to the sino tubular junction at the maximum pressure limit. The root was considered to be competent if the pressure head had not dropped to 80 mmHg (for aortic) or 20 mmHg (for pulmonary) within a cut-off period of 30 minutes for aortic and 20 minutes for pulmonary heart valve roots.

### 2.4.7 Hydrodynamic Performance II: Pulsatile Flow Testing

Quantitative hydrodynamic performance of the heart valve roots was assessed by testing the root under physiological pressure and flow conditions similar to those occurring in a human heart in a pulsatile flow simulator.

**Table 2.4 The Major Performance Specifications required during optimisation of the Pulsatile Flow Simulator**

No	Specification
1	Easy mounting and removal of the heart valve roots without causing damage
2	Able to clean thoroughly with disinfectant
3	Able to capture valve images during testing
4	Accurate measurement of the flow and pressure
5	Leakage free

The pulsatile flow simulator has been widely used in previous studies (Fisher et al., 1986, Jennings, 2001, 2014) to assess hydrodynamic performance of the heart valve roots. However, the instrumentation for this pulsatile flow simulator was relatively old and difficult to use. The simulator had the potential to work, but suffered frequent failures of the flow meter, pump controller and waveform generator. Replacing these units with the most recently available versions of the units was an ideal solution. In addition, another key requirement of the new pulsatile flow simulator was the capability to mount a cellular and decellularised human heart valve root into the loop in the position of the aortic valve. The major performance specifications for the optimised pulsatile flow simulator are described in Table 2.4.

#### 2.4.7.1 Optimisation of Pulsatile Flow Simulator

To satisfy the performance specifications described in Table 2.4, the pulsatile flow simulator used by Fisher et al. (1986) was upgraded and optimised to make certain processes easier and more practical. For instance, it used to take a long time to mount a heart valve root into the existing flow loop and there were risks of damaging the heart valve root during mounting. Therefore, the heart valve root mounting technique in the simulator was optimised (Section 2.4.7.3) which greatly

increased the ease in which studies could be carried out in the simulator. In addition, new gaskets and O-rings were implemented into the new flow loop to prevent leaks. The newer versions of instrumentations and flow loop were improved. A schematic diagram of the optimised pulsatile flow simulator is shown in Figure 2.8.

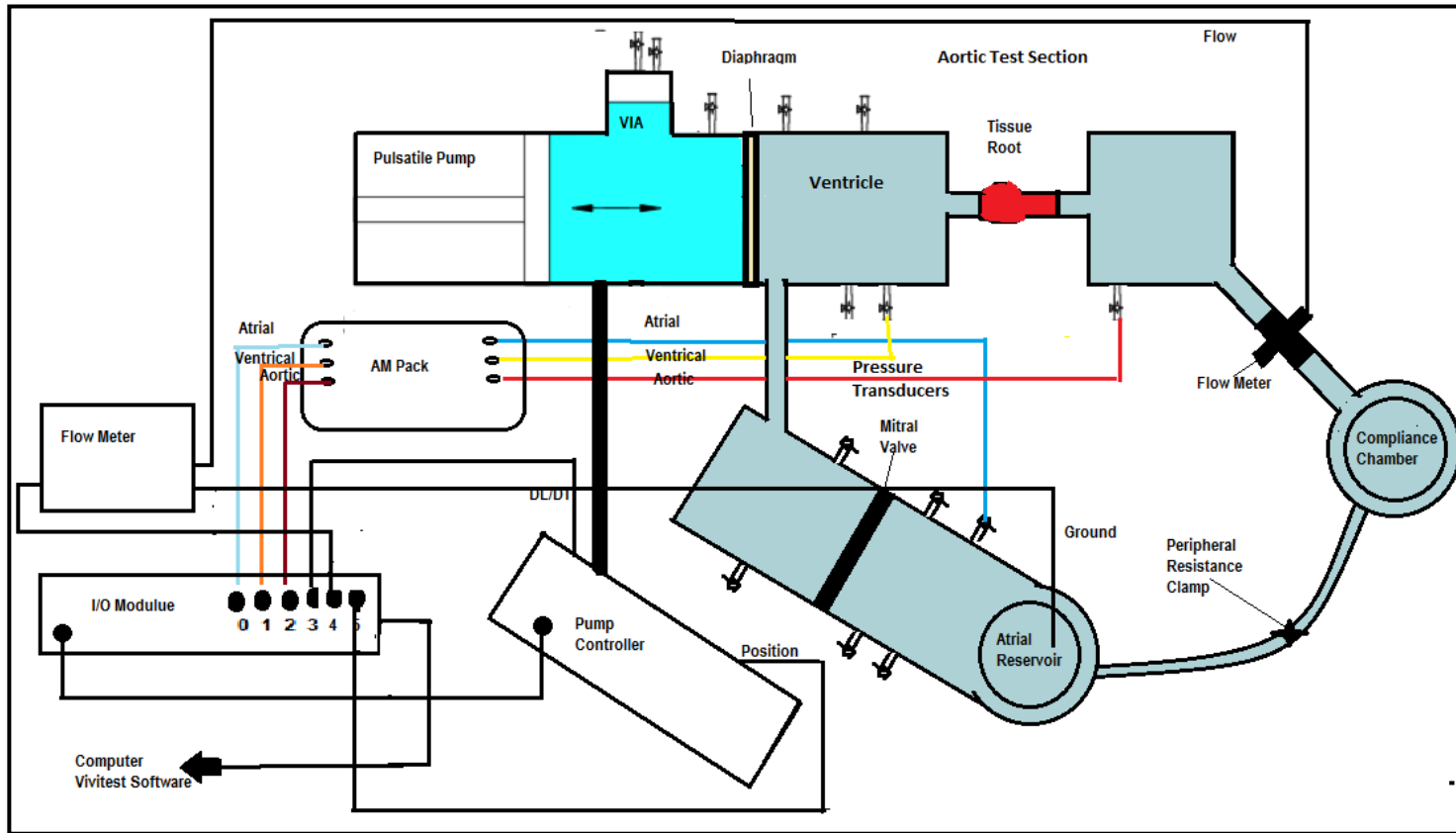
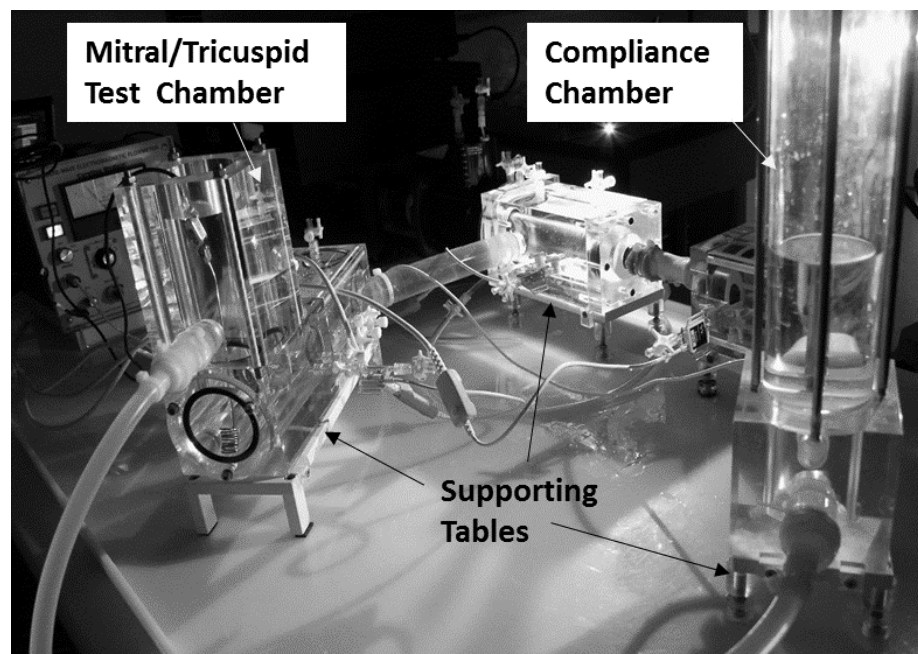


Figure 2.8 Pulsatile Flow Simulator Schematic Diagram used to assess Hydrodynamic Performance of the Heart Valve Roots

The simulator replicated the function of either side (left or right) of the heart. The simulator consisted of a positive displacement pulsatile pump, SuperPump (Vivitro Systems Inc, Victoria BC, Canada), a viscoelastic impedance adapter (VIA), two test chambers for testing valves in the aortic/pulmonary or mitral/tricuspid valve positions, a ventricular and an atrial chamber, a compliance chamber (after load), silicon tubing simulating the peripheral circulation, a peripheral resistance tap, and the pressure and flow measurement (Vivitro Systems Inc, Victoria BC, Canada) instruments. The simulator was controlled and monitored by a data acquisition system and the ViviTest software (Vivitro Systems Inc, Victoria BC, Canada) installed on an attached computer.



**Figure 2.9 Pulsatile Flow Simulator Showing the Test Chambers with Supporting Tables**

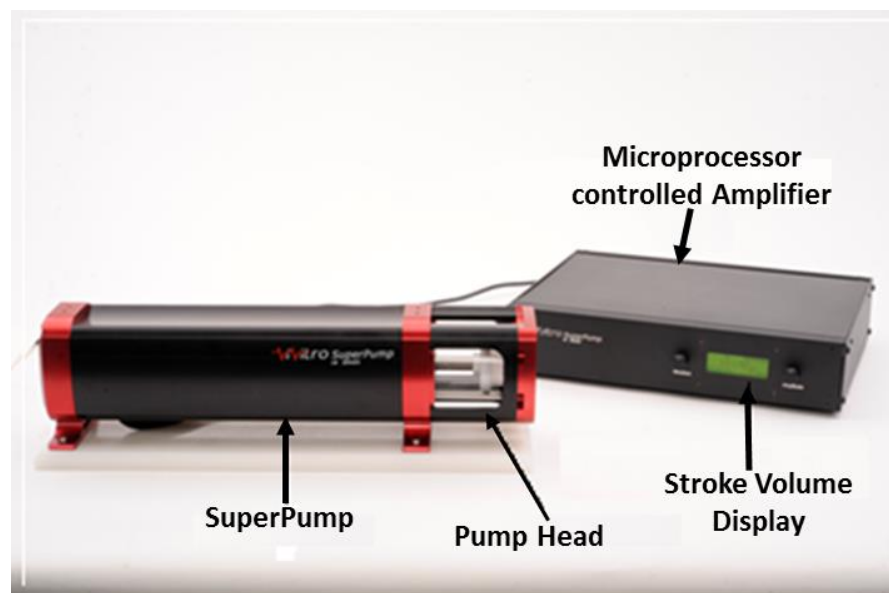
All the test chambers had supporting tables for easy specimen mounting and cleaning as shown in Figure 2.9.

#### **2.4.7.1.1 SuperPump and Viscoelastic Impedance Adapter (VIA)**

The SuperPump (AR Series, Vivitro Systems Inc, Victoria BC, Canada) was a microprocessor controlled piston-in-cylinder pump that creates physiological cardiac flows (Figure 2.10). The SuperPump system consisted of an amplifier, a linear actuator, a pump head, and interconnecting cables. The amplifier had a capacity to



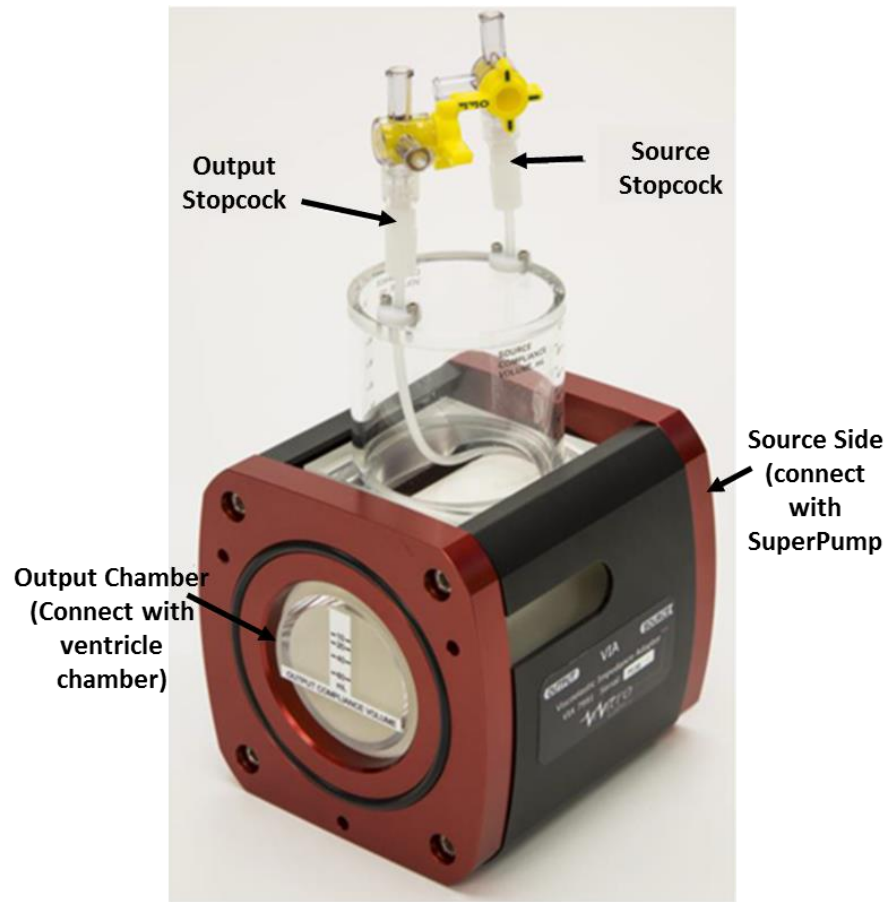
store five programmable physiological waveforms at different heart rates ranging from 30 to 200 bpm. Additional user defined waveforms could be programmed in the amplifier using the ViViGen software. The amplitude of the input waveforms, in terms of stroke volume, was controllable by an amplitude switch on the amplifier. A sinusoidal (S50) input waveform was used to drive the SuperPump throughout this study as this waveform was found to produce smoother pressure waveforms for the biological heart valve roots (Jennings, 2001).



**Figure 2.10 SuperPump System used for Pulsatile Flow Simulator**

A viscoelastic impedance adapter (VIA), (VIA 7991, Vitro Systems Inc, Victoria BC, Canada) (Figure 2.11) was placed between the SuperPump and the ventricle test chamber. It added resistance and compliance to pump waveforms to produce physiological pressure and flow waveforms. A diaphragm separated the VIA from the ventricle chamber and the pump to prevent the test fluid (saline) from entering the VIA.

The VIA consisted of a fixed resistive element and adjustable compliance chambers, simulating ventricular viscoelastic behaviour. The VIA was adjusted to maximum compliance by setting air volumes to 60 mL and 125 mL on the output and input side respectively.



**Figure 2.11 A Viscoelastic Impedance Adapter**

Minimum compliance was achieved by completely filling the VIA with distilled water. Adjusting the VIA to maximum compliance reduced the oscillations in the ventricle pressure and provided the smoothest possible flow waveforms, similar to those seen on porcine cellular heart valve roots tested in the pulse duplicator simulator by Jennings et al. (2001).

#### **2.4.7.1.2 Aortic Test Section**

The aortic test section comprised of a ventricle chamber and aorta. In the human body, the left ventricle is responsible for pumping blood through the aortic valve, on to the ascending aorta, and out to the rest of the body. In this experimental flow loop, the ventricle was powered by a pulsatile positive displacement pump to push fluid through the system.

#### **2.4.7.1.3 Compliance Chamber**

Compliance is characterised by the ability of the walls of a heart to contract and expand as the interior pressure changes. In the simulator, the compliance chamber is the section of the flow loop that compensates for the requirement to expand and contract according to the arterial pressure and maintains the physiological nature of the waveforms produced by the device. After leaving the aortic valve and passing through the flow probe, the test solution (saline) enters the compliance chamber.

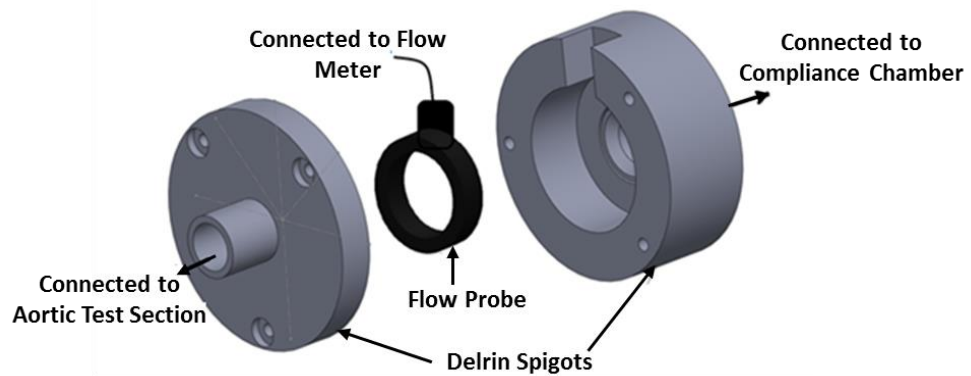
This compliance chamber consisted of a long vertical cylindrical Perspex column partially filled with air, an analogue pressure gauge and a rubber tubing with a clamp. The clamp on the flexible rubber tubing was used to control the resistance and the level of saline inside the cylindrical Perspex column.

#### **2.4.7.1.4 Mitral Valve Test Section**

The mitral valve test section consisted of two parts: the atrium and ventricle, with the mitral valve positioned between them. The outlet of the test section was connected to the ventricle section. The atrium chamber primarily served as a reservoir that held excess saline not used by the system. Saline supplied to the flow loop enters the system through the atrium. The atrium chamber was designed with a cavity on top to tolerate fluctuations in volume without causing a drastic increase in pressure through the rest of the system. A 29 mm Björk-Shiley mono-leaflet mechanical valve *was used* throughout the study *as* the standard valve in the mitral position.

#### **2.4.7.1.5 Measuring Instruments**

The flow measuring system consisted of a Carolina Medical electromagnetic variable range analogue flow meter (model: FM501, Carolina Medical Electronics, Inc) and electromagnetic flow probe (EP688, Carolina Medical Electronics, Inc). The flow meter had a range from 5 mL.min<sup>-1</sup> to 19.99 L. min<sup>-1</sup> depending on probe selected.



**Figure 2.12 Flow Probe Mounting Arrangements**

The flow probe works on the principle of electromagnetic induction. The probe had an internal diameter of 28 mm and probe factor was 53800 provided by the manufacturer. The probe factor was useful to adjust flowmeter gain and permitted full scale direct reading on the flow meter display in millilitres or litre per minute. It was held between two Delrin spigots, as shown in Figure 2.12, and mounted at an angle between the aortic test section and the compliance chamber.

To measure the pressure in the system, several small ports were built into the chambers at various locations. These ports consisted of small through holes running inside a chamber to the exterior and attached to three way connectors. Pressure transducers were attached to the three way connectors. Pressure was measured directly upstream and downstream of the test heart valve root using Vivitro pressure transducers (Model: HCM018, Vivitro Systems Inc, Victoria BC, Canada). The pressure transducers had a range of -50 to +300 mmHg with  $5 \mu\text{V}/\text{V}/\text{mmHg}$ . Data from the transducers was filtered by the attached amplifier unit. Each transducer was filled with saline, and bubbles were removed before every experiment for accurate pressure measurement.

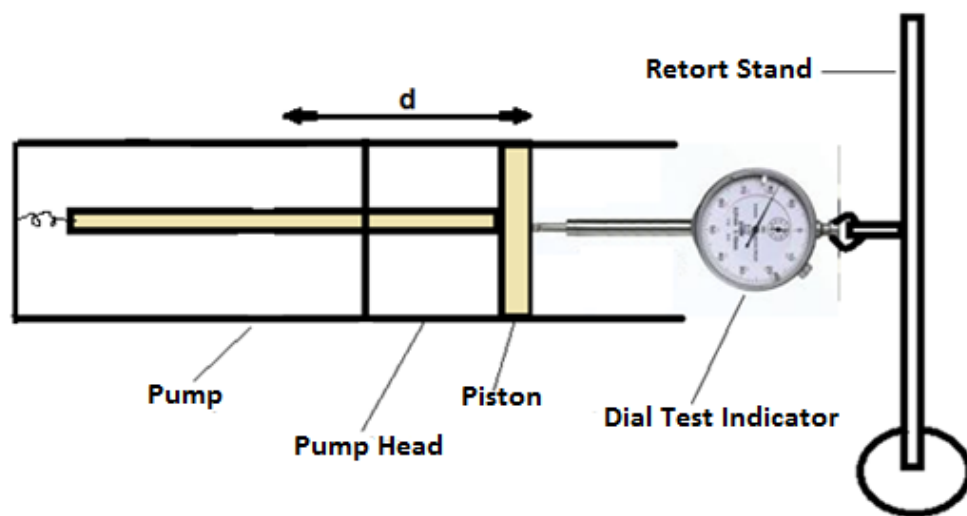
#### **2.4.7.1.6 Data Acquisition**

A 12 bit digital data acquisition device was used to acquire data from the piston position sensor, the flow meter, and the three pressure transducers. Data was sampled at a rate of 300 Hz. Low pass filters with cut-off of 30 Hz and 10 Hz were set for the pressure and flow sensors respectively to remove excessive electrical interference from the pressure and flow output waveforms. This filter settings

allowed smoother pressure and flow waveforms. The ViViTest software (Vivitro Systems Inc, Victoria BC, Canada) was used to monitor, collect, and analyse the pressure and flow data which is explained in detail in the Section 2.4.7.5 .

#### 2.4.7.2 Calibration and Verification of Pulsatile Flow Simulator Components

Stroke volume verification: The accuracy and consistency of the stroke volume measured by the pump controller and recorded by the ViViTest software was verified as follows:



**Figure 2.13 Stroke Volume Verification Setup**

The volume of fluid displaced by the piston in a single stroke is the output data of the pump controller. This stroke volume value was verified using an analogue dial test indicator (DTI) connected to the pump as shown in Figure 2.13. The pump was adjusted to displace 60 mL of fluid per stroke for a corresponding heart rate of 60 bpm with a sine waveform. The movement of the DTI plunger for the forward stroke was recorded. The stroke volume (SV) is the amount of blood the left ventricle pumps through the aortic valve with each heartbeat. The volume of test fluid being pumped in each stroke was calculated using the formula shown below:

$$\text{Stroke volume (SV)} = \text{Area} \times [\text{stroke distance}]$$

$$\text{Where Area } A = \pi r^2 = 38.32 \text{ cm}^2 \text{ (provided by manufacturer)}$$

This process was repeated three times under the same test conditions and the mean of the three results was used. The data output of the pump controller and value displayed by the ViViTest software were within  $\pm 0.2$  mL of the calculated stroke volume.

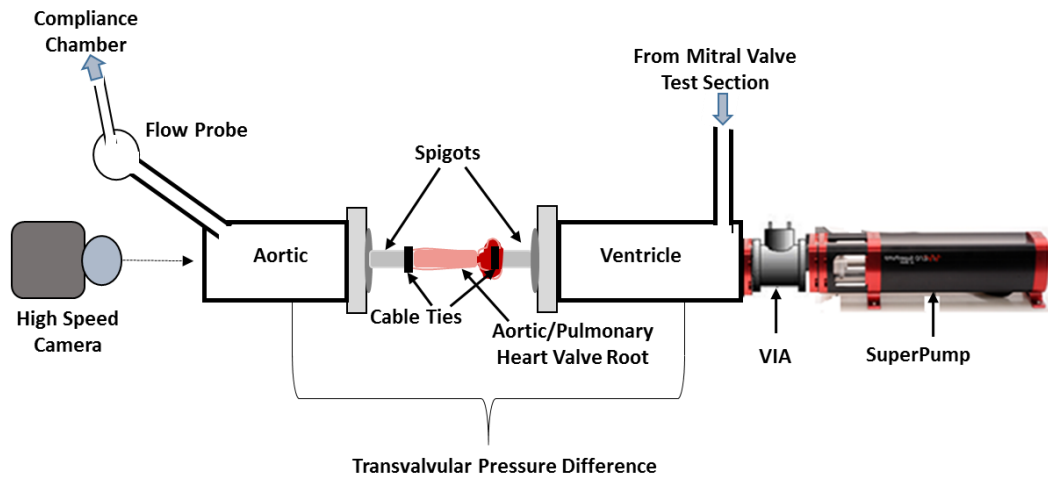
**Flow meter calibration:** The flow meter was calibrated using the ViViTest software. An open spacer ring was mounted in the aortic site and an occluding solid plug in the mitral site. The pump was adjusted for 60 bpm and 60 mL stroke volume with sine wave. The calibration wizard steps of ViViTest software were followed. The stroke volume automatically adjusted calibration factor to equate the flow meter signal with pump displacement signal.

**Pressure transducer calibration:** Three digital pressure transducers were used to measure pressure at various locations in the pulsatile flow simulator. A two point pressure calibration, guided by ViViTest software, was performed with each of the pressure transducers using the following procedure: A transducer was kept open to the atmosphere, without any external pressure, to record the initial base value - the output voltage of the transducer. Pressure equivalent to 200 mmHg was then applied to the transducer with an external digital pressure transducer (S/N: 63204/3, Comark Instruments, Inc). The resulting output voltage of the transducer was recorded. At the end of this calibration process, a calibrated value in mV/mmHg was calculated for each pressure transducer by ViViTest software. These values were compared with their historical values.

#### **2.4.7.3 Heart Valve Root Mounting in Pulsatile Flow Simulator**

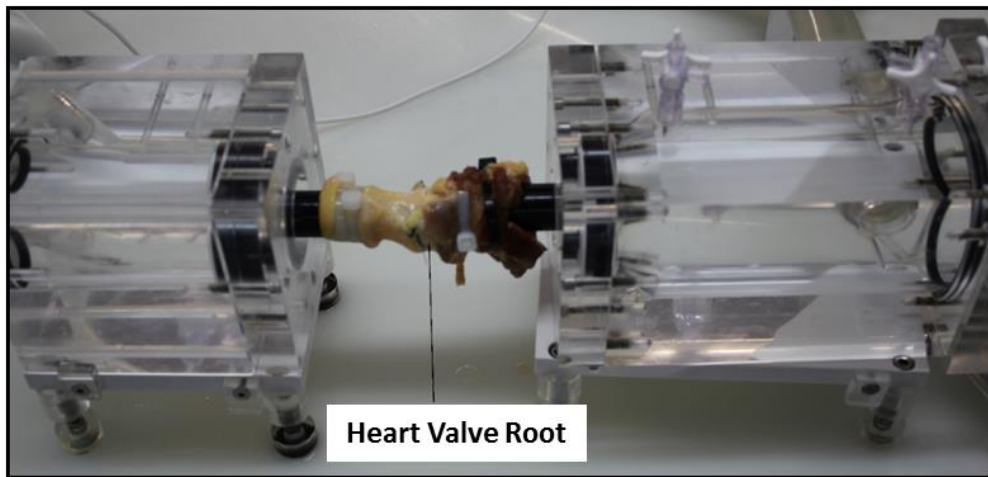
One of the key aspects of the modification of the pulsatile flow simulator was the capability to mount cellular and decellularised human roots into the flow loop in the position of the aortic valve. The problem with testing these roots was that they were well hydrated and soft, so they slipped off the spigot with clamping fittings due to pulsatile forces during the testing. In addition, in this study the same root was tested for multiple test conditions and multiple test procedures. Therefore, it was essential not to damage the heart valve root even after completion of this test procedure.

The heart valve roots were positioned and clamped at the downstream end of ventricular chamber and upstream end of the aorta as shown in Figure 2.14.



**Figure 2.14 Schematic Diagram of Heart Valve Root Position and Mounting in Pulsatile Flow Simulator**

All the cellular and decellularised roots under test were mounted on Delrin mounting spigots and secured with cable ties as shown in Figure 2.15.



**Figure 2.15 Heart Valve Root Mounting in Pulsatile Flow Simulator**

It was a requirement to tighten the cable ties without damaging the heart valve root. A cable tie gun (part no: STHV, Panduit Europe Ltd) (Figure 2.16) was used to tension and cut the cable ties. The cable ties were sufficiently tight to prevent axial movement along the heart valve root and push them out under pulsatile flow conditions.



**Figure 2.16 Cable Tie Gun**

#### **2.4.7.4 Test Procedure**

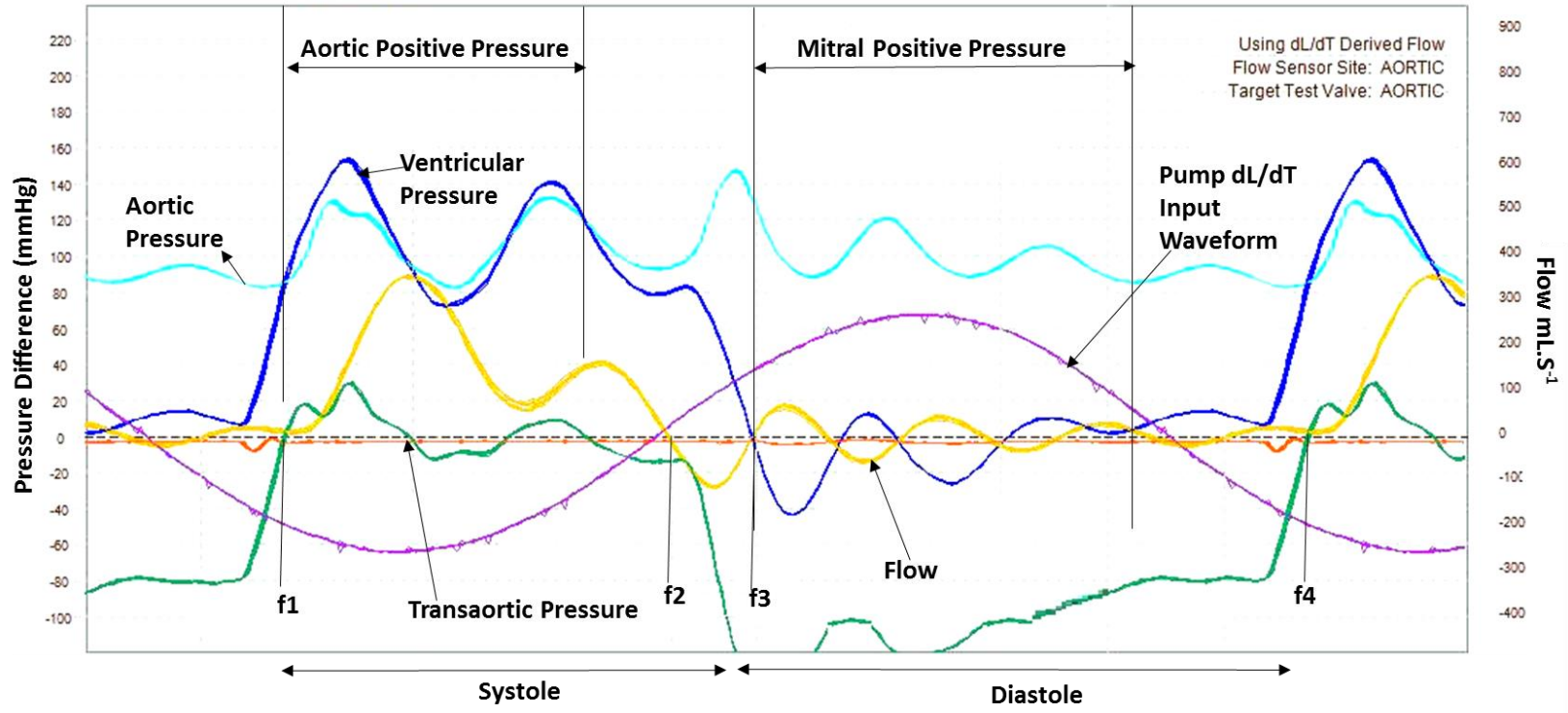
The hydrodynamic performance of the heart valve roots was assessed using this upgraded Leeds pulsatile flow simulator. A Viscoelastic Impedance Adapter (VIA) (Vivitro System Inc., Victoria BC, Canada) was used to deliver physiological ventricle pressure and flow waveform to the simulator. This simulator system allowed for physiological pressure and flow waveforms as well as high speed video recording of leaflet motion as described in detail by Jennings et al. (Jennings et al., 2001). As described in Section 2.4.7.3, a test heart valve root was mounted in the aortic position. It was a two stage testing procedure for biological heart valve roots due to the nature of their compliance. Firstly, at minimum VIA compliance, the simulator was adjusted for with heart rates 60, 72, 80 and 100 bpm with corresponding stroke volumes 60, 72, 70 and 80 mL. The systemic pressure was held between 120 to 80 mmHg for aortic heart valve roots and between 45 to 15 mmHg for pulmonary heart valve roots to represent *in vivo* conditions of the heart. The process was repeated with the VIA adjusted to its maximum compliance setting, with 125 mL air in the source chamber and 60 mL in the output chamber to produce physiological pressure and flow waveforms. It was observed that the VIA with maximum compliance adjustment reduced the forward flow volume displaced by the pump piston. Therefore, peak flow was used as the test condition rather than the stroke volume (Jennings et al., 2001). Therefore, VIA with maximum compliance and peak flow were considered as test conditions. The precise pulsatile flow conditions for specific heart valve root tests have been detailed in the relevant chapters. After setting the heart



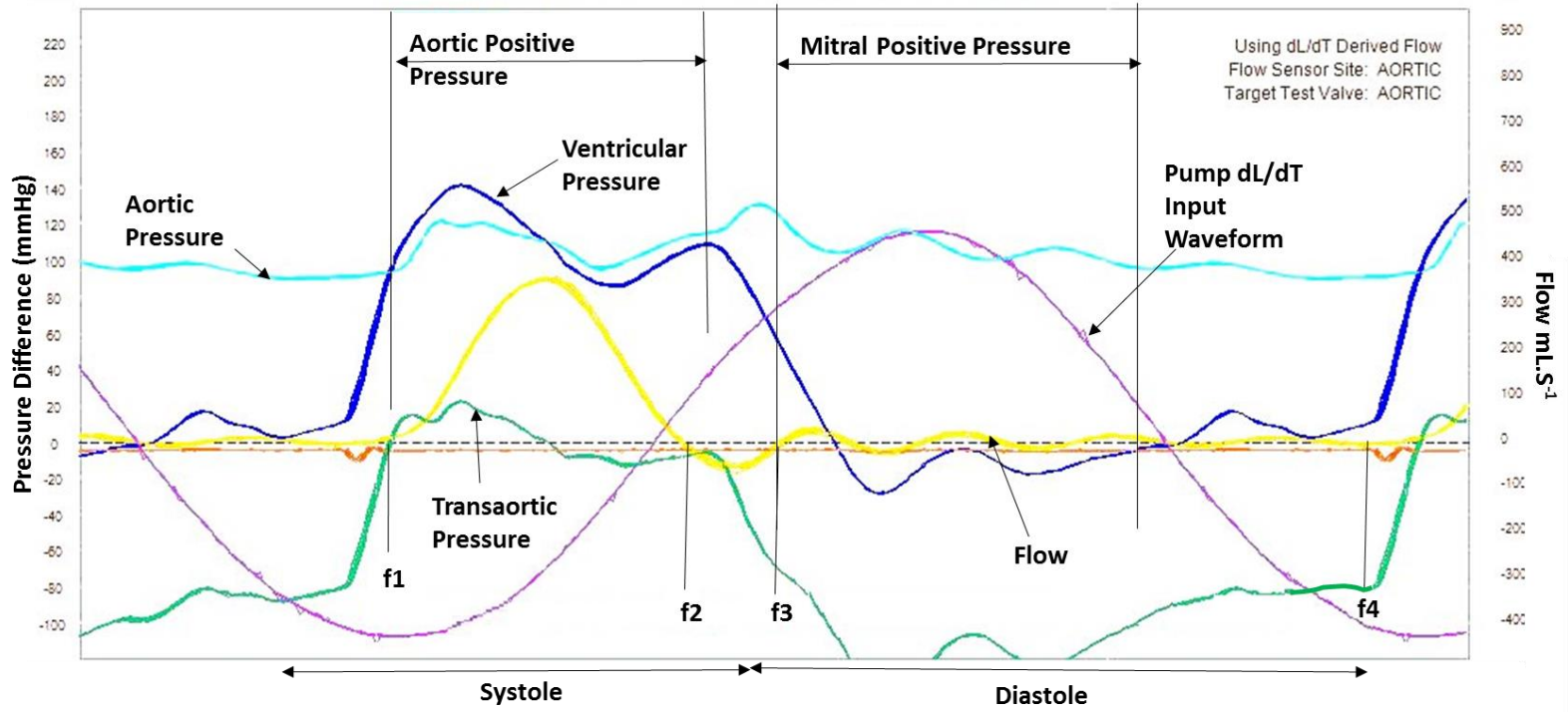
rate to 72 bpm and adjusting stroke volume or peak flow, a 2 second video clip of leaflet motion under pulsatile conditions was recorded using an AOS Technologies S-PRI high speed camera set to a capture rate of 500 frames.s<sup>-1</sup>.

#### **2.4.7.5 Data Processing**

The performance of the heart valve roots was characterised by evaluating the leaflet dynamics, transvalvular pressure difference ( $\Delta P$ ) during forward flow, the heart valve root mean square (RMS) forward flow ( $Q_{RMS}$ ), and effective orifice area (EOA). The EOA was calculated using the formula that was derived by Gabbay et al. (1978),  $EOA = Q_{RMS} \text{ (mL/s)} / 51.6\sqrt{\Delta P \text{ (mmHg)}}$ . Typical pressure and flow waveforms obtained by ViVitro software for the BSM mechanical control valve are shown in Figure 2.17. All the flow and pressure crossover positioning, data acquisition, and analysis were in accordance with ISO 5840 (2015). During the test, the software captured data for 10 cycles. Once all pressure and flow crossover adjustment of 10 cycles was completed, means and standard deviations for the 10 cycles were saved as a .csv file (excel file) for further analysis. It was possible to obtain regurgitant volumes from pulsatile flow testing, but the data was not reliable due to artifacts in flow oscillations in the heart valve root during diastole (Jennings, 2001). Hence this data was not included in the results. However, closed regurgitant flow rates were determined in the competency testing to give an indication of performance during the closed phase.



(a)



(b)

Figure 2.17 Example of Acquired Pressure and Flow Curve (a) Minimum (b) Maximum Compliance

The flow and pressure crossover points detailed in Figure 2.17 are defined as follows:

**Flowrate**

f1	forward flow at the beginning of systole
f2	forward flow at the end of systole
f3	flow when the valve leakage begins or mitral valve starts to close
f4	flow at end of the cycle

**Pressure**

Aortic (positive)	pressure difference between the beginning and the end of systole positive pressure drop
Mitral (positive)	pressure difference between the beginning and the end of diastole positive pressure drop

All the tests were performed using physiological 0.9% (w/v) saline to maintain compatibility with the flow probe which measures the voltage of a conductive solution flowing through a magnetic field. The hydrodynamic performance of the heart valve roots were expressed as transvalvular pressure gradient versus RMS forward flow ( $Q_{RMS}$ ) and EOA. The RMS Forward Flow and transvalvular pressure was automatically calculated in the software with below formula:

$$\text{RMS forward flow } (Q_{RMS} \text{ mL}\cdot\text{s}^{-1}) = \text{RMS Flowrate } (f1 \text{ to } f2) * 1000 / 60 \text{ (s}\cdot\text{min}^{-1})$$

Transvalvular pressure difference ( $\Delta P$  mmHg) = Mean of pressure difference between outflow and inflow of points between f1 to f2.

The valve leaflet dynamics were assessed using an AOS Technologies S-PRI high speed camera recording at a rate of 500 frames per second during a complete cardiac cycle under pulsatile condition, when the heart rate was 72 bpm.

#### **2.4.7.5.1 Statistical Analysis**

Regression analysis was performed to assess the trend and the difference between transvalvular pressure of the heart valve roots (cellular and decellularised human pulmonary and aortic) for different RMS flow conditions. A second order polynomial trend line was fitted with R-squared value close to 1 in Microsoft Excel 2013. The mean EOA is presented as the mean  $\pm$  95 % confidence intervals. Statistical significance between the cellular and decellularised aortic heart valve roots (porcine and human), and between the cellular and decellularised human pulmonary heart valve roots, was determined using Student's t test using SPSS for Windows (version 21.0; SPSS, Inc., USA).  $P < 0.05$  was considered statistically significant.

#### **2.4.7.5.2 Validation of Pulsatile Flow Simulator**

The performance of the simulator was verified using a 23 mm Björk-Shiley mono leaflet (Shiley Corporation Incorporated, USA) mechanical control valve before each test. This valve was tested at heart rates of 60, 72, 80, 100 and 120 bpm with corresponding stroke volumes 60, 70, 70, 80 and 80 mL. A 50% input sine wave was used for all iterations. The systemic pressure was adjusted between 120 and 80 mmHg. The VIA was set for minimum compliance. The function of the valve was assessed using the mean  $\Delta p$ ,  $Q_{RMS}$ , and EOA. All data were processed and analysed using Microsoft Excel and compared with the historical data and test data for the same valve obtained during previous testing using a previous version of this pulsatile flow simulator by Jennings (2001). The recorded data was within a range of  $\pm$  5 % of the mean of the historical data.

### **2.4.8 Biomechanical Performance**

#### **2.4.8.1 Biomechanical Performance I: Expansion Characteristics (Dilation Testing)**

The circumferential expansion of each heart valve roots (cellular porcine aortic and pulmonary, human cellular and decellularised aortic, human cellular and decellularised pulmonary) was determined in terms of percentage dilation using a dilation test procedure adapted from previous studies (Wilcox et al., 2005, Jennings et al., 2002). Circumferential expansion is influenced by material properties of wall

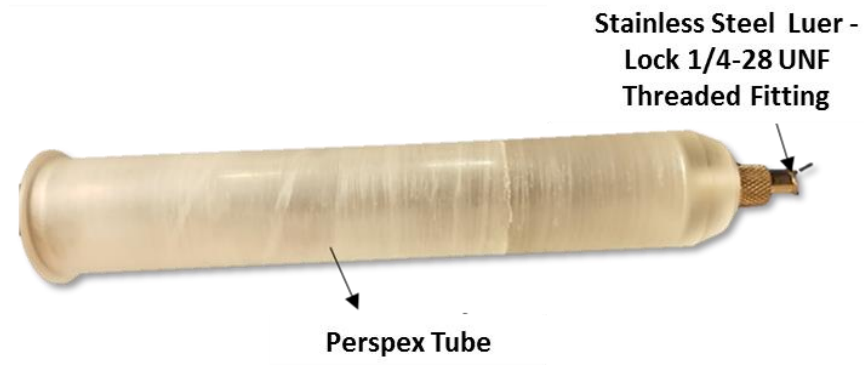
layers (Roach and Burton, 1957), but it is not indicative of wall stiffness because the expansion is also affected by heart valve root size and wall thickness. Jennings (2001) used different sizes of syringe to mount porcine heart valve roots. However, due to limitations in syringe size availability it was limited to test different sizes of the heart valve roots. Also there were a few other problems with the method such as pressure control, valve leakage and repeatability of the method. Therefore, it was essential to develop a robust dilation testing method. The design specification for the dilation tester is described in the Table 2.5.

**Table 2.5 Design Specification for Dilation Tester**

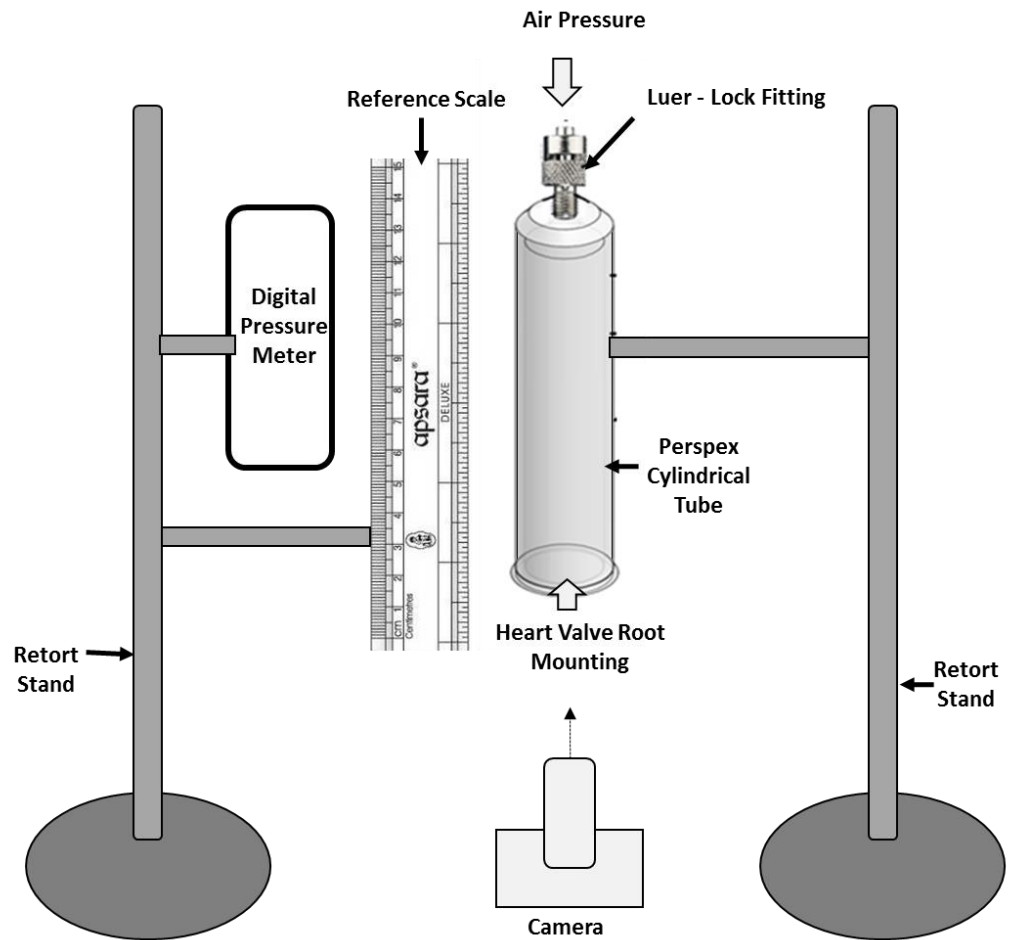
<b>Feature</b>	<b>Requirement/ Specification</b>
Dimensions	Able to fit various sizes of the heart valve roots ( $\varnothing$ 20-32 mm)
Material	Durable enough to withstand repeated use Able to clean thoroughly with disinfectant Able to see test fluid level
Operation	Easy mounting and removal of the specimen without causing damage Able to apply maximum pressure of 120 mmHg and easy to control

#### **2.4.8.1.1 Dilation Tester**

Cylindrical Perspex tubes of different sizes were designed to accommodate heart valve root sizes with diameters ranging from 20 to 32 mm. The narrow end of the Perspex tube was connected to a stainless steel luer lock 1/4-28 UNF threaded fitting for easy and leak free connection of tubing with air pressure supply (Figure 2.18).



**Figure 2.18 Perspex Tube for Dilation Test Setup**



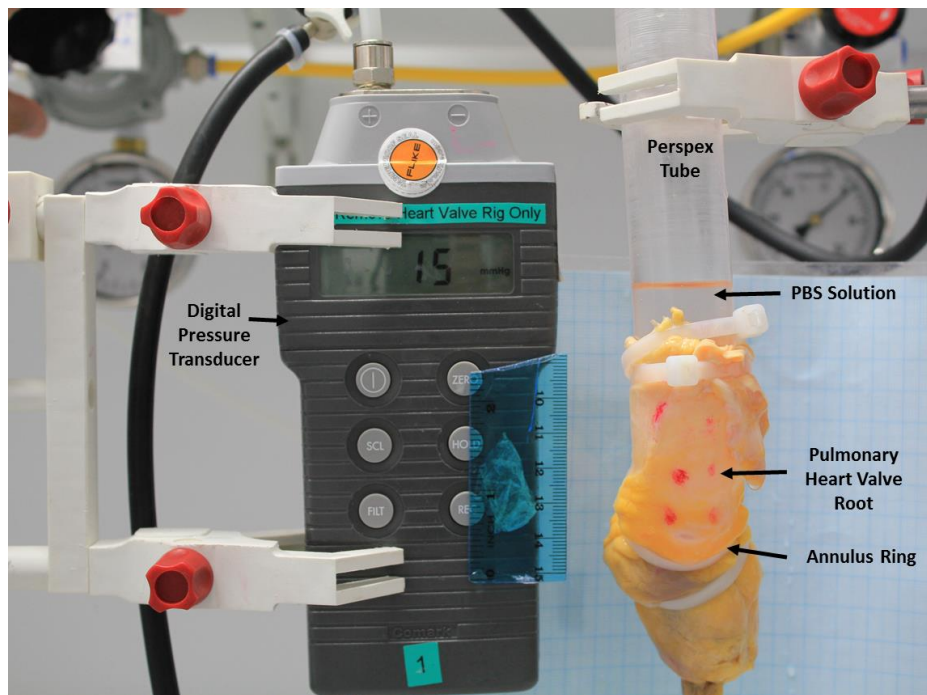
**Figure 2.19 Schematic Diagram of Dilation Test Setup**

The schematic diagram of dilation test set up is shown in Figure 2.19. A Canon digital SLR 550 D camera was mounted perpendicular to the Perspex column (or heart valve root) to take images of the heart valve root. A reference scale and a digital pressure transducer (S/N: 63204/3, Comark Instruments, Inc.) were mounted on a

retort stand in the same plane as the Perspex column (or a heart valve root) for calibration.

#### 2.4.8.1.2 Test Procedure

The heart valve root outflow was mounted onto the wide end of the tube and secured with a cable tie. The myocardial end of the heart valve root was free to move longitudinally, allowing the heart valve root to expand freely in the axial direction. For the pulmonary heart valve roots, an appropriately sized annulus ring (Figure 2.20) was used due to the fact that when removed from the heart the pulmonary heart valve root is hardly supported by the thin right ventricle myocardium, whereas aortic heart valve root is supported by the thick left ventricle myocardium.

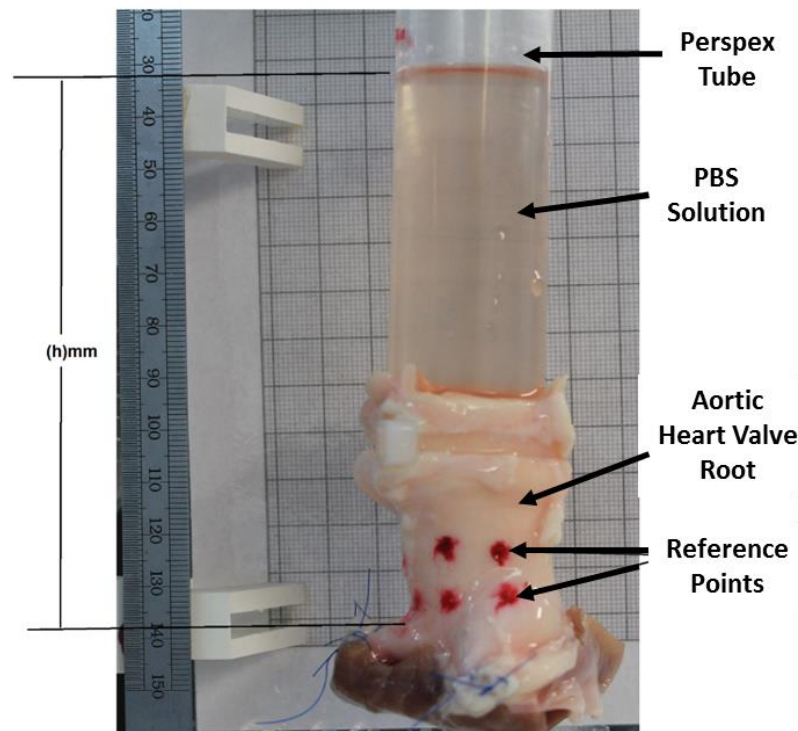


**Figure 2.20 Dilation Testing Setup for Pulmonary Heart Valve Root with Annulus Ring**

One end of the 3 way connector was connected to a digital pressure transducer and another to a pneumatic air regulator. The Perspex tube was filled with PBS solution through the three-way connector and gradually pressurized using a pneumatic air regulator. The root was marked with reference points at least 5 mm above the sinotubular junction to help identify relative deformation using a tissue marking dye. Pressure was increased in increments of at least 5 mmHg and the heart valve root was photographed at each increment. The images were taken such that



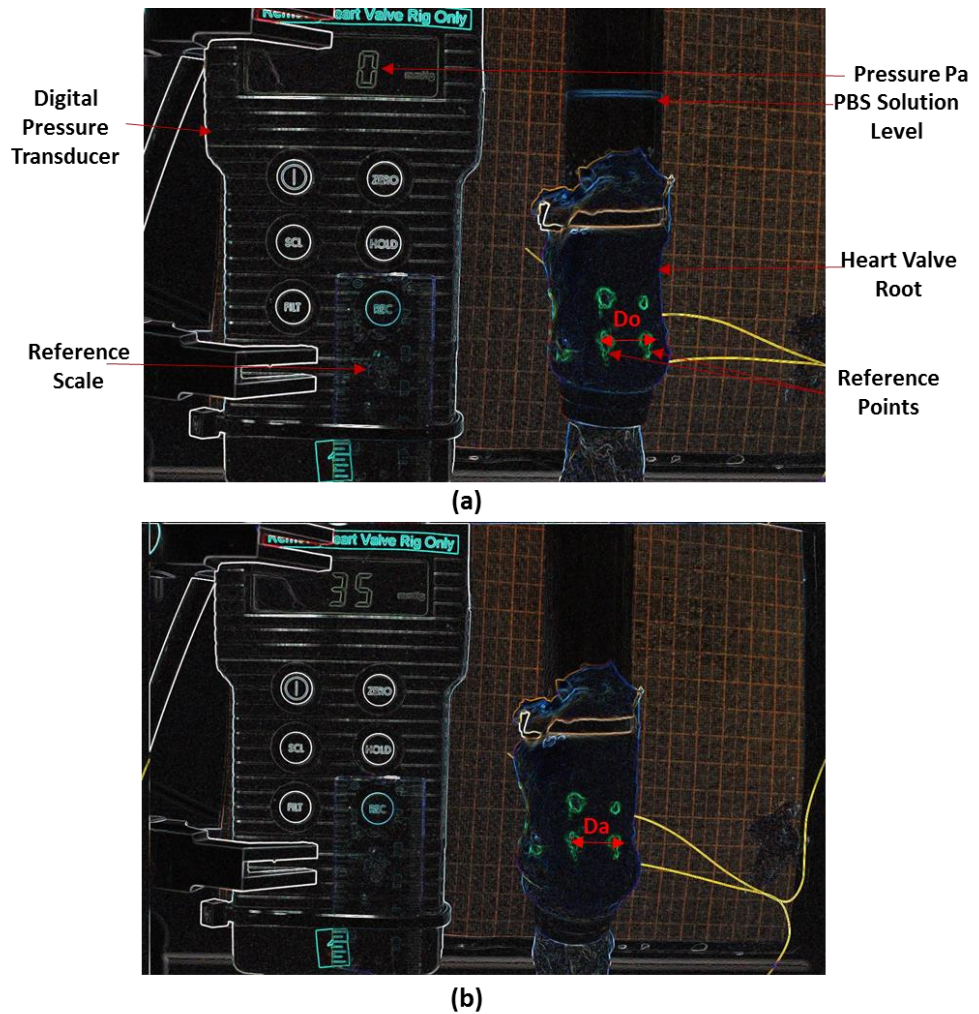
the digital display of the pressure meter and the reference scale were in the field of view. The process stopped when the maximum pressure was reached or until the heart valve root “failed”, whichever occurred first. The maximum applied pressure for aortic and pulmonary heart valve roots was 120 and 35 mmHg respectively. Failure was considered when the PBS solution leaked out of the heart valve root faster than the pressure could be applied.



**Figure 2.21 Static Pressure Calculation during Dilation Testing**

A preliminary image, without application of any external pressure, was also captured to help calculate the static pressure experienced by the heart valve root due to PBS solution level in the Perspex tube (Figure 2.21). First the scale was calibrated using the reference scale (10 mm) as the reference to convert pixels to millimeters. Then the measured height ( $h$ ) of the column of PBS solution divided by 13.6 (mercury is approximately 13.6 times denser than the PBS solution) to measure the static pressure ( $P_o$ ) in millimetres of mercury. This static pressure value,  $P_o$ , was added to all the other applied pressure values ( $P_a$ ). The height ( $h$ ) of PBS at the start of the test was different for each heart valve root, resulting in different final pressure values  $P_f$  ( $P_f = P_a + P_o$ ) for all the heart valve roots.

### 2.4.8.1.3 Data Analysis



**Figure 2.22 Representative images taken during dilation test at (a) 0 mmHg and (b) 35 mmHg**

All the images were uploaded into ImageJ, a Java-based open source image processing software ImageJ (NIH, Bethesda, MD), for analysis.

Image stacks of pressure measurements for each heart valve root were collected and aligned on a single canvas using the ImageJ plug-in called Montage. An edge detection plug-in in ImageJ was used to find the edges of the reference marks and the heart valve root (Figure 2.22).

The distance  $D_a$  between two reference marks were measured for each pressure  $P_a$ . Similarly, the distance  $D_o$  was measured at pressure  $P_o$ . The formula shown below was used to measure percentage dilation for each pressure measurement:

$$\text{Percentage Dilation} = \frac{D_a - D_o}{D_o} \times 100$$

The results for each heart valve root are presented in terms of percentage dilation as a function of internal pressure. The mean percentage dilation is presented at 20 mmHg for pulmonary and 40 mmHg for aortic heart valve roots.

#### **2.4.8.1.4 Statistical Analysis**

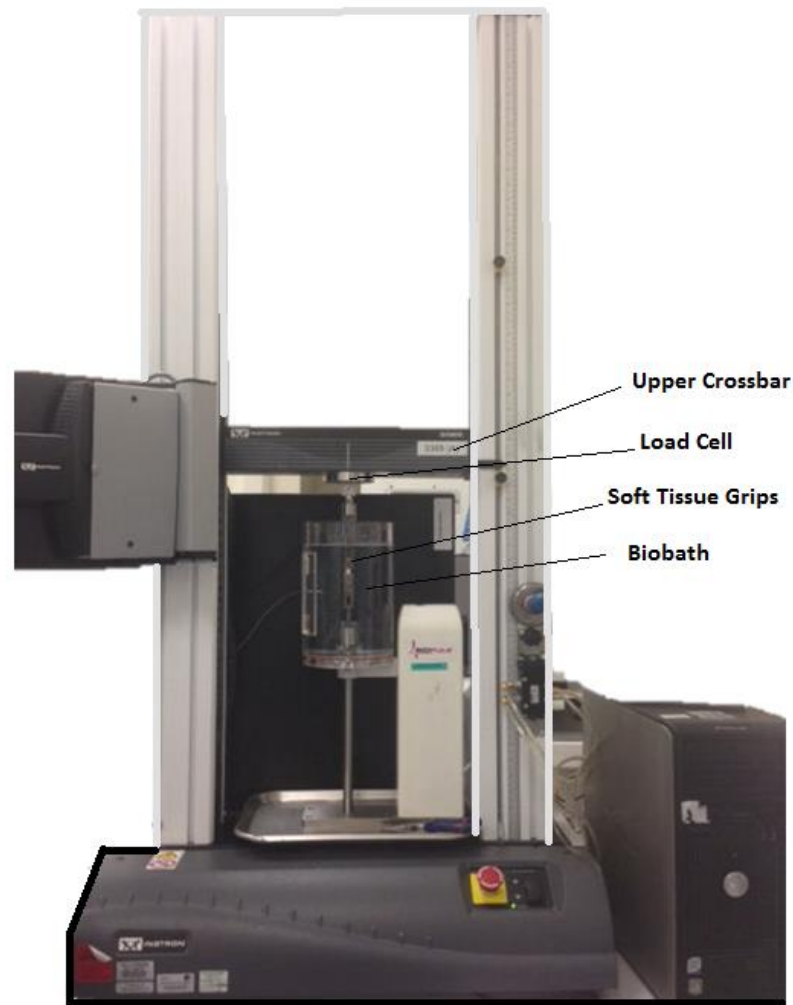
Statistical significance between two groups was determined by applying Student's t-test using SPSS for Windows (version 21.0; SPSS, Inc., USA). The significance level was set at 0.05.

#### **2.4.8.2 Biomechanical Performance II: Uniaxial Tensile Test and Suture Pull-Out Test**

The mechanical testing of soft biological heart valve roots is often confounded by local complexities introduced at sample-grip interfaces (i.e., bending, preloading, cross-section area measurement, stress concentrations, tearing). This requires additional diligence in ensuring the accuracy of measurements of all parameters. Also, it was important to develop an accurate, reliable, and repeatable test method to test this tissue under uniaxial tension.

##### **2.4.8.2.1 Uniaxial Tensile Tester: Instron 3365 (Instron® Corporation)**

Tensile material properties of the heart valve root (cellular porcine aortic and pulmonary, human cellular and decellularised aortic, human cellular and decellularised pulmonary, cellular ovine pulmonary, explanted decellularised porcine pulmonary, decellularised porcine pulmonary, cryopreserved cellular porcine pulmonary) wall and leaflets were determined using uniaxial tensile tests. Suture pull-out properties of the wall and myocardium of the heart valve root (cellular porcine aortic and pulmonary, human cellular and decellularised aortic, human cellular and decellularised pulmonary) were determined using suture pull-out tests. These tests were performed with an Instron 3365 materials testing machine (3365K5747, Instron® Corporation).



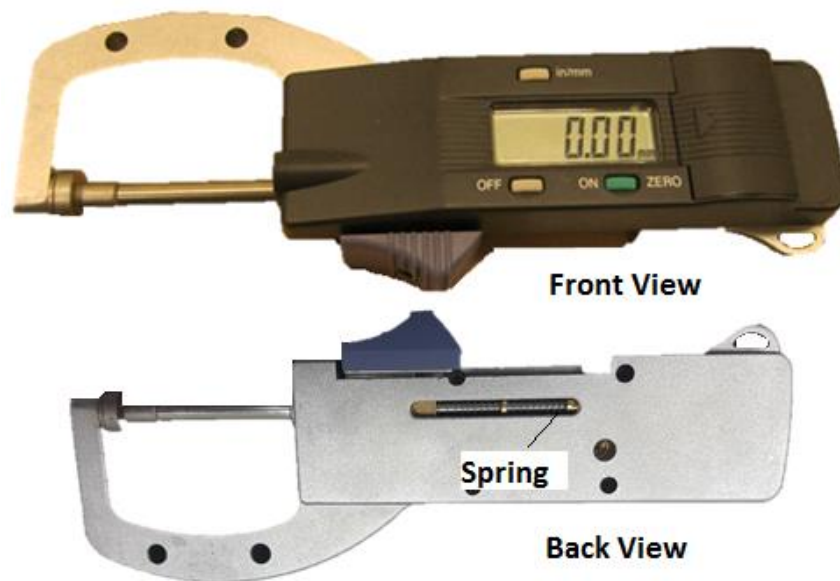
**Figure 2.23 Uniaxial Tensile Tester 3365 with Biobath**

The machine was equipped with a 50 N load cell (UKAS traceable calibrated), a biobath containing PBS, and a temperature control system (Figure 2.23). The Instron 3365 is a dual column table-top testing system, ideal for tension and/or compression applications. It has a capacity of 5 kN, maximum speed 1000 mm/min, and 1193 mm vertical test space.

#### **2.4.8.2.2 Thickness Measurement**

The thicknesses of the heart valve root wall and leaflet specimens were measured at six locations in gauge length area using two different tissue thickness gauges (Mitutoyo 700-122, James H. Heal J-40-V). Heart valve root wall and leaflet specimens are compressible. This means that they change their thickness depending on the vertical force applied on them. Therefore, great care was taken during

thickness measurements and thickness gauge with minimum specimen compression during thickness measurement was chosen.



**Figure 2.24 Mitutoyo Digital Thickness Gauge 700-122**

The porcine heart valve root specimens thickness were measured with a lightly spring loaded Mitutoyo (Model No: 700-122) quick mini digital thickness gauge (Figure 2.24). The thickness gauge was used in previous other studies to measure pulmonary valve wall (2011) and patellar tendon (Herbert et al., 2016). It had a 0-25.4 mm range and 0.01 mm resolution. The applied force on the tissue specimen was variable as it was hand held. The limitations of the thickness gauge were identified during the method evaluation study. As the heart valve root specimens were wet and the loading spring of the thickness gauge was exposed and resulted in frequent replacement of the spring due to stiction and corrosion. Also, it was difficult to hold the gauge length region of the tissue specimens (wall and leaflets) between the two anvils of the thickness gauge whilst holding the thickness gauge at the same time.

To eliminate limitations with the Mitutoyo thickness gauge a low load (0.05 N/cm<sup>2</sup>) digital thickness gauge J-40-V (James H. Heal and Company Limited) (Figure 2.25) with an accuracy of  $\pm 0.01$  mm was used. The J-40 V thickness gauge consisted of a fixed bottom anvil and a moving upper anvil with a diameter of 50 mm. The large upper anvils of the thickness gauge made it difficult to mount small specimen in the middle of the anvils for the thickness measurement. This issue was mitigated by Chapter 2

reducing the diameter of the top anvil to 10 mm which allowed for precise positioning of the specimen between the anvils. The modified size of the top anvil relative to the bottom anvil is shown in Figure 2.25.



**Figure 2.25 Digital Thickness Gauge J-40 V (James H. Heal and Company Limited)**

During measurement, the specimen was carefully placed on the middle of the bottom anvil and the top anvil was moved downward until it touched an area of the specimen. The resulting height was recorded. To prevent the specimens from drying out, PBS was regularly applied with a syringe during measurement, as dehydration may have led to underestimation of the specimen thickness due to shrinkage. This method gave an accurate measure of the thickness and was free of any error due to change in load associated with spring loaded thickness gauge.

#### **2.4.8.2.3 Uniaxial Tensile Test**

Uniaxial tensile testing of heart valve tissue specimens has always raised the question of test reliability. Because of their viscoelastic characteristics and low friction between the holder material and wet soft biological tissue specimen, it is difficult to hold them rigidly at *in vitro* strain and tensile load. Excessive compression on the soft tissue will elevate stress around the contact area, which leads to rupture

before target loads are achieved, too little compression will result in slippage. Therefore, it was deemed important to develop a holder for tensile testing of heart valve tissue specimens. To achieve to the best holder design to allow effective characterisation of the tensile properties of the heart valve tissue specimen. Design specification for the holder is described in Table 2.6.

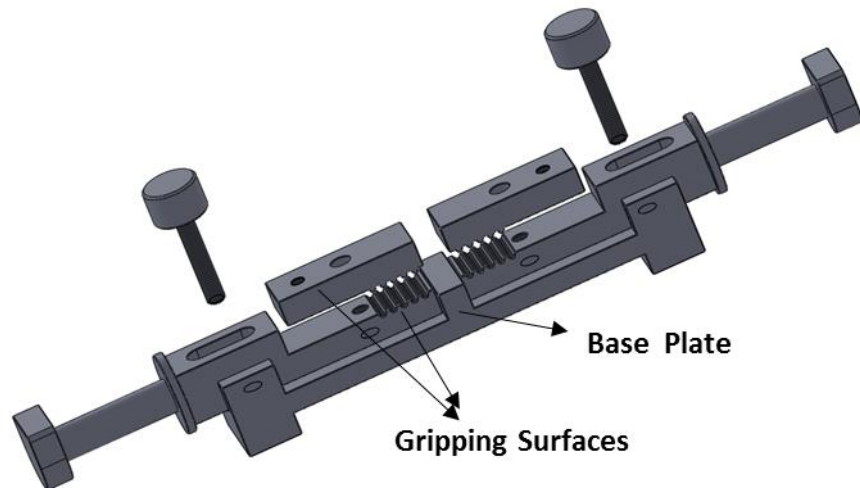
**Table 2.6 Design Specification for the Holder to Test Heart Valve Specimens under Uniaxial Tensile Testing**

Feature	Requirement/ Specification
Dimensions	Must be able to fit in the uniaxial tensile tester 3365 and able to connect with 50 N Load cell and Bio bath
Material	Durable enough to withstand repeated use Able to clean thoroughly with disinfectant /Autoclavable
Operation	Easy mounting and removal of the specimen without causing damage Able to hold specimen rigidly at maximum load 30 N Able to hold specimen with different thickness and texture (aortic and pulmonary walls and leaflets)

#### **2.4.8.2.3.1.1 Holder Design and Specimen Clamping**

Securing the wall and leaflet specimens to the grips for uniaxial tensile testing for accurate tensile testing posed many challenges and required some innovative solutions. In order to measure accurate stress strain characteristics of the specimens, it was imperative to ensure a firm grip between the specimen and the grips without damaging the specimen. Designing a holder with gripping surfaces that could hold the specimens tightly without damaging them was one of the important criteria as described in Table 2.6. For this purpose, a holder was redesigned. The new design (Figure 2.26) was simple, light weight, and easy to mount in the Instron machine.



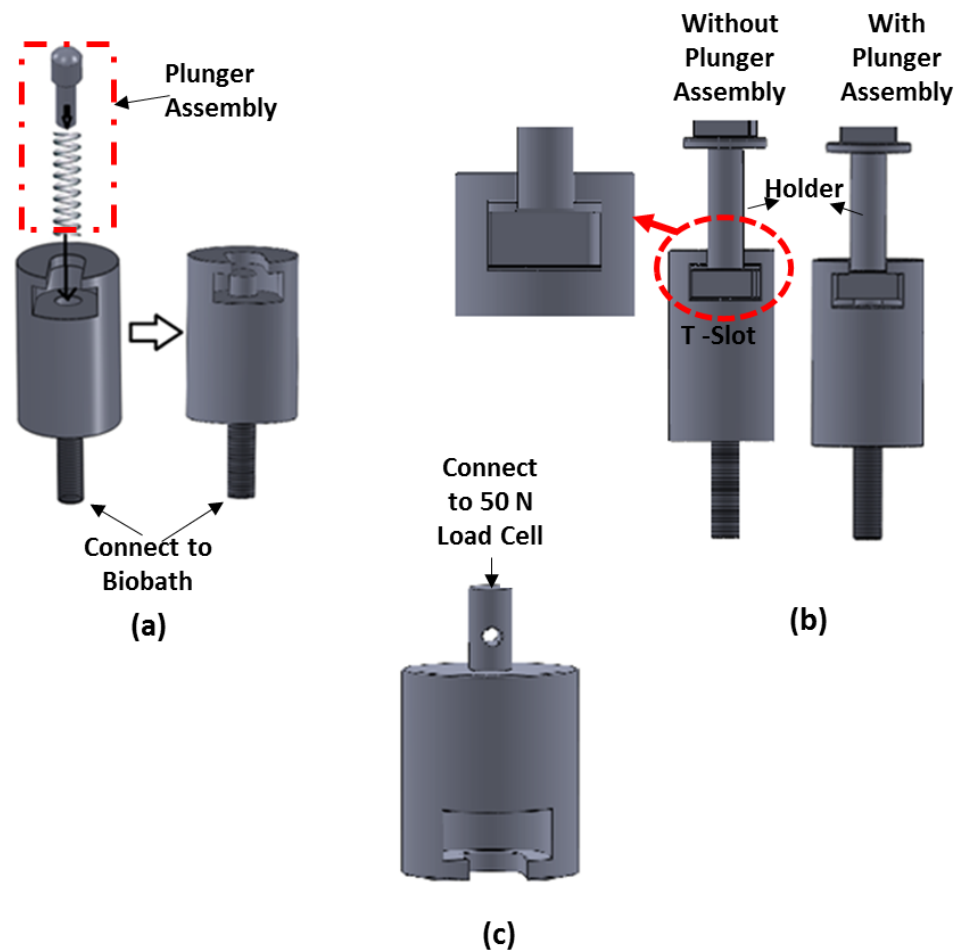


**Figure 2.26 Tissue Specimen Holder for the Uniaxial Tensile Tester**

The holder was made of titanium and had two different gripping surfaces for testing different types of tissues such as leaflet and wall of the heart valve root. It was required that holder should fit with the Bio bath and 50 N load cell. Therefore, two adapters (bottom adaptor – connect to Bio bath Figure 2.27 (a), Top adaptor – connect to 50 N load cell Figure 2.27 (C)) were designed. Both the adapters were T-slotted as shown in Figure 2.27, so the holder could be easily mounted and removed from the Instron. The plunger assembly was inserted in the hole of the bottom adaptor (connected to the Bio bath) as shown in Figure 2.27 (a). As the plunger assembly was spring loaded, it allowed automatic adjustment of the slack between the holder and adaptor as shown in Figure 2.27 (b).

One challenge in the tensile testing of the heart valve tissues was defining the gauge length and mounting the tissue in its fully relaxed state, therefore not pre-tensioning the tissue. The gauge length refers to reference length of a test specimen at which it begins to resist load. The holder design allowed adjustment of the specimen gauge length before it was mounted in the Instron. Base plates with different gauge blocks were used to set up different gauge lengths (Figure 2.26).

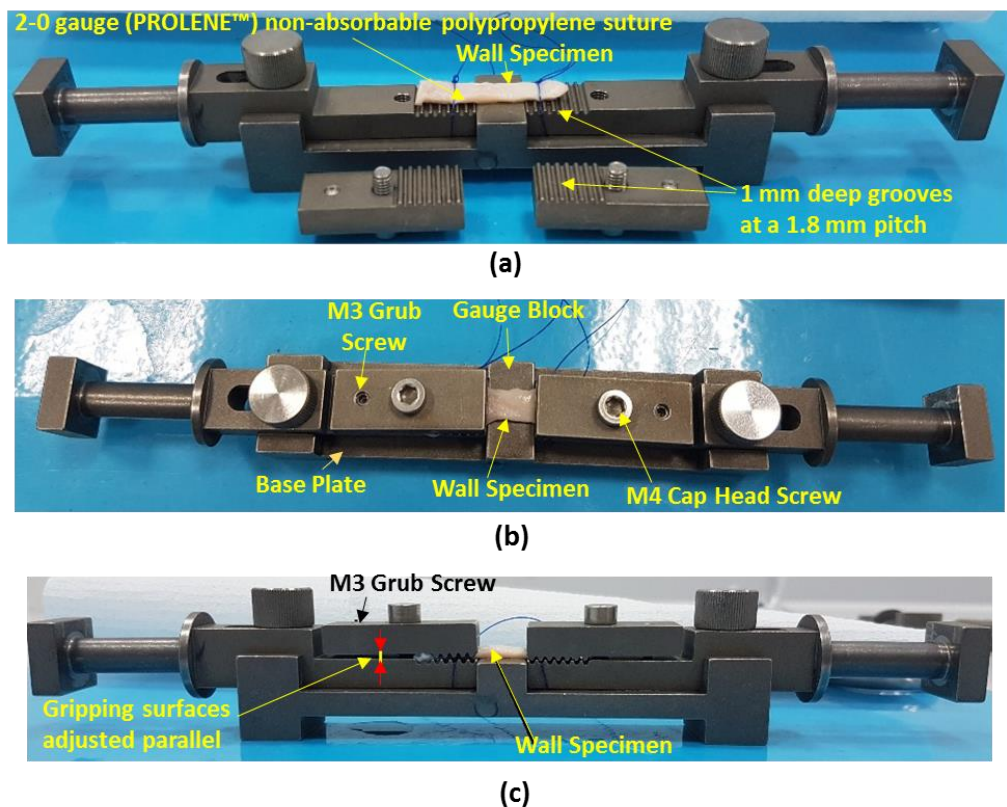




**Figure 2.27 (a) Bottom Adaptor with Plunger Assembly – Connect to Bio Bath (b) Spring Loaded Plunger Assembly Automatically Adjusts Holder Slack (c) Top Adaptor –Connect to 50 N Load Cell**

As described in Table 2.6, the other requirement of the holder design was the capability to hold specimens without damage. The tissue wall specimens were thick and slippery, whereas the leaflet tissue specimens were very thin and fragile. All the preliminary prototypes which were used in previous studies were tried to prevent the grip-specimen slippage during testing including serrated jaws (Jennings, 2001), sandpaper (Warnock et al., 2010, Sokolis et al., 2002), tissue paper (Seebacher et al., 2008), etc. None of the gripping techniques were capable of holding the specimen without damaging it. It was observed that wall tissue specimens were much more 'slippery' compared to leaflet tissue specimens. The answer to this challenge consisted of two parts: redesigned grips and sutures to hold the tissue. The gripping surfaces for wall and leaflet tissues were redesigned to minimise damage to specimens during the mounting and to avoid premature failure at grip edges during

the testing. A holder with gripping surfaces consisting of 1 mm deep grooves at a 1.8 mm pitch was used for wall tissue specimens. A holder with finer gripping surfaces, 0.5 mm deep grooves at 0.8 mm pitch, was used for leaflet tissue specimens. Slipping or failing at the grips during specimen mounting was prevented by using a 2-0 gauge (PROLENE™) non-absorbable polypropylene suture to hold the wall tissue specimen in the middle of the grips. Both ends of the tissue specimens were tied with suture to the lower face of the grips as shown in the Figure 2.28 (a) and (b).



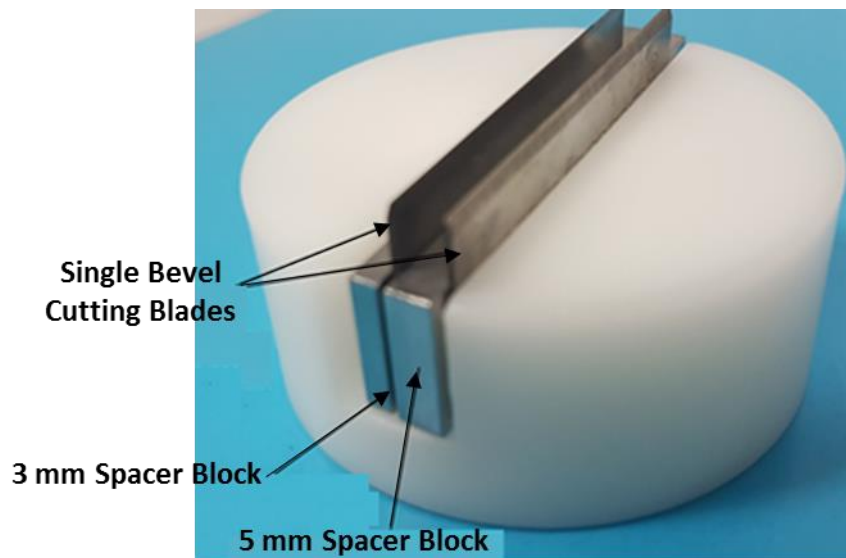
**Figure 2.28 Clamping of the Wall Tissue Specimen (a) with Polypropylene Suture to hold the wall specimen in the middle of the grips (b) Top View (c) Side View**

One M4 cap head screw was used to fix the clamps together. Also a M3 grub screw was used to keep the two gripping surfaces parallel as shown in Figure 2.28 (c). The specimen was mounted in its fully relaxed state and care was taken to prevent specimen bending or stretching. This technique reduced the stress concentration at the grip specimen interface. It was predicated that the suture, which helped to keep the specimen in the middle of the grips during the mounting and act as a dissipater to reduce stress at grip-specimen interface.

The tissue specimen holder and adapters (Appendix B) were drawn in SolidWorks by technician Rhys Moore, Faculty of Engineering, University Of Leeds.

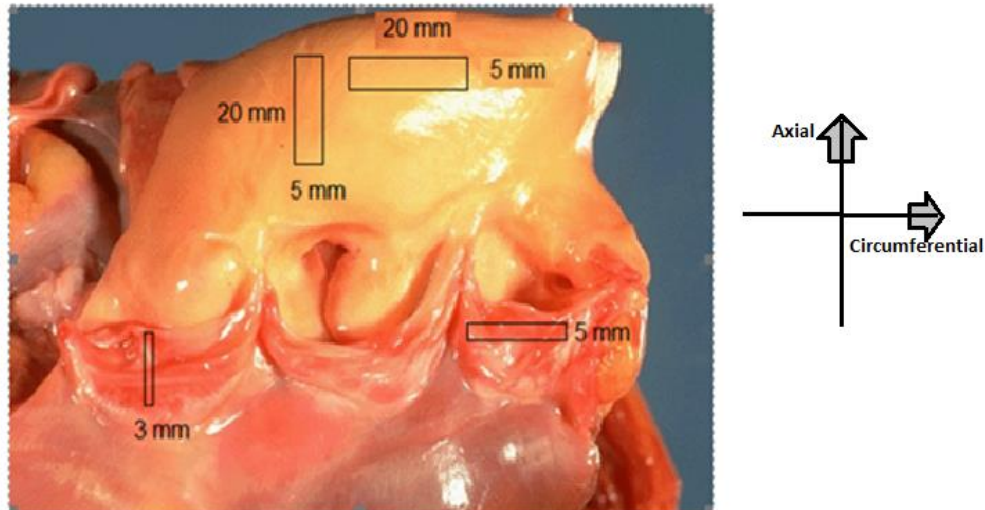
#### 2.4.8.2.3.1.2 Specimen Preparation and Cross Sectional Area Measurement

Accurate measurement of cross-sectional area of wall and leaflet tissue specimens is critical for calculation of their material properties. In this study, the specimen width was controlled using a custom made cutter shown in Figure 2.29. The cutter consisted of two single bevel cutting blades with two stainless steel spacer blocks. The spacer block (5 mm or 3 mm) between the two blades defined the gauge width of the tissue specimen.



**Figure 2.29 Specimen Cutter**

Specimens with an approximate length of 20 mm and width of 5 mm were taken from each heart valve root wall in the axial and circumferential directions. These strips were cut at least 2-3 mm above the sinotubular junction (Figure 2.30). Sections of the leaflet were cut from the same heart valve root in the radial and circumferential directions. Due to sample size limitations, valve leaflets were cut into width of 5 mm in circumferential and 3 mm in radial direction with maximum possible lengths from each valve.



**Figure 2.30 Specimen Preparation**

The gauge length was 10 mm for the wall tissue specimens in both the axial and circumferential directions and leaflet specimens in the circumferential direction. Whereas, the gauge length was 6 mm for all the leaflet radial specimens. It was notably difficult to cut the leaflet specimens to the correct dimensions. To ease the cutting process, the leaflets were placed on a thin transparent plastic sheet over coloured paper. The leaflets were kept hydrated with PBS solution during the cutting process. The thickness of the specimens was measured as described in Section 2.4.8.2.2.

#### **2.4.8.2.3.1.3 Test Procedure**

Consistency in the physiological environment during testing, for factors such as hydration and temperature, helps to make procedures repeatable and reliable. A bio bath with PBS solution at 37°C was used to achieve a controlled physiological environment. First the bio bath and grips with specimens were mounted in the Instron. Then the specimen thickness, width, and length were entered in the software. Initial extension and load measurement were reset to zero. Test data was recorded as the change in length of the tissue and the corresponding force detected on the load cell. The data was stored in Microsoft Excel format. A strain rate of 10 mm.min<sup>-1</sup> (0.028 s<sup>-1</sup>) was used for all the specimens. A similar strain rate had been used in previous studies to test similar tissues, such as human thoracic aorta (Duprey et al., 2010), mitral valve tissue (Kunzelman and Cochran, 1992) and porcine

pulmonary valve tissue (Bader et al., 1998). No preloading or preconditioning was used. The intrinsic properties of the test specimen in the elastin phase may alter due to preloading by starting the data collection at an arbitrary value rather than the relaxed state of the specimen.

#### **2.4.8.2.3.1.4 Data Processing**

The load (N) and corresponding displacement (mm) was recorded for each test by the Bluehill 2 software (Version 2.35.917). This data was stored in Microsoft Excel files for further analysis. The data (load and displacement) were converted to stress (MPa) and strain as follows:

$$\text{Engineering Stress } (\sigma) = \frac{F}{A_0}$$

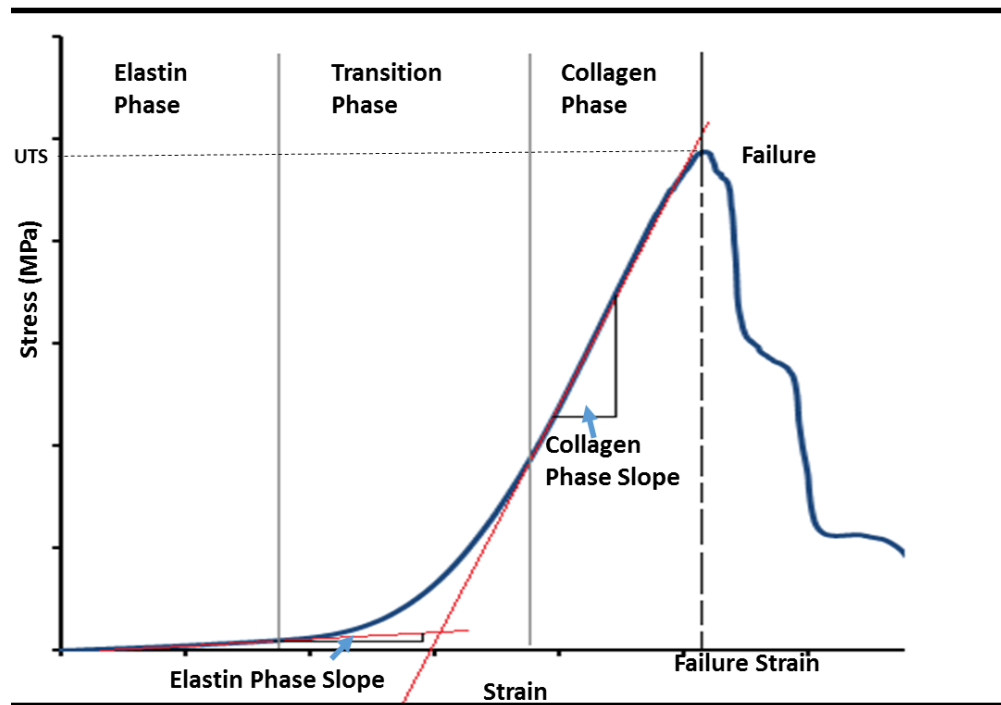
Where  $A_0$  is the initial cross-sectional area = specimen width x specimen thickness, and  $F$  is the load in Newtons registered by the Instron machine.

$$\text{Engineering Strain } (\epsilon) = \frac{L}{L_0}$$

Where  $L_0$  is the original gauge length during tensile testing, and  $L$  is the extension from the original gauge length.

The engineering stress–engineering strain data must be interpreted with caution because during uniaxial tensile testing the specimens experience significant change from their original dimensions during testing. Conversely, the true stress–true strain can give a more direct measure of the material's response instantaneously. Hence, for testing associated with large strain and significant reduction in cross-sectional area, the true stress (force divided by instantaneous area) and a higher order strain may be preferable. However, to determine true stress-strain, it requires the right equipment in order to measure the instantaneous changing values of width and length of specimen during testing.

Therefore, the data was analysed using engineering stress versus engineering strain graphs, considering uniform cross-sectional during testing; this made the measurement easier to perform, but the results can be only comparative, not absolute.



**Figure 2.31 Typical Stress-Strain Graph of Heart Valve Tissue Specimen Subjected to Uniaxial Tensile Loading to Failure.**

For each specimen, a stress-strain graph was created. Two linear regions (elastin and collagen) of the stress-strain graphs were approximated. Elastin phase slope and collagen phase were created through linear regression of the linear portions of the stress-strain graph performed in Microsoft Excel. In order for a test to be valid the trend line was required to have an  $R^2 > 0.85$ . The maximum failure stress value was referred to as the ultimate tensile strength (UTS).

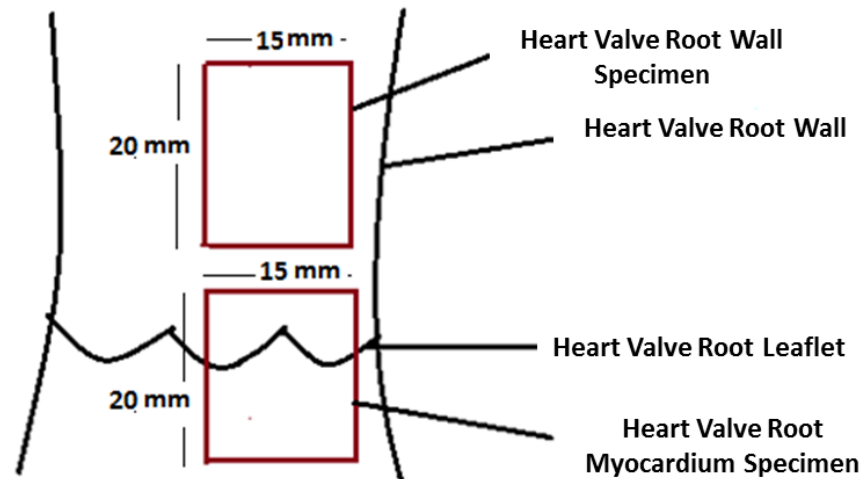
#### **2.4.8.2.4 Suture Pull-out Test**

The suture retention properties of heart valve root tissues were investigated in this study because the decellularised heart valve roots must have adequate suture retention strength, and hence, be capable of resisting sutures from pulling through.

The suture pull out method was adopted from the method described by ISO 7198 (2016) for Cardiovascular implants - Tubular vascular prostheses.

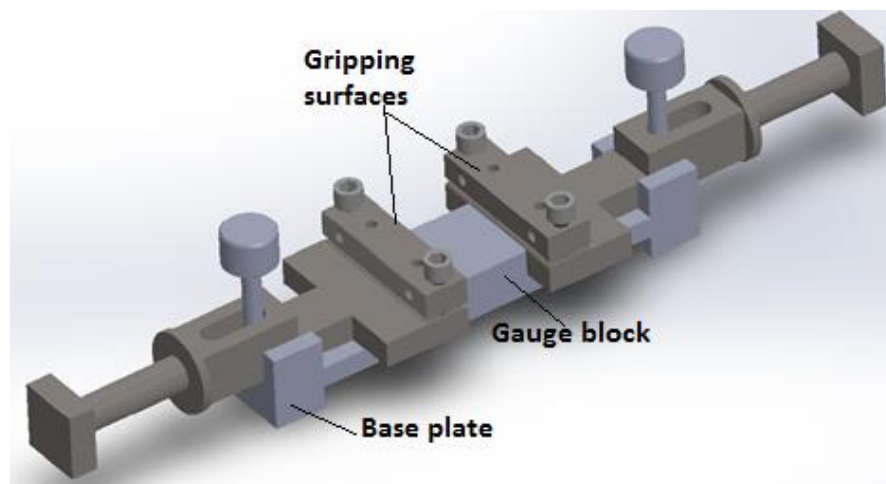
##### **2.4.8.2.4.1.1 Specimen Preparation**

The specimens were taken from the wall and myocardium of each heart valve root. All specimens were cut axially into a 20 mm x 15 mm strip as shown in Figure 2.32.



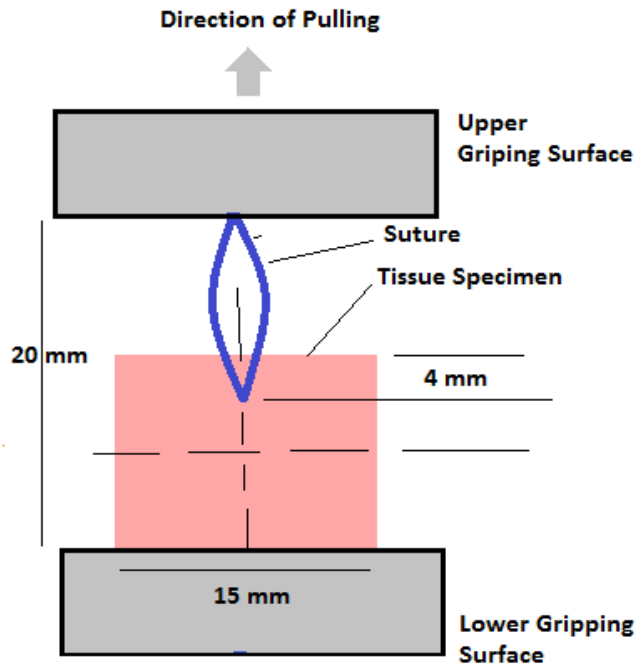
**Figure 2.32 Specimen Preparation for Suture Pull-Out Testing**

A holder with wider custom made grips (Figure 2.33 ) was designed on the basis of the holder used for tensile testing (Section 2.4.8.2.3.1.1) to secure the wider tissue specimen.



**Figure 2.33 Tissue Specimen Holder for the Suture Pull-Out Testing**

One end of the specimen was clamped. A 5 mm suture loop (4-0 non-absorbable monofilament suture with taper needle, Premilene®) (Karck and Haverich, 2005, Park et al., 2012) was created at the centre of the other end of the specimen, 4 mm from the free edge (Figure 2.34).



**Figure 2.34 A Sample Specimen Showing the Position of Suture through Material**

The suture was clamped on the upper gripping surface. The full specimen clamping arrangement was mounted in the Instron 3365 (Instron, Bucks, UK), uniaxial tensile tester. A 50 N load cell was used and strain was applied at a rate of 10 mm/min. The thickness of the specimens were measured at the suture insertion point using a thickness gauge J- 40 V as described in Section 2.4.8.2.2. The tests were continued until the suture was completely pulled out from the specimens.

#### **2.4.8.2.4.1.2 Data Processing**

The peak load was recorded as the maximum suture pull-out force and the type of failure was recorded. The peak load recorded was reported as the suture pull-out force. Also resistance to tearing was calculated by using the formula below.

$$T = F_{\max} / t$$

Where  $T$  = Resistance to tearing (N/mm)

$F_{\max}$  = Maximum suture pull-out load measured in Newton

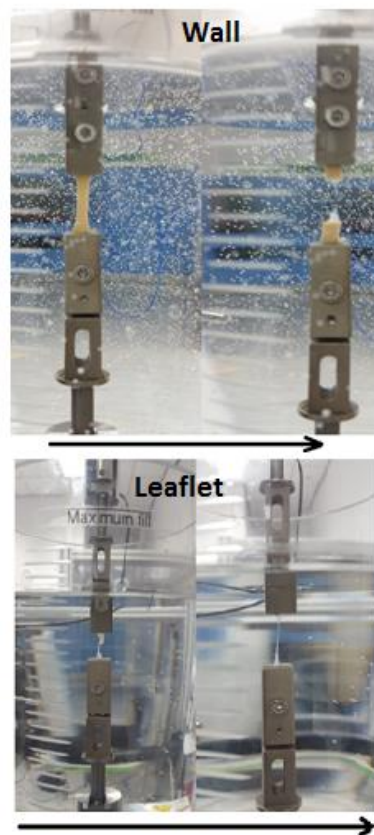
$t$  = Thickness measured in mm

#### **2.4.9 Tissue Behavior**

Images were taken during the uniaxial tensile testing of the wall and leaflet specimens and suture pull-out testing of the wall specimens. It was observed that the

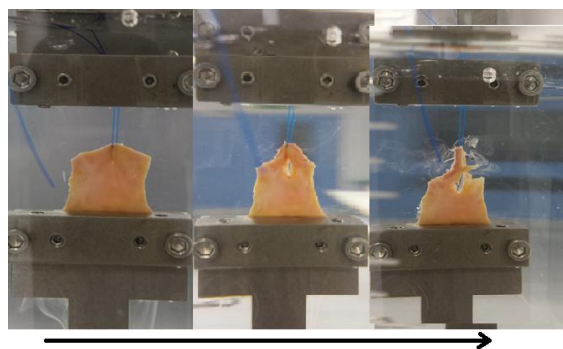


majority of the wall and leaflet tissue specimens (aortic and pulmonary) failed in the gauge length during uniaxial tensile testing (Figure 2.35).



**Figure 2.35 Representative Images of Tissue Specimens Undergoing Uniaxial Tensile Testing**

During suture pull-out testing of the wall specimens (aortic and pulmonary) the first sign of failure was the appearance of a small hole behind the suture. This was followed by a wedge shaped cut spreading from the suture in the circumferential direction perpendicular to the axial axis (direction of pulling) (Figure 2.36).



**Figure 2.36 Circumferential Wedge Propagation in the Wall Specimen due to a Suture Pull-Out Load in the Axial Axis.**

#### **2.4.10 Statistical Analysis for Uniaxial Tensile Test and Suture Pull-Out**

##### **Test**

Analysis was carried out in Microsoft Excel 2013 and numerical data presented as the mean  $\pm$  95 % confidence intervals. The 95 % confidence intervals were calculated using Microsoft Excel. Differences between two means were assessed using a Student's t-test. For all analyses, the significance value was set to  $p \leq 0.05$ . All analyses were performed using the SPSS for Windows (version 21.0; SPSS, Inc., USA).

#### **2.5 Summary**

The use of experimental methods for *in vitro* pre-clinical analysis is a well-established practice. However, the complex collagenous structure inherent in human heart valve roots warrants a truly complete picture of performance of heart valve roots. This requires accurate and robust *in vitro* analysis of functional performance of heart valve root. Keeping this objective in mind, the preceding sections in this chapter described robust, repetitive, and accurate biomechanical and hydrodynamic test methods to test biological heart valve roots.

### **3 *In vitro* Hydrodynamic and Biomechanical Performance of Cellular Porcine Aortic and Pulmonary Heart Valve Roots**

#### **3.1 Introduction**

This study addressed the practical aspects of implementing and evaluating the research methods described in Chapter 2 to assess hydrodynamic (competency and pulsatile flow) and biomechanical (dilation, uniaxial tensile and suture pull-out) performance of heart valve roots before applying the methods to decellularised human (aortic and pulmonary) and decellularised porcine pulmonary heart valve roots. This method evaluation process was designed to ensure that the methods produced results that were consistent with existing data in the literature. In this method evaluation study porcine heart valve roots were used because they are "healthy" and more consistent in properties compared to human roots which are highly variable due to age and lifestyle of the donors. Cellular porcine samples are widely used in cardiovascular research due to the circulatory system being comparable to that of humans (Schuster et al., 2010). In addition, low infection risk, ease of availability, and low cost have led to the extensive use of porcine samples in biomedical research. The hydrodynamic (Syedain et al., 2013, Fisher et al., 1986, Reimer et al., 2015, Jennings et al., 2002) and biomechanical (Korossis et al., 2002, 2014, Anssari-Benam et al., 2011) performance of porcine heart valve roots has been accepted as a near equivalent measure of human heart valve roots. In addition, robust hydrodynamic and biomechanical performance data for porcine aortic and pulmonary heart valve roots provided confidence in test methods as well as a benchmark control for comparison with decellularised heart valve roots.

#### **3.2 Aim and Objectives**

The aim of this study was to derive hydrodynamic and biomechanical performance of cellular porcine aortic and pulmonary heart valve roots and compare the performance with data published in the literature.

Specifically, the objectives of this study were:

1. To determine the hydrodynamic performance of cellular porcine aortic and pulmonary heart valve roots and compare to published data.
2. To determine the biomechanical performance of cellular porcine aortic and pulmonary heart valve roots and compare to published data.

### **3.3 Materials**

Six pulmonary (assigned identification PP1 to PP6) and six aortic (assigned identification PA1 to PA6) heart valve roots were dissected from porcine hearts, obtained from M & C Meats, Crossgates, Leeds and John Penny & Sons, Rawdon, Leeds, UK. For each performance assessment, six independent cellular porcine pulmonary and six independent cellular porcine aortic heart valve roots were used. The cellular porcine pulmonary and aortic heart valve roots were sized between 19 and 24 mm. The details of the heart valve root storage and defrosting procedure was described in Chapter 2 Section 2.4.4.

### **3.4 Methods**

#### **3.4.1 Hydrodynamic Performance of Cellular Porcine Aortic and Pulmonary Heart Valve Roots**

##### **3.4.1.1 Hydrodynamic Performance I: Competency**

The competency of each cellular porcine aortic and pulmonary heart valve root was measured in terms of leakage flow rate by applying a maximum static back pressure of 120 and 60 mmHg respectively. The time taken for this test fluid to drop to 80 mmHg (aortic) and 20 mmHg (pulmonary) were recorded. The root was considered to be competent if the pressure head had not dropped to 80 mmHg (for aortic) or 20 mmHg (for pulmonary) within a cut-off period of 30 minutes for aortic and 20 minutes for pulmonary heart valve roots. The detailed test procedure and test conditions for the competency testing of porcine pulmonary and aortic heart valve roots were described in Chapter 2 Section 2.4.6.1.3.

It was not considered necessary to measure the arterial diameter of the heart valve root during the competency assessment since this would not have given any further information to support the method evaluation.

### 3.4.1.2 Hydrodynamic Performance II: Pulsatile Flow

The hydrodynamic performance of the cellular porcine aortic and pulmonary heart valve roots was measured in terms of root mean square flow, transvalvular pressure difference and effective orifice area (EOA) using a pulsatile flow simulator. The EOA is presented as the mean  $\pm$  95% confidence intervals. The leaflet dynamics of the roots were measured with a high speed camera at 500 frames.  $s^{-1}$  at a heart rate 72 bpm.

**Table 3.1 Test Conditions Used in the Pulsatile Flow Performance of Cellular Porcine Aortic and Pulmonary Heart Valve Roots (Maximum Compliance Condition)**

	Aortic Heart Valve Root	Pulmonary Heart Valve Root
Heart Rate (bpm)	Mean Peak Flow (mL .s <sup>-1</sup> )	
60	249	239
72	352	348
80	383	388
100	546	537

The heart valve roots were mounted on the appropriate size of spigots as described in Chapter 2 Section 2.4.7.3 and tested as described in Chapter 2 Section 2.4.7.4. The heart valve roots were initially tested in the pulsatile flow simulator at minimum compliance with heart rates 60, 72, 80 and 100 bpm with corresponding stroke volumes 60, 70, 80 and 80 ml to determine the peak flow conditions required for the testing at maximum compliance, which are detailed in Table 3.1. The systemic pressure was held between 120 to 80 mmHg for aortic heart valve roots and between 45 to 15 mmHg for pulmonary heart valve roots to represent *in vivo* conditions.

### 3.4.2 Biomechanical Performance of Cellular Porcine Aortic and Pulmonary Heart Valve Roots

#### 3.4.2.1 Biomechanical Performance I: Dilation (Expansion Characteristics)

The circumferential expansion characteristics of each cellular aortic and pulmonary heart valve root wall was derived in terms of percentage dilation. As described in Chapter 2 Section 2.4.8.1.2, the test involved attaching the heart valve root (aortic and pulmonary) outflow to the end of a Perspex cylindrical tube with a

cable tie. The maximum applied pressures were 120 (aortic) and 35 mmHg (pulmonary) or until the valve “failed”. The percentage dilation was calculated for each pressure measurement. The results are presented as percentage dilation as a function of increasing pressure. The mean percentage dilation was recorded at 20 mmHg for the pulmonary and 40 mmHg for aortic heart valve roots. All data are presented as the mean  $\pm$  95% confidence intervals.

#### **3.4.2.2 Biomechanical Performance II: Uniaxial Tensile and Suture Pull-**

##### **Out**

The tensile material properties of the wall and leaflets from each cellular aortic and pulmonary heart valve root were characterised using the uniaxial tensile testing method. Two walls (axial and circumferential) and two arbitrary leaflets (radial and circumferential) specimens from each heart valve root were tested. The specimen sizes and test method were described in Chapter 2 Section 2.4.8.2.3.1.3. The ultimate tensile stress (UTS), failure strain and slopes for the elastin and collagen phases were determined for each specimen tested.

The maximum suture pull-out force was determined for additional wall specimens from each pulmonary and aortic heart valve root. The specimen sizes and test methods were described in the Chapter 2 Section 2.4.8.2.4. The peak load for each tested specimen was recorded as the maximum suture pull-out force. It was not considered necessary to determine the suture pull-out force of the myocardial specimen from the heart valve root since this would not have given any further information to support the method evaluation procedure.

The specimen thickness was measured with a Mitutoyo digital thickness gauge. All data are presented as the mean  $\pm$  95% confidence intervals.

### **3.5 Results**

#### **3.5.1 Hydrodynamic Performance of Cellular Porcine Aortic and Pulmonary Heart Valve Roots**

##### **3.5.1.1 Hydrodynamic Performance I: Competency**

The valve competency in terms of mean leakage flow times and rates for the cellular porcine aortic and pulmonary heart valve roots is shown in Table 3.2.

**Table 3.2 Mean Leakage Flow Times ( $T_L$ ) and Mean Leakage Flow Rates ( $F_L$ ) for the Cellular Aortic and Pulmonary Heart Valve Roots**

Cellular Porcine Aortic Heart Valve Roots				Cellular Porcine Pulmonary Heart Valve Roots			
Valve	$T_L$ second	$F_L$ $\text{mL}\cdot\text{s}^{-1}$	Competent Yes <sup>+</sup> Or No <sup>++</sup>	Valve	$T_L$ second	$F_L$ $\text{mL}\cdot\text{s}^{-1}$	Competent Yes* Or No**
PA1	832	1.86	No <sup>++</sup>	PP1	577	2.66	No**
PA2	>1800	<0.85	Yes <sup>+</sup>	PP2	684	2.97	No**
PA3	>1800	<0.85	Yes <sup>+</sup>	PP3	414	3.71	No**
PA4	>1800	<0.85	Yes <sup>+</sup>	PP4	262.5	5.85	No**
PA5	>1800	<0.85	Yes <sup>+</sup>	PP5	118	13.01	No**
PA6	>1800	<0.85	Yes <sup>+</sup>	PP6	421	3.65	No**

Yes<sup>+</sup> - leakage flow rate  $\leq 0.85 \text{ mL}\cdot\text{s}^{-1}$ , No<sup>++</sup> leakage flow rate  $> 0.85 \text{ mL}\cdot\text{s}^{-1}$

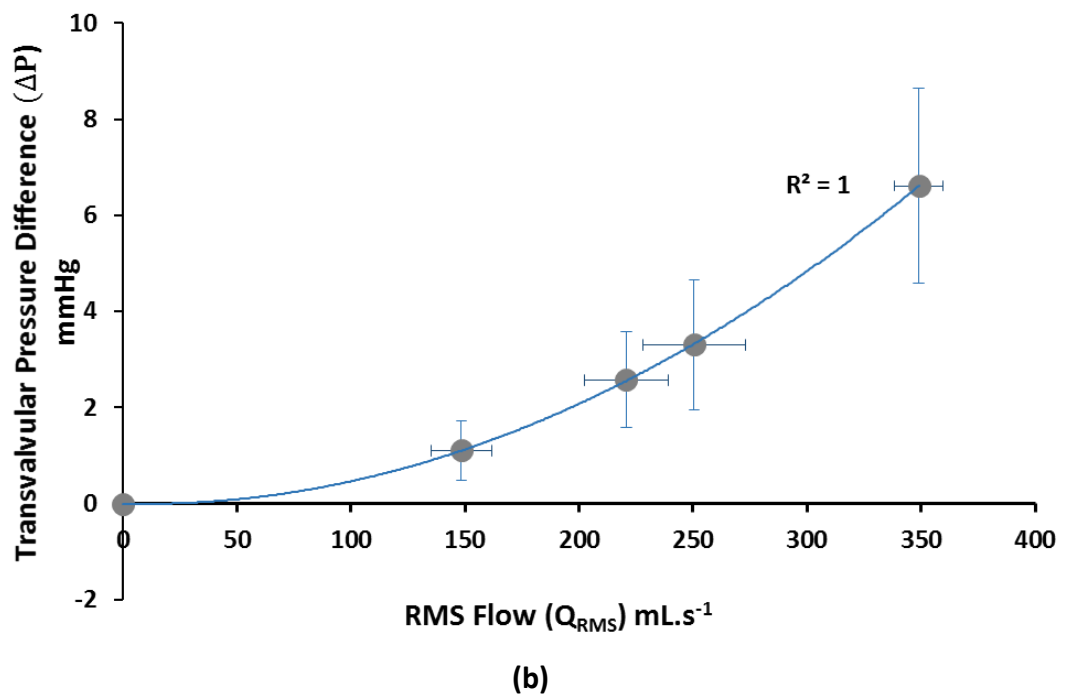
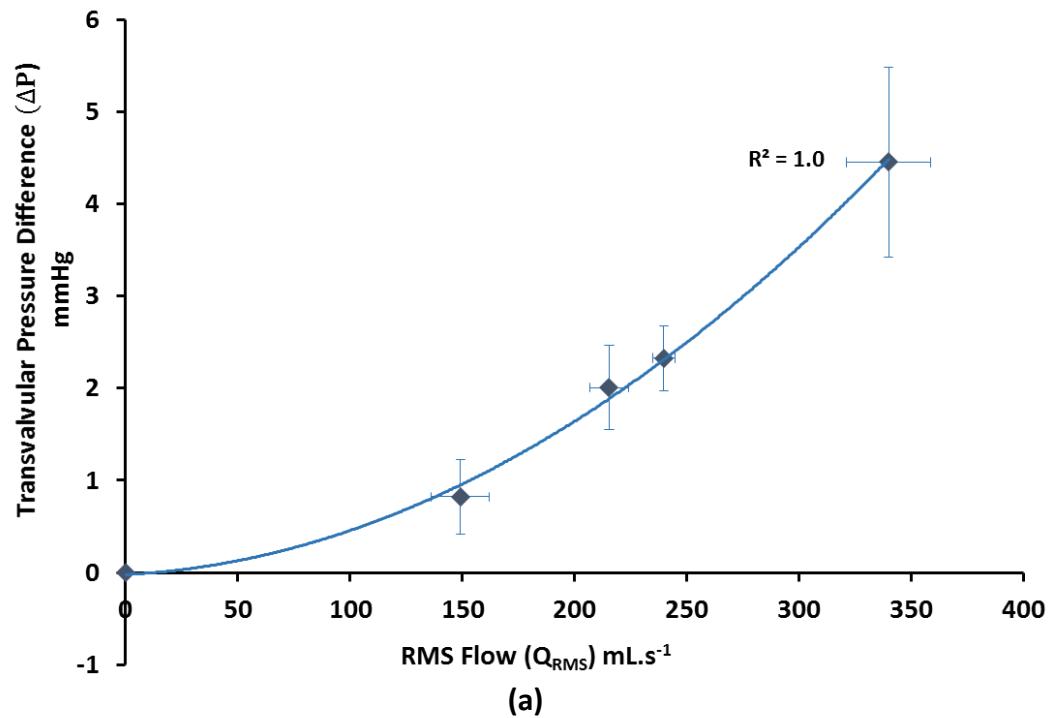
Yes\* - leakage flow rate  $\leq 1.28 \text{ mL}\cdot\text{s}^{-1}$ , No\*\* leakage flow rate  $> 1.28 \text{ mL}\cdot\text{s}^{-1}$

The majority of the cellular porcine aortic heart valve roots were competent with leakage flow rates lower than  $0.85 \text{ mL}\cdot\text{s}^{-1}$ , except heart valve root PA1 which had a mean leakage flow rate of  $1.86 \text{ mL}\cdot\text{s}^{-1}$ .

All six cellular porcine pulmonary heart valve roots were regurgitant and had a central regurgitant jet, taking on average 413 seconds to drop from 80 to 20 mmHg, giving a mean leakage flow rate of  $5.31 \text{ mL}\cdot\text{s}^{-1}$ .

### 3.5.1.2 Hydrodynamic Performance II: Pulsatile Flow

The mean transvalvular pressure difference and mean RMS forward flow for the six cellular porcine aortic and pulmonary heart valve roots is shown in Figure 3.1 (a) and (b) respectively. At a heart rate 72 bpm, the mean transvalvular pressure difference and the mean RMS flow for the porcine aortic heart valve roots was  $2.01 \pm 0.46 \text{ mmHg}$  and  $215.42 \pm 8.66 \text{ mL}\cdot\text{s}^{-1}$  respectively; and mean transvalvular pressure was  $2.57 \pm 0.99 \text{ mmHg}$  and RMS flow was  $220.73 \pm 18.31 \text{ mL}\cdot\text{s}^{-1}$  for the pulmonary heart valve roots.



**Figure 3.1 Mean Transvalvular Pressure Difference versus RMS Flow for Cellular Porcine (a) Aortic (b) Pulmonary Heart Valve Roots – Data fitted with second order polynomial trend line - The error bars indicate 95 % confidence limits**

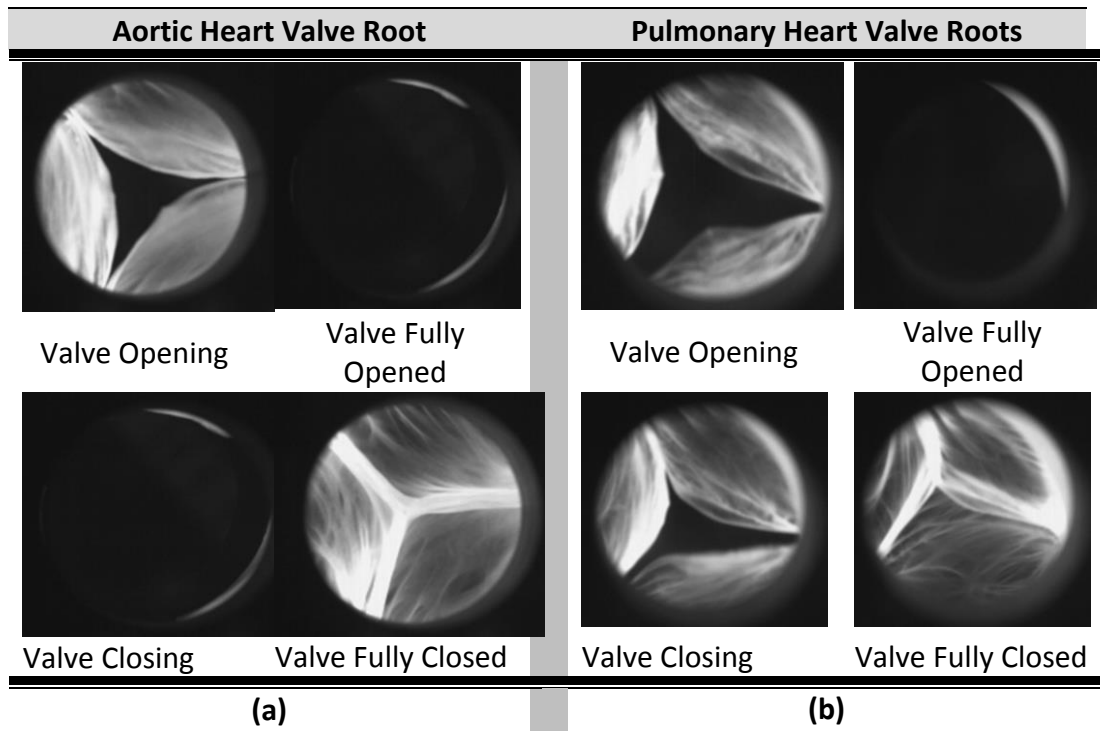
The effective orifice area (EOA) for each aortic and pulmonary heart valve root was averaged over all tested conditions as shown in Table 3.3. The mean EOA with  $\pm$  95 % confidence limits for cellular porcine aortic and pulmonary heart valve roots was  $3.03 \pm 0.34 \text{ cm}^2$  and  $2.84 \pm 0.56 \text{ cm}^2$  respectively.



**Table 3.3 Mean Effective Orifice Areas for Cellular Porcine Pulmonary and Aortic Heart Valve Root**

<b>Aortic</b>	PA1	PA2	PA3	PA4	PA5	PA6
Heart Valve Root EOA (cm <sup>2</sup> )	2.88	3.48	3.24	3.26	2.91	3.43
<b>Pulmonary</b>	PP1	PP2	PP3	PP4	PP5	PP6
Heart Valve Root EOA (cm <sup>2</sup> )	3.75	2.60	3.24	2.45	2.39	2.64

The leaflet kinematics were assessed during the opening, fully opened, closing and fully closed phases and representative images of these phases are shown in Figure 3.2 for the cellular porcine (a) aortic and (b) pulmonary heart valve roots respectively.



**Figure 3.2 Valve Opening, Valve Fully Opened, Valve Closing and Valve Fully Closed Images of a Typical Cellular Porcine (a) Aortic and (b) Pulmonary Heart Valve Root at Heart Rate 72 bpm, Captured from the Front View by a High-Speed Camera**

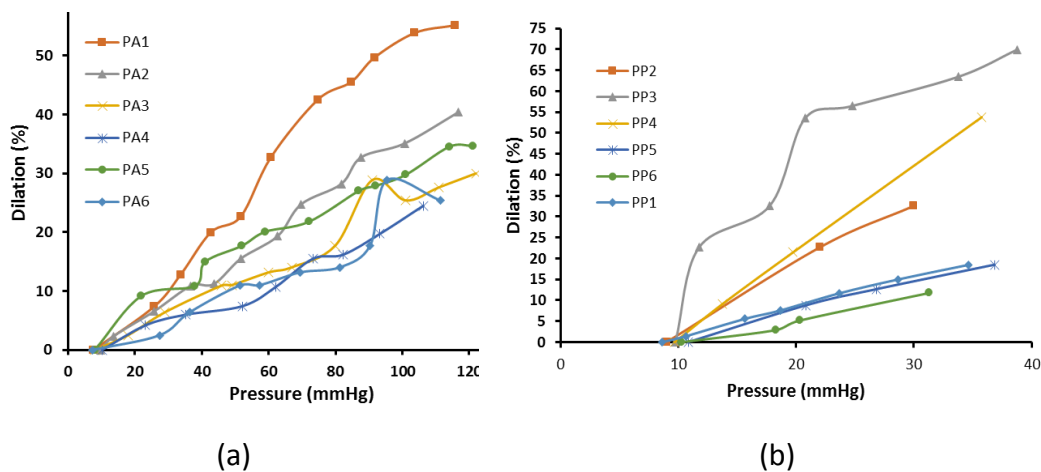
All the cellular porcine aortic heart valves roots showed a triangular orifice during the opening phase and circular orifice in the fully opened phase. There was no leaflet folding observed. During the closing phase, all the aortic valves were observed to fully close, with no visible leakage orifice during the fully closed phase.

For all the cellular porcine pulmonary heart valve roots, synchronous opening was observed. During the closed phase, a small central leakage orifice at lower heart rates and redundant leaflet material was observed.

### 3.5.2 Biomechanical Performance of the Cellular Porcine Aortic and Pulmonary Heart Valve Roots

#### 3.5.2.1 Dilation (Expansion Characteristics)

The percentage dilation as a function of the internal pressure for all the cellular porcine aortic and pulmonary heart valve roots is shown in Figure 3.3 (a) and (b) respectively.



**Figure 3.3 Percentage Dilation as a Function of Applied Pressure of all Cellular Porcine (a) Aortic and (b) Pulmonary Heart Valve Roots - Data fitted with a second order polynomial trend line**

The figures showed that percentage dilation with respect to pressure relationship seemed to be linear for both the cellular aortic and pulmonary heart valve roots.

The mean percentage dilation was  $11.58 \pm 5.56$  % at 40 mmHg internal pressure for aortic heart valve roots and it was  $20.54 \pm 18.44$  % at 20 mmHg pressure for pulmonary heart valve roots.

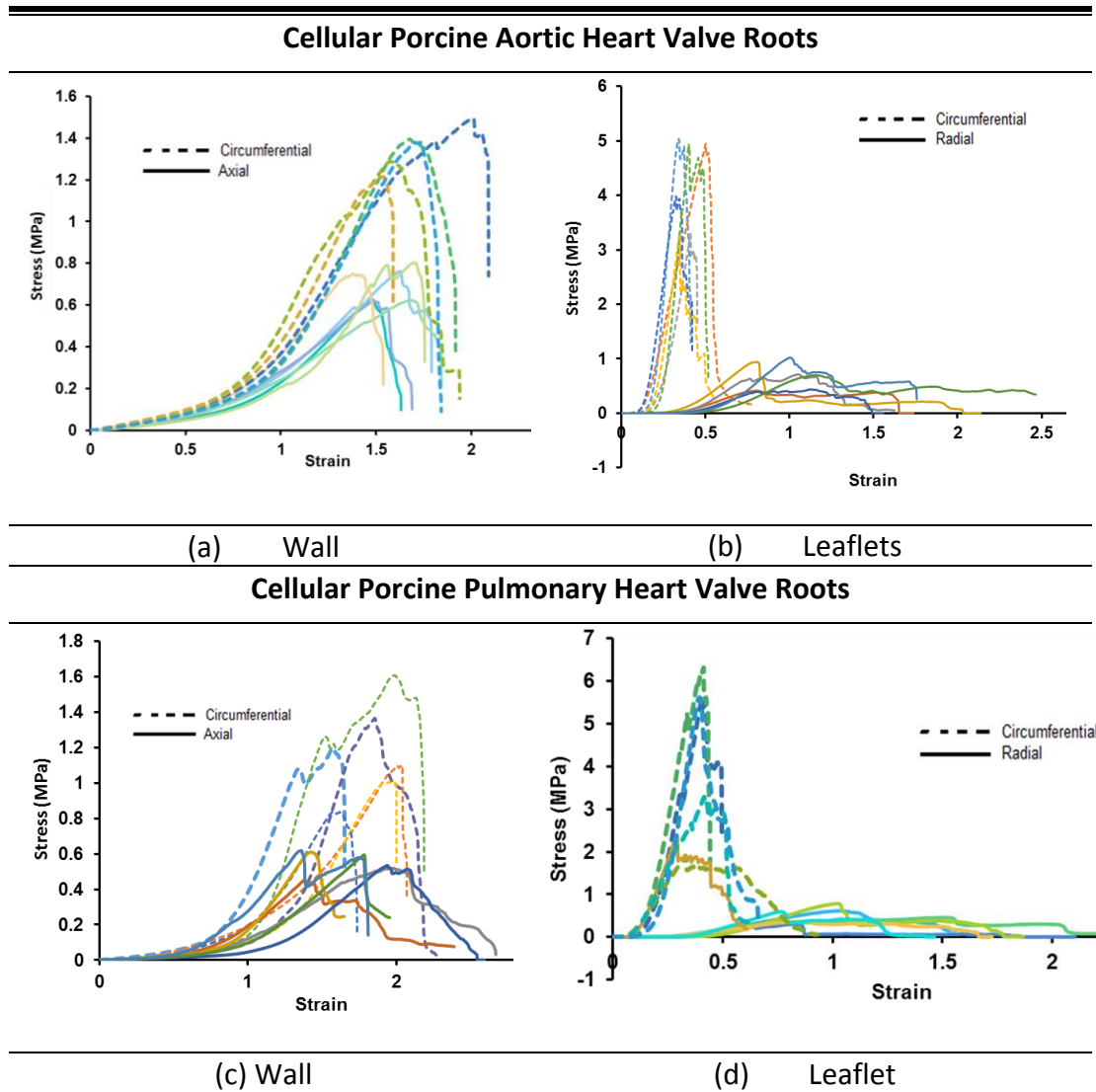
#### 3.5.2.2 Uniaxial Tensile and Suture Pull – Out Characteristics

The mean wall and leaflet specimen thicknesses  $\pm$  95 % confidence limits of the porcine pulmonary and aortic heart valve roots are shown in Table 3.4.

**Table 3.4 Mean Thickness  $\pm$  95 % Confidence Limits for the Cellular Porcine Aortic and Pulmonary Heart Valve Root Specimens (Wall and Leaflet)**

Specimen Type	Mean Thickness $\pm$ 95 % confidence limits (mm)	
	Aortic Heart Valve Root	Pulmonary Heart Valve Root
Root wall axial	3.02 $\pm$ 0.29	2.22 $\pm$ 0.28
Root wall circumferential	2.62 $\pm$ 0.24	1.88 $\pm$ 0.28
Leaflet radial	0.52 $\pm$ 0.11	0.39 $\pm$ 0.09
Leaflet circumferential	0.63 $\pm$ 0.13	0.38 $\pm$ 0.09

The stress-strain graphs of six specimens of the cellular porcine pulmonary and aortic heart valve root wall in the axial and circumferential and leaflet in radial and circumferential directions are shown in Figure 3.4.



**Figure 3.4 Stress-Strain Graphs for the Cellular Porcine (a) Aortic Wall, (b) Aortic Leaflets, (c) Pulmonary Wall and (d) Pulmonary Leaflets Specimens [Wall Specimens: Axial (Solid Lines) and Circumferential (Dotted lines)] and Leaflet Specimens [Radial (Solid Lines) and Circumferential (Dotted lines)]**

The leaflet specimens demonstrated a noticeable anisotropy between the radial and circumferential directions for both pulmonary and aortic heart valve roots. The stress-strain characteristics of the aortic and pulmonary heart valve root walls had a similar three-phased behaviour to the leaflet tissue, with a low modulus region during the elastin phase and a high modulus region during the collagen phase but no clear anisotropy between the axial and circumferential directions.

The mean biomechanical parameters with 95 % confidence limits for the porcine aortic and pulmonary specimens (wall and leaflet) are shown in Table 3.5.

**Table 3.5 Mean Collagen Phase Slope (Ec), Mean Elastin Phase Slope (Ee), Mean Ultimate Tensile Stress (UTS) and Mean Failure Strain ( $\epsilon_f$ ) ( $\pm$  95 % Confidence Limits) for the Cellular Porcine Aortic and Pulmonary Wall and Leaflet Specimens**

	<b>Ec</b> MPa	<b>Ee</b> MPa	<b>UTS</b> MPa	<b><math>\epsilon_f</math></b>
<b>Aortic Wall</b>				
<b>Axial</b>	0.86 $\pm$ 0.22	0.15 $\pm$ 0.02	0.70 $\pm$ 0.09	1.56 $\pm$ 0.13
<b>Circumferential</b>	1.55 $\pm$ 0.18	0.23 $\pm$ 0.02	1.38 $\pm$ 0.12	1.69 $\pm$ 0.20
<b>Aortic Leaflet</b>				
<b>Radial</b>	1.42 $\pm$ 0.52	0.03 $\pm$ 0.01	0.70 $\pm$ 0.26	1.01 $\pm$ 0.17
<b>Circumferential</b>	22.07 $\pm$ 6.44	0.81 $\pm$ 0.82	4.17 $\pm$ 0.85	0.38 $\pm$ 0.05
<b>Pulmonary Wall</b>				
<b>Axial</b>	0.76 $\pm$ 0.26	0.04 $\pm$ 0.01	0.55 $\pm$ 0.07	1.65 $\pm$ 0.30
<b>Circumferential</b>	1.52 $\pm$ 0.45	0.10 $\pm$ 0.03	1.19 $\pm$ 0.29	1.83 $\pm$ 0.22
<b>Pulmonary Leaflet</b>				
<b>Radial</b>	0.92 $\pm$ 0.51	0.03 $\pm$ 0.01	0.51 $\pm$ 0.19	1.05 $\pm$ 0.27
<b>Circumferential</b>	18.22 $\pm$ 9.55	0.44 $\pm$ 0.31	3.84 $\pm$ 1.96	0.40 $\pm$ 0.04

The mean maximum suture pull-out force for the aortic and pulmonary wall specimens was  $4.14 \pm 1.43$  N and  $8.07 \pm 5.19$  N respectively.

### 3.6 Discussion

This study assessed the hydrodynamic and biomechanical performance of cellular porcine aortic and pulmonary heart valve roots. The majority of the cellular porcine aortic heart valve roots were shown to be competent, whereas all the cellular porcine pulmonary heart valve roots were regurgitant. This was possibly due to the anatomy of the pulmonary heart valve root combined with a test artefact. Physiologically the pulmonary heart valve root is supported by thin and delicate myocardium, in comparison with the aortic heart valve root, which is strongly supported by its thick myocardium and in a position wedged between the left and right atrioventricular annuli and bulging thick left ventricular wall (Misfeld and Sievers, 2007). It was hypothesised that the pulmonary valve regurgitation was due to the lack of annulus support, resulting in a lack of coaptation of the leaflets of the

valves. Modification in the competency assessment method by adding annulus support was a possible way to solve this issue and this hypothesis and solution is investigated further in Chapter 5.

An *in vitro* assessment of EOA gives information about valve performance and this provides clinicians and engineers of a way to compare different types of heart valves. The porcine aortic heart valve roots showed excellent performance in terms of valve opening and closing characteristics under pulsatile flow conditions. The EOA derived in this study ( $3.03 \pm 0.34 \text{ cm}^2$ ) for the aortic heart valve roots was similar to the EOA derived by Nagy et al. (2000) and Jennings (2001). Both Nagy et al. (2000) and Jennings (2001) investigated the hydrodynamic performance of cellular porcine aortic heart valve roots in a similar experimental set up. Nagy used varying sizes of aortic heart valve roots and found the mean EOA to be  $2.73 \pm 0.47 \text{ cm}^2$  at a heart rate 72 bpm. Jennings (2001) used 23 mm size of porcine aortic heart valve root and the mean EOA was determined to be  $2.59 \pm 1.53 \text{ cm}^2$ .

Under pulsatile flow conditions, all the cellular porcine pulmonary heart valve roots showed synchronous leaflet opening, the fully open leaflet configuration and leaflet fluttering characteristics. A small central leakage orifice was observed for lower heart rates during the fully closed phase. It was observed that porcine pulmonary heart valve roots had some redundant leaflet above the coaptation surface. These findings were also reported in previous studies (Jennings, 2001, 2014). The mean EOA for the pulmonary heart valve roots was  $2.84 \pm 0.56 \text{ cm}^2$ , which agreed well with the values  $2.85 \pm 0.61 \text{ cm}^2$  and  $2.74 \pm 0.39 \text{ cm}^2$  derived by Nagy et al. (2000) and Jennings (2001) respectively. The hydrodynamic parameters (EOA, transvalvular pressure) for porcine pulmonary heart valve roots derived in this study showed good agreement with previous studies (Jennings, 2001, Nagy et al., 2000). Overall the repeatability of the pulsatile flow tests was comparable with literature.

The mean percentage dilation was  $11.58 \pm 5.56 \%$  at 40 mmHg pressure for the aortic heart valve roots. However, the pulmonary heart valve root was much more expansible in the circumferential direction with a mean percentage dilation of  $20.54 \pm 18.44 \%$  at 20 mmHg. The dilation characteristics of the cellular porcine aortic heart valve roots at 40 mmHg agreed well with those reported (mean percentage dilation

12.22 ± 5.04 %) by Jennings (2001). Jennings (2001) however reported higher mean percentage dilation at 20 mmHg of cellular porcine pulmonary heart valve roots to be 33.93 ± 14.75 %. This could have been due to different test set up used for heart valve root dilation measurements. In this study, the annulus of pulmonary heart valve root was supported with an appropriately sized annulus ring during dilation measurement, whereas Jennings (2001) did not use annulus support during dilation measurement of pulmonary heart valve root. The circumferential expansion of the aortic and pulmonary root artery has been shown to be an important element of the leaflets opening (Nagy et al., 2000). Circumferential expansion was chosen as the indicator of arterial stiffness due to its direct representation of the overall arterial compliance and close correlation with the volume of blood flow through the artery of the heart valve root. Also maintaining the heart valve root as a whole structure as opposed to manipulating tissue into flat strips provided more informed analysis of the heart valve biomechanical function under physiological conditions. Dilation testing has the ability to preserve the physiological structure of the heart valve root and thus provides characteristics that more closely mimic those of a clinical setting. The extensibility of the heart valve root in the circumferential and axial directions was studied using pressure inflation tests with radiopaque markers, sonomicrometric crystals or syringe test set up either *in vitro* or *in vivo* animal models by several research groups (Dagum et al., 1999, Hansen et al., 1995, Vesely et al., 1991). Jennings (2001) has used different sizes of syringes to mount the heart valve roots which limited the ability to test different sizes of the heart valve roots. In this study, the purposely designed Perspex tubes in various sizes allowed the measurement of dilation of various sizes of the heart valve roots with diameters ranging from 20 to 32 mm. Furthermore, during the dilation measurement it was important to mark the heart valve root wall with reference points, so the percentage dilation could be measured accurately between the reference points for small incremental pressure intervals from the captured images. A tissue marking dye was used to mark the reference points on the heart valve root wall which were clearly visible in the captured images and hence dilation was able to be accurately measured.

It was important to develop a robust method for the determination of material properties so that the effects of decellularisation on cellular porcine and human heart

valve roots could be assessed. The clamping of fragile biological specimens and preventative slippage or premature failure is problematical during tensile testing. Many authors have designed or adapted clamping holders or techniques specifically for the tissue they were investigating (Gallagher et al., 2012, Lei et al., 2018, Marei et al., 2015, Guedes et al., 2018). In this study, the majority of the wall specimens failed in the middle of the gauge length during uniaxial tensile testing, this indicated that the utilisation of the new holder design combined with a new suture technique substantially reduced the stress concentration at the grip-specimen interface. The new valve holder design and clamping technique for uniaxial tensile testing (Chapter 2 Section 2.4.8.2.3.1.1) was able to facilitate the accurate measurement of the material properties of porcine aortic and pulmonary heart valve root wall and leaflet specimens. This was one of the vital steps in the accurate measurement of the material properties of the biological heart valve root specimens with the tensile test method to ensure that the specimen did not slip from the grip edge during the testing.

It was also important to measure the thickness of the specimens accurately during uniaxial tensile testing of the heart valve root specimens, since the thickness directly affected the stress calculation. The aortic wall was thicker than the pulmonary wall in both the axial and circumferential directions. The mean thickness of the cellular porcine pulmonary wall (axial:  $2.22 \pm 0.28$  mm, circumferential:  $1.88 \pm 0.28$  mm) and leaflet (radial:  $0.39 \pm 0.09$  mm, circumferential:  $0.52 \pm 0.11$  mm) specimens was higher than the wall (axial: 1.74 mm, circumferential: 1.66 mm) and leaflet (radial and circumferential: 0.16 mm) thickness, reported by , 2011). The mean thickness of the aortic leaflets measured in this study was  $0.58 \pm 0.07$  which was similar in thickness (0.5 mm) measured by Sauren et al. (1983). In this study, the aortic wall specimen mean thicknesses were  $3.02 \pm 0.29$  mm (axial) and  $2.62 \pm 0.24$  (circumferential) which were higher than the thicknesses ( $2.40 \pm 0.09$  mm) measured by Jennings (2001). It was likely that variation in thickness measurements in porcine pulmonary and aortic heart valve leaflet specimens between different studies was due to user accuracy during the thickness measurement procedure, the choice of measuring equipment and arbitrarily selection of leaflets for tensile testing. The posterior leaflets tend to be thicker, have a larger surface area, and weigh more than



the right or left leaflet in the pulmonary heart valve roots; and the average width of the right coronary leaflet is greater than that of the other two leaflets in the aortic heart valve roots (Chandran et al., 2012). This study used a lightly loaded Mitutoyo (Model No: 700-122) digital thickness gauge, which when exerting a small compressive force on the tissue specimen would have given more consistent result. However, the thickness gauge had the following limitations: 1) failure due to spring corrosion and stiction and 2) difficult to hold the tissue specimens between the two anvils of the thickness gauge whilst holding the thickness gauge at the same time. In addition, the high water content of the specimens made it difficult to measure thickness accurately. To reduce experimental error and variation, thickness was measured six times and an average was taken. To address the limitations of the Mitutoyo thickness gauge a low load ( $0.05 \text{ N/cm}^2$ ) digital thickness gauge J-40-V (James H. Heal and Company Limited) was used to measure wall and leaflet thickness of the heart valve root (Chapter 4, 5, 6 and 8).

For the aortic leaflet specimens, the average collagen phase slopes (circumferential:  $22.07 \pm 6.44 \text{ MPa}$  and radial:  $1.42 \pm 0.52 \text{ MPa}$ ) obtained in this study were lower than the collagen phase slopes of  $54.6 \pm 7.4 \text{ MPa}$  and  $7.82 \pm 0.58 \text{ MPa}$  for the circumferential and radial directions respectively, reported by Lee et al. (1984) and  $28 \pm 10 \text{ MPa}$  in the circumferential direction reported by Sauren et al. (1983). Similar discrepancies were obtained in the wall tensile parameters. The elastic phase slope for circumferential aortic wall specimen was  $0.23 \pm 0.02 \text{ MPa}$ , which was larger than the  $0.12 \pm 0.02 \text{ MPa}$  reported by Korossis et al. (2002) and  $0.113 \pm 0.036 \text{ MPa}$  reported by Zhou et al. (1997). Similarly in the axial direction, the elastic phase slope for the aortic wall specimen derived in this study was  $0.15 \pm 0.02 \text{ MPa}$ , which was larger than  $0.087 \pm 0.021 \text{ MPa}$  reported by Korossis et al. (2002). It was clear that the elastic moduli for the leaflets were highly dependent upon test specimen orientation. The leaflet circumferential specimens had significantly higher elastic modulus than the radial specimens. This anisotropy was expected since the load bearing collagen fibers are preferentially aligned in the circumferential direction.

The mean elastic phase slopes obtained in this study were considerably lower than the elastic phase of  $0.76$  and  $0.34 \text{ MPa}$  in the circumferential and radial

directions respectively for the pulmonary leaflet specimens, reported by , 2011). Whereas, the mean collagen phase for the pulmonary leaflet specimens reported in this study were higher than the collagen phase of 0.15 and 0.12 MPa in the circumferential and radial directions respectively, reported by , 2011). The mean collagen phase slope for pulmonary wall specimens derived here was  $0.76 \pm 0.26$  MPa and  $1.52 \pm 0.45$  MPa in the axial and circumferential directions respectively which were larger than the values obtained by , 2011).

There was a high variability in the tensile wall and leaflets parameters for the porcine aortic and pulmonary heart valve roots, obtained in various studies (Sauren et al., 1983, 2011, Korossis et al., 2002, Lee et al., 1984). This could have been due to the fact that a few studies (2011, Korossis et al., 2002) used preconditioning and preloading. , 2011) preloaded pulmonary heart valve specimens with 0.02 N to obtain an accurate measure of the tissue gauge length and hence, zero extension was taken at the point where a 0.02 N was measured. Korossis et al. (2002) preconditioned aortic leaflet specimens for 50 cycles to produce a steady-state load-elongation response. However, the intrinsic properties of the test specimen in the elastin phase may alter due to preloading by starting the data collection at an arbitrary value rather than the relaxed state of the specimen. It has been reported that tissue preconditioning does not contribute to the generation of repeatable stress-strain curves for heart valve tissue (Carew et al., 2004). A need for preconditioning in the determination of heart valve tissue material properties will be dependent upon the purpose of the study. For example, for comparative studies, preconditioning can be omitted as long as the test conditions for each test groups are kept same. Also the tensile properties of the heart valve root specimen depend on specimen hydration and test conditions such as strain rate and test temperature.

### **3.7 Conclusion**

The hydrodynamic and biomechanical performance of cellular porcine pulmonary and aortic heart valve roots suggested that the methods developed have the ability to generate accurate and repeatable hydrodynamic and biomechanical performance of any type of biological heart valve roots.

These *in vitro* methods will be used for human cellular and decellularised aortic (Chapter 4) and pulmonary (Chapter 5) heart valve roots to derive the effect of decellularisation and the uniaxial tensile test method will be used for different types of xenogenic pulmonary heart valve roots (Chapter 6) to derive the effect of 12 months implantation in sheep on decellularised porcine pulmonary heart valve roots before they can be utilised in clinical studies.

## **4 Effect of Decellularisation on Hydrodynamic and Biomechanical Performance of Human Aortic Heart Valve Roots**

### **4.1 Introduction**

The characteristics of low concentration sodium dodecyl sulphate (SDS) decellularised human aortic heart valve roots (Vafaei et al., 2016) were investigated in this study to determine whether the hydrodynamic and biomechanical performance has been affected as a result of the decellularisation treatment. Cryopreserved cellular aortic human heart valve roots were included as the control, against which all the decellularised heart valve roots were compared, since cryopreserved cellular human aortic heart valve roots are the existing clinical product. This study was carried out in collaboration with NHS BT TES, Speke, Liverpool with a view to manufacturing decellularised aortic heart valve roots and supplying them for clinical use for the replacement of severely damaged aortic heart valves.

### **4.2 Aim and Objectives**

The aim of this chapter was to fully assess the effects of low concentration SDS decellularisation on the hydrodynamic and biomechanical performance of human aortic heart valve roots.

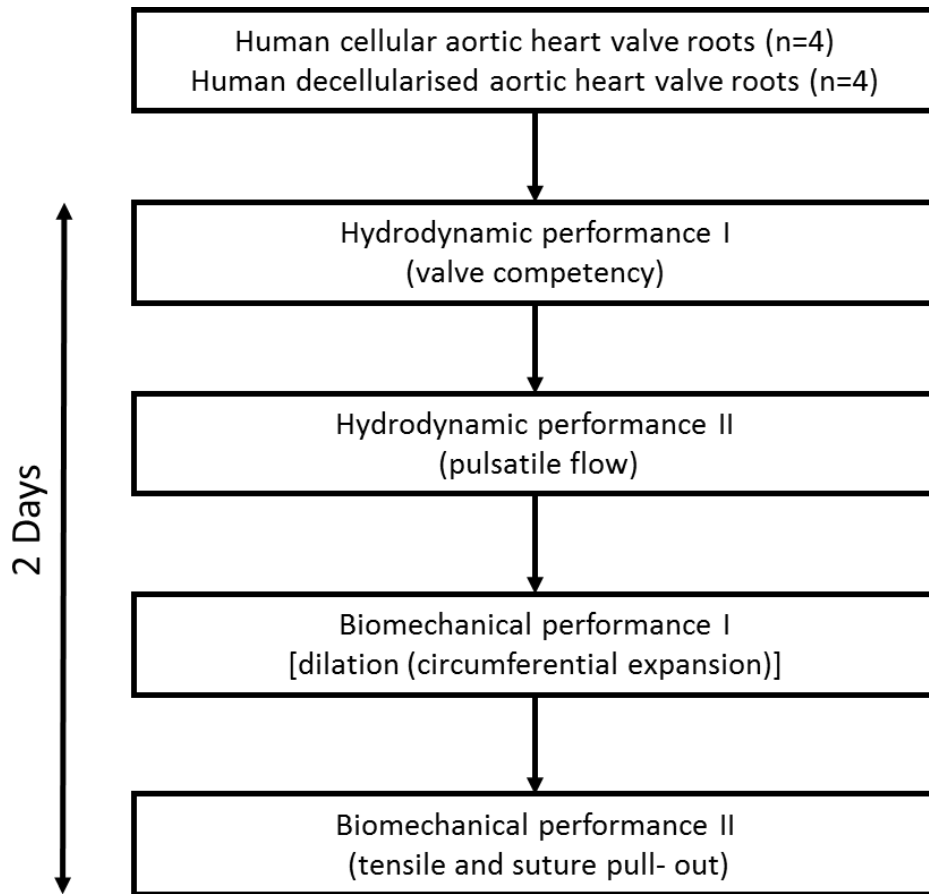
The specific objectives were:

1. To determine and compare the hydrodynamic (competency, pulsatile flow) and biomechanical (dilation, tensile, suture pull-out) performance of cellular and decellularised human aortic heart valve roots.
2. To determine and compare the biomechanical (dilation, tensile, suture pull-out) performance of cellular and decellularised human aortic heart valve roots.

### **4.3 Study Experimental Design**

This study was designed to assess the effect of decellularisation on the hydrodynamic (competency, pulsatile) and biomechanical (dilation, tensile, suture pull-out) performance of human aortic heart valve roots (un-paired comparison). The hydrodynamic and biomechanical performance of each aortic heart valve root

(cellular and decellularised) was evaluated in the sequence shown in Figure 4.1 within two consecutive days.

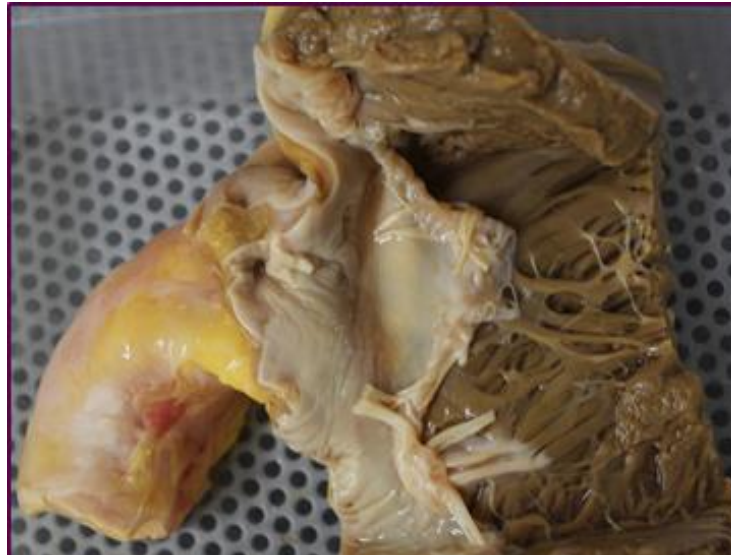


**Figure 4.1 Flow Chart Indicating Cellular and Decellularised Aortic Heart Valve Root Hydrodynamic and Biomechanical Performance Assessment Sequence**

#### 4.4 Materials

The cryopreserved human donor aortic heart valve roots were supplied by NHS BT TES, Speke, Liverpool. The valves were found to be unsuitable for therapeutic use but had full research and development consent. The study was conducted under UK NHS Health Research Authority approval (REC 09/H1307/02). The decellularised human aortic heart valve roots were prepared by Dr Tayyebeh Vafae in the Faculty of Biological Sciences (University Of Leeds). The protocol used to decellularise human aortic heart valve roots has been described in detail by Vafae et al. (2016). Following decellularisation the heart valve roots were cryopreserved using the standard NHS BT TES process and stored at  $-80^{\circ}\text{C}$ . All cryopreserved cellular and decellularised human aortic heart valve roots detailed in Table 5.1 and Table 4.2 were thawed on

the day before testing and stored in 100 ml Cambridge antibiotic solution at 4 °C to inhibit antibacterial growth. The heart valve root defrosting procedure is described in detail in Chapter 2 Section 2.4.4. A representative image of a thawed human aortic heart valve root is shown in Figure 5.2. Immediately before testing, the heart valve roots were rinsed with PBS. In between the tests the heart valve roots were stored in Cambridge antibiotic solution at 4 °C.



**Figure 4.2 Representative Image of Human Aortic Heart Valve Root**

As received, the sizes (internal diameter) of all the valves were measured with obturators.

**Table 4.1 Details of Cellular and Decellularised Aortic Heart Valve Roots Including Patient Age, Patient Sex and Valve Size Used for Hydrodynamic and Biomechanical Performance Testing**

Cellular Aortic Heart Valve Roots				Decellularised Aortic Heart Valve Roots			
ID Number	Patient Age (Year)	Patient Sex	Valve Size (mm)	ID Number	Patient Age (Year)	Patient Sex	Valve Size (mm)
HA045	56	M	22	HA048	71	M	25
HA044	76	F	21	HA046	57	M	23
HA049	50	M	23	HA047	47	M	24
HA057	27	M	19	HA050	75	F	21

Due to the quality and variability in cellular human aortic valve roots, it was difficult to prepare enough samples to test, especially from the leaflets. Therefore, four additional cellular aortic heart valve roots (Table 4.2) were obtained from NHS BT TES, Speke, Liverpool for uniaxial tensile and suture pull-out testing; giving a total of eight cellular aortic and four decellularised aortic heart valve roots.

**Table 4.2 Details of the Four Additional Cellular Aortic Heart Valve Roots including Patient Age and Patient Sex Used for Uniaxial and Suture Pull-Out Testing**

Cellular Aortic Heart Valve Roots		
ID Number	Patient Age (Years)	Patient Sex
HA056	50	F
HA059	60	F
HA060	46	M
HA061	61	M

## 4.5 Methods

### 4.5.1 Hydrodynamic Performance I: Competency

In order to assess valve competency, the leakage flow rate of each valve was measured by applying static back pressure. The maximum static back pressure for aortic heart valve roots was 120 mmHg and the time (TL) taken for the pressure of the test fluid to drop to 80 mmHg was recorded. The leakage flow rate ( $F_L$ ) for each heart valve was calculated. The aortic heart valve root was classified as competent if the pressure head had not dropped to 80 mmHg pressure within a cut-off period of 30 minutes (or leakage rate  $\leq 0.85 \text{ mL} \cdot \text{s}^{-1}$ ). The detailed test procedure for competency testing is described in Chapter 2 Section 2.4.6.1.3. When the maximum static back pressure was applied, the diameter of the root was measured at 4 to 5 mm above the sinotubular junction using a digital Vernier Calliper.

### 4.5.2 Hydrodynamic Performance II: Pulsatile Flow

To evaluate hydrodynamic performance, each aortic heart valve root was function tested in the pulsatile flow simulator. A 23 mm Björk-Shiley mono leaflet mechanical control valve (BSM; Shiley Corporation Incorporated, USA) was also

tested and compared with previous results to verify the performance of the pulsatile flow rig prior to testing of the aortic heart valve roots.

**Table 4.3 Test Conditions Used in the Pulsatile Flow Performance of Cellular and Decellularised Aortic Heart Valve Roots**

Heart Rate (bpm)	Peak Flow (mL .s <sup>-1</sup> )
60	225
72	325
80	409

The aortic heart valve roots were initially tested in the pulsatile flow simulator at minimum compliance with heart rates 60, 72 and 80 bpm with corresponding stroke volumes 60, 70 and 80 ml to determine the peak flow conditions required for the testing at maximum compliance, which are detailed in Table 4.3.

The aortic heart valve roots were subsequently tested at maximum compliance using the three pulsatile flow conditions detailed in Table 4.3 following the procedure detailed in Chapter 2 Section 2.4.7.4. The systemic pressure was held between 120 to 80 mmHg to mimic *in vivo* conditions. The pump input profile was a 50 % systolic duration sine waveform in both cases to replicate physiological cardiac waveforms benchmarked in previous studies (Jennings, 2001, 2011) .

As previously discussed the pulsatile flow testing allowed the evaluation of hydrodynamic performance of the aortic heart valve roots by producing measurements of transvalvular pressure across the valve, root mean square (RMS) flow and Effective Orifice Area (EOA). High speed video imaging at 500 frames. s<sup>-1</sup> allowed the leaflet dynamics to be assessed.

#### **4.5.3 Biomechanical Performance I: Dilation (Expansion Characteristics)**

The circumferential expansion of each heart valve root was determined in terms of percentage dilation using the dilation test procedure described in Chapter 2 Section 2.4.8.1.2. The test procedure involved attaching the heart valve root outflow to the end of a Perspex cylindrical tube, filling with PBS solution, and subjecting to various incremental internal static pressures. The maximum applied pressure for aortic heart valve roots (cellular and decellularised) was 120 mmHg or until the valve



failed. The mean percentage dilation is presented at 40 mmHg for aortic heart valve roots.

#### **4.5.4 Biomechanical Performance II: Uniaxial Tensile and Suture Pull-Out**

Tensile material properties of the wall (axial and circumferential) and leaflets (radial and circumferential) from each aortic heart valve root were characterised using the uniaxial tensile testing method described in Chapter 2 Section 2.4.8.2.3.1.3. The specimen thickness was measured with a digital thickness gauge J-40-V (James H. Heal and Company Limited). The tensile material parameters: elastin phase slope, collagen phase slope, ultimate tensile stress (UTS) and failure strain were calculated from the stress-strain graphs.

To determine the resistance to tearing of the wall and myocardial from each heart valve root, the suture pull - out test was performed on the wall and myocardium. The peak load was recorded as the maximum suture pull-out force and the resistance to tearing for all the samples was determined. The detailed test procedure and resistance to tearing calculation is described in Chapter 2 Section 2.9.6.4.

#### **4.5.5 Statistics**

All the hydrodynamic and biomechanical performance data for the cellular and decellularised aortic heart valve roots are presented as the mean  $\pm$  95% confidence limits and statistical significance between the cellular and decellularised aortic heart valve roots performance was determined using Student's t-test. A significance level of  $p < 0.05$  was applied. Statistical analyses were performed using SPSS for Windows (version 21.0; SPSS, Inc., USA).

### **4.6 Results**

#### **4.6.1 Hydrodynamic Performance of Human Cellular and Decellularised Aortic Heart Valve Roots**

##### **4.6.1.1 Competency**

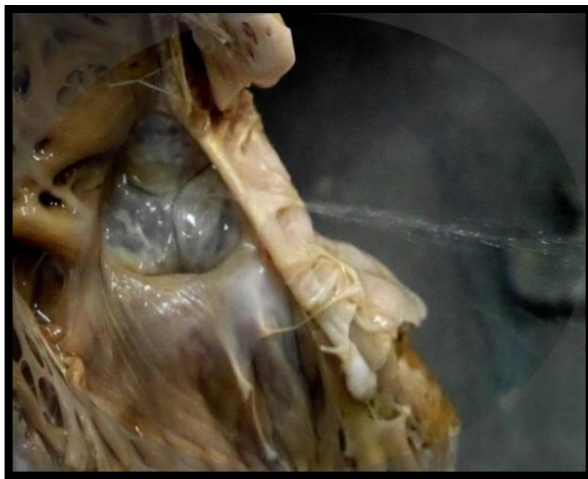
Three out of four of the cellular aortic heart valve roots were judged to be fully competent (Table 4.4).

**Table 4.4 Mean Leakage Flow Times ( $T_L$ ), Mean Leakage Flow Rates ( $F_L$ ), Competency and Arterial Diameters at 120 mmHg Pressure of Tested Human Cellular and Decellularised Aortic Heart Valve Roots**

ID Number	$T_L$ (Second)	$F_L$ ( $\text{mL}\cdot\text{s}^{-1}$ )	Competent	Arterial Diameter ( $D_1$ ) mm
			Yes or No	
Cellular Aortic Heart Valve Roots				
HA045	>1800	<0.85	Yes	31
HA044	>1800	<0.85	Yes	32
HA049	>1800	<0.85	Yes	34
HA057	857.2	1.78	No	28
Decellularised Aortic Heart Valve Roots				
HA048	83	18.48	No	42
HA046	162.5	9.44	No	32
HA047	1145	1.34	No	35
HA050	539	2.84	No	28

Competent- Yes: Leakage flow rate  $\leq 0.85 \text{ mL}\cdot\text{s}^{-1}$ , No: Leakage flow rate  $> 0.85 \text{ mL}\cdot\text{s}^{-1}$

However, all the decellularised aortic heart valve roots were regurgitant with leakage flow rate greater than  $0.85 \text{ mL}\cdot\text{s}^{-1}$ . An image of a decellularised aortic regurgitant valve during competency assessment is shown in Figure 4.3.



**Figure 4.3 Decellularised Aortic Heart Valve HA050 Showing Central Regurgitant Jet**

The arterial diameters for all the aortic heart valve roots (cellular & decellularised) at 120 mmHg pressure are shown in Table 4.4. At 120 mmHg, the

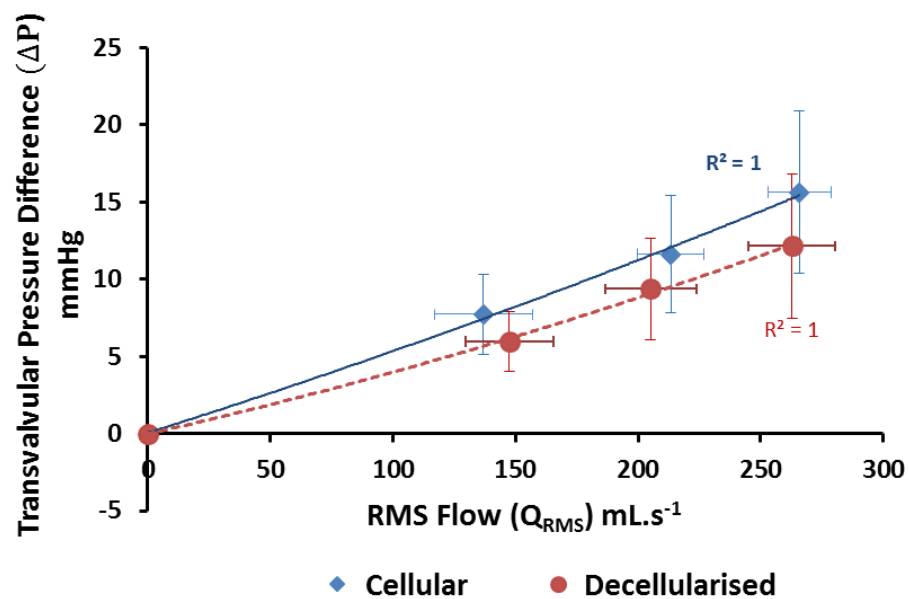
arterial diameters of the cellular aortic heart valve roots ranged between 28 to 34 mm and for the decellularised heart valve roots, the arterial diameters ranged between 28 to 42 mm.

#### 4.6.1.2 Pulsatile Flow

The mean transvalvular pressure versus mean RMS forward flow for the cellular and decellularised aortic heart valve roots is shown in Figure 4.4.

The cellular aortic heart valve roots had similar pressure flow characteristics to the decellularised aortic heart valve roots.

The mean transvalvular pressure with 95% confidence limits for the cellular aortic heart valve roots at 72 bpm was  $11.6 \pm 3.8$  mmHg and for the decellularised aortic heart valve roots the transvalvular pressure was  $9.3 \pm 3.2$  mmHg.



**Figure 4.4 Mean Transvalvular Pressure versus Mean RMS Flow for Human Cellular and Decellularised Aortic Heart Valve Roots - Data fitted with a second order polynomial trend line - The error bars indicate 95 % confidence limits**

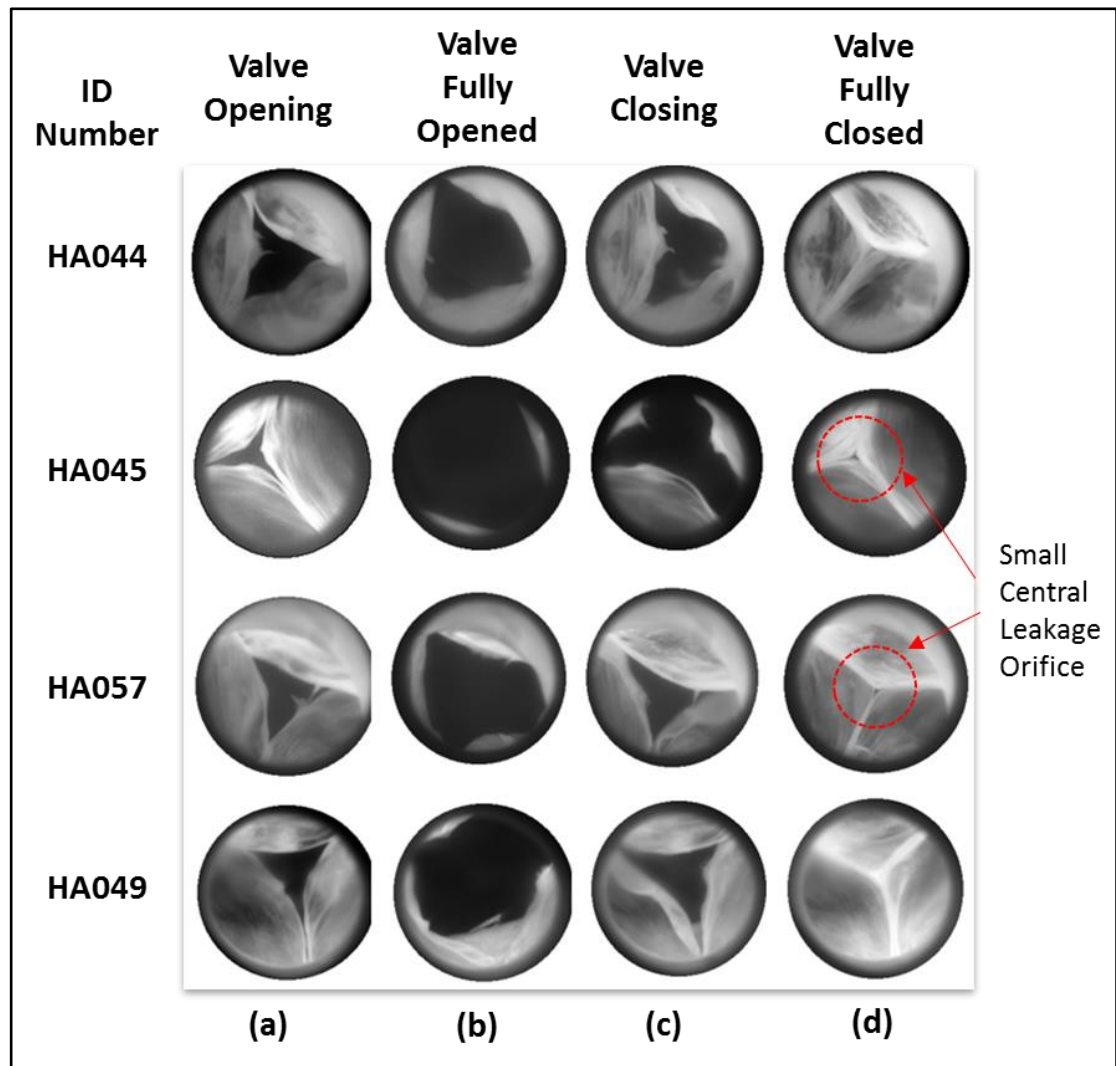
The EOA averaged over three heart rate conditions for all the cellular and decellularised aortic heart valve roots is shown in Table 4.5.

**Table 4.5 Effective Orifice Area for Each Human Cellular and Decellularised Aortic Heart Valve Root Averaged over 3 Heart Rate conditions**

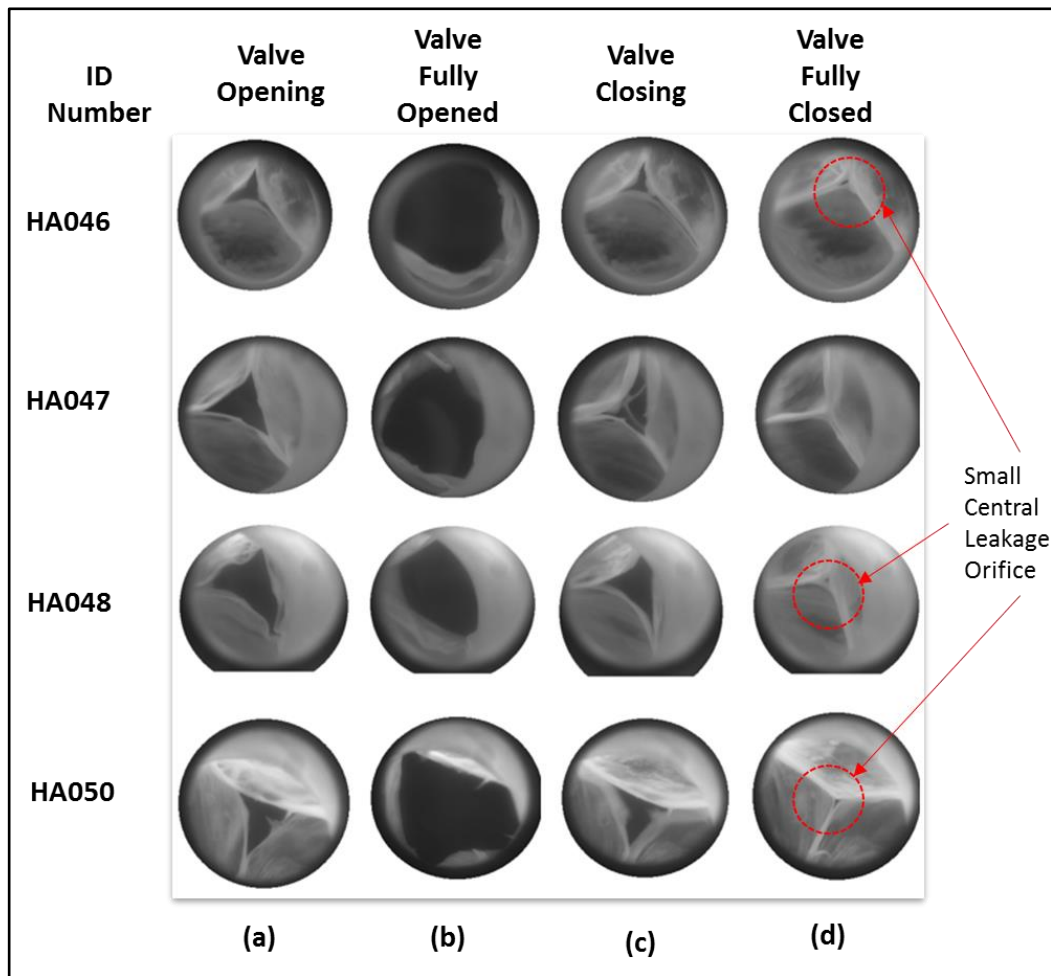
Cellular Aortic Heart Valve Roots		Decellularised Aortic Heart Valve Roots	
ID Number	Effective Orifice Area (EOA) cm <sup>2</sup>	Valve ID Number	Effective Orifice Area (EOA) cm <sup>2</sup>
HA044	1.16	HA046	1.55
HA045	1.22	HA047	1.52
HA057	1.14	HA048	1.99
HA049	1.66	HA050	1.16

The mean EOA for decellularised aortic valve heart valve roots ( $1.55 \pm 0.33$  cm<sup>2</sup>) was not significantly different than the cellular aortic heart valve roots ( $1.29 \pm 0.39$  cm<sup>2</sup>; P=0.26, Student's t-test)

Images of all tested cellular and decellularised heart valve roots in opening, fully opened, closing and fully closed phases are shown in Figure 4.5 and Figure 4.6 respectively.



**Figure 4.5 (a) Valve Opening, (b) Valve Fully Opened, (c) Valve closing and (d) Valve Fully Closed Images of Human Cellular Aortic Heart Valve Roots at Heart Rate 72 bpm, captured from the Front View by a High-Speed Camera**



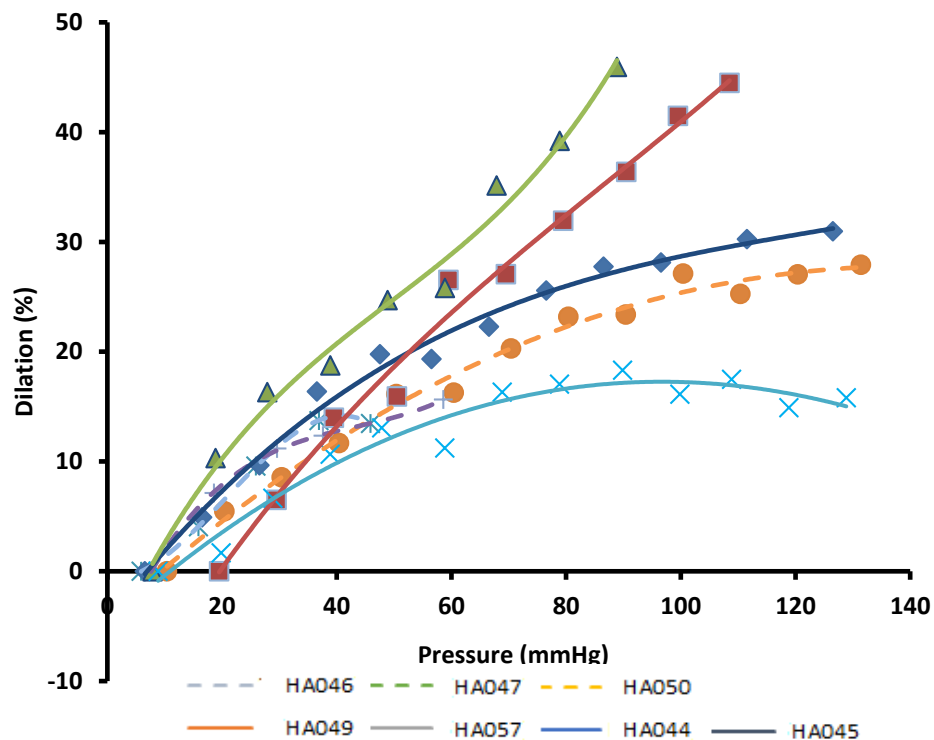
**Figure 4.6 (a) Valve Opening, (b) Valve Fully Opened, (c) Valve closing and (d) Valve Fully Closed Images of Human Decellularised Aortic Heart Valve Roots at Heart Rate 72 bpm, captured from the Front View by a High-Speed Camera**

The Cellular heart valve root HA044, HA049 and decellularised heart valve root HA047 showed excellent closed leaflet configuration, with perfect coaptation at the free edge of the leaflets. However, the cellular heart valve root HA045, HA057 and decellularised heart valve root HA046, HA048 and HA050 had a small central leakage orifice. The cellular heart valve roots HA044, HA057 and decellularised heart valve root HA050 did not fully open resulting in a restricted triangular orifice, whereas the other heart valves had a fully opened leaflet configuration. The cellular heart valve root HA049 and decellularised heart valve roots HA047, HA048 had a fully open configuration.

## 4.6.2 Biomechanical Performance of Human Cellular and Decellularised Aortic Heart Valve Roots

### 4.6.2.1 Dilation

The percentage dilations for all the tested aortic heart valve roots (cellular and decellularised) are shown as a function of applied internal pressure in Figure 4.7. The data showed that there was a variation within the cellular heart valve root group in dilation properties after 60 mmHg pressure. The dilation of the decellularised heart valve root HA048 could not be determined as it was leaking faster than the pressure applied.



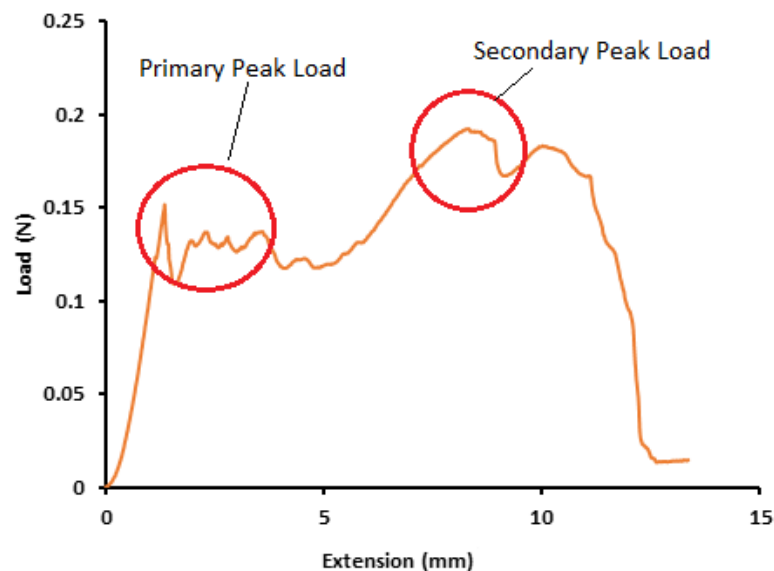
**Figure 4.7 Percentage Dilation as a Function of Applied Pressure of all Cellular (Solid line, n=4) and Decellularised (Dotted line, n=3) Aortic Heart Valve Roots - Data fitted with a third order polynomial trend line**

The expansion characteristics of decellularised aortic heart valve roots were similar to cellular heart valve roots at an internal pressure of 40 mmHg. The external wall diameters of the decellularised and cellular aortic heart valve roots, at 40 mmHg pressure, dilated by  $12.6 \pm 2.6$  % and  $15.4 \pm 5.4$  % respectively, which were not significantly different ( $p=0.23$ , Student's t test).

#### 4.6.2.2 Tensile Properties

Images were captured during the uniaxial and suture pull-out testing of cellular and decellularised tissue. It was observed that all the cellular and decellularised wall and leaflet tissue failed in the gauge length during uniaxial tensile testing as explained in Chapter 2 Section 2.4.9.

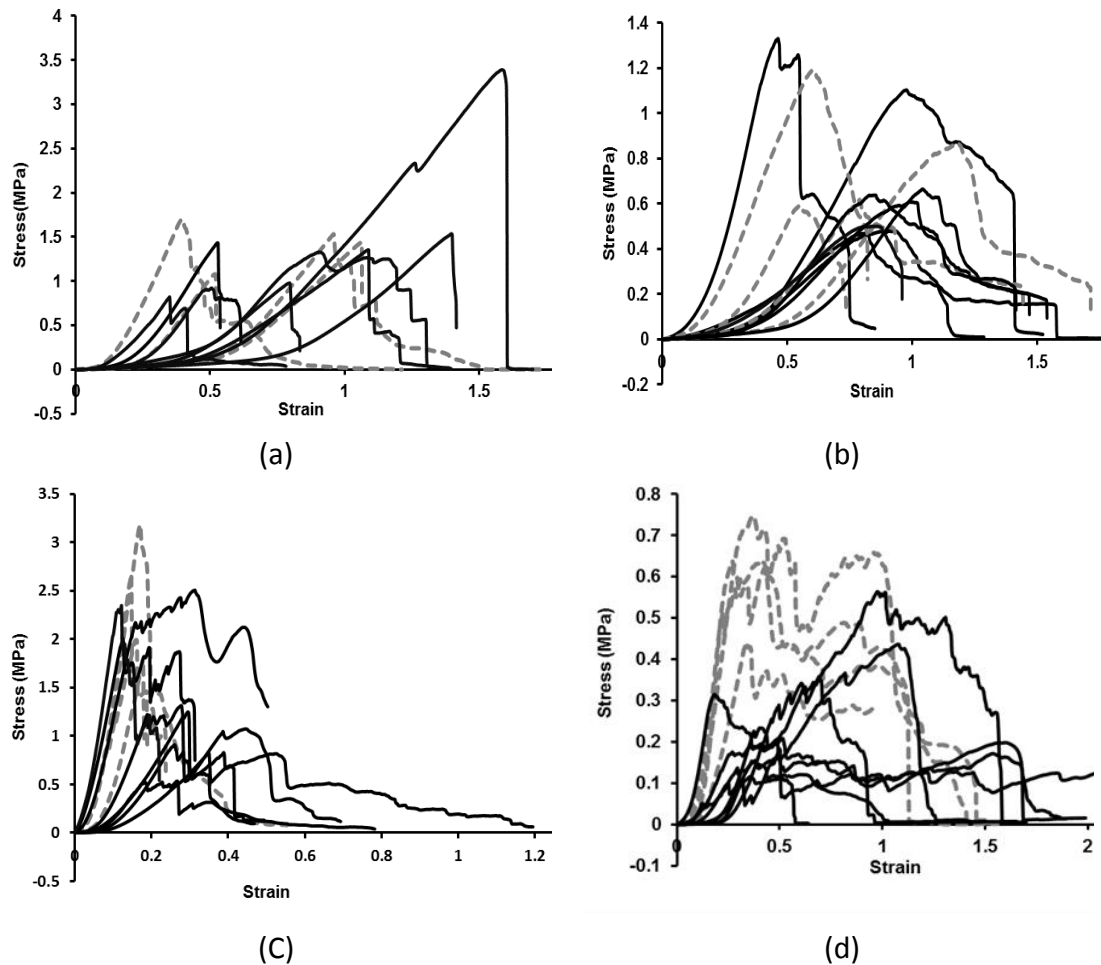
During the uniaxial tensile testing, two decellularised circumferential, two decellularised radial, two cellular circumferential and four cellular radial leaflet specimens tended to fail first at one point and then failure propagated across the leaflet and showed primary and secondary peak loads (Figure 4.8). For the UTS calculation, the primary peak load was considered.



**Figure 4.8 Load versus Extension Graph with Two Peaks for the Leaflet Specimen Undergoing Uniaxial Tensile Testing**

The stress-strain graphs for all the cellular and decellularised aortic wall and leaflet specimens are shown in Figure 4.9. The graphs demonstrated the typical tri-phasic characteristics. The decellularised wall stress-strain characteristics were similar to that of the cellular wall in the circumferential and axial directions. However, stress-strain leaflet characteristics in radial and circumferential directions demonstrated a rise in the ultimate tensile stress after decellularisation [Figure 4.9 (c) and (d)].





**Figure 4.9 Stress-Strain Graphs for the Cellular (solid line, n=8) and Decellularised (dotted line, n=4) (a) Circumferential Aortic Wall (b) Axial Aortic Wall (c) Circumferential Aortic Leaflet (d) Radial Aortic Leaflet Specimens**

Table 4.6 shows mean thickness with 95 % confidence limits and Table 4.7 shows tensile parameters with 95 % confidence limits for the cellular and decellularised aortic heart valve root wall (axial and circumferential) and leaflet (radial and circumferential) specimens.

The initial linear region of the stress-strain curve was used to derive the elastin phase modulus and it was not distinct for one decellularised and two cellular circumferential leaflet specimens. Hence these samples were omitted and only six cellular and three decellularised samples were used for the mean elastin phase slope calculation.

There was no significant difference between the mean cellular and decellularised aortic wall and leaflet specimen thickness in both the axial and circumferential directions ( $p > 0.05$ , Student's t-test).

**Table 4.6 Mean Thickness for the Cellular and Decellularised Aortic Heart Valve Root Wall and Leaflet specimens – p values: statistical probability in the comparison between cellular and decellularised aortic heart valve roots**

	Specimen Direction	Mean Thickness (mm)		p Value
		Cellular	Decellularised	
Aortic Heart valve root <b>wall</b>	Number of Specimens	8	4	
	Axial	1.99 ± 0.32	2.03 ± 0.11	0.89
	Circumferential	2.11 ± 0.18	2.23 ± 0.27	0.33
Aortic Heart valve root <b>Leaflet</b>	Number of Specimens	8	4	
	Radial	0.58 ± 0.14	0.49 ± 0.12	0.37
	Circumferential	1.11 ± 0.94	0.72 ± 0.20	0.23

**Table 4.7 Tensile Parameters (Collagen Phase Slope  $E_c$ , Elastin Phase Slope  $E_e$ , Ultimate Tensile Stress  $\sigma_{UTS}$ , Failure Strain  $\epsilon_{failure}$ ) for Cellular and Decellularised Aortic Wall in the Axial (A) and Circumferential (C) Directions and Leaflet Specimens in the Radial (R) And Circumferential (C) Directions, Number of Specimens (n). \*- Statistical significant difference ( $p < 0.05$ ; Student's t-test) for decellularised versus cellular heart valve roots.**

Aortic Heart Valve Roots	n	$E_c$ MPa	$E_e$ MPa	$\sigma_{UTS}$ MPa	$\epsilon_{failure}$
<b>Wall (A)</b>					
Cellular	8	1.72 ± 1.09	0.14 ± 0.10	0.72 ± 0.27	0.86 ± 0.15
Decellularised	4	1.98 ± 1.07	0.16 ± 0.17	0.82 ± 0.44	0.78 ± 0.45
P Value		0.72	0.79	0.62	0.57
<b>Wall (C)</b>					
Cellular	8	3.23 ± 0.74	0.19 ± 0.07	1.47 ± 0.68	0.89 ± 0.37
Decellularised	4	4.24 ± 2.64	0.21 ± 0.09	1.44 ± 0.42	0.74 ± 0.52
P Value		0.19	0.70	0.95	0.55
<b>Leaflet (R)</b>					
Cellular	8	1.30 ± 0.56	0.04 ± 0.04	0.19 ± 0.07	0.32 ± 0.82
Decellularised	4	4.06 ± 2.56*	0.15 ± 0.18	0.59 ± 0.21*	0.30 ± 0.10
P Value		0.002	0.05	0.00009	0.67
<b>Leaflet (C)</b>					
Cellular	8 <sup>x</sup>	11.91 ± 7.18	0.36 ± 0.25	1.40 ± 0.56	0.21 ± 0.69
Decellularised	4 <sup>xx</sup>	20.62 ± 9.08	1.76 ± 0.92*	2.41 ± 1.02*	0.16 ± 0.22
P Value		0.1	0.0004	0.03	0.28

<sup>x</sup>n=8 for all cellular leaflet parameters except n=6 for mean elastin phase slope, <sup>xx</sup>n=4 for all decellularised leaflet parameters except n=3 for mean elastin phase slope

The tensile wall parameters for the decellularised aortic heart valve roots were similar to the cellular aortic heart valve roots (Student's t-test,  $p>0.05$ ). There was no significant difference among the cellular and decellularised leaflet for the following parameters: the collagen phase slope in the circumferential direction, elastin phase slope in the radial direction, failure strain in the radial and circumferential direction ( $p>0.05$ , Student's t-test). The mean collagen phase slope for decellularised radial leaflet specimens was significantly higher than for cellular specimens ( $p=0.002$ , Student's t-test). There was also a significant increase in elastin phase slope for decellularised specimens compared to cellular specimens in the circumferential direction ( $p=0.0004$ , Student's t-test). The mean ultimate tensile stress was significantly increased for decellularised specimens compared to the cellular specimens in radial and circumferential directions ( $p<0.05$ , Student's t-test).

#### 4.6.2.3 Suture Pull – Out Properties

During suture pull-out testing of wall and myocardial specimens, failure was seen as a wedge shaped cut spreading from the suture in the circumferential direction perpendicular to the axial axis as explained in Chapter 2 Section 2.4.9.

The mean suture pull-out force and mean resistance to tearing for decellularised aortic heart valve root wall and myocardial specimen was not significantly different than the cellular aortic heart valve root wall and myocardium specimen (Table 4.7;  $p>0.05$ , Student's t-test).

**Table 4.8 Mean Maximum Suture Pull-Out Force and Mean Resistance to Tearing for the Cellular and Decellularised Aortic Heart Valve Root Wall and Myocardial specimens (Where n- Number Specimens) - p values: statistical probability in the comparison between cellular and decellularised aortic heart valve roots**

Specimen Type	n	Maximum Suture Pull-Out Force (N)		Resistance to Tearing (N/mm)	
		Wall	Myocardial	Wall	Myocardial
Cellular	8	6.87 ± 3.26	5.71 ± 1.07	0.91 ± 0.21	2.63 ± 1.00
Decellularised	4	6.63 ± 1.90	6.12 ± 7.83	0.27 ± 1.74	2.75 ± 1.21
P value		0.91	0.83	0.86	0.45

## 4.7 Discussion

### 4.7.1 Effect of Decellularisation on Hydrodynamic Performance of Human Cellular Aortic Heart Valve Roots

The *in vitro* hydrodynamic performance of decellularised aortic heart valve roots was shown to be improved compared to cellular aortic heart valve roots with lower transvalvular pressure gradients for all the tested conditions, indicating a reduced resistance against forward flow. Indeed, the mean pressure - flow characteristics for the decellularised group were slightly superior. This superiority was also observed with a larger mean EOA for decellularised aortic valve heart valve roots of  $1.55 \pm 0.33 \text{ cm}^2$  compared to  $1.29 \pm 0.39 \text{ cm}^2$  for the cellular aortic valve heart valve roots. However, the EOA values were not significantly higher for decellularised aortic heart valve roots ( $p=0.29$ ).

Analysis of high speed videos demonstrated that fully closed leaflet configuration was excellent for two of the cellular aortic heart valve roots with no visible central leakage orifice and a minor central leakage orifice was observed in the two remaining cellular heart valve roots. The images of closed leaflet configuration for cellular aortic heart valve roots correlated well with measured leakage flow rate under static back pressure.

For most of the decellularised aortic heart valve roots, the leaflets opened fully or near-fully, producing circular or near-circular orifices. However, for one of the decellularised aortic heart valve roots, the leaflets did not fully open resulting in a restricted triangular orifice. All the decellularised aortic heart valve roots appeared competent since a central leakage orifice was negligible or not observed during closed phase. Nevertheless, the valve competency assessment under static back pressure showed that all the decellularised aortic heart valve roots appeared to be regurgitant (having a leakage rate of  $> 0.85 \text{ mL}\cdot\text{s}^{-1}$ ). Although two out of four decellularised heart valve roots had a mean leakage flow rate of  $2.09 \text{ mL}\cdot\text{s}^{-1}$ , this was lower than the baseline value of  $4.95 \pm 1.78 \text{ mL}\cdot\text{s}^{-1}$  derived for a clinical heart valve (23 mm Björk-Shiley mono leaflet valve; Chapter 2 Section 2.4.6.1.2). The decellularised aortic heart valve root HA048 had the highest leakage flow rate along with the highest arterial diameter (42 mm at 120 mmHg). Conversely, heart valve

root HA048 showed good closed leaflet configuration under pulsatile flow. This may have been related to the lack of annulus support during competency testing. Also, the arterial diameters of these heart valve roots were not measured before the decellularisation treatment so it could not be ascertained whether this was a result of decellularisation processing. These pulsatile flow results must be interpreted with care due to the complex dynamic movement of the heart valve root during the pulsatile flow testing.

#### **4.7.2 Effect of Decellularisation on Biomechanical Performance of Human Cellular Aortic Heart Valve Roots**

The biomechanical performance of the decellularised human aortic heart valve roots was evaluated and compared with human cellular aortic heart valve roots. The decellularised aortic heart valve root walls had similar expansion characteristics to the cellular heart valve roots. The mean dilation for decellularised and cellular aortic heart valve root wall was  $12.6 \pm 2.6$  % and  $15.4 \pm 5.4$  % respectively at 40 mmHg. In addition, the maximum suture pull - out force and resistance to tearing were similar for the decellularised and cellular aortic specimens (wall and myocardial).

The tensile properties of decellularised aortic wall specimens were not significantly changed in terms of stiffness, elasticity and strength compared to the cellular specimens when tested in the axial and circumferential directions. There were however significant differences between the tensile properties of the cellular and decellularised leaflet specimens. The decellularised circumferential leaflet specimens were significantly stronger with mean ultimate tensile stress  $2.41 \pm 1.02$  MPa compared to  $1.40 \pm 0.56$  MPa for cellular circumferential specimens. Also decellularised circumferential leaflet specimens were stiffer with a collagen phase slope  $20.62 \pm 9.08$  MPa compared to  $11.91 \pm 7.18$  MPa for cellular specimens, this difference was not statistically significant ( $p=0.1$ ). The reason behind decellularised leaflets being stiffer and significantly stronger than cellular leaflets in the circumferential direction was possibly due to loosening and un-crimping of the collagen fibre network (Freed and Doehring, 2005) which leads to an increased in stiffness of the tissue. Also, results from this study showed that the extensibility of the decellularised circumferential aortic leaflet specimens was higher than the

cellular specimens. The radial elasticity of the aortic leaflet remained unaffected by the decellularisation procedure. The ultimate tensile stress and collagen phase slope was higher for decellularised leaflet specimens compared to cellular leaflet specimens in the radial direction. The findings from this study correlated well with a previous study which tested porcine aortic leaflets and found that after decellularisation treatment, their extensibility and failure strain significantly increased in the circumferential direction, while in the radial direction, the increase in strength was not significant (Korossis et al., 2002). Nonetheless, consideration must be taken to allow for species-related differences when interpreting these results. Although, the strength and stiffness of the aortic leaflets was affected by the decellularisation procedure, it did not appear to negatively affect valve function. Moreover, the expansion characteristics of the decellularised aortic wall were similar to the cellular aortic wall in the physiological pressure range, contributing to its positive performance.

In this study, human aortic heart valve roots were decellularised using hypotonic buffer, 0.1 % (w/v) sodium dodecyl sulphate (SDS) and nuclease digestion to remove cells from all regions (wall, leaflet and myocardium) (Vafaei et al., 2016). Decellularised heart valve roots for heart valve replacement may be used either pre-seeded with the patient's own autologous cells before implantation (Steinhoff et al., 2000, Lichtenberg et al., 2006) or implanted directly with a view to the patient's own endogenous cells repopulating and regenerating the decellularised scaffolds *in vivo* (da Costa et al., 2010). Nevertheless, harvesting of cells from patients and pre-seeding of decellularised scaffolds would be a time consuming, costly and potentially risky procedure. When this project commenced, it was decided to consider a strategy whereby decellularised human heart valve roots would be directly implanted, remodelled and regenerated *in vivo*. The aim of this study was to characterise human aortic heart valve roots decellularised using a proprietary process developed at the University of Leeds (Booth et al., 2002) before using them in clinic as a replacement valve. Aortic allograft valves that have been decellularised using different processes are already delivering promising *in vivo* results. Zehr and colleagues reported favourable clinical results on the use of SynerGraft® decellularised aortic valve allografts for aortic valve replacement (Zehr et al., 2005). These valves had been

implanted in patients with a mean age of  $53 \pm 14$  years. Although the small number of patients ( $n=22$ ) and short term mean follow up (30.3 months) limits the results. Zehr et al. (2005) demonstrated no calcification in the wall or leaflets with stable hemodynamic function without major complications during echocardiography. Calcification of cellular aortic valve allografts rarely occurs immediately after implantation (Doty et al., 1998), hence long term results are required. da Costa et al. (2010) implanted decellularised aortic allografts in 41 patients with a mean age of 34 years. da Costa et al. (2010) used a similar decellularisation protocol to the one used in this study. The post-operative results showed stable structural integrity, low rate of calcification, and adequate hemodynamics in the short term follow-up (maximum 19 months); however, one patient underwent reoperation due to mitral valve stenosis (da Costa et al., 2010). Tudorache et al. (2016) analysed results of 69 decellularised aortic allograft implants in children and young patients. Hemodynamic performance of these decellularised allografts was excellent up to 7.6 years of follow up. Most importantly, this study showed clinical data of decellularised aortic allograft implanted in 16 patients younger than 10 years (Tudorache et al., 2016). The data from this younger group of patients raised concerns about supra-avalvular stenosis and valvular regurgitation. However, the mean short term follow up, the small number of patients and complex surgical procedure in these young patients, limit the discussion of the results. Overall the results from these studies (da Costa et al., 2010, Zehr et al., 2005, Tudorache et al., 2016) are promising; even though the decellularisation protocols were different to the decellularisation protocol used in this study, this can nevertheless be seen as another sign of the excellent preliminary results achieved using decellularised allografts.

#### **4.7.3 Limitations**

There are several limitations to this study. First, the *in vitro* nature of this study meant the test methodologies used were a simplification of the environmental conditions under which the decellularised aortic heart valve roots will be placed *in vivo*; there was also no consideration of the effects of inflammation, cell repopulation or tissue remodelling, all of which may influence the mechanical properties and flow characteristics of the valves. Second, the relatively small sample size meant a lack of

statistical power to discriminate/provide significant differences between biomechanical properties of the cellular and decellularised aortic heart valve roots. The statistical power was also influenced by inherent biological variation and quality of the tissue.

#### **4.8 Conclusion**

In conclusion, an extensive *in vitro* hydrodynamic and biomechanical comparison of decellularised and cellular human aortic heart valve roots has been performed. Neither pulsatile flow parameters nor expansion properties of human aortic heart valve roots were significantly affected by the low concentration SDS decellularisation treatment. However, decellularisation significantly altered hydrodynamic performance under static back pressure and some of the directional material properties of aortic heart valve leaflets. This work has been published in the *The Journal of the Mechanical Behavior of Biomedical Materials*, and publication details can be found in Appendix A.



## **5 Effect of Decellularisation on Hydrodynamic and Biomechanical Performance of Human Pulmonary Heart Valve Roots**

### **5.1 Introduction**

In addition to developing a process for decellularisation of human aortic heart valve roots, the study by Vafae et al. (2016) also developed a process for decellularisation of human pulmonary heart valve roots, in collaboration with NHS BT TES, with a view to supplying them for clinical use in the pulmonary valve switch operation (Ross procedure). The decellularised pulmonary heart valve roots were developed on the basis of hypothesis that removal of the major cellular immunogenic components had been achieved without adverse effects on the extracellular matrix (ECM). To determine whether the ECM had been affected as a result of the low concentration sodium dodecyl sulphate (SDS) decellularisation (Vafae et al., 2016) treatment, the hydrodynamic and biomechanical performance of human cellular and decellularised pulmonary heart valve roots was evaluated. Cryopreserved cellular human pulmonary heart valve roots were included as the control to which all the decellularised pulmonary heart valve roots were compared, since cryopreserved cellular human pulmonary heart valve roots are the existing clinical product. The importance of physiological boundary conditions during the assessment of valve competency was also explored in this study.

### **5.2 Aim and Objectives**

The aim was to fully assess the effects of low concentration SDS decellularisation on the hydrodynamic and biomechanical performance of human pulmonary heart valve roots.

The specific objectives were:

1. To determine and compare the hydrodynamic (competency, pulsatile flow) and biomechanical (dilation, tensile, suture pull-out) performance of cellular and decellularised human pulmonary heart valve roots (in an un-paired comparison).
2. To determine the influence of a specific processing step (scraping) on the functional biomechanical performance (competency, dilation) of cellular and

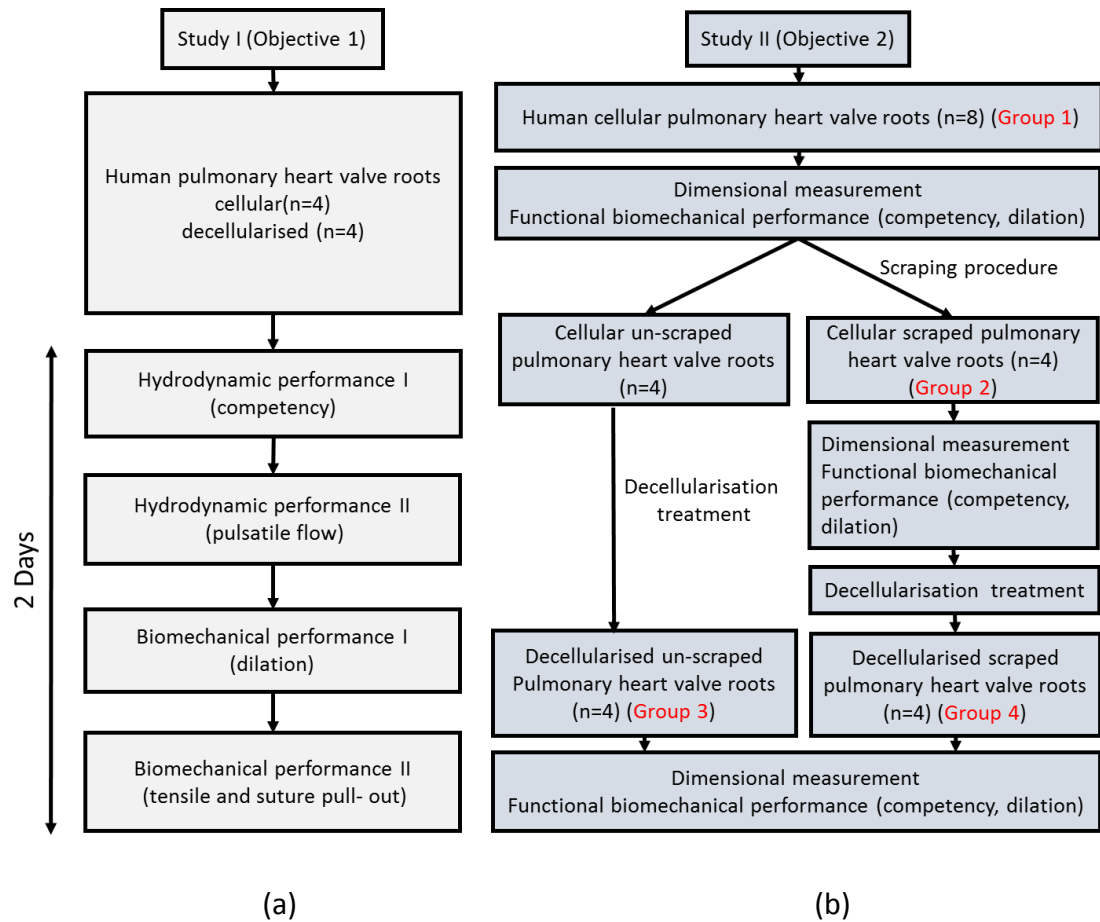
decellularised (scraped and un-scraped) pulmonary heart valve roots (in a paired comparison).

### **5.3 Study Experimental Design**

This study was conducted in two phases. Study I was designed to assess the effect of decellularisation on the hydrodynamic (competency, pulsatile) and biomechanical (dilation, tensile, suture pull-out) performance of human pulmonary heart valve roots in an un-paired comparison (Objective 1). The hydrodynamic and biomechanical performance of each pulmonary heart valve root (cellular and decellularised) was evaluated in the sequence shown in Figure 5.1(a) within two consecutive days. The decellularised heart valve roots were processed as reported by (Vafaei et al., 2016), which included the removal of excess fat, connective tissue and the adventitial layer of the pulmonary heart valve root wall by scraping using a scalpel blade (referred to throughout as 'scraping'), to allow diffusion of decellularisation solutions. It was not known whether this scraping process disrupted the structure of the valve in any way and altered the mechanical properties of the tissue. Therefore, a further study (Study II) was introduced to investigate the influence of this scraping step on the functional biomechanical properties of the pulmonary heart valve roots (Objective 2).

Study II used a repeated measure design approach, in which functional biomechanical performance (competency and dilation) of the cellular and decellularised pulmonary heart valve roots was evaluated [Figure 5.1 (b)] and compared in a paired comparison. Here functional mechanical performance of all the cellular pulmonary heart valve roots was evaluated and then the heart valve roots were divided into two groups with each group assigned a different decellularisation processing protocol either with or without the scraping step [Figure 5.1(b)]. Following the decellularisation treatment, the functional biomechanical performance of the pulmonary heart valve roots was again evaluated. The dimensional quantification of heart valve roots before and after decellularisation (with and without scraping) could be an indication of whether the internal tissue structure was altered. Therefore, the functional assessments, the dimensions of each pulmonary heart valve root were

measured throughout. This approach helped to reduce variability and hence sample size.



**Figure 5.1 Flow Chart Indicating Pulmonary Heart Valve Roots Performance Assessment Sequence used in (a) Study I and (b) Study II**

### 5.3.1 Materials (Study I and Study II)

In Study I, four cellular and four decellularised human pulmonary heart valve roots were used as detailed in Table 5.1.

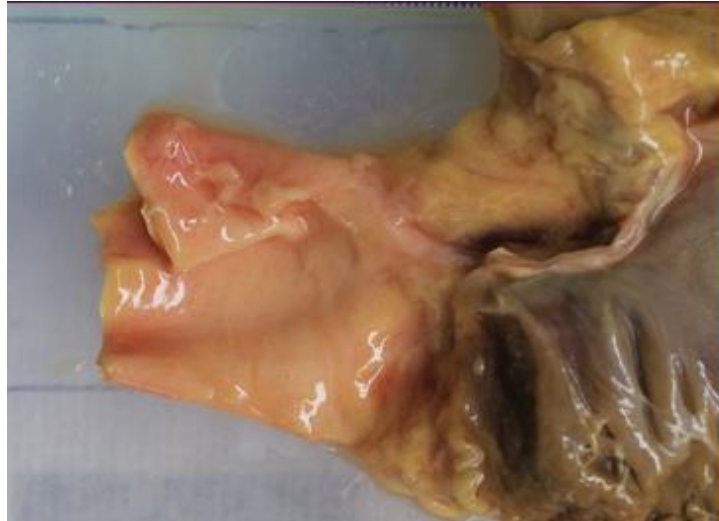
In Study II, eight human cellular pulmonary heart valve roots were used as detailed in Table 5.1.

**Table 5.1 Details of Pulmonary Heart Valve Roots Assessed in Study I, Including Patient Age, Sex and Valve Size.**

Pulmonary Heart Valve Roots							
Study I				Study II			
ID Number	Age (Years)	Sex	Valve Size (mm)	ID Number	Age (Year)	Sex	Valve Size (mm)
<b>Cellular</b>							
HP041	44	F	26	HP056	56	M	23
HP045	75	M	23	HP058	59	F	23
HP044	69	M	25	HP063	72	M	22
HP055	66	M	23	HP062	70	F	22
<b>Decellularised</b>				HP060	64	M	21
HP042	75	M	22	HP061	18	F	20
HP046	59	M	26	HP057	57	F	25
HP043	72	M	26	HP059	68	M	24
HP040	84	F	25				

The cryopreserved human donor pulmonary heart valve roots used in this study were supplied by NHS BT TES, Speke, Liverpool. The study was conducted under UK NHS Health Research Authority approval (REC 09/H1307/02). The decellularised human pulmonary heart valve roots were prepared by Dr Tayyebah Vafae in the Faculty of Biological Sciences (University Of Leeds). A detail decellularisation protocol used to decellularise heart valve roots is described by Vafae et al. (2016). Following decellularisation the pulmonary heart valve roots were cryopreserved using the standard NHS BT TES process and stored at  $-80^{\circ}\text{C}$ . All cryopreserved cellular and decellularised human pulmonary heart valve roots were thawed on the day before testing and stored in 100 ml Cambridge antibiotic solution at  $4^{\circ}\text{C}$ . The heart valve root defrosting procedure is described in detail in Chapter 2 Section 2.5. Immediately, before testing, the heart valve roots were rinsed with PBS. In between the tests the heart valve roots were stored in Cambridge antibiotic solution at  $4^{\circ}\text{C}$ . A representative image of a thawed cellular human pulmonary heart valve root is shown in Figure 5.2.

As received, the sizes (internal diameter) of all the valves were measured with obturators.



**Figure 5.2 Representative Image of Cellular Human Pulmonary Heart Valve Root**

## **5.4 Methods**

### **5.4.1 Methods Used in Study I**

#### **5.4.1.1 Hydrodynamic Performance**

##### **5.4.1.1.1 Competency**

In order to assess valve competency under static back pressure the leakage flow rate ( $F_L$ ) of each heart valve root was measured as described in Chapter 2 Section 2.4.6.1.3. The heart valve roots were deemed to be competent if the pressure head had not dropped from 60 to 20 mmHg within the cut-off period of 20 minutes (or leakage rate  $\leq 1.28 \text{ mL}\cdot\text{s}^{-1}$ ). The time ( $T_L$ ) taken for the test fluid to drop from 60 to 20 mmHg was recorded. The diameter of the heart valve root was measured at 4 to 5 mm above the sinotubular junction using a Vernier Calliper.

##### **5.4.1.1.2 Pulsatile Flow**

To evaluate hydrodynamic performance, each human pulmonary heart valve root was function tested in the pulsatile flow simulator. The heart valve root was initially tested in the pulsatile flow simulator at minimum compliance following the procedure detailed in Chapter 2 Section 2.4.7.4 to determine the peak flow conditions required for testing at maximum compliance, which are detailed in Table 5.2. The systemic pressure was held between 45 mmHg to 15 mmHg to mimic *in vivo* conditions. The test was repeated with the viscoelastic impedance adapter (VIA)

adjusted to its maximum compliance setting to produce relevant physiological pressure and flow characteristics.

**Table 5.2 Test Conditions Used in the Pulsatile Flow Performance of Cellular and Decellularised Pulmonary Heart Valve Roots**

Heart Rate (bpm)	Peak Flow (mL .s <sup>-1</sup> )
60	241
72	342
80	405

The evaluation of hydrodynamic performance of the pulmonary heart valve roots was achieved by producing measurements of transvalvular pressure across the valve and root mean square (RMS) flow and the Effective Orifice Area (EOA). The opening and closing of the valve was recorded with a high speed digital camera at 500 frames.s<sup>-1</sup>.

#### **5.4.1.2 Biomechanical Performance**

##### **5.4.1.2.1 Dilation (Expansion Characteristics)**

The circumferential expansion of each heart valve root was determined in terms of percentage dilation using the dilation test procedure described in Chapter 2 Section 2.4.8.1.2. The maximum applied internal pressure was 35 mmHg or until the valve failed. The mean percentage dilation was calculated at 20 mmHg.

##### **5.4.1.2.2 Uniaxial Tensile and Suture Pull-Out**

The tensile material properties of the wall (axial and circumferential) and leaflets (radial and circumferential) from each heart valve root were characterised using the uniaxial tensile testing method. The sample sizes and test method were described in Chapter 2 Section 2.4.8.2.3.1.3. The specimen thickness was measured with a digital thickness gauge J-40-V (James H. Heal and Company Limited). The tensile material parameters (elastin phase slope, collagen phase slope, ultimate tensile stress (UTS) and failure strain) were calculated from the stress strain graphs.

To determine the suture pull-out force and resistance to tearing of the wall and myocardial from each heart valve root, the suture pull - out test was performed on

the wall and myocardium as described in Chapter 2 Section 2.4.8.2.4. The peak load was recorded as the maximum suture pull-out force and the resistance to tearing for all the samples was determined.

## **5.4.2 Statistics**

All the hydrodynamic and biomechanical performance data for the cellular and decellularised pulmonary heart valve roots are presented as the mean  $\pm$  95 % confidence limits and statistical significance between the cellular and decellularised pulmonary heart valve roots performance was determined using Student's t-test. A significance level of  $p < 0.05$  was applied. Statistical analyses were performed using SPSS for Windows (version 21.0; SPSS, Inc., USA).

## **5.4.3 Methods Used in Study II**

### **5.4.3.1 Dimensional Measurements**

To derive the effect of decellularisation treatments with and without scraping on the heart valve root external morphology, the dimensions of each root, whilst laid flat were measured before and after each treatment as described in Chapter 2 Section 2.4.5. The scraping procedure and treatment resulted in four groups of heart valves [cellular un-scraped (Group 1), cellular scraped (Group 2), decellularised un-scraped (Group 3) and decellularised scraped (Group 4)]. The annulus width W1 and width W2 (Chapter 2, Figure 2.4) in the wall region were measured for each root before and after each treatment (scraping and decellularisation). The percentage change in the widths for W1 ( $\Delta W_{13}$  and  $\Delta W_{14}$ ) and W2 ( $\Delta W_{23}$  and  $\Delta W_{24}$ ) for Group 3 (un-scraped decellularised) relative to Group 1 (un-scraped cellular) and Group 4 (scraped decellularised) relative to Group 2 (cellular scraped) were compared.

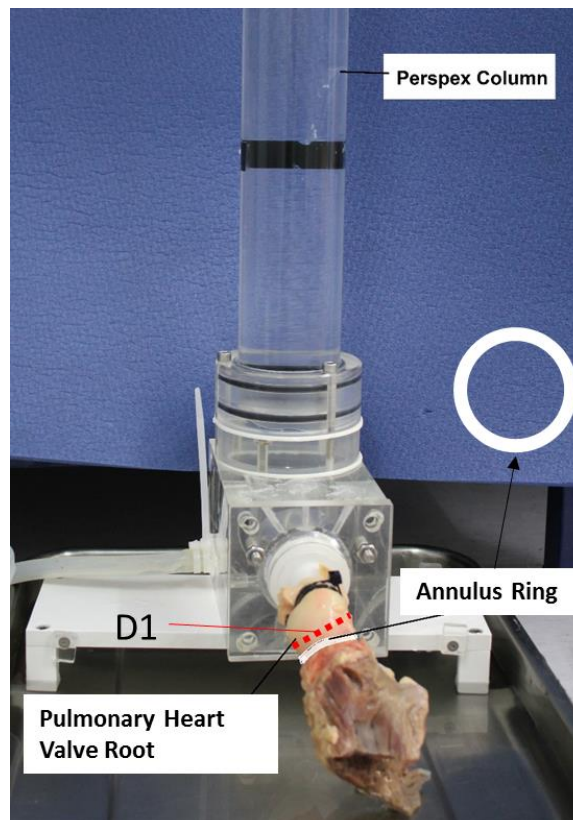
As explained in Chapter 2 Section 2.4.5.2, the accuracy of the valve dimensional measurements using imageJ was  $\pm 5\%$ , all the changes in widths less or equal to  $\pm 5\%$  were considered as no change.

### **5.4.3.2 Functional Biomechanical Performance**

#### **5.4.3.2.1 Competency with Annulus Support**

In order to assess valve closure after each treatment (scraping and decellularisation), competency tests were performed under a physiological static  
Chapter 5

back pressure range for each human pulmonary heart valve root [cellular un-scraped (Group 1), cellular scraped (Group 2), decellularised un-scraped (Group 3) and decellularised scraped (Group 4)]. The test set up used in Study II was modified compared to Study I (Section 5.4.1.1). In this phase, the annulus of each heart valve root was supported with an appropriately sized annulus ring as shown in Figure 5.3. This annulus ring helped to restore the shape and size of the valve annulus to its physiological dimensions and provided support that would physiologically be provided by the heart.



**Figure 5.3 Pulmonary Heart valve root with Annulus Ring Mounted in Static Leakage Tester**

The competency test was performed with and without annulus support for each pulmonary heart valve root as described in Chapter 2 Section 2.4.6.1.3. The time taken ( $T_L$ ) for the test fluid to drop from 60 mmHg to 20 mmHg was recorded. The mean leakage flow rate ( $F_L$ ) was calculated for each heart valve root. The heart valve root was considered to be competent if the pressure head had dropped to 20 mmHg within a cut-off of period of 20 minutes (or leakage rate  $\leq 1.28 \text{ mL}\cdot\text{s}^{-1}$ ).



The change in arterial diameter D1 of each heart valve root for group 3 (un-scraped decellularised) relative to group 1 (un-scraped cellular) and group 4 (scraped decellularised) relative to group 2 (cellular scraped) was calculated.

#### **5.4.3.2.2 Dilation (Expansion Characteristics)**

Following the dimensional measurement of each pulmonary heart valve root, the circumferential wall expansion characteristics were determined in terms of percentage dilation using the dilation test procedure which was identical to Study I (Section 5.4.1.2). Before converting dilation data to percentage, data distribution was tested using the Shapiro–Wilk test, and the data were considered normal if the probability value was  $P > 0.05$ . The data obtained were homogeneous ( $p=0.2$ ) and hence analysis was continued using the one-way analysis of variance (ANOVA) test. To evaluate the difference in the mean dilation between the four pulmonary heart valve root groups (cellular, cellular scraped, un-scraped decellularised and scraped decellularised), one-way ANOVA was performed, followed by Gabriel post-hoc test. Analysis was performed using the SPSS statistics program, and p-value of  $\leq 0.05$  was considered to be statistically significant.

### **5.5 Results**

#### **5.5.1 Study I**

##### **5.5.1.1 Hydrodynamic Performance of Human Cellular and Decellularised Pulmonary Heart Valve Roots**

###### **5.5.1.1.1 Competency**

The valve competency, mean leakage flow times, mean leakage flow rates and arterial diameter for the cellular and decellularised pulmonary heart valve roots are shown in Table 5.3.

**Table 5.3 Mean Leakage Flow Times ( $T_L$ ), Mean Leakage Flow Rates ( $F_L$ ), Competency and Arterial Diameters of Human Cellular and Decellularised Pulmonary Heart Valve Roots, assessed in Study I**

Valve ID Number	$T_L$ (second)	$F_L$ (mL.s <sup>-1</sup> )	Competent Yes Or No	Arterial Diameter (D1) (mm)
Cellular Pulmonary Heart Valve Roots				
HP041	449.5	3.41	No	30
HP045	389	3.95	No	29.8
HP044	>1200	<0.85	Yes	31.5
HP055	>1200	<0.85	Yes	31
Decellularised Pulmonary Heart Valve Roots				
HP042	634	2.42	No	28
HP046	303.5	5.05	No	33.5
HP043	241.5	6.37	No	32.5
HP040	90	17.25	No	37

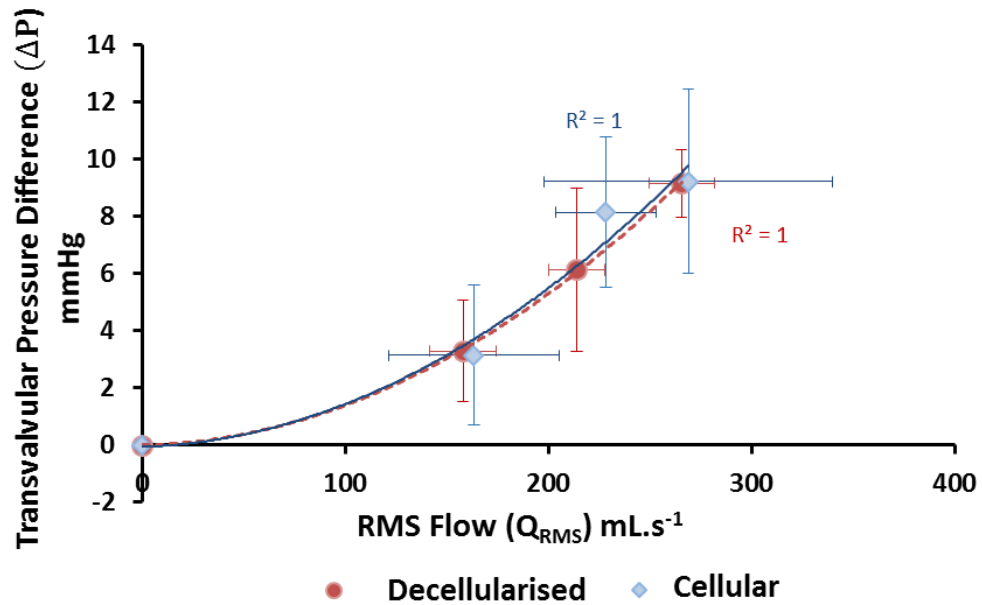
**Competent: Yes: Leakage flow rate  $\leq 1.28$  mL.s<sup>-1</sup>; No: Leakage flow rate  $> 1.28$  mL.s<sup>-1</sup>**

The majority of cellular and decellularised pulmonary heart valve roots were regurgitant. Two of the cellular heart valve roots (HP044 and HP055) were competent with mean leakage flow rates less than 0.85 mL.s<sup>-1</sup>. The decellularised heart valve root, HP040, had the highest mean leakage flow rate of 17.25 mL.s<sup>-1</sup>. The other three decellularised pulmonary heart valve roots had mean leakage flow rates below 7 mL.s<sup>-1</sup>.

At 60 mmHg, the measured arterial diameters of the cellular pulmonary heart valve roots ranged between 29.8 mm and 31 mm. The arterial diameters of the decellularised pulmonary heart valve roots ranged between 28 mm and 37 mm (Table 5.3).

#### 5.5.1.1.2 Pulsatile Flow

The mean transvalvular pressures versus mean RMS flows for human cellular and decellularised pulmonary heart valve roots for tested heart rates is shown in Figure 5.4.



**Figure 5.4 Mean Transvalvular Pressure versus Mean RMS Flow for Human Cellular and Decellularised Pulmonary Heart Valve Roots - Data fitted with second order polynomial trend line - The error bars indicate 95 % confidence limits**

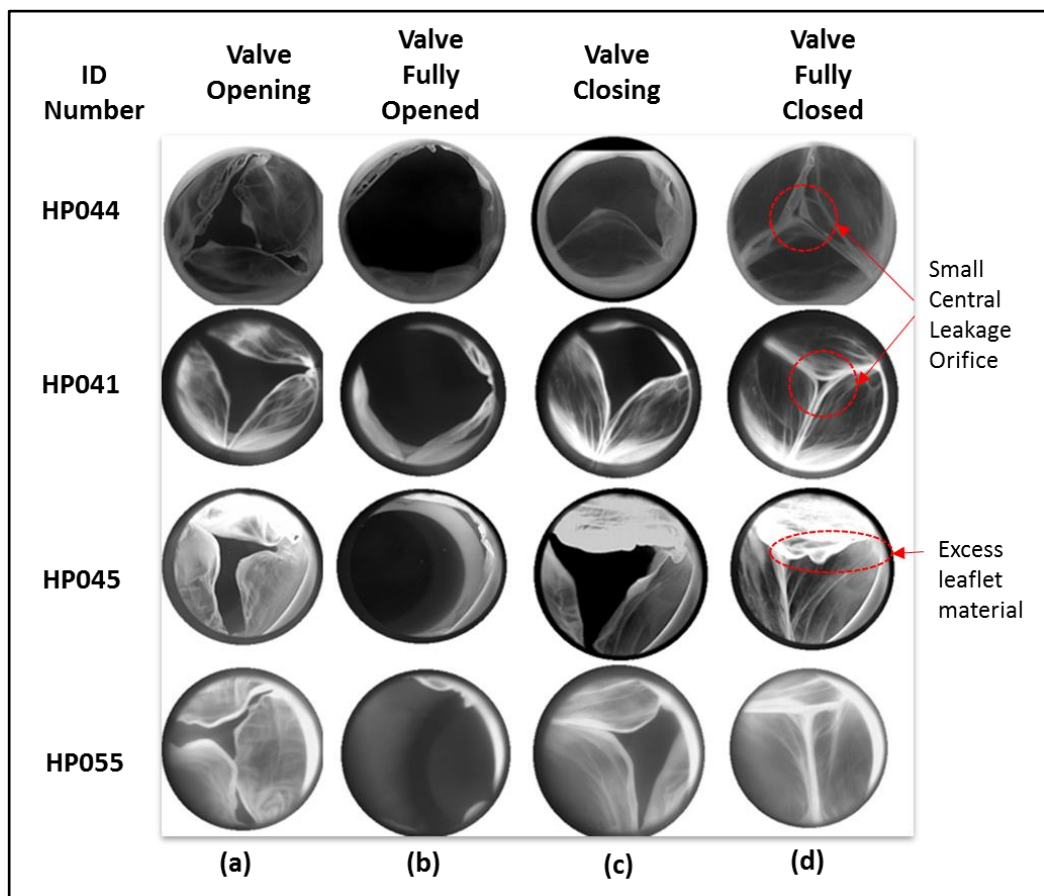
At a heart rate of 72 bpm, the mean transvalvular pressure with 95 % confidence limits across the decellularised pulmonary heart valve roots was  $6.1 \pm 2.8$  mmHg and for the cellular pulmonary heart valve roots was  $8.1 \pm 2.6$  mmHg. When comparing between the cellular and decellularised heart valve roots the mean transvalvular pressure across the decellularised heart valve roots was similar to the cellular heart valve roots for all three tested conditions ( $p > 0.05$ ).

**Table 5.4 Effective Orifice Area (EOA) for each Human Cellular and Decellularised Pulmonary Heart Valve Root averaged over the three Cycle Rates**

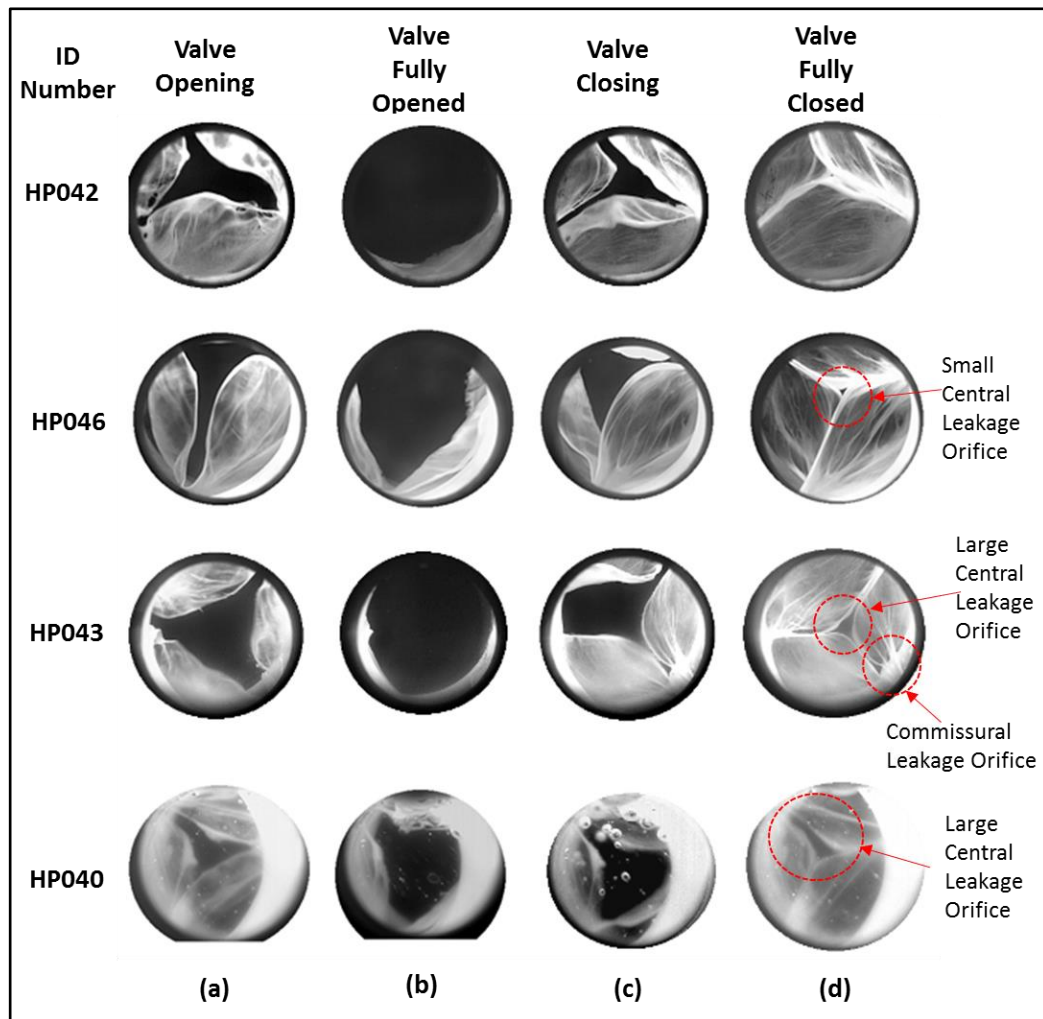
Cellular Pulmonary Heart Valve Root		Decellularised Pulmonary Heart Valve	
ID Number	Effective Orifice Area (EOA) $\text{cm}^2$ (PF)	ID Number	Effective Orifice Area (EOA) $\text{cm}^2$ (PF)
HP044	2.09	HP042	2.37
HP041	2.12	HP046	2.07
HP045	2.44	HP043	2.12
HP055	2.59	HP040	1.82

The EOA of each cellular and decellularised heart valve root, averaged over three cycle rates tested is shown in Table 5.4. The mean EOA with 95 % confidence limits was  $2.31 \pm 0.39 \text{ cm}^2$  and  $2.10 \pm 0.36 \text{ cm}^2$  for the cellular and decellularised pulmonary heart valve roots respectively which were similar (Student's t-test,  $p=0.2$ ).

Images of all the tested cellular and decellularised pulmonary heart valve roots in their closing, fully closed, opening and fully opened configuration are shown in Figure 5.5 and Figure 5.6 respectively.



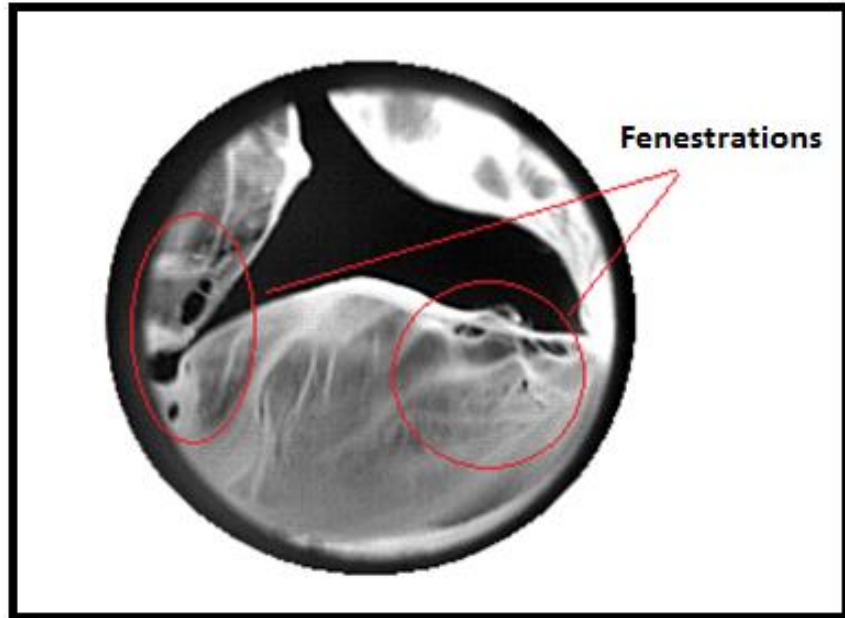
**Figure 5.5 (a) Valve Opening, (b) Valve Fully Opened, (c) Valve closing and (d) Valve Fully Closed Images of Human Cellular Pulmonary Heart Valve Roots at Heart Rate 72 bpm, captured from the Front View by a High-Speed Camera**



**Figure 5.6 (a) Valve Opening, (b) Valve Fully Opened, (c) Valve closing and (d) Valve Fully Closed Images of Human Decellularised Pulmonary Heart Valve Roots at Heart Rate 72 bpm, captured from the Front View by a High-Speed Camera**

It was observed that most of the cellular and decellularised heart valve roots demonstrated synchronous and triangular leaflet opening with leaflet fluttering during systole. In the decellularised heart valve roots HP040 and HP043, a large central leakage orifice was clearly visible. The decellularised heart valve roots HP040 and HP043 showed incomplete leaflet coaptation where the leaflet edges appeared to be taut, resulting in large central and commissural regurgitant orifices (Figure 5.6). Also the cellular heart valve roots HP044, HP041 and decellularised valve HP046 had minor central leakage orifices. The fully closed leaflet configuration for the cellular heart valve root HP055 and decellularised heart valve root HP042 showed full coaptation of the leaflets. The fully closed configuration of the cellular heart valve root HP045 exhibited an excess redundant free edge material. Also there were a few

small holes (fenestrations) observed in the tips of the leaflets for the cellular valve HP044 and decellularised valve HP042 as shown in Figure 5.7. Fenestration of valve leaflets is commonly noted at medical examination and surgery.



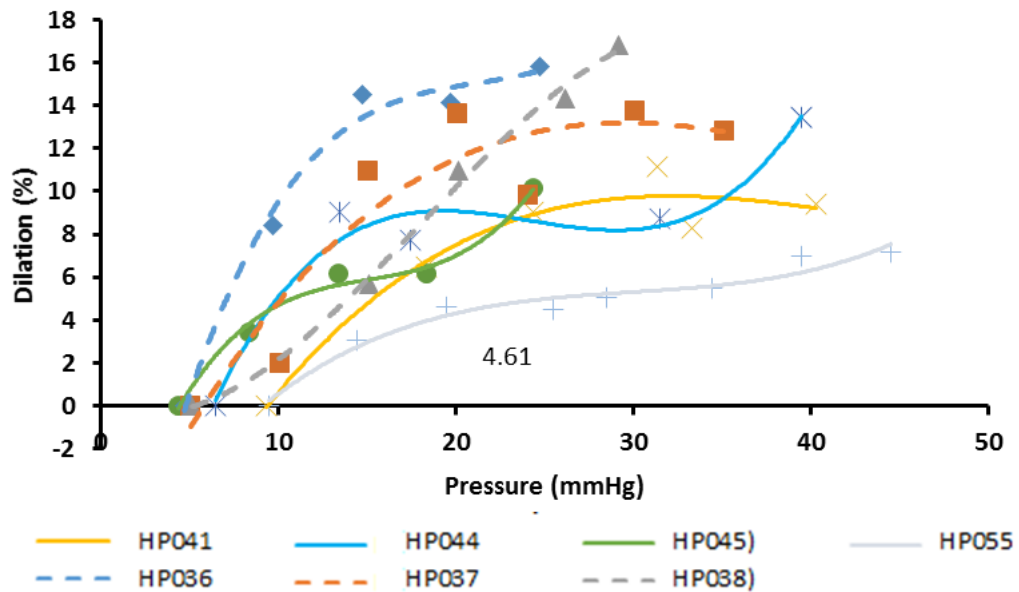
**Figure 5.7 Human Decellularised Pulmonary Heart Valve HP042 with Fenestrations Visible**

### **5.5.1.2 Biomechanical Performance of Human Cellular and Decellularised Pulmonary Heart Valve Roots**

#### **5.5.1.2.1 Dilation (Expansion Characteristics)**

The expansion characteristics in terms of percentage dilation as a function of applied internal pressure for the cellular and decellularised pulmonary heart valve roots are shown in Figure 5.8.

The expansion characteristics of the decellularised heart valve root HP040 could not be determined as it was leaking faster than the pressure applied. The expansion characteristics show that decellularised pulmonary heart valve roots (dotted lines) were more compliant than the cellular heart valve roots (solid lines).



**Figure 5.8 Percentage Dilation as a Function of Applied Pressure of Cellular (Solid Line, n=4) and Decellularised (Dotted Line, n=3) Porcine Heart Valve Roots-Data fitted with a third order polynomial trend line**

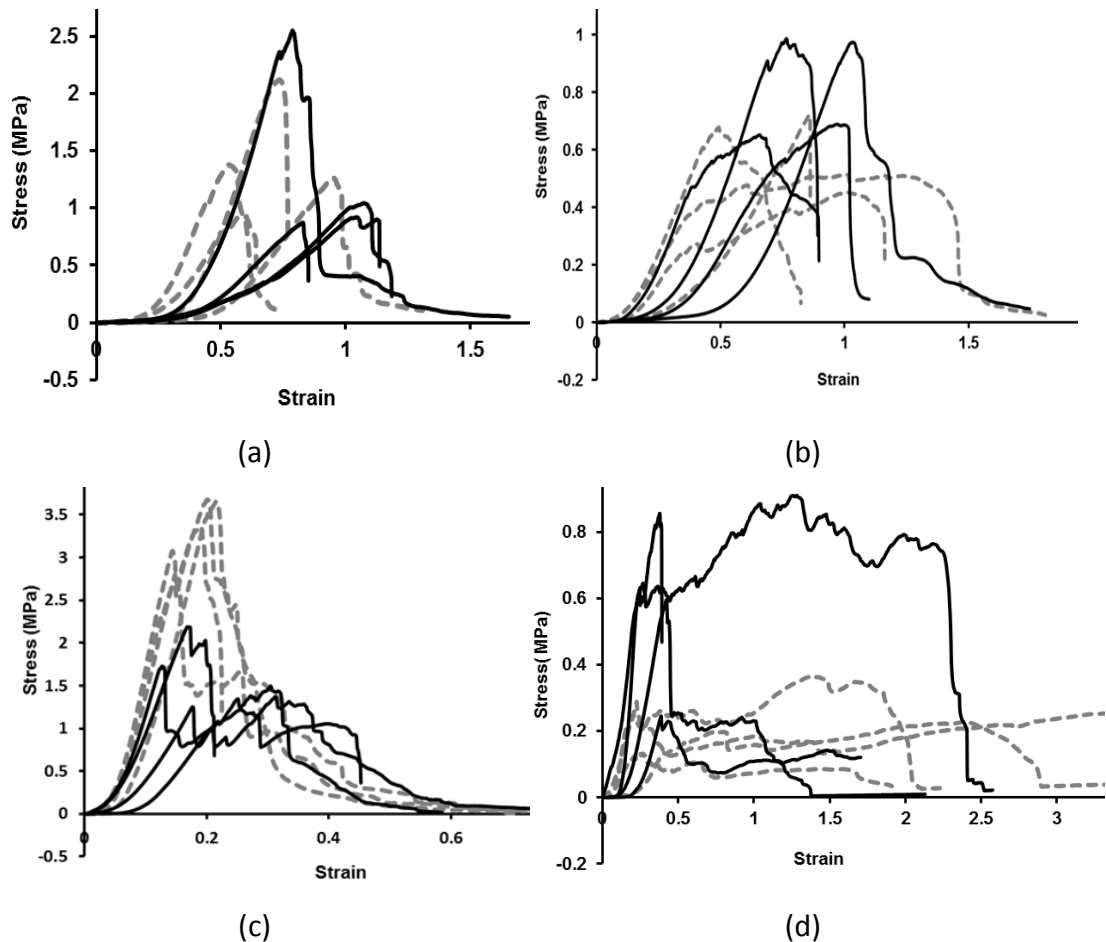
During the dilation testing, the starting pressure due to the height of saline was different for all the pulmonary heart valve roots. Although subsequent pressure was applied in similar regular intervals, it resulted in discrete final pressure values for all the heart valve roots. Therefore percentage dilation at the measurement point closest to 20 mmHg was used in the calculation of the mean percentage dilation.

These mean percentage dilation for cellular and decellularised was  $6.23 \pm 2.02$  and  $12.90 \pm 4.27$  mmHg respectively at 20 mmHg pressure. The decellularised pulmonary heart valve roots were significantly more compliant than the cellular pulmonary heart valve roots ( $P=0.002$ , Student's t-test).

#### 5.5.1.2.2 Tensile Properties

The majority of the cellular and decellularised wall and leaflet tissue specimens failed in the gauge length during uniaxial tensile testing.

The stress-strain graphs for all cellular and decellularised pulmonary wall and leaflet tissue specimens are illustrated in Figure 5.9.



**Figure 5.9 Stress-Strain Graphs for the Cellular (solid line, n=4) and Decellularised (dotted line, n=4) (a) Circumferential Pulmonary Wall (b) Axial Pulmonary Wall (c) Circumferential Pulmonary Leaflet (d) Radial Pulmonary Leaflet Specimens**

The graphs demonstrated the typical tri phasic characteristics. Figure 5.9 (a) and (b) clearly showed no obvious differences between the tensile wall characteristics (axial and circumferential) of the decellularised and cellular heart valve roots. However, tensile leaflet characteristics in circumferential directions demonstrated a rise in ultimate tensile stress after decellularisation. [Figure 5.9 (c)].

The mean thickness with 95 % confidence limits and tensile parameters with 95 % confidence limits for the cellular and decellularised pulmonary heart valve root wall (axial and circumferential) and leaflet (radial and circumferential) specimens are presented in Table 5.5 and Table 5.6 respectively.



**Table 5.5 Mean Thickness for the Cellular and Decellularised Pulmonary Heart Valve Root Wall and Leaflet Specimens - p values: statistical probability in the comparison between cellular and decellularised pulmonary heart valve roots**

	Specimen Direction	Mean Thickness (mm)		p Value
		Cellular	Decellularised	
Pulmonary Heart valve root <b>wall</b>	Axial	1.27 ± 0.28	1.11 ± 0.20	0.18
	Circumferential	1.20 ± 0.22	1.09 ± 0.15	0.23
Pulmonary Heart valve root <b>Leaflet</b>	Radial	0.26 ± 0.20	0.22 ± 0.07	0.57
	Circumferential	0.33 ± 0.28	0.22 ± 0.07	0.33

There was no significant difference among the mean cellular and decellularised pulmonary wall and leaflet specimen thickness in both tested directions ( $p > 0.05$ , Student's t-test).

**Table 5.6 Tensile Parameters (collagen phase slope  $E_c$ , elastin phase slope  $E_e$ , ultimate tensile stress  $\sigma_{UTS}$ , failure strain  $\epsilon_{failure}$ ) based on the Engineering Stress versus Engineering Strain behaviour of the Cellular and Decellularised Pulmonary Heart Valve Root Wall Specimens [Axial (A) and Circumferential (C) Directions] and Leaflet Specimens [Radial (R) and Circumferential (C) Directions] \*-Statistical significant difference ( $p < 0.05$ ) for decellularised versus cellular heart valve roots**

Pulmonary Heart Valve Root Specimen	$E_c$ MPa	$E_e$ MPa	$\sigma_{UTS}$ MPa	$\epsilon_{failure}$
<b>Wall (A)</b>				
Cellular	2.14 ± 0.70	0.15 ± 0.18	0.83 ± 0.28	0.86 ± 0.28
Decellularised	1.59 ± 0.55	0.10 ± 0.02	0.59 ± 0.20	0.84 ± 0.38
<b>p Value</b>	0.10	0.42	0.08	0.91
<b>Wall (C)</b>				
Cellular	3.20 ± 3.95	0.10 ± 0.02	1.35 ± 1.28	0.93 ± 0.23
Decellularised	4.23 ± 2.71	0.15 ± 0.14	1.42 ± 0.79	0.70 ± 0.30
<b>p Value</b>	0.52	0.27	0.87	0.10
<b>Leaflet (R)</b>				
Cellular	3.81 ± 3.73	0.33 ± 0.75	0.53 ± 0.30	0.33 ± 0.14
Decellularised	1.76 ± 1.33	0.33 ± 0.43	0.20 ± 0.13*	0.24 ± 0.18
<b>p Value</b>	0.15	0.99	0.02	0.25
<b>Leaflet (C)</b>				
Cellular	15.44 ± 9.72	1.07 ± 1.72	1.54 ± 0.84	0.17 ± 0.53
Decellularised	29.50 ± 6.31*	1.80 ± 2.18	3.28 ± 0.73*	0.18 ± 0.58
<b>p Value</b>	0.008	0.43	0.003	0.79

There was no significant difference between cellular and decellularised pulmonary heart valve root wall tensile parameters in the axial and circumferential directions ( $p > 0.05$ , Student's t-test)

The collagen phase slope and UTS of the decellularised pulmonary leaflet was significantly higher in the circumferential direction compared to cellular leaflet ( $p < 0.05$ , Student's t-test). However, in the radial direction the ultimate tensile stress for decellularised pulmonary leaflet specimens was significantly lower than decellularised specimens ( $p = 0.02$ , Student's t-test).

### 5.5.1.2.3 Suture Pull-Out Properties

During suture pull-out testing of wall and myocardial specimens, failure was seen as a wedge shaped cut spreading from the suture in the circumferential direction perpendicular to the axial axis.

The mean suture pull-out force and mean resistance to tearing for decellularised pulmonary heart valve root wall and myocardial specimen was not significantly different than the cellular pulmonary wall and myocardium specimen (Table 5.7;  $p > 0.05$ , Student's t-test).

There was no significant difference between the cellular and decellularised groups for the following factors: mean maximum suture pull out force for wall and myocardial specimens and resistance to tearing for the wall and myocardium specimens ( $p > 0.05$ ).

**Table 5.7 Mean Maximum Suture Pull-Out Force and Mean Resistance to Tearing for the Cellular and Decellularised Pulmonary Heart Valve Root Wall and Myocardial specimens - p values: statistical probability in the comparison between cellular and decellularised pulmonary heart valve roots**

Specimen Type	Mean Maximum force $\pm$ 95 % confidence limits (N)		Resistance to Tearing (N.mm <sup>-1</sup> )	
	Wall	Myocardium	Wall	Myocardium
Cellular	3.97 $\pm$ 1.98	1.74 $\pm$ 1.00	2.58 $\pm$ 1.57	0.60 $\pm$ 0.42
Decellularised	3.18 $\pm$ 1.04	2.14 $\pm$ 0.56	2.47 $\pm$ 1.10	1.05 $\pm$ 0.43
<b>p Value</b>	0.30	0.31	0.85	0.05

## 5.5.2 Study II

### 5.5.2.1 Dimensions of Human Pulmonary Heart Valve Roots (Cellular Un scraped, Cellular Scraped, Decellularised Un-Scraped and Decellularised Scraped Heart Valve Roots)

The dimensions of each pulmonary heart valve root when laid flat for all the groups are detailed in Table 5.8.

As shown in Table 5.8, a paired width comparison ( $\Delta W_{13}$ ,  $\Delta W_{14}$ ,  $\Delta W_{23}$   $\Delta W_{24}$ ) was made between the appropriate pair of groups i.e., Group 3 (decellularised un-scraped) was compared with Group 1 (cellular) and Group 4 (decellularised scraped) was compared with Group 2 (cellular scraped). As the sensitivity of measurement technique was  $\pm 5\%$ , all the changes in width less than or equal to  $\pm 5\%$  were considered as no change. The results in Table 5.8 showed that the measurements for cellular and decellularised heart valve roots did not exhibit any trend. These results were highly dependent on the quality and consistency of the captured images and sensitivity of the diameter measurement technique in imageJ.

**Table 5.8 Wall Widths (W1 and W2) of each Human Pulmonary Heart Valve Root for all the Groups [Cellular Un- Scraped (Group 1), Cellular Scraped (Group 2), Decellularised Un-Scraped (Group 3), Decellularised Scraped (Group 4)] and Percentage Change in Widths W1 ( $\Delta W_{13}$  and  $\Delta W_{14}$ ) and W2 ( $\Delta W_{23}$  and  $\Delta W_{24}$ ) for Decellularised Un-Scraped (Group 3) and Decellularised Scraped (Group 4) Human Pulmonary Heart Valve Roots**

ID	Heart Valve Root Width				Change in Width		Heart Valve Root Width				Change in Width	
	W1 (mm)						W2 (mm)					
	Group						Group					
	1	2	3	4	$\Delta W_{13}$	$\Delta W_{14}$	1	2	3	4	$\Delta W_{23}$	$\Delta W_{24}$
HP056	41.1	42.8		47.9		↑	32.6	34.4		36.8		↑
HP058	47.8	60.3		51.1		↓	35.3	42.1		42.2		-
HP063	41.8		41.9		-		36.8		39.5		↑	
HP062	49.4		47.9		-		45.4		40.7		↓	
HP060	37.3	39.2		42.0		↑	34.2	33.4		34.8		-
HP061	33.6	35.9		33.3		↓	32.1	32.9		36.8		↑
HP057	51.4		52.7		-		42.9		42.7		-	
HP059	44.4		46.8		↑		33.1		33.2		-	

↑:Increase, ↓:Decrease, -: No change

### **5.5.2.2 Functional Biomechanical Performance of Human Pulmonary Heart valve roots (Cellular Un scraped, Cellular Scraped, Decellularised Un-Scraped and Decellularised Scraped Heart Valve Roots)**

#### **5.5.2.2.1 Competency with and without Annulus Support**

The valve competency ( $C_p$ ) and mean leakage flow rates ( $F_L$ ) for all the heart valve roots of all the groups [cellular un- scraped (Group 1), cellular scraped (Group 2), decellularised un-scraped (Group 3) and decellularised scraped (Group 4)] are shown in Table 5.9.

As shown in Table 5.9, the heart valve root competency assessment revealed that without annulus support the majority of cellular un-scraped, cellular scraped, decellularised un-scraped and decellularised scraped pulmonary heart valve roots were regurgitant.

The mean leakage flow rate for the cellular group (un-scraped and scraped) of heart valve roots was under  $2.5 \text{ mL}\cdot\text{s}^{-1}$  with annulus support, with the majority being competent. After decellularisation treatment the mean leakage flow rate for these heart valve roots were also under  $2.5 \text{ mL}\cdot\text{s}^{-1}$  with annulus support with the exception of the decellularised un-scraped heart valve root HP059 ( $4.4 \text{ mL}\cdot\text{s}^{-1}$ ). The competency of the cellular un-scraped heart valve roots HP057 could not be measured without the annulus ring as the valve was leaking faster than the static pressure applied and when the competency was assessed again with annulus ring it was still an incompetent valve with the highest mean leakage flow rate of  $26.0 \text{ mL}\cdot\text{s}^{-1}$ . However, after decellularisation, the valve appeared more competent and the mean flow rate was reduced to  $1.01 \text{ mL}\cdot\text{s}^{-1}$ . The reason for this was not clear. The mean leakage rates for the valves HP056, HP058, HP060 and HP061 before (Group 1) and after scraping (Group 2) were similar. The arterial diameters for each heart valve root for all the groups at 60 mmHg pressure are shown in Table 5.10. The dimension of heart valve root HP057 could not be measured before and after the treatments (scraping and decellularisation), as the valve leakage was too fast and it was difficult to control pressure at 60 mmHg. The data did not show any trend in arterial diameters of the pulmonary heart valve roots groups.

**Table 5.9 Mean Leakage Flow Rates ( $F_L$  mL.s<sup>-1</sup>) and Competency (Cp) for each Human Pulmonary Heart Valve Root for all the Groups [Cellular Un- Scraped (Group 1), Cellular Scraped (Group 2), Decellularised Un-Scraped (Group 3), Decellularised Scraped (Group 4)]**

	Group 1				Group 2				Group 3				Group 4			
	Without		With		Without		With		Without		With		Without		With	
	Support				Support				Support				Support			
	$F_L$	Cp	$F_L$	Cp	$F_L$	Cp	$F_L$	Cp	$F_L$	Cp	$F_L$	Cp	$F_L$	Cp	$F_L$	Cp
HP056	3.41	No	1.28	Yes	3.05	No	1.28	Yes					3.40	No	2.13	No
HP058	1.26	Yes	1.28	Yes	1.30	No	1.28	Yes					2.16	No	1.28	Yes
HP063	2.26	No	0.99	Yes					6.39	No	2.49	No				
HP062	3.63	No	1.28	Yes					6.64	No	1.44	No				
HP060	1.55	No	1.28	Yes	2.51	No	1.28	Yes					3.18	No	1.94	No
HP061	3.97	No	1.47	No	1.47	No	1.28	Yes					4.79	No	2.35	No
HP057	~~	~~	26.0	No					1.01	Yes	1.28	Yes				
HP059	3.55	No	2.39	No					4.93	No	4.40	No				

~~ - Leakage rate not measured. Cp - Competency (Yes- leakage rate  $\leq 1.28$  mL.s<sup>-1</sup>, No -leakage rate  $\geq 1.28$  mL.s<sup>-1</sup>)

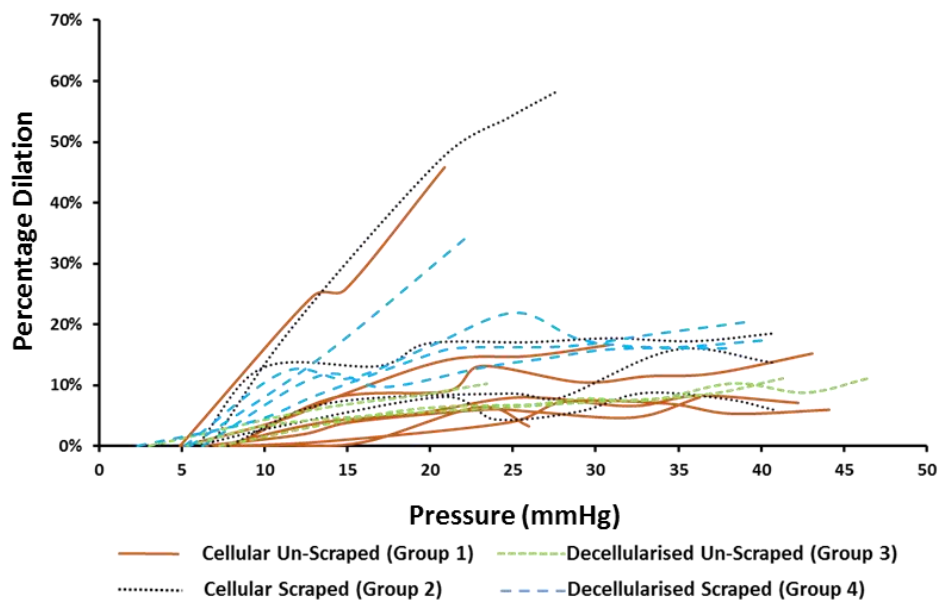
**Table 5.10 Diameters D1 of each Human Pulmonary Heart Valve Root for all the Groups [Cellular Un- Scraped (Group 1), Cellular Scraped (Group 2), Decellularised Un-Scraped (Group 3), Decellularised Scraped (Group 4)] at 60 mmHg Static Pressure and Change in Diameter  $\Delta D1$**

ID	Heart Valve Root Diameter D1 (mm)				$\Delta D1$ mm	
	Group					
	1	2	3	4	3	4
HP056	35.4	36.5		34.9	-	
HP058	40.1	32.4		34.8	↑	
HP063	35.9		30.9		↓	
HP062	30.3		30.4		-	
HP060	33.9	31.9		31.6	-	
HP061	37.0	38.0		36.0	↑	
HP057	~~		~~		~~	
HP059	36.8		34.2		↑	

↑: Increase, ↓: Decrease, -: No change, ~~ : Diameter not measured

#### 5.5.2.2.2 Dilation (Expansion Characteristics)

The percentage dilations for the pulmonary heart valve roots (cellular, cellular scraped, decellularised un-scraped and decellularised scraped) are shown as a function of applied pressure in Figure 5.10.

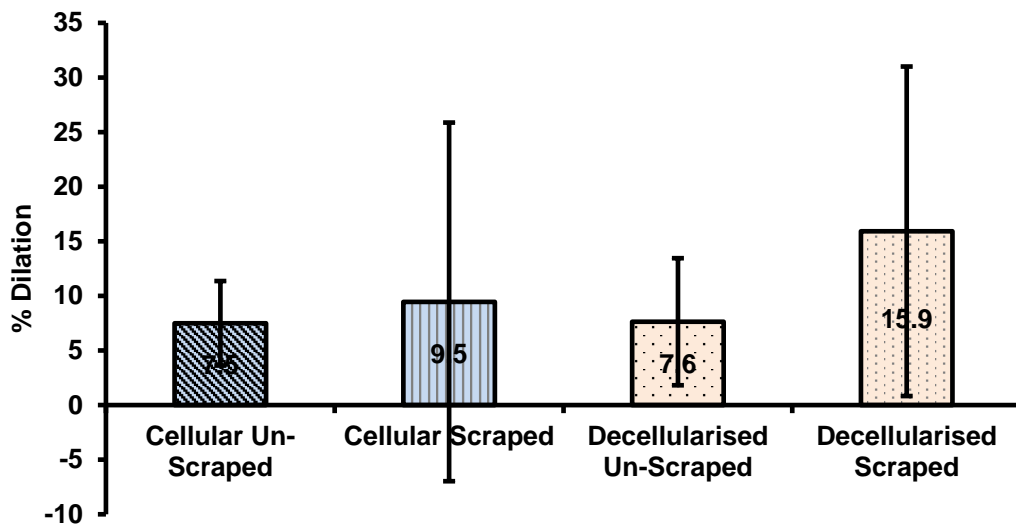


**Figure 5.10 Percentage Dilation as a Function of Applied Pressure of Cellular Un-scraped (Group 1, n=7) and Cellular Scraped (Group 2, n=4), Decellularised Un-Scraped (Group 3, n=3) and Decellularised Scraped (Group 4, n=4) Heart valve roots**

The percentage dilation for the heart valve root HPO57 could not be determined as it was leaking faster than the pressure applied. The donor age for the valve HP061 (18 years) was not in the same range as the other valves and also the dilation results for the valve before and after decellularisation were not in range with the other heart valve roots. Hence the dilation data for valve HP061 was omitted from the analysis.

The mean percentage dilation for all the groups of heart valve roots at 20 mmHg pressure was similar ( $p > 0.05$ , one way Anova).

As shown in Figure 5.11, the mean dilation for the decellularised scraped pulmonary heart valve roots (Group 4) was higher than that of all the other groups, but not significantly ( $p > 0.05$ ).



**Figure 5.11 Mean Percentage Dilation at Approximately 20 mmHg For All the Pulmonary Cellular (Group 1, n=6), Cellular Scraped (Group 2, n=3), Decellularised Un-Scraped (Group 3, n=3) and Decellularised Scraped (Group 4, n=3) Heart Valve Roots. - The error bars indicate 95 % confidence limits.**

## 5.6 Discussion

### 5.6.1 Effect of Decellularisation on Hydrodynamic Performance of Human Cellular Pulmonary Heart Valve Roots

The decellularised pulmonary heart valve roots demonstrated similar hydrodynamic characteristics to cellular pulmonary heart valve roots. The mean EOA for the decellularised pulmonary heart valve roots was also very similar to that of



cellular pulmonary heart valve roots ( $2.10 \pm 0.36 \text{ cm}^2$  vs  $2.31 \pm 0.39 \text{ cm}^2$  respectively,  $p=0.5$ ). The high speed video analysis showed that one cellular and one decellularised pulmonary heart valve root showed good closed leaflet configuration, and a further two cellular and one decellularised heart valve root showed minor central leakage orifices under pulsatile flow conditions. It was observed however that two decellularised heart valve roots HP043 and HP040 had poor closed leaflet configuration with visible large leakage orifices. The images of closed leaflet configuration correlated well with measured reverse flow rates. The decellularised heart valve root HPO40, showed poor closed leaflet configuration during pulsatile flow assessment and the highest leakage flow rate of  $17.25 \text{ mL}\cdot\text{s}^{-1}$  with the largest arterial diameter of 37 mm during the valve competency assessment. Overall the decellularised heart valve root HPO40 did not perform well under the pulsatile flow and static back pressures. In contrast, two of the four cellular pulmonary heart valve roots were classified as competent as they had leakage rates less than  $1.28 \text{ mL}\cdot\text{s}^{-1}$ . Two of the cellular and majority of the decellularised pulmonary heart valve roots were regurgitant with large variation in the leakage flow rates and heart valve root diameters, noticeably in decellularised group. Also the decellularised pulmonary human heart valve roots were more expansible in the circumferential direction (Section 5.5.1.2.1) than cellular human pulmonary heart valve roots. During this phase, there was a concern that before application of the decellularisation treatment excess fat, connective tissue and the adventitial layer from the pulmonary heart valve roots were removed (scraping process) which may have disrupted the outer layer of the adventitia. This layer has an important role in the structural support of the vessel wall in preventing overstretching (2011, Laflamme et al., 2006). Damage to the adventitial layer may adversely affect the biomechanical properties of the artery and hence function of the heart valve root.

It was also apparent that the study was based on a small sample size, and was therefore of low statistical power and there was a large variation between samples within a group, limiting the interpretation of the results. It was also apparent that it was not known whether the human decellularised heart valve roots that had been decellularised had a large diameter prior to decellularisation or whether the heart valve roots had increased in diameter as a result of the decellularisation process.

After data analysis, it was recognised that the method for competency assessment was unsuitable for pulmonary heart valve roots due to the thin right myocardium of the pulmonary heart valve root which was not supported during competency assessment and this is not the case *in vivo*. This meant that the annulus of the pulmonary heart valve root was not being fully supported and therefore, the leaflets were not coapting fully. In addition, the competency assessment protocol was adopted from the previous study (Jennings, 2001), in which the annulus of the heart valve root was not supported, because the majority of the tested heart valve roots were fixed with glutaraldehyde and hence they had fixed geometry. Therefore it was necessary to improve the method for competency assessment by incorporating a more physiological condition. To clarify all these findings, Study II was conducted.

In Study II, the setup for valve competency assessment was modified to incorporate an annulus ring in order to mimic the annulus support provided from the heart. The annulus supported competency assessment of the eight cellular pulmonary heart valve roots showed that five out of eight heart valve roots had low regurgitant flow rates below  $2.4 \text{ mL}\cdot\text{s}^{-1}$  under physiological static back pressure. Maintaining valve competency of biological heart valve roots is dependent on the coordinated actions of the annulus, leaflets and associated wall collectively. Therefore, stiffening or dilation of the wall or stiffening of the leaflets can impede proper coaptation of the valve leaflets during closure and thereby promote regurgitation (Sabbah et al., 1986). After the application of the decellularisation treatment to these valves, the leakage flow rates remained under  $2.5 \text{ mL}\cdot\text{s}^{-1}$  with the exception of one heart valve root ( $4.4 \text{ mL}\cdot\text{s}^{-1}$ ). The competency assessment was performed with and without annulus support and from those results it was clear that the use of an annulus support ring reduced the leakage flow rate, as this ring provided structural support to restore the shape and size of the valve annulus to its physiological geometrical dimensions. In addition to leakage flow rate, the arterial diameter of each heart valve root was measured at 60 mmHg during competency testing. The data did not show any trend in annulus or arterial diameters between cellular and decellularised heart valve roots. These results should, however be considered cautiously, as physiologically the heart valve roots were delicate and

covered with fatty tissue, so it was difficult to mount heart valve roots in exactly the same orientation each time for an exact comparison.

The aim of this study was to characterise human pulmonary heart valve roots that had been decellularised using low concentration SDS before using them in the clinic as a replacement valve, in particular in the Ross procedure to reconstruct the right ventricular outflow tract. Several studies (Bechtel et al., 2008, Konuma et al., 2009, Burch et al., 2010, Brown et al., 2011) have reported short-term and medium-term *in vivo* performance of pulmonary human heart valves that have been decellularised using different processes (CryoValve SynerGraft®, CryoLife Inc, Kennesaw, GA) in comparison to standard cryopreserved allografts. Overall, 399 CryoValve SynerGraft® pulmonary human heart valves were implanted in several centres for pulmonary valve replacement between 2000 and 2005 and results were favourable with respect to structural deterioration and endocarditis. Da Costa et al. have demonstrated that decellularised pulmonary allografts showed excellent hemodynamic behaviour and reduction in immunogenic response compared to standard allografts in the right ventricular outflow tract (RVOT) (da Costa et al., 2005). Another recent study by Da Costa reported higher reoperation-free survival with decellularised pulmonary allografts compared to conventional cryopreserved allografts for RVOT reconstruction up to 6 years of follow-up, and, in addition, pressure gradients were lower in the decellularised pulmonary allografts (da Costa et al., 2014).

### **5.6.2 Effect of Decellularisation on Biomechanical Performance of Human Cellular Pulmonary Heart Valve Roots**

The biomechanical performance of the decellularised pulmonary heart valve roots was evaluated and compared with cellular pulmonary heart valve roots through assessment of wall circumferential expansion characteristics, uniaxial tensile testing to failure and suture pull out.

The decellularised pulmonary heart valve root walls were more extensible in the circumferential direction than the cellular pulmonary heart valve root walls. The dilation of decellularised pulmonary heart valve root walls increased to  $12.9 \pm 4.3\%$ , compared to  $6.2 \pm 2.0\%$  for cellular heart valve root walls at approximately 20 mmHg

internal pressure. However, this was an unpaired comparison. It was believed that this increase in dilation could be due to several reasons such as the wall of the decellularised heart valve roots being thinner than the cellular heart valve roots (although this was not significant); the variability and accuracy in the measurement technique; or could have simply been due to inherent biological variation. Also, as discussed in Section 5.6.1, the scraping procedure may have induced disruption in the wall mechanical properties. Therefore Study II was introduced to investigate the influence of the scraping step in the decellularisation protocol on the functional biomechanical performance of the heart valve roots. Study II made a paired comparison and showed that scraping of the adventitia layer of the wall or decellularisation treatment had no significant effect on the circumferential characteristics of the pulmonary heart valve root wall. The circumferential expansion characteristics of the pulmonary heart valve root walls showed that the processing step (scraping) and decellularisation treatment had no significant effect on the dilation properties of the pulmonary heart valve roots. Although, 95 % confidence limits were high in the dilation test results (Study II), particularly within the cellular scraped and decellularised scraped compared to cellular un-scraped and decellularised un-scraped pulmonary heart valve roots. These large confidence limits may be attributed to the small number of sample sizes ( $n=3$ ) used in the calculation of the mean value.

To determine effect of heart valve root wall scraping and decellularisation treatment on the dimensions of human pulmonary heart valve roots, dimensions of the same roots were measured before and after wall scraping and after decellularisation. The dimensional measurement data of the pulmonary heart valve root groups (cellular un-scraped, cellular scraped, decellularised un-scraped and decellularised scraped) did not exhibit any trend. These results were highly dependent on the quality and consistency of the captured images and sensitivity of measurement analysis in imageJ.

The decellularised heart valve root wall specimen had similar stress-strain characteristics (extensibility and stiffness) in the axial and circumferential directions to that of the cellular heart valve root wall specimen. This leads to the conclusion that

the heart valve root wall maintains its natural material tensile properties following decellularisation due to the preservation of the elastin and collagen content of the wall. However, the stress-strain characteristics of decellularised pulmonary leaflets differed compared to the cellular leaflets. The decellularised pulmonary leaflets were stronger in the circumferential direction with a significant increase in mean collagen phase slope and ultimate tensile stress (UTS), compared to cellular leaflets. Such changes may be due to the significant reduction of glycosaminoglycan (GAGs) and removal of cells reported by Vafaei et al. (2016). The loss of GAGs in the decellularised leaflets, may have led to loosening of the fibrous structure and uncrimping of the circumferentially aligned collagen fibers. This could potentially cause an earlier than normal recruitment and reorientation of the collagen fibers in the direction of applied strain during tensile testing (Williams et al., 2009). Previous work on decellularised tissues has shown similar findings in bone tissue (Banse et al., 2002), ligaments (Frank et al., 1995, Herbert et al., 2016) and soft tissue (Freed and Doehring, 2005). It is hypothesised that the leaflets of the decellularised heart valve roots will recellularise *in vivo* and regain their physiological tensile properties. Conversely, the extensibility of decellularised pulmonary leaflets was comparable to the cellular leaflets in both the radial and circumferential directions, while UTS for decellularised specimens was significantly reduced in the radial direction. However, it is important to note that the biomechanical performance of decellularised and cellular heart valve roots was not a paired comparison. Previous results on porcine pulmonary heart valve roots decellularised with a similar protocol did not show leaflet stiffening but showed wall stiffening in both the axial and circumferential directions in the initial elastin phase (2014). These findings related to material properties of the decellularised pulmonary heart valve roots, showed that the resultant changes due to decellularisation treatment can be highly dependent on species, tissue type and method (Gilbert et al., 2006), this highlights the need to carry out robust pre-clinical testing of all types of decellularised tissues prior to their implantation.

The decellularised human pulmonary heart valve root wall and myocardial specimens had similar suture pull-out forces to cellular human pulmonary heart valve root wall and myocardial specimens respectively. However, the resistance to tearing

for the decellularised myocardial specimens was significantly higher than the cellular specimens. This increase might have been due to the large variation in specimen thickness and also quality of the myocardial specimens. A few of the myocardial specimens may have become damaged during prior test procedures, which required the clamping of the myocardial with cable ties.

The limitations of this study include the small number of samples giving low statistical power, simplification of the *in vivo* environmental conditions and the biological variation within the pulmonary heart valve root groups.

## 5.7 Conclusion

In conclusion, an extensive *in vitro* hydrodynamic and biomechanical comparison of decellularised and cellular human pulmonary heart valve roots has been performed. Neither hydrodynamic nor expansion properties of human pulmonary heart valve roots were significantly affected by the low concentration SDS decellularisation treatment. Also, the processing step (scraping) during decellularisation treatment did not alter functional biomechanical properties of human pulmonary heart valve roots. However, decellularisation significantly altered some of the directional material properties of pulmonary heart valve leaflets. Also, there was a trend for increased leakage flow rate following decellularisation although after decellularisation treatment the mean static leakage rate for the pulmonary valves were also under  $2.5 \text{ mL}\cdot\text{s}^{-1}$  with annulus support with the exception of one heart valve root ( $4.4 \text{ mL}\cdot\text{s}^{-1}$ ). This work has been published in the Journal of the Mechanical Behavior of Biomedical Materials and publication details can be found in Appendix A.

## **6 *In vitro* Material Properties of Non- and Post-Implanted Decellularised Porcine Pulmonary Heart Valve Roots**

In this chapter, material properties of the non-implanted and post-implantation decellularised porcine pulmonary heart valve roots were evaluated to assess the material properties of decellularised porcine pulmonary heart valve roots after 12 months implantation in sheep. Comparison of the material properties of the non - implanted and implanted decellularised porcine pulmonary heart valve roots provided understanding of any biomechanical changes that occurred as a result of cellular population *in vivo*. The material properties assessment of 12 months implanted decellularised porcine pulmonary heart valve roots was part of a larger collaborative study with Professor Francisco Da Costa, Pontificia Universidade Catolica do Parana, Curitiba, Brazil.

### **6.1 Introduction**

Decellularised porcine pulmonary heart valve roots, in various sizes, have been developed with a view to their clinical use in the Ross procedure (2014). An *in vivo* proof of concept study of these decellularised porcine pulmonary heart valve roots was conducted in collaboration with Professor Francisco Da Costa, Pontificia Universidade Catolica do Parana, Curitiba, Brazil. The decellularised porcine heart valve roots were implanted in the orthotopic position (right ventricular outflow tract; pulmonary position) of juvenile sheep (120 days) and explanted at 1 (n=4), 3 (n=4), 6 (n=4) and 12 (n=8) months. The *in vivo* functional performance was monitored by weight gain and Doppler echocardiography. Roots explanted at 1, 3, 6 and 12 months (n=4 per group) were assessed by gross analysis, histology, immunohistochemistry and quantitative calcium analysis to assess the regenerative process over time. The *in vivo* and biological data is not described here as it was out with the scope of this study (manuscript in preparation). In summary, the functional performance of decellularised porcine pulmonary roots over a 12 month period was excellent, with evidence of cellular population. However, the levels of calcium in the pulmonary wall and leaflets of the 12 month explanted decellularised porcine pulmonary heart valve

roots, although low (278-401 ppm) were significantly greater than in the non-implanted decellularised porcine and cellular ovine pulmonary heart valve roots (Berry et al., 2017).

The aim of this part of the study was to characterise the material of the decellularised porcine pulmonary heart valve roots (n=4) following 12 months implantation in sheep. Cryopreservation was used to preserve the decellularised porcine pulmonary heart valve roots before they were implanted in the sheep. In this context, this study was designed to test the following hypotheses:

1) The pre-implantation treatments (decellularisation and cryopreservation) alter the material properties of the porcine pulmonary heart valve roots.

2) The material properties of decellularised porcine pulmonary heart valve roots changes as a result of post-implantation structural changes, inflammatory response and graft incorporation.

There are many methods to evaluate the material properties of heart valve roots, however uniaxial tensile testing is the most practical method and allows measurement of stress-strain behavioural properties of the wall and leaflets.

## **6.2 Aim**

The aim of the study was to assess the effects of low concentration sodium dodecyl sulphate (SDS) decellularisation and cryopreservation on the material properties of porcine pulmonary heart valve roots and determine the material properties of decellularised porcine pulmonary heart valve roots following 12 months implantation in three months old sheep.

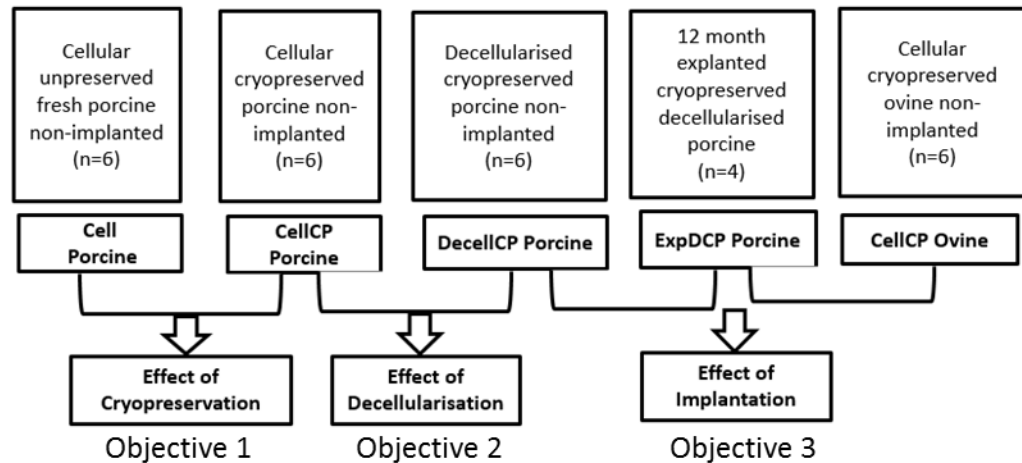
The objectives of this study (Figure 6.1) were:

1. To determine and compare the material properties of the pulmonary artery wall and leaflets of cryopreserved cellular porcine non-implanted and non-cryopreserved cellular porcine non-implanted pulmonary heart valve roots in order to investigate the effect of cryopreservation.
2. To determine and compare the material properties of the pulmonary artery wall and leaflets of cryopreserved decellularised porcine non-implanted and



cryopreserved cellular porcine non-implanted pulmonary heart valve roots in order to investigate the effect of decellularisation.

- To determine and compare the material properties of cryopreserved 12 months explanted decellularised porcine, cryopreserved decellularised porcine non-implanted and cryopreserved cellular ovine non-implanted pulmonary heart valve roots to determine the effects of 12 months implantation in juvenile sheep.



**Figure 6.1 Pulmonary Heart Valve Root Experimental Groups**

### 6.3 Materials

Five pulmonary heart valve root groups were studied and each group had n=6 with the exception of 12 month explanted cryopreserved decellularised porcine pulmonary heart valve root group (n=4) as described in Table 6.1.

The cellular porcine and cellular ovine pulmonary heart valve roots were dissected from hearts which were obtained from *M & C Meats, Crossgates, Leeds* or *John Penny & Sons, Rawdon, Leeds, UK*. within 4 hours of slaughter.

The decellularised porcine pulmonary heart valve roots were prepared in the Faculty of Biological Sciences (University of Leeds, Leeds) using established decellularisation procedures (2014). The heart valve roots were cryopreserved using the protocol utilised by NHS Blood Transplant Tissue & Eye Services (Speke; Liverpool, UK) and stored at -80 °C until use.

Four decellularised porcine pulmonary heart valve roots were explanted from sheep after 12 months *in vivo* at the Pontificia Universidade Catolica do Parana, Curitiba, Brazil and shipped to Leeds for material properties assessment.

Phosphate buffered saline (PBS) was used to keep the roots hydrated during the test procedure.

**Table 6.1 Details of Pulmonary Heart Valve Roots Groups Assessed Including Abbreviation, Age of the Animal and Number of Specimens in Each Group**

<b>Pulmonary Heart Valve Root Group</b>	<b>Abbreviation</b>	<b>Age of the Animal (Months)</b>	<b>Number of Specimens (n)</b>
Cellular cryopreserved ovine non-implanted	CellCP Ovine	15	6*
12 month explanted cryopreserved decellularised porcine	ExpDCP Porcine	15	4
Decellularised cryopreserved porcine non-implanted	DecellCP Porcine	6 - 8	6
Cellular cryopreserved porcine non-implanted	CellCP Porcine	6 - 8	6
Cellular unpreserved porcine non-implanted	Cell Porcine	6 - 8	6

\*n=4 for leaflets tested in the radial direction

## 6.4 Methods

### 6.4.1 Preparation, Shipment and Storage of Heart Valve Roots for Material properties Assessment

The cryopreserved decellularised porcine pulmonary heart valve roots were shipped on dry ice to Brazil through a courier with an import licence (authorisation No MP.000.1/13PR). The heart valve roots were stored at -80 °C at the University Veterinary Hospital (Hospital Veterinário Para Animais De Companhia) Brazil until implantation. The decellularised porcine pulmonary heart valve roots were implanted in the right ventricle outflow tract (RVOT) of juvenile sheep (3 months old) at the Hospital Veterinário Para Animais De Companhia, Brazil, in accordance with

the institutional guidelines for animal care. The Ethics Research Committee on Animal Research of Pontifícia Universidade Católica in Paraná (PUC-PR) approved this experiment. The cryopreserved roots were gently thawed at 37 °C, washed aseptically in 0.9% (w/v) saline solution, myocardial and artery trimmed to appropriate length and kept moist until implantation. The details of the heart valve roots implantation in sheep are not described here as it was not required for the purpose of this study. The implanted pulmonary heart valve roots were retrieved from the sheep after 12 months under terminal anaesthesia for *in vitro* material properties assessment. The pulmonary heart valve root explants were cryopreserved and stored at - 80 °C. The roots were shipped to the University of Leeds, Leeds, UK on dry ice by a courier with appropriate export and import licences. The explanted heart valve roots were stored at -80 °C at the University of Leeds until testing. The cryopreserved explanted heart valve roots were gently thawed at 37 °C, washed aseptically in 0.9% (w/v) saline solution and stored in 200 ml PBS solution on the day of testing.

#### **6.4.2 Material properties Assessment of Heart Valve Roots**

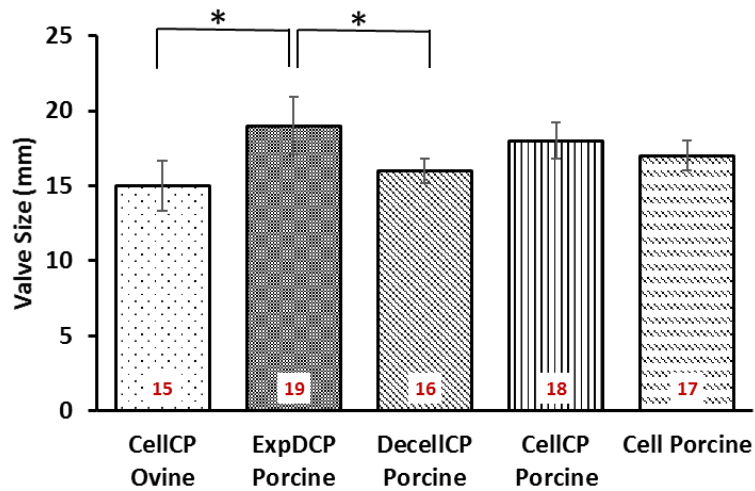
In order to determine the material properties of the heart valve roots, a uniaxial tensile test to failure was performed on the wall (axial and circumferential) and leaflets (radial and circumferential). Before tensile testing the sizes (internal diameter) of the heart valve roots were measured with obturators. The specimen sizes, method of specimen preparation and test procedures are described in Chapter 2 Section 2.4.8.2. The following material parameters were derived from the stress-strain graphs: collagen phase slope, elastin phase slope and ultimate tensile stress (UTS).

Results are presented as mean  $\pm$  95 % confidence limits. One-way analysis of variance (ANOVA) was employed for evaluating the existence of difference among the valve groups. If significant variation in the data was detected, Gabriel post hoc analysis was used to determine the significance between the two relevant groups to investigate the effect of decellularisation (DecellCP Porcine/CellCP Porcine), cryopreservation (CellCP Porcine/Cell Porcine) and post-implantation (ExpDCP

Porcine/DecellCP Porcine and ExpDCP Porcine/CellCP Ovine). A p-value of <0.05 was considered to be statistically significant.

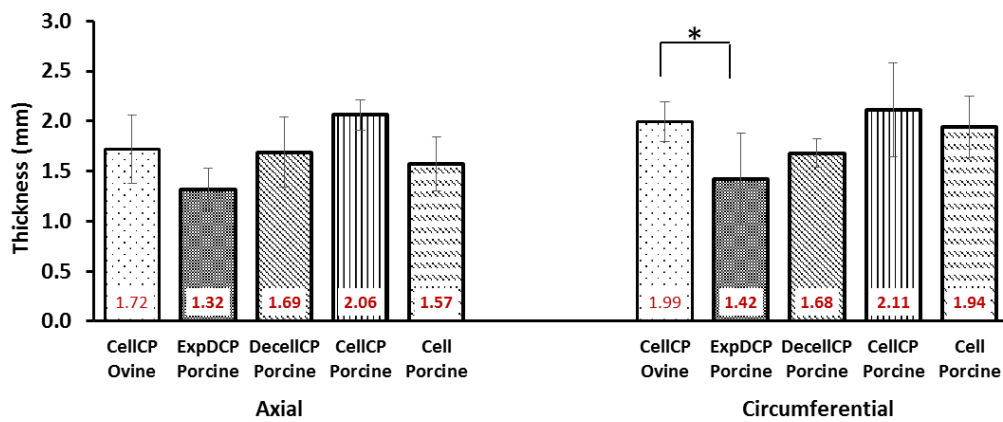
### 6.5 Results

The mean valve size for all the tested pulmonary heart valve root groups is shown in Figure 6.2. The ExpDCP Porcine valves were significantly larger than CellCP Ovine and DecellCP Porcine valves ( $p < 0.05$ , one-way ANOVA).



**Figure 6.2 Mean Valve Size (Internal Diameter) for Pulmonary Heart Valve Root Groups - The error bars indicate 95 % confidence limits. \* - Denotes significant difference ( $p < 0.05$ )**

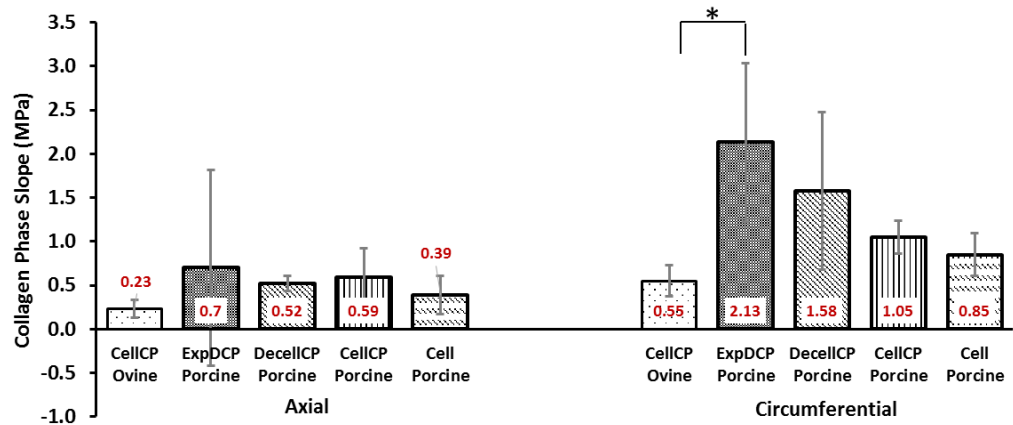
The mean wall thickness in the axial and circumferential directions for all the tested pulmonary heart valve root groups is shown in Figure 6.3.



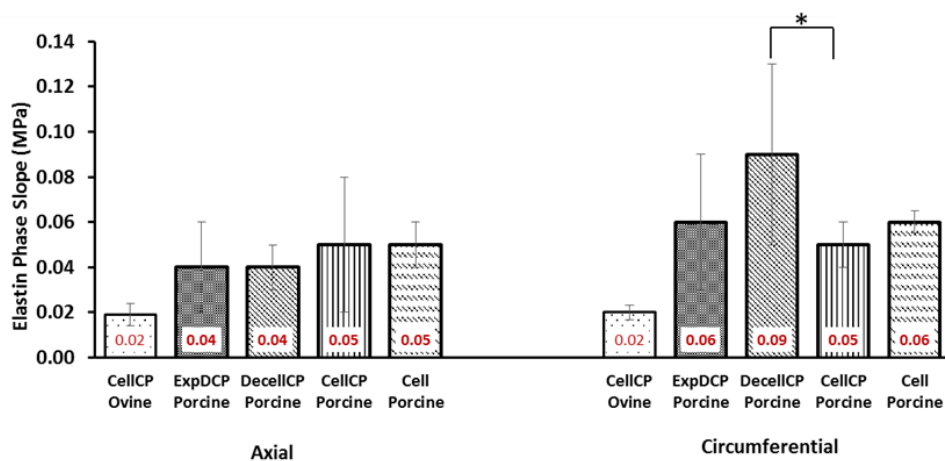
**Figure 6.3 Mean Pulmonary Heart Valve Root Wall Groups Thickness in the Axial and Circumferential Directions - The error bars indicated 95 % confidence limits. \* - Denotes significant difference ( $p < 0.05$ )**

In the axial direction, the mean wall specimens thickness for all the tested pulmonary heart valve root groups were similar. The mean wall thicknesses for CellCP Porcine and Cell Porcine heart valve roots were similar in the radial and circumferential directions. However, in the circumferential direction, the mean wall thickness for ExpDCP Porcine heart valve roots ( $1.42 \pm 0.46$  mm) was significantly lower than the CellCP Ovine heart valve roots ( $1.99 \pm 0.2$  mm) ( $p=0.04$ ; Gabriel post-hoc test).

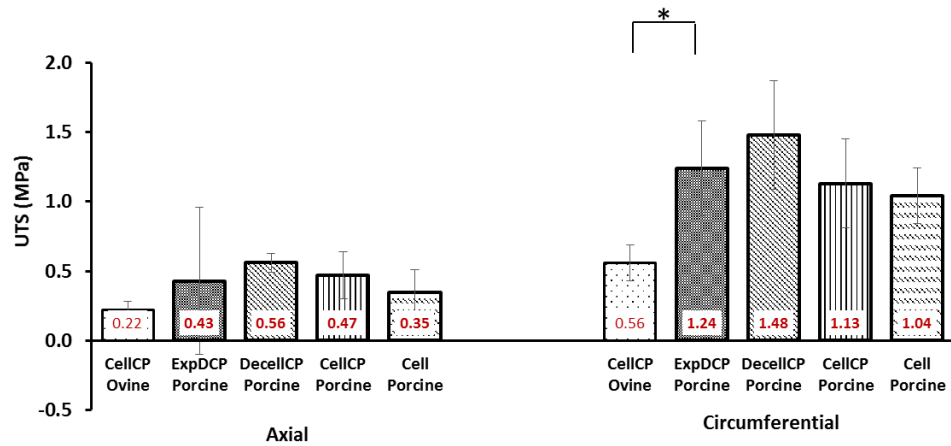
The mean biomechanical parameters for all pulmonary heart valve root wall groups are shown in Figure 6.4, Figure 6.5 and Figure 6.6.



**Figure 6.4 Mean Collagen Phase Slope for the Pulmonary Heart Valve Root Wall Groups in the Axial and Circumferential Directions - The error bars indicate 95 % confidence limits. \* - Denotes significant difference ( $p<0.05$ )**



**Figure 6.5 Mean Elastin Phase Slope for the Pulmonary Heart Valve Root Wall Groups in the Axial and Circumferential Directions - The error bars indicate 95 % confidence limits. \* - Denotes significant difference ( $p<0.05$ )**



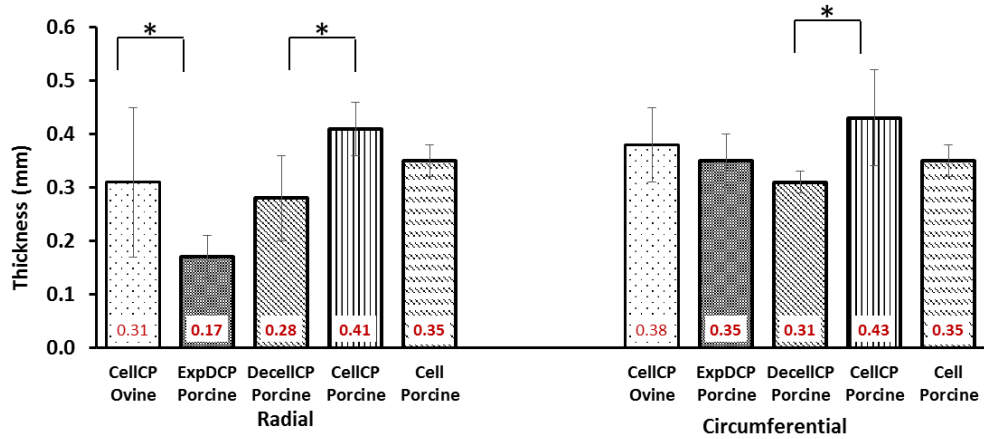
**Figure 6.6 Mean Ultimate Tensile Stress (UTS) for the Pulmonary Heart Valve Root Wall Groups in the Axial and Circumferential Directions. The error bars indicate 95 % confidence limits. \* - Denotes significant difference ( $p < 0.05$ )**

There was no significant difference between the ExpDCP Porcine and DecellCP Porcine pulmonary heart valve root wall specimens for the following parameters: the mean collagen phase slope (Figure 6.4), the mean elastin phase slope (Figure 6.5) and the mean UTS (Figure 6.6) in the axial directions ( $p > 0.05$ ). However, ExpDCP Porcine pulmonary heart valve root wall specimens had significantly higher mean collagen phase slope (Figure 6.4) and mean UTS (Figure 6.6), when compared to the CellCP Ovine pulmonary heart valve root wall specimens in the circumferential direction ( $p < 0.05$ ). In addition, DecellCP Porcine pulmonary heart valve root wall specimens had a mean elastin phase slope of  $0.09 \pm 0.04$  MPa, significantly higher than the CellCP Porcine pulmonary heart valve root wall ( $0.05 \pm 0.01$  MPa) in the circumferential direction (Figure 6.5) ( $p = 0.01$ ; Gabriel post-hoc test).

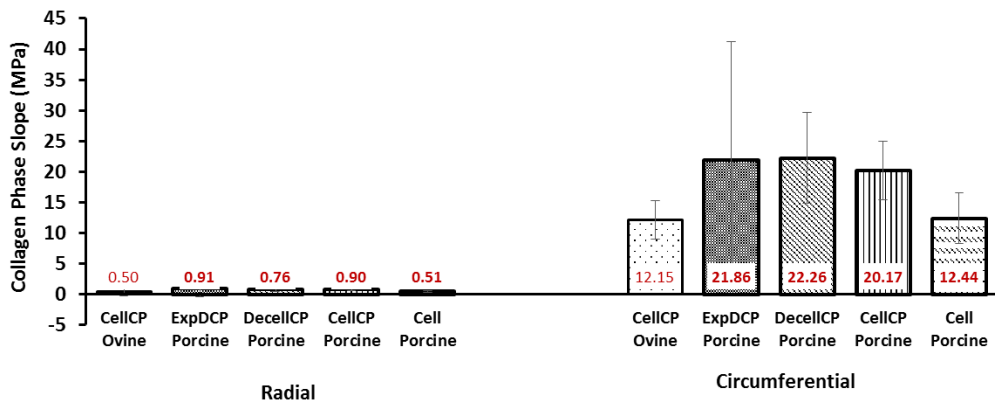
For the heart valve root leaflets, the initial linear region of the stress-strain graph was used to derive elastin phase modulus and it was not distinct for two CellCP Ovine leaflet radial specimens. Hence these samples were omitted and only four CellCP Ovine samples were used in the calculation of mean thickness, elastin phase slope, collagen phase slope and UTS.

The mean leaflet thicknesses (Figure 6.7) for CellCP Porcine and Cell Porcine heart valve roots were similar in the radial and circumferential directions. However, the DecellCP Porcine pulmonary heart valve root leaflet specimens were significantly thinner than CellCP Porcine in the radial ( $p = 0.01$ ; Gabriel post-hoc test) and

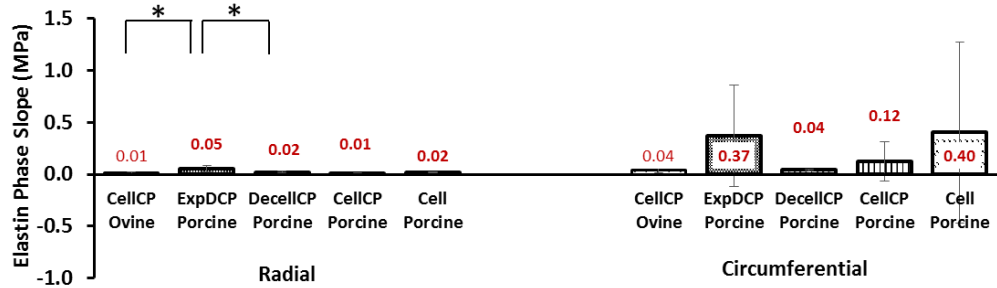
circumferential ( $p=0.005$ ; Gabriel post-hoc test) directions. In addition, ExpDCP Porcine pulmonary heart valve root leaflet radial specimens ( $0.17 \pm 0.04$  mm) were significantly thinner than the CellCP Ovine ( $0.31 \pm 0.14$  mm) ( $p=0.02$ ; Gabriel post-hoc test).



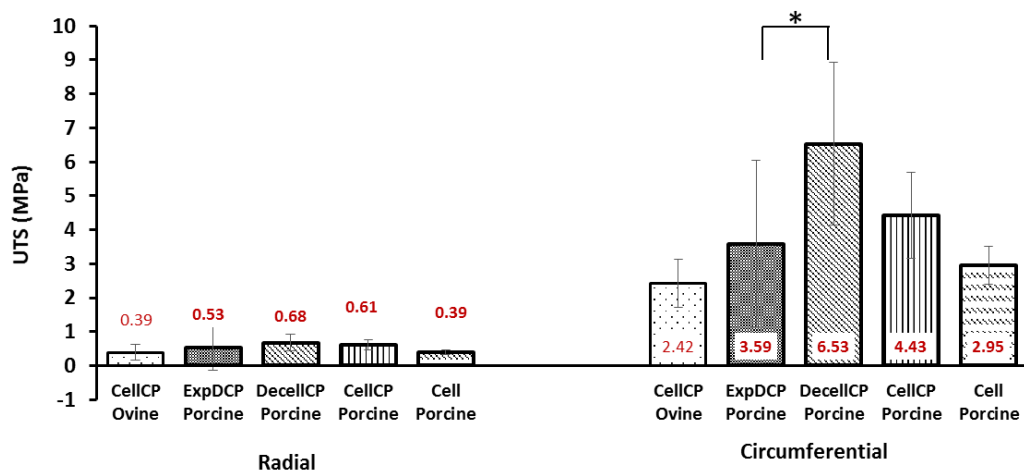
**Figure 6.7 Mean Thickness for the Pulmonary Heart Valve Root Leaflets in the Radial and Circumferential Directions - The error bars indicate 95 % confidence limits. \* - Denotes significant difference ( $p<0.05$ )**



**Figure 6.8 Mean Collagen Phase Slope for the Pulmonary Heart Valve Root Leaflets in the Radial and Circumferential Directions- The error bars indicate 95 % confidence limits.**



**Figure 6.9 Mean Elastin Phase Slope for the Pulmonary Heart Valve Root Leaflets in the Radial and Circumferential Directions - The error bars indicate 95 % confidence Limits. \* - Denotes significant difference ( $p < 0.05$ )**



**Figure 6.10 Mean Ultimate Tensile Stress (UTS) for the Pulmonary Heart Valve Root Leaflets in the Radial and Circumferential Directions - The error bars indicate 95 % confidence limits. \* - Denotes significant difference ( $p < 0.05$ )**

The mean collagen phase slopes in the radial and circumferential direction for Cell Porcine pulmonary heart valve root leaflet specimens were not significantly altered after decellularisation or the cryopreservation process (Figure 6.8). However, the mean elastin phase slope was significantly increased for ExpDCP Porcine pulmonary radial leaflet specimens ( $0.05 \pm 0.03$  MPa) compared to the non-implanted DecellCP Porcine specimens ( $0.02 \pm 0.01$  MPa) ( $p=0.02$ ; Gabriel post-hoc test; Figure 6.9). There was also a significant reduction in UTS for ExpDCP Porcine pulmonary leaflet specimens ( $3.59 \pm 2.45$  MPa) compared to non-implanted DecellCP Porcine pulmonary heart valve root leaflet specimens ( $6.53 \pm 2.40$  MPa) in the circumferential direction ( $p=0.03$ ; Gabriel post-hoc test; Figure 6.10).



The mean elastin phase slope for ExpDCP Porcine radial leaflet specimens ( $0.05 \pm 0.03$  MPa) was significantly higher when compared to the CellCP Ovine specimens ( $0.01 \pm 0.01$  MPa) ( $p=0.001$ ; Gabriel post-hoc test; Figure 6.9).

Failure of both the wall and leaflet tissue occurred at or near to the centre of the gauge length.

## **6.6 Discussion**

### **6.6.1 Effect of Cryopreservation on Material Properties of the Porcine Pulmonary Heart Valve Roots**

The cryopreservation process did not appear to alter the tensile material properties of the wall and leaflets of the pulmonary heart valve roots. For example, the tensile material parameters (elastin and collagen phase slopes, UTS) of the CellCP Porcine wall and leaflet specimens tested in both directions were very similar to these of the Cell Porcine specimens. These results agreed with other published studies (Langerak et al., 2001, Theodoridis et al., 2016).

### **6.6.2 Effect of Decellularisation on Material Properties of the Porcine Pulmonary Heart Valve Roots**

The effects of decellularisation on the biomechanical function of porcine pulmonary heart valve roots were evaluated by comparing material properties of DecellCP Porcine with CellCP Porcine pulmonary heart valve roots. The majority of the tensile material properties of pulmonary heart valve roots were preserved after decellularisation. For example, the wall and leaflet material parameters (collagen phase slope, elastin phase slope and UTS) for the DecellCP Porcine specimens in axial and circumferential directions were similar when compared to the CellCP Porcine, with the exception of elastin phase slope for wall specimens which was significantly higher in the circumferential direction for the DecellCP Porcine group. Conversely, (2014) found that the elastin phase slope for decellularised porcine pulmonary heart valve roots wall specimens was significantly higher in both axial and circumferential directions compared to cellular wall specimens. This was despite (2014) using a similar decellularisation protocol. This discrepancy compared to this study was likely due to differences in each experimenter's methodology and repeatability of

experiments, especially with respect to determining the fully relaxed state of tissue specimens. The fact that no changes in the collagen phase slopes and ultimate tensile stresses indicated that the small increase in elastin phase slope in the circumferential direction of the arterial wall may not affect function, observed during the Doppler echocardiography of the implanted decellularised pulmonary heart valve roots in all sheep at 1, 3, 6 and 12 months of implantation (manuscript in preparation).

The DecellCP Porcine radial and circumferential leaflet specimens were thinner than CellCP Porcine specimens. This was likely due to a previously reported reduction in glycosaminoglycan (GAG) levels in the decellularised porcine pulmonary leaflets and due to absence of cells (2011). GAGs are, however, very important components in the middle layer (spongiosa) of the porcine pulmonary leaflets which can retain water and are believed to contribute to the material properties and the viscoelastic properties of the valve (Sacks et al., 2009). Nevertheless, the reduction in GAGs did not appear to adversely affect the material properties of these leaflets.

### **6.6.3 Effect of 12 Months Implantation in Sheep on Material Properties of the Decellularised Porcine Pulmonary Heart Valve Roots**

The material properties of the 12 months explanted decellularised pulmonary heart valve roots were derived and compared with non-implanted DecellCP Porcine and CellCP Ovine. The tensile parameters for ExpDCP Porcine pulmonary heart valve root wall in the axial and circumferential directions were similar to non-implanted DecellCP Porcine pulmonary heart valve root wall. However, the tensile leaflet material properties of DecellCP pulmonary heart valve roots appeared to alter following 12 months of implantation in sheep. The mean elastin phase slope of the ExpDCP Porcine heart valve root radial leaflet specimens was significantly higher than the non-implanted DecellCP Porcine heart valve root radial leaflet specimens. Furthermore, in the circumferential direction the mean UTS for ExpDCP Porcine heart valve root leaflet specimens was significantly lower than DecellCP Porcine heart valve root leaflet specimens, but similar to CellCP Ovine pulmonary heart valve root leaflet specimens. In addition, the UTS in the axial and circumferential directions for ExpDCP Porcine heart valve root wall and leaflets were reduced, although not significantly. The trend for decreasing stiffness and strength showed the ExpDCP porcine

pulmonary root wall and leaflets were becoming more like cellular ovine. Indeed, it was observed in the histological and the immunohistochemical analysis that the wall and leaflets of the decellularised porcine pulmonary heart valve roots were repopulating with ovine cells following 12 months implantation in sheep (Berry et al., 2017). These findings have shown that studying the decellularised porcine heart valve roots material properties after the effect of *in vivo* physiological forces is useful to better understand the remodeling process.

#### **6.6.4 Study Limitations**

This study had the following limitations:

- The study included a small number of explanted heart valve roots giving low statistical power.
- There was biological variation within the experimental porcine and ovine pulmonary heart valve groups.
- Only uniaxial tensile assessment was used to derive material properties of the heart valve roots which ignores *in vivo* multiaxial loading conditions.
- The study was limited by a lack of an experimental group (pulmonary heart valve root homograft from sheep) comparing material properties of the explanted decellularised pulmonary heart valve roots to interpret the results.

#### **6.7 Conclusion**

From this study, the following conclusions can be made:

- Cryopreservation did not alter material properties of the cellular porcine pulmonary heart valve roots.
- The decellularisation process had minimal effect on the material properties of the porcine pulmonary heart valve root wall and leaflets.
- After 12 months implantation in sheep, the decellularised porcine pulmonary heart valve root wall and leaflets did not appear to be getting stiffer. Indeed, the trend for decreasing stiffness and strength showed the decellularised porcine pulmonary heart valve root wall and leaflets were becoming more like cellular ovine, potentially indicating constructive remodelling.

Overall, the current study demonstrated that cryopreserved decellularised porcine pulmonary heart valve roots maintained tissue integrity in an *in vivo* environment. The current study showed adequate biomechanical function following 1) trans-species implantation of decellularised porcine pulmonary heart valve roots for 12 months 2) a low concentration SDS decellularised treatment on a porcine pulmonary heart valve root. Thus, the study provides valuable pre-clinical biomechanical data that can support clinical studies.

To minimise *in vivo* testing in large animal, *in vitro* real time fatigue or durability testing could be used to predict heart valve root fatigue and durability, which will be addressed in the next chapter (chapter 7), discussing newly developed *in vitro* real time fatigue assessment method for biological heart valve roots. However, the *in vivo* regeneration response will still need to be evaluated with animal studies.

## **7 Development of a Pre-Clinical Method for Assessment of Real Time Fatigue and Durability of Biological Heart Valve Roots**

This chapter describes the development of an *in vitro* fatigue and durability testing method for biological heart valve roots under cyclic physiological conditions. It includes the various stages undertaken to characterise and validate the real time wear tester (RWT; Section 7.5), development of a method to determine the real time fatigue of biological heart valve roots including the design of a heart valve root holder (Section 7.8.1) and modification of the RWT (Section 7.8.2). The method will then be used to investigate effect of decellularisation on the durability of decellularised porcine aortic heart valve roots to be described in Chapter 8.

### **7.1 Introduction**

The prediction of long-term performance and investigation and quantification of the effects of factors that influence long term performance of prosthetic heart valves are vitally important in the development process in order to improve *in vivo* fatigue and durability. The characterisation of the long term performance or durability of a prosthetic heart valve is also one of the requirements established by the FDA (2010) and specified in the ISO 5840 (2015) standard.

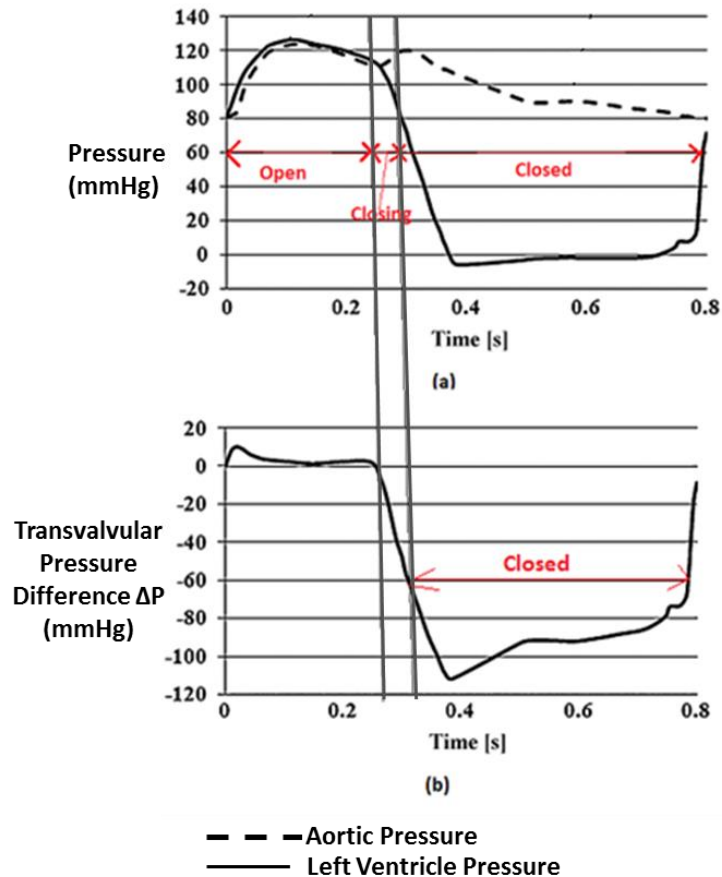
With the potential clinical use of decellularised heart valve roots, biomechanical performance, hydrodynamic performance and durability are important considerations. The biomechanical and hydrodynamic performance of human cellular and decellularised aortic and pulmonary heart valve roots have been described in Chapters 4 and 5. This chapter describes the development stages of an *in vitro* test method to determine fatigue and durability of biological heart valve roots under real time cyclic test conditions. It describes an advancement of methods currently used to assess the durability of prosthetic and bioprosthetic heart valves.

Cyclic testing of heart valve roots under simulated physiological conditions can provide evidence of the possible failure modes and lifespan. It can also aid heart valve root development and improvement and can guide future designs. Previous studies (Iwasaki et al., 2002, D'Souza et al., 2003, Butterfield and Fisher, 2000) on prosthetic and bioprosthetic heart valve durability have used accelerated fatigue testers to

Chapter 7

attain valve leaflet motion (valve leaflet opening and closing) under non physiological test conditions. Accelerated fatigue testers were used at significantly higher frequencies (15 to 20 Hz) than physiological frequencies, in order to achieve failure in a shortened period of time. These accelerated fatigue testers are not appropriate for use with biological heart valve roots such as allografts and decellularised heart valve roots, because these valves exhibit highly time dependent viscoelastic behaviour and accelerated testing produces highly abnormal biomechanics (D'Souza et al., 2003). Accelerated fatigue testers were used at significantly higher frequencies than physiological frequencies, so the biological valves did not have enough relaxation time and additional forces were applied to the leaflets of the test heart valve roots which do not exist in the physiological environment (D'Souza et al., 2003, Sacks, 2001). Therefore biological heart valve roots require testing under more physiological frequencies and pressures. The test frequency has also been shown to influence the life time of polymer valves. Iwasaki et al. (2002) demonstrated that a polymer valve known as a Jellyfish valve had varied lifetime with cyclic frequency even when the maximum transvalvular pressure difference was constant; therefore, using appropriate time dependent test conditions is important. In effect, for biological and polymer valves, durability is dependent on the number of cycles, the peak pressure and the duration that the pressure is applied in a single cycle (the cycle frequency) (D'Souza et al., 2003). Hence, it is important to consider viscoelasticity and frequency of testing of the biological heart valve roots during fatigue testing in order to predict accurate fatigue and durability of the biological heart valve roots.

To derive *in vitro* real time fatigue and durability performance of the heart valve roots, a testing equipment was required which could replicate physiological pressures and flow waveforms in a simplified, yet effective, controllable and cost-effective way.



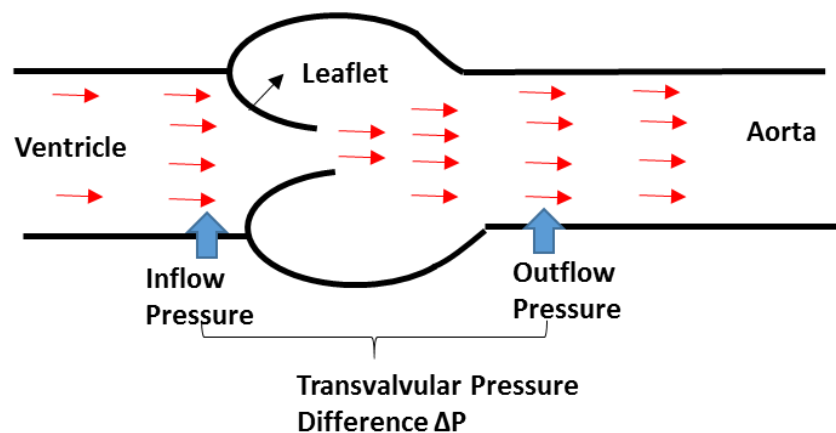
**Figure 7.1 (a) Left Ventricle and Aortic Pressure Waveforms During a Cardiac Cycle at Heart Rate of 60 bpm (b) Transvalvular Pressure across Aortic Valve, Image Adapted from (Conti et al., 2010)**

It was considered to use aortic heart valve roots in the fatigue testing method development due to their straight tubular shape which is supported with thick myocardium and aortic valve roots are larger in size than pulmonary heart valve roots. Hence, the method development and the performance requirements were based on the human aortic heart valve roots. The aortic heart valve opens during systole when the ventricle is contracting and then closes during diastole as the ventricle relaxes. The mean aortic pressure of a healthy human is 100 mmHg (Guyton and Hall, 2006), whereas diastolic pressure in the aorta is approximately 70 mmHg (Malamed, 2007). A physiological, time-dependent aortic pressure waveform inside the aortic heart valve root, ventricular pressure waveform experienced by the leaflets and a consistent transvalvular pressure drop ( $\Delta P$ ) to the closed leaflet surfaces respectively is shown in Figure 7.1 (a) and (b). Therefore, the first criterion of the fatigue tester was that it should be able to operate over a transvalvular pressure of

100 mmHg at a physiological heart rate range of 60–120 bpm for adult and children (Chirakanphaisarn et al., 2018).

To mimic physiological pressure conditions, the pressures at the entrance (inflow) and exit (outflow) of the test valve needed to be able to be tuned to the mean transvalvular pressure difference ( $\Delta P$ ) found in humans (Figure 7.2). Also the arterial wall has elastic and viscous properties and their difference reflects the time-dependent response of the stress–strain relationship (arterial pressure–arterial diameter changes). Therefore, in addition to  $\Delta P$  a pressure across the wall (outflow pressure) of the heart valve root needed to be able to be tuned to mimic pressure–diameter function.

A real time wear tester (RWT) was purchased from Vivitro Systems Inc, Victoria BC, Canada to test biological heart valve roots under physiological test conditions. The characterisation and validation of the new equipment was required in order to verify that it met the requirements of the user and that it was able to function reliably.

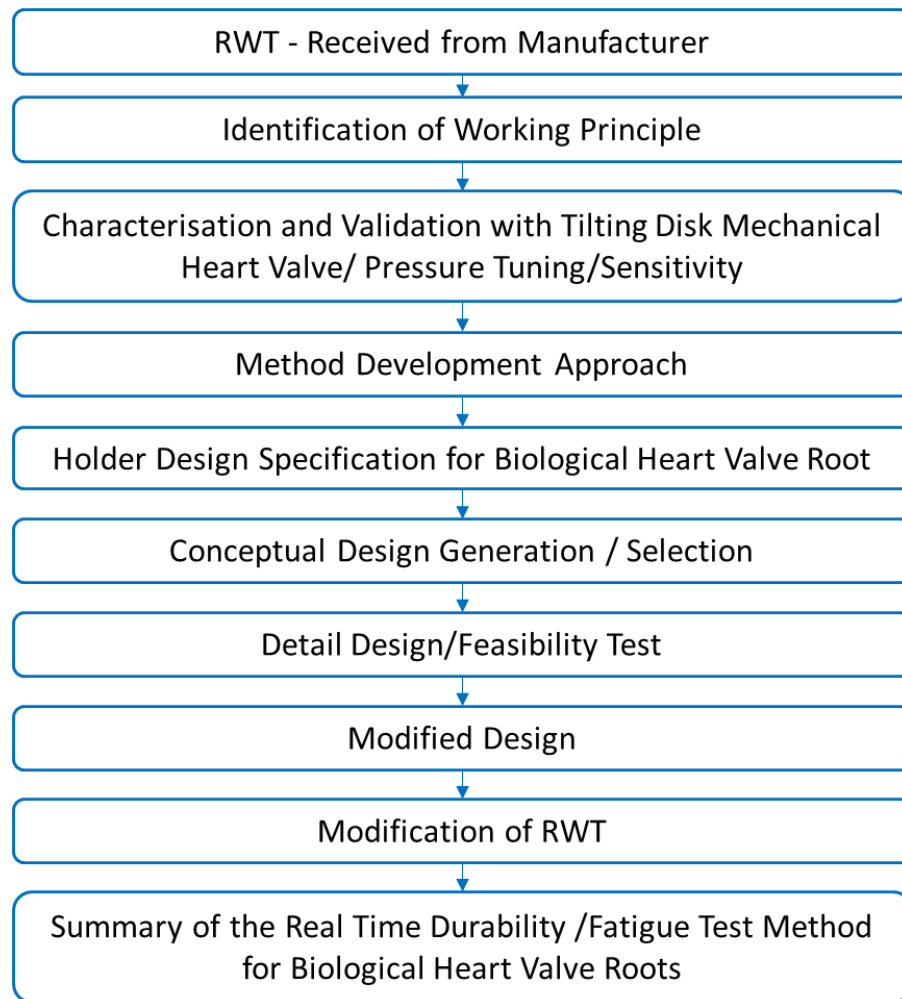


**Figure 7.2 Inflow and Outflow Pressures in the Heart Valve Root**

Developing the method to investigate the fatigue and durability of the biological heart valve roots under real time physiological test conditions was one of the most novel aspects of this research. An overview of the process used for the method development is given in Figure 7.3. The RWT was designed predominantly for frame mounted heart valves so required modification to test biological heart valve roots. The development involved characterisation and validation of the RWT, and developing an in-house protocol for the real time fatigue and durability testing of



biological heart valve roots with the simulation of human physiological and systemic pressure conditions.



**Figure 7.3 Flowchart of the Method Development Process to Investigate the Fatigue and Durability of Biological Heart Valve Roots**

## 7.2 Aim and Objectives

The aim of this chapter was to develop a test method to predict fatigue and durability of biological heart valve roots under cyclic physiological test conditions. The specific objectives were:

1. To characterise and validate the RWT with a tilting disc mechanical heart valve
2. To design a biological heart valve root holder
3. To modify the RWT, so that it could be used for testing the biological heart valve roots
4. To establish a method for real fatigue and durability testing of biological heart valve roots in the RWT

## 7.3 Materials and Methods

### 7.3.1 Mechanical Valves



**Figure 7.4 Tilting Disc Mechanical Heart Valve**

Three 25 mm tilting disc mechanical *heart* valves (Figure 7.4) were used for characterisation and validation of the RWT due to easier and faster mounting/dismantling in the RWT; and to get consistent, repeatable and reproducible results.

### 7.3.2 Cellular and Glutaraldehyde Fixed Porcine Aortic Heart Valve Roots

Cellular and glutaraldehyde fixed porcine aortic heart valve roots were used for both the initial method development stage and as a control to understand any potential confounding mechanical factors in the system which were likely to affect the biological root testing. Also these heart valve roots were included in the study as the “control” against which all the other types of heart valve roots were compared. It was decided to use aortic heart valve roots because they are well supported with thick myocardium, easy to handle and larger in size than pulmonary heart valve roots. Also pulmonary heart valve roots have an arch whereas aortic heart valve roots are a straighter tubular shape, so it was more practical to use aortic heart valve roots for method development. The geometry of the fixed heart valve roots make the roots easier to mount and the inert characteristics help to extend handling time and thus, the root holder design could be checked more easily. The fixation procedure is described in Chapter 2 Section 2.4.2.

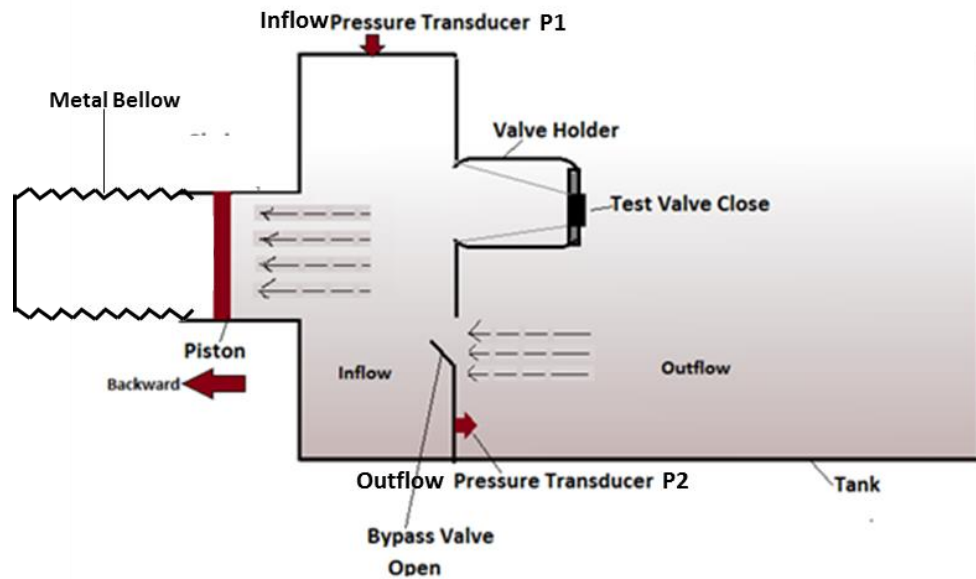
#### 7.4 Real Time Wear Tester (RWT)

Fundamentally the RWT is intended for the use of durability assessment of prosthetic valves under various types of time dependent waveforms (sinusoidal, non-sinusoidal, square, triangle etc).

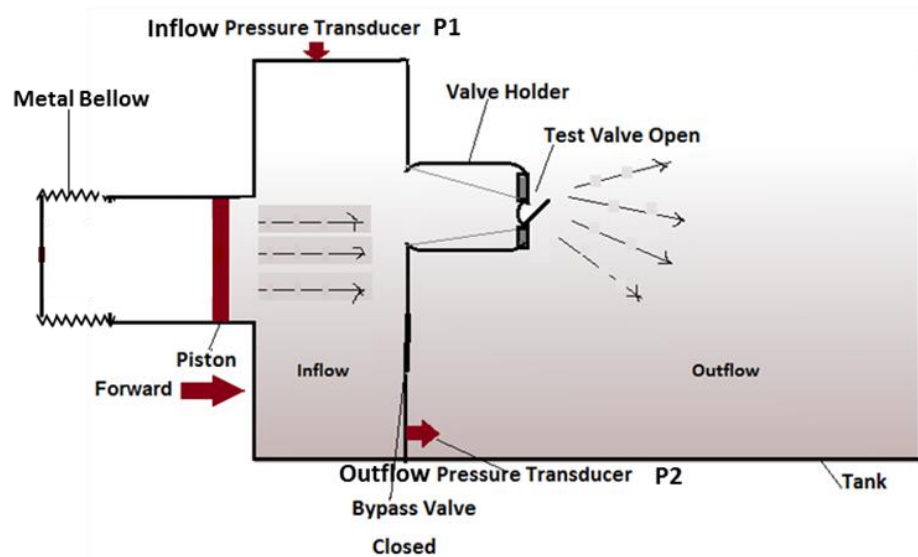


**Figure 7.5 Real Time Wear Tester**

The real time wear tester consisted of a positive displacement SuperPump with control system (Vivitro Systems Inc, Victoria BC, Canada), a Perspex tank, silicone tubing and pressure measurement system (Vivitro Systems Inc, Victoria BC, Canada) (Figure 7.5). The RWT was monitored by HiTest software (Vivitro Systems Inc, Victoria BC, Canada). The tank was divided into two chambers, the inflow chamber attached to the piston with a metal bellow. The outflow chamber was open to the air. The RWT allowed the mounting of six test valves between the inflow and outflow chamber.



(a)



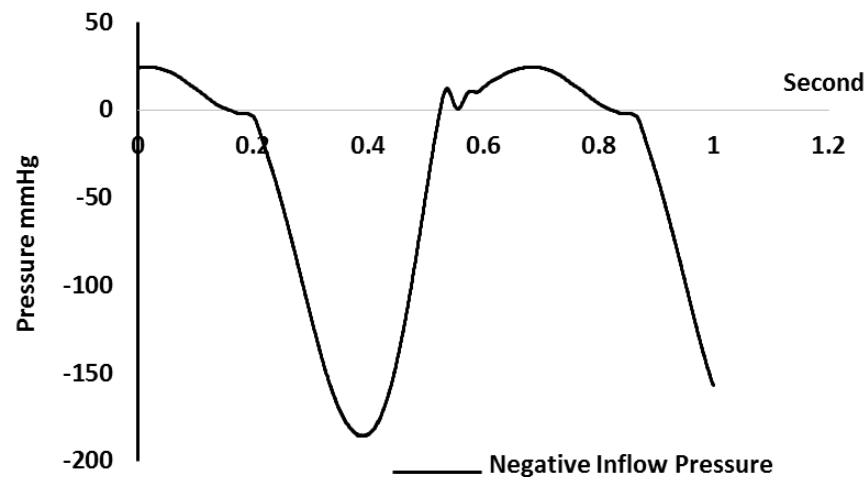
(b)

**Figure 7.6 Basic Working Principle of the RWT (a) Backward Piston Stroke Closes the Test Valve (b) Forward Piston Stroke Opens the Test Valve**

Figure 7.6 (a) and (b) shows the basic principle of the RWT which can be explained as follows: The piston motion was designed to control with physiological input waveforms. When the piston stroke travels backwards (moves away from the test valve), the metal bellow expands, a volume of test solution is drawn into the inflow chamber through the test valve and closes the valve leaflets [Figure 7.6 (a)]. On the forward piston stroke, the test solution is expelled, the metal bellow compresses and opens the test valve [Figure 7.6 (b)]. The RWT comprised of a one-

way adjustable bypass valve to control the inflow pressure and negative back pressure on the test valve.

The functionality of the bypass valve will be discussed later in the chapter. In summary, the RWT was designed on the principle of dynamic pressurisation, where valve closure occurs during the closed part of the input waveform and applied negative pressure on the test valve as measured by inflow pressure transducer P1 [Figure 7.6(a)]. During the open part of the input waveform, the piston moved forward and opened the test valve Figure 7.6 (b). The pressure measured by outflow pressure transducer P2 [Figure 7.6 (b)] was approximately zero. Therefore, the pressure across the closed valve (transvalvular pressure difference  $\Delta P$ ) was similar to inflow pressure P1 (Figure 7.7).



**Figure 7.7 Negative Pressure in the Inflow Chamber Measured by Inflow Pressure Transducer P1 at 60 bpm**

One cycle at a heart rate of 60 bpm lasts for one second, during which time 2000 data points are collected by the inflow pressure transducer in the RWT (Figure 7.7).

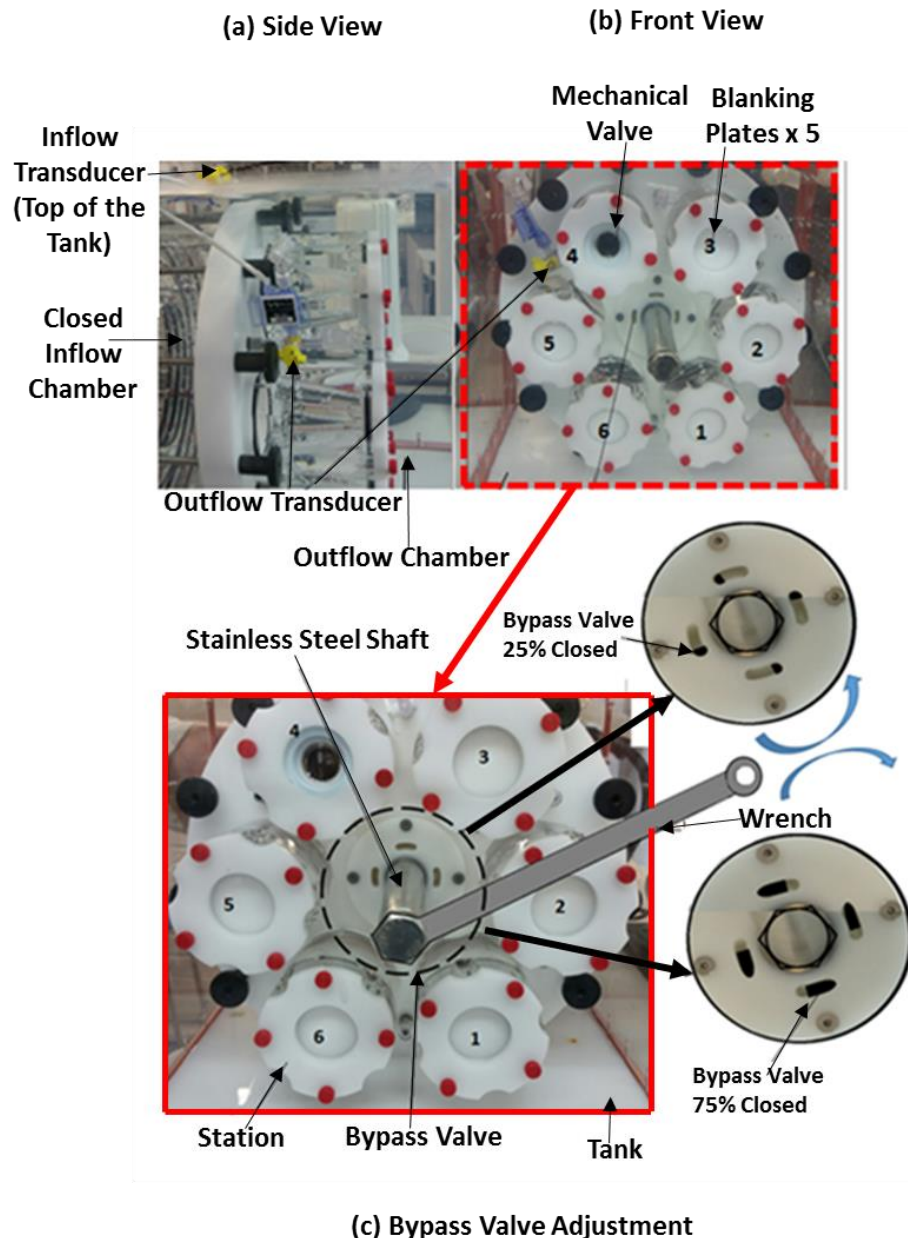
#### 7.4.1.1 SuperPump and Pump Controller

The SuperPump (AR Series, Vivitro Systems Inc, Victoria BC, Canada) was a digitally controlled microprocessor based piston-in-cylinder pump that creates physiological cardiac flows. The complete SuperPump system included a digital amplifier with stroke volume and cycle count display, pre-programmed waveforms, and inter-connecting cables. The amplifier had capacity to store five programmable

physiological waveforms at different heart rates ranging from 30 to 200 bpm. The stroke volume in terms of percentage gain (amplitude) of the waveforms was controllable by an amplitude controller on the amplifier.

#### 7.4.1.2 Tank Assembly

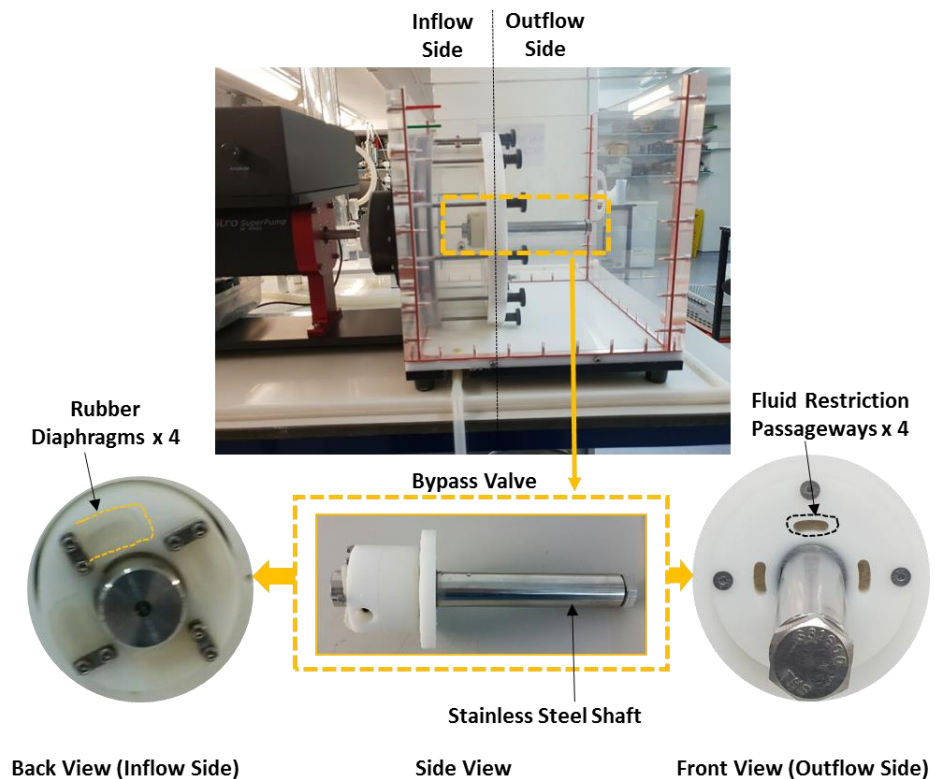
There were six equally spaced stations (numbered 1 to 6) for mounting the test valves housed in the tank (Figure 7.8).



**Figure 7.8 Real Time Wear Tester with (a) Side View (b) Front View with one Mechanical Valve in Station 4 and five Stations blanked off (C) Tank Assembly with one Mechanical Valve in Station 4 and five Stations blanked off and Bypass Valve Adjustment (Front View)**

The tank was divided into two chambers: the inflow chamber was a closed chamber attached to the pump through a metal bellow and a piston; and the outflow chamber was open to the air as shown in Figure 7.6. Approximately 31 litres of test fluid was required to fill the tank. The tester had a pressure controlled one way bypass valve between the two chambers to regulate the fluid flow (a valve that opens only with forward or reverse flow) as shown Figure 7.8.

The bypass valve had flexible rubber diaphragms which moved in the direction of the flow and were attached to fluid restriction passageways (Figure 7.9). Flow in the reverse direction deflected the diaphragms backwards, allowing free passage of the test fluid in the inflow chamber [(Figure 7.10 (a))] and the amount of test fluid passing into the inflow chamber was dependent on the opened/closed percentage of the fluid restriction passageways.

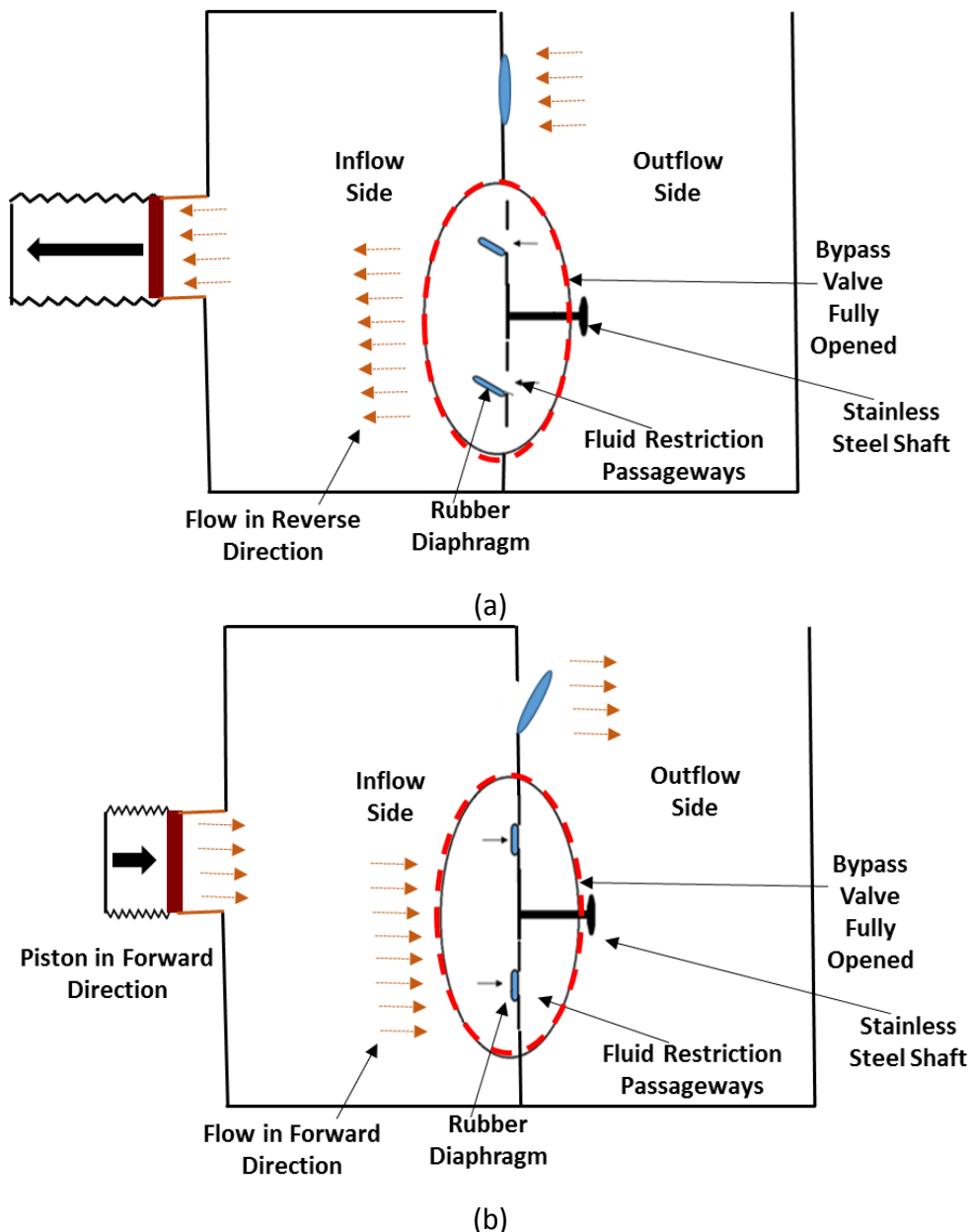


**Figure 7.9 Bypass Valve Assembly**

To adjust the fluid restriction passageway, the bypass valve consisted of a stainless steel shaft, which could be rotated clockwise or anticlockwise with a wrench, as shown in Figure 7.8. Conversely, flow in the forward direction closed the



diaphragms, therefore closing the fluid restriction passageways completely [Figure 7.10 (b)].



**Figure 7.10 Working Principle of the Bypass Valve showing Movement of Rubber Diaphragms with Flow in (a) Reverse and (b) Forward Directions**

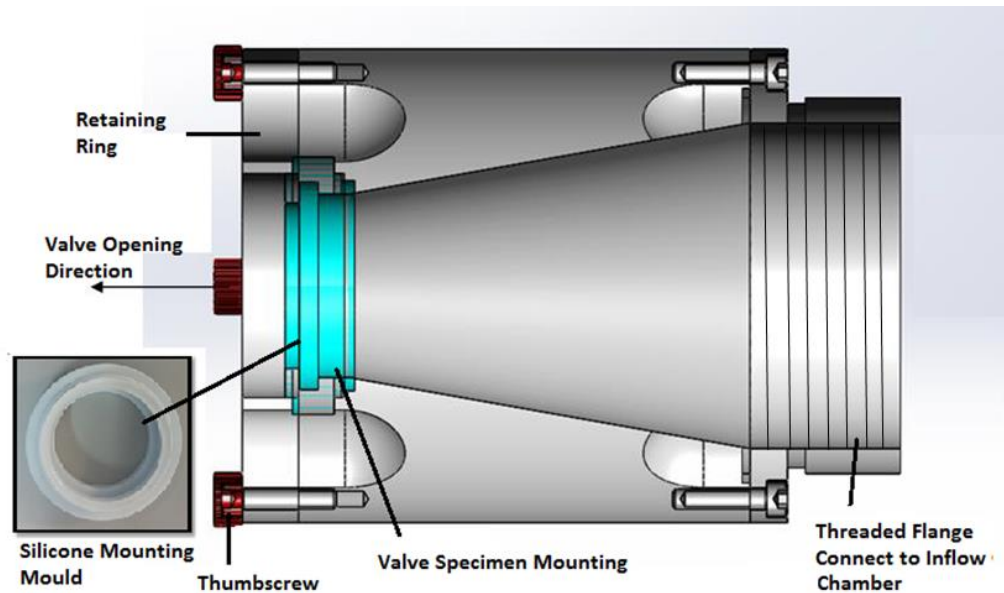
#### 7.4.1.3 Valve Holder

There were six valve holders in total, these were the original holders of the RWT which were designed to work with standard mechanical heart valves or frame mounted bioprosthetic heart valves (Figure 7.11). Each valve holder had four thumbscrews and a retaining ring for test specimen mounting and dismantling. The default configuration for the test valve to open was towards the front of the tank as



shown in Figure 7.11. The valve holder had a threaded flange, so it was easy to install or remove from the valve stations.

A silicone mounting mould (Figure 7.11) was supplied with the valve holder and could be used to seal the appropriate boundaries between the valve specimen and the valve holder.



**Figure 7.11 Standard Valve Holder (Side View), Image Adapted from Vivitro Systems Inc, Victoria BC, Canada Manual**

#### **7.4.1.4 Pressure Measurement Instruments and Data Acquisition**

The RWT had two Vivitro pressure transducers (Vivitro Systems Inc, Victoria BC, Canada) to measure the inflow and outflow chamber pressures. The inflow pressure can be described as valve closing pressure or back pressure on the valve and the outflow pressure can be described as the aorta pressure. Both pressure transducers were connected to the amplifier.

To collect output test data, the RWT was connected with a 16 bit analogue to digital Vivitro I/O module. The output data consisted of test set up information (valve details, targeted pressure) and raw pressure (inflow and outflow) measurements for any of the captured cycles during the test. The recorded data was processed using HiTest software (Vivitro Systems Inc, Victoria BC, Canada). The HiTest software consisted of various programs allowing; calibration, analysis, individual valve display,

data acquisition and results panel (Figure 7.12). The results panel showed live data regarding pressure values as follows:

- **Targeted pressure boundary** (Targeted or defined transvalvular pressure difference  $\Delta P$  mmHg): this value showed the predefined transvalvular pressure value across the closed test valve. For an aortic heart valve root the target transvalvular pressure difference was 100 mmHg.
- **Mean peak differential pressure** (mean transvalvular pressure): this value monitored the mean transvalvular pressure value across the closed valve during the test procedure by calculating the difference between inflow and outflow pressure.

During the closed part of the cycle, due to expansion of the metal bellows, a large negative inflow pressure was generated and closed the valve leaflets. Consequently, the mean transvalvular pressure was negative.

- **% All peak pressure meeting target:** this value monitored percentage of test cycles achieving the targeted peak transvalvular pressure ( $\Delta P$ ) across the closed valve during testing [As per ISO 5840 (2015), the defined transvalvular pressure value across the closed valve ( $\Delta P$ ) should be maintained for 95% or more of all test cycles and must be maintained for at least 5% of the test cycle duration]
- **Mean % of cycle time meeting target:** this value monitored percentage of each cycle achieving the minimum peak transvalvular pressure across the closed valve during testing [As per ISO 5840 (2015), at least 5% of each cycle, the transvalvular pressure value ( $\Delta P$ ) across the closed valve must be at least at the defined transvalvular pressure]

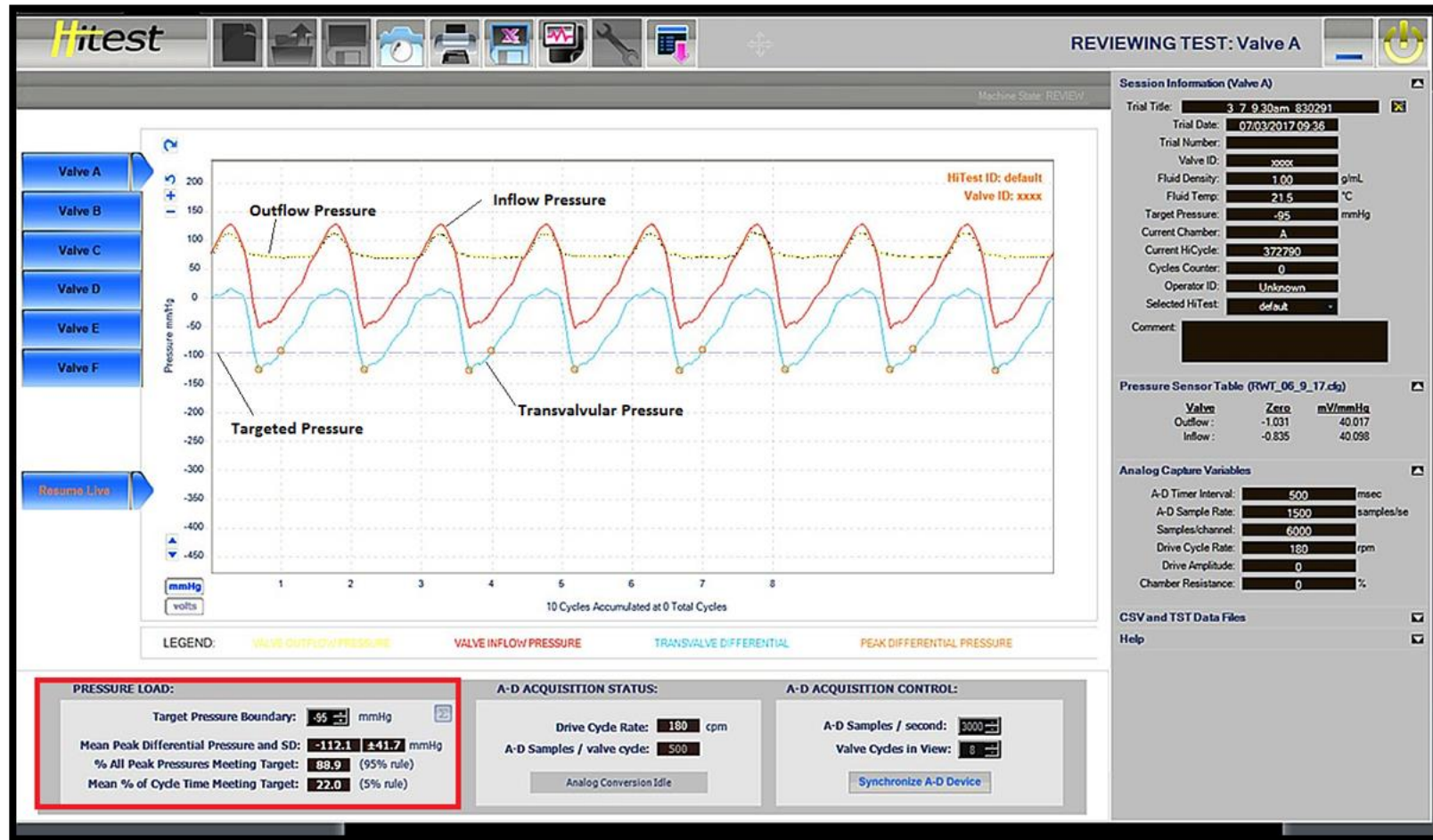
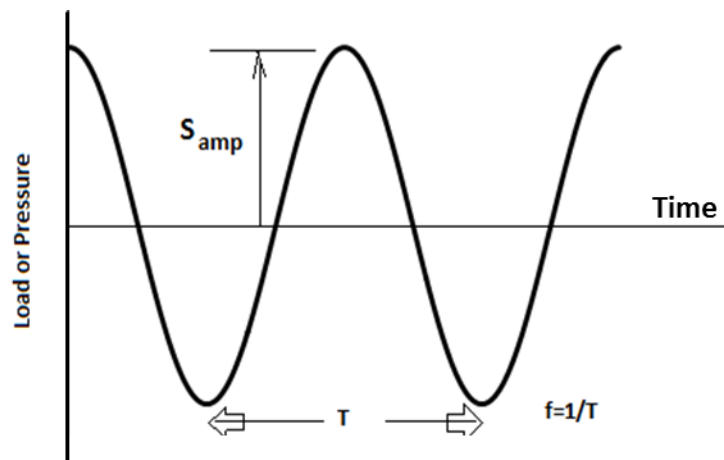


Figure 7.12 The HiTest Software Process Display

#### 7.4.1.5 Data Analysis

The inflow and outflow data was analysed by HiTest software for 10 consecutive cycles. The difference between the inflow and outflow pressure was the transvalvular pressure, this was automatically calculated by the software and saved in Microsoft Excel. Graphs were plotted in Microsoft Excel for inflow, outflow and transvalvular pressures.

### 7.5 Terminology and Conditions Used During Characterisation, Validation and Method Development



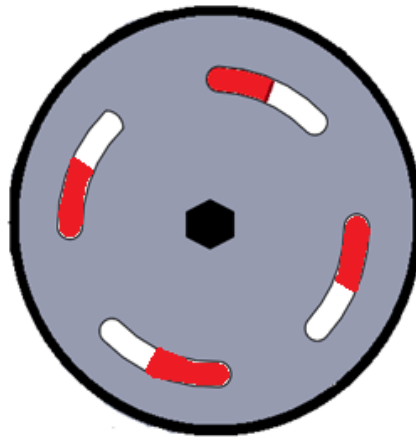
**Figure 7.13 Constant Amplitude Sine Wave (S50) with 50% Systolic and 50% Diastolic Phase**

**Amplitude (Gain):** As shown in Figure 7.13 the input sine waveform was characterised by the parameters of amplitude and frequency. The peak amplitude  $S_{amp}$  represented the maximum forward or backward displacement of the piston and hence maximum volume of test fluid displaced by the piston during the positive or negative part of the input cycle (sine wave). The amplitude of the input waveform was adjusted in terms of percentage of  $S_{amp}$  with the amplifier controller and the value was presented as a percentage of maximum amplitude ( $S_{amp}$ ).

**Frequency:** The frequency ( $f \text{ Hz} = \text{heart rate (bpm)}/60$ ) of the input waveform was adjusted as per the test requirement.

**% Bypass Valve Closing:** The RWT tank had a pressure controlling bypass (Figure 7.8). The detailed working principle of the bypass valve is explained in Section

7.4.1.1. As shown in Figure 7.14, visually 50 % of the fluid restriction passageways could be closed to control test fluid flow and pressure in the RWT.



**Figure 7.14 Schematic showing Fluid Restriction Passageways of Bypass Valve Visually 50 % Closed Configuration**

In all tests, in this chapter the test solution was 0.9 % w/v saline and input waveform was a sine wave (S50) (Figure 7.13). The RWT was allowed to run for 30 min for each test to ensure that a steady state had been reached.

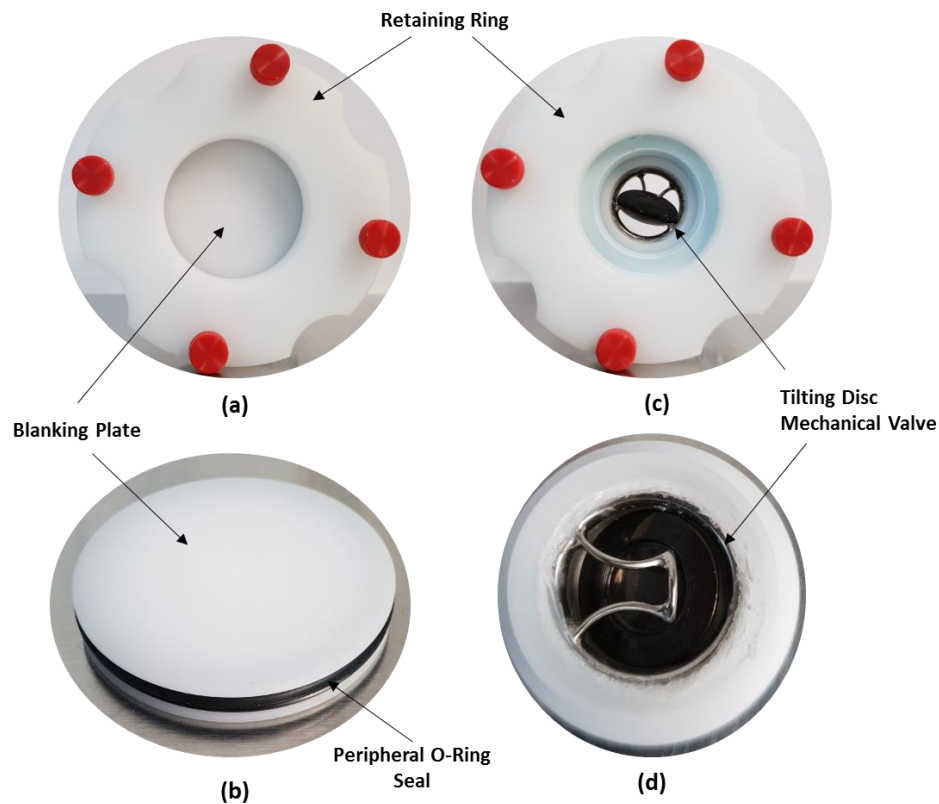
## **7.6 Approach to Characterisation and Validation of the RWT**

The RWT was purchased specifically for this research. It was manufactured by Vivitro Systems Inc, Victoria BC, Canada and therefore little was known about the equipment and testing procedure. This led to a need for the tester to be characterised, validated and calibrated. A characterisation and validation of the RWT was conducted using the assumption that it was designed for frame mounted valves. Part of the validation procedure involved controlling closing pressure of the standard tilting disc mechanical heart valve and measuring transvalvular pressure across the valve.

### **7.6.1 Mounting of Tilting Disc Mechanical Heart Valves in the RWT**

To validate the RWT and ensure the output was accurate, a simplified sinusoidal input waveform (Figure 7.13) and tilting disc mechanical valves were used, the remaining stations were blanked off. Circular 43 mm diameter blanking plates were designed and manufactured to blank off the other five valve stations as shown Figure 7.15 (a). The blanking plate had a peripheral o-ring seal [Figure 7.15 (b)]. Upon

ensuring the attachment of the mechanical valve to the holder [Figure 7.15 (c) and (d)], the whole device was secured into the RWT and inflow and outflow pressure transducers were mounted as shown in Figure 7.8 (a) and (b).



**Figure 7.15 (a) Blanking Plate Sealed in the Valve Holder (Top View) (b) Blanking Plate (c) A Tilting Disc Mechanical Heart Valve Mounted in the Valve Holder (Top View) (d) A Tilting Disc Mechanical Heart Valve Mounted in a Delrin Fixture (Looking from Inflow Side)**

### 7.6.2 Pressure Transducers Calibration

In order to collect accurate pressure data from the tester, the pressure sensors had to be calibrated before any experiment was conducted. Part of the calibration and characterisation of the tester had to be carried out simultaneously.

Before the start of the test, the pressure transducers were calibrated. Both pressure transducers were initially zeroed by keeping them open to the atmosphere until the software read zero and then both were assigned with the corresponding voltage, approximately 0 volt. A pressure of 200 mmHg was then applied until the software assigned the corresponding voltage, approximately 7 Volts. Following this procedure, the HiTest software automatically calculated and stored calibration values

in mV/mmHg. Once the calibration process was completed, the software prompted the user to measure the static head zero offset values for the pressure sensors.

### 7.6.3 Pressure Tuning

The pump controller was designed with a rotary encoder to determine acceleration, and that combined with the precision glass cylinders produced the stroke volume. However if there are any constraints present such as narrow tubing or a variation in heart valve diameters the pump could slow down due to an internal current limit which is part of the pump controller feedback loop. Hence, the characterisation and validation of the RWT was performed using the pressure measurement across the test valve as opposed to the measurement of piston displacement or stroke volume.

**Table 7.1 Test Plan for the Evaluation of Pressure Controlling Mechanism in the RWT**

<b>Input Conditions</b>	<b>Variables</b>	<b>Case 1</b>	<b>Case 2</b>	<b>Case 3</b>	<b>Case 4</b>
<b>S50 Sine Wave</b>	<b>Heart Rate</b>	1) 60 bpm 2) 120 bpm 3) 200 bpm	120 bpm	120 bpm	120 bpm
	<b>Amplitude</b>	50 % gain	75 % gain	1) 25 % gain 2) 50 % gain 3) 75 % gain	25 % gain
	<b>Bypass Valve</b>	50 % gain	1) 25 % closed 2) 50 % closed	50 % Closed	100 % (fully) closed
	<b>Number of Specimens (tilting disc mechanical heart valve)</b>	One	One	One	1) One 2) Three

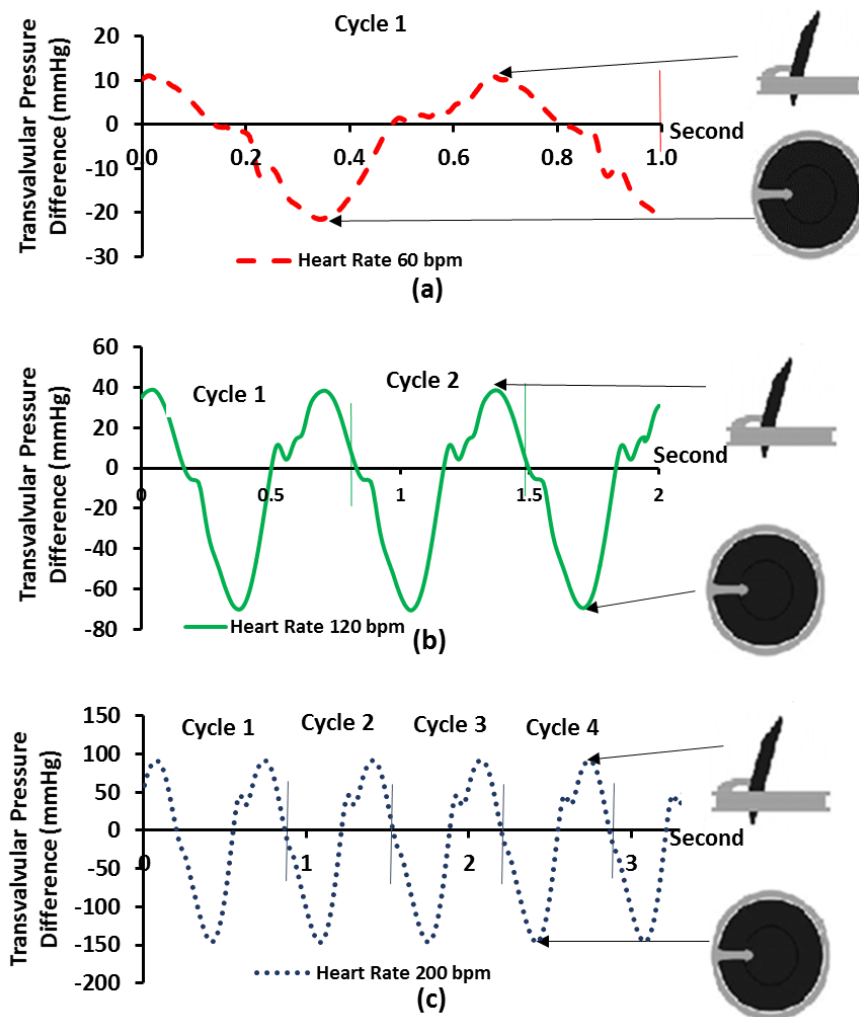
The FDA (2010) and ISO 5840 (2015) standards require that a minimum peak transvalvular pressure of 90 mmHg must be established on the closed aortic valve and should be maintained for 95 % or more of all test cycles during durability testing. As described in Section 7.4.1.4, the HiTest software had the capability to measure peak transvalvular pressure and monitor how much percentage peak transvalvular pressure was meeting the target during the operation of the RWT. However, the controlling mechanism to adjust desired transvalvular pressure across the closed valve needed to be evaluated to establish a method for RWT pressure tuning, as no previous data was available with the RWT. Therefore, to understand the pressure controlling mechanism in the RWT, a transvalvular pressure difference was recorded with different combinations of variables as described in Table 7.1. The transvalvular pressure data were acquired using the HiTest software for 10 consecutive cycles and saved to Microsoft Excel.

#### **Case I: Variable Heart Rate, Fixed Bypass Valve, Fixed amplitude and Fixed Number of Specimens**

To begin with the heart rate was adjusted to 60 bpm (1 Hz) with the bypass valve and the sine wave amplitude (gain) adjusted to 50 % to assess the operational performance of the RWT. This procedure was repeated at 120 bpm (2 Hz) and 200 bpm (3.3 Hz), keeping all other conditions the same.

Transvalvular pressure waveforms were generated for the different heart rates and each of the three generated waveforms corresponded to the piston movement (Figure 7.16).





**Figure 7.16 Transvalvular Pressure across Tilting Disc Mechanical Heart Valve at Heart Rate (a) 60, (b) 120 and (c) 200 bpm**

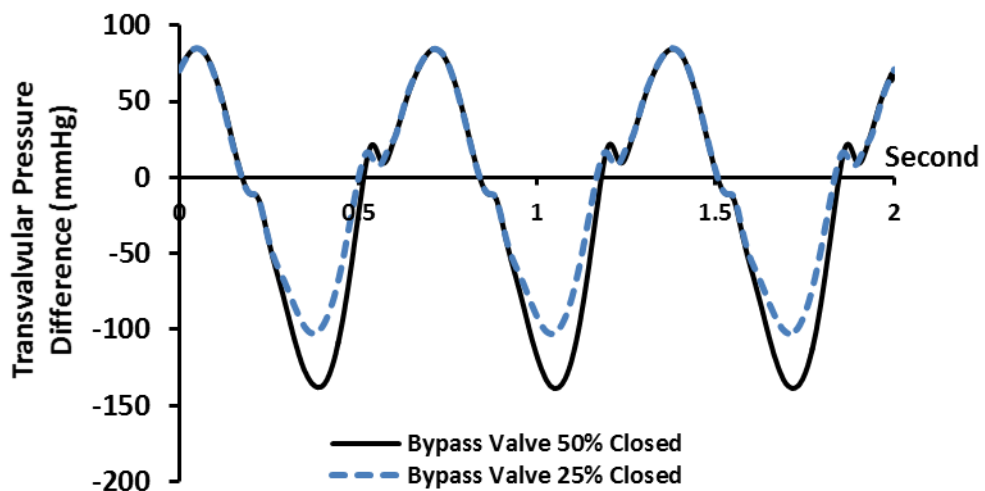
The outflow pressure was close to zero for all the tested conditions, as the valve opened to the outflow chamber, which was opened to the air. Therefore, the transvalvular pressure waveforms were similar to the inflow pressure waveforms. There was a maximum pressure (negative) spike when the valve was closed and a low level of positive spike in pressure when the valve was open producing forward flow. The results also showed that the valve was fully closed 1, 2 and 4 times with heart rate 60, 120 and 200 bpm respectively in 1 second as shown in Figure 7.16.

### **Case 2: Variable Bypass Valve, Fixed Heart Rate, Fixed amplitude and Fixed Number of Specimens**

One tilting disc mechanical heart valve was mounted in the RWT as described in Section 7.6.1. The sine wave was adjusted for a frequency of 2 Hz (heart rate 120

bpm) and amplitude of 75%. Transvalvular pressure waveforms were obtained for the flow bypass valve set at 25 % and 50 % closed as shown in Figure 7.17.

The transvalvular pressure waveforms demonstrated that there was a higher negative pressure drop for the 50 % bypass valve closed than the bypass valve 25 % closed, whereas positive pressures were same for both conditions. This means that the percentage amount of bypass valve closing affected the transvalvular pressure across the closed valve (negative pressure) but not across the opened valve (positive pressure).

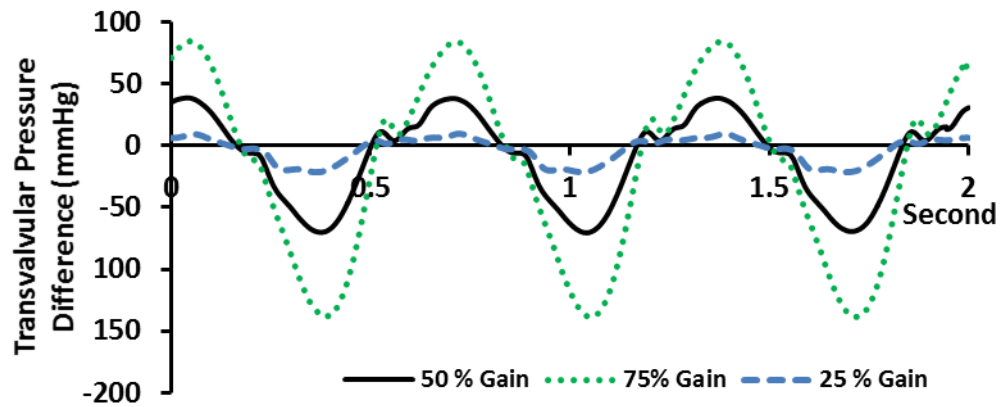


**Figure 7.17 Transvalvular Pressure across one Tilting Disc Mechanical Heart Valve for Different Bypass Valve Conditions**

### **Case 3: Variable Amplitude, Fixed Heart Rate, Fixed Bypass Valve and Fixed Number of Specimens**

The RWT with one tilting disc mechanical heart valve was set to 120 bpm heart rate and 50 % bypass valve closed. The transvalvular pressure waveforms were obtained for 25, 50 and 75% amplitude (gain) (Figure 7.18).

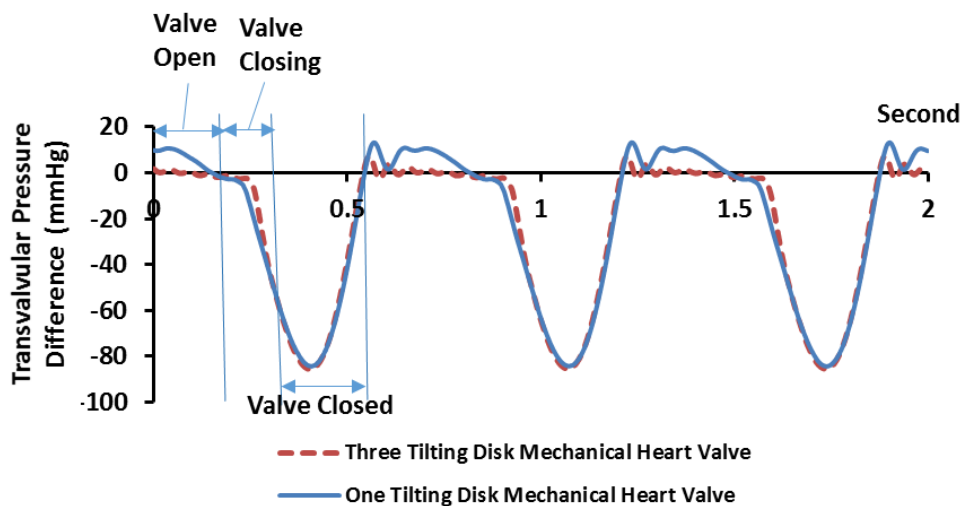
These transvalvular pressure waveforms showed that there was an overall higher pressure drop (positive and negative) across the valves for the higher amplitude value. Therefore, the pressure across the closed and opened valve was increased with increments in the amplitude value of the input sine waveform.



**Figure 7.18 Transvalvular Pressure Difference across one Tilting Disc Mechanical Heart Valve for Different Amplitude Conditions**

**Case 4: Variable Number of Specimens, Fixed Heart Rate, Fixed Amplitude and Fixed Bypass Valve**

A sensitivity analysis to investigate the impact of varying the number of test specimens on the inflow pressure of the test valves was carried out. The RWT had six equally spaced stations numbered 1 to 6 (Figure 7.8), these were not independent in that they had common inflow and outflow. Therefore, it was important to understand the effect of the number of test specimens on the system pressures, especially the inflow pressure.



**Figure 7.19 Transvalvular Pressures Difference across Tilting Disc Mechanical Heart Valve**

To investigate this, a valve holder with a tilting disc mechanical valve was placed in station 5 and five valve holders with blank plates were placed in all other stations.

The heart rate was adjusted to 120 bpm with the bypass valve fully closed and the gain was adjusted to 25 %. Following that the pressure data was captured for ten consecutive cycles. This procedure was repeated for three tilting disc mechanical valves mounted in stations 1, 3 and 5 and blank plates in stations 2, 4 and 6, by keeping all other test conditions the same as before. By inserting the valves in this manner even loading of the tester was achieved. The transvalvular pressure waveforms were captured for both cases as shown in Figure 7.19.

The negative part of the inflow pressure represented valve closing and valve closed pressures and the positive part of the inflow pressure represented valve open pressure. The valve closed pressures were the same in both cases. However, the outflow positive pressures were different in both cases but less than 10 mmHg as there was nothing to restrict flow on the outflow chamber and the outflow chamber was open to the air. Hence the transvalvular pressure across the closed valve was approximately the same as inflow pressure. In summary, the increment in the number of test specimens did not affect the inflow closed pressure and hence transvalvular pressure on the closed valve. All test valves experienced the same transvalvular pressure when they were fully closed.

#### **7.6.4 Discussion and Conclusions Following Characterisation and Validation of the RWT**

The RWT was tested with a tilting disc mechanical heart valve to understand the operation of the RWT and to verify consistency and repeatability to control physiological test pressure.

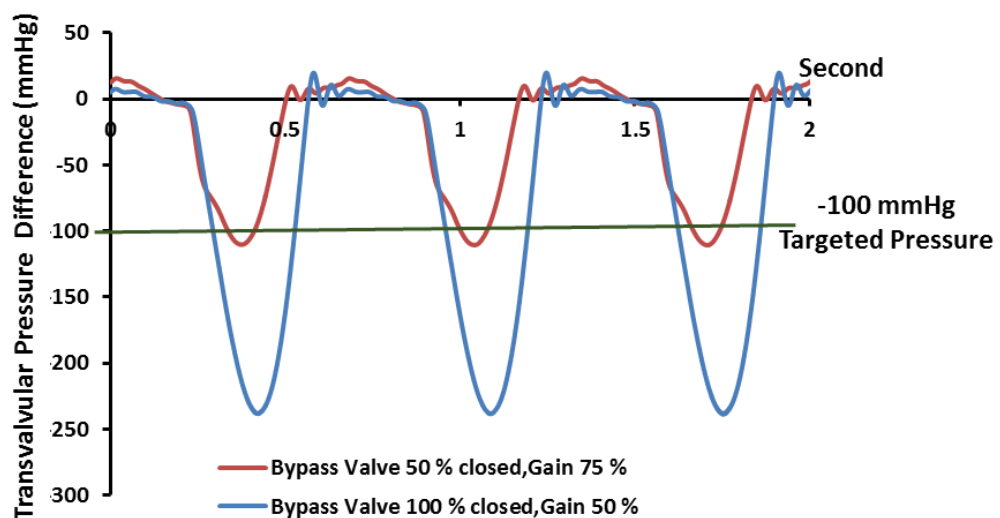
The following observations and conclusions were made during this study:

- An important aspect of the RWT from this data was verified, that the piston moved a shorter distance as the frequency increased. This was most likely due to the pump trying to “keep pace” at higher frequencies meaning that if it moves a shorter distance, it can move at a faster rate. As the frequency increased, systolic duration decreased and as stroke volume increased, volumetric flow rate also increased. The tester also naturally increased pressure as the frequency increased and this allowed the piston to move a shorter distance while still maintaining the correct pressure measurements.

- The amplitude dial set the drive level of the piston in terms of percentage gain, which increased or decreased the peak to peak movement of the piston, and thus the pressures. The amplitude control was used as a tool for setting the transvalvular pressure only, and not the piston displacement. The relationship between the amplitude control number (percentage gain) and the test pressures or the piston displacement was not absolute but dynamic, as it depends on several factors, including frequency (heart rate), bypass valve settings, type of the valves, and biological variation between the heart valve roots under test.
- Due to the lack of flow probes in the RWT, cardiac output relied on the metal bellow size and piston displacement. The piston waveform (input waveform) was scaled by frequency and piston displacement, in order to achieve physiological valve opening and closing. The amplitude of the piston waveform was adjusted to the length of the displacement of the piston and hence the volume of fluid being displaced. During the positive portion of the input waveform, the positive upstroke forces compressed the metal bellow, moved the test fluid forward and opened the test valve. During the negative or depressurisation portion of the test cycle, i.e., that portion of the input waveform having negative percentage amplitude values, expanded the metal bellow, the flow was reversed and the test valve was closed. As the negative portion of the cycle began, the fluid moved through the bypass valve into the inflow chamber. During return flow, the test valve remained closed due to the flow reversal and transvalvular pressure present between the inflow and outflow chamber. The pump drive system returned to its starting position and the process was repeated, cyclic opening and closing of the test valve.
- Transvalvular pressure waveforms were influenced by the heart rate (frequency) of the input waveforms. The transvalvular pressure waveforms showed that, during the specific amount of time  $t$  (Figure 7.16), the tilting disc mechanical heart valve was fully closed and opened 5, 3 and 1 times for frequency 3.33, 2 and 1 Hz respectively. This explained that the valve stayed closed for a long period of time at a specific transvalvular pressure for the lower frequency compared to the higher frequency.

- The RWT was designed to control the back pressure acting on the test valve as a primary variable. The input sine waveform controlled the negative pressure for a desired duration while limiting a peak reverse pressure on the valve. The bypass valve helped to control the excessive negative pressure on the valve.

A pressure tuning process across the test valve which involved making systematic adjustments to the amplitude of the input waveform and the flow bypass valve setting was developed. Figure 7.20 shows representative waveforms obtained during the process to achieve full opening and closing of the mechanical test valves (n=3) and simultaneously controlling transvalvular pressure across the closed valve by adjusting the closing of the bypass valve and amplitude of the input waveforms.



**Figure 7.20 Transvalvular Pressure Waveforms Obtained for Different Bypass Valve Setting and Amplitude Values**

The following sequence for RWT Pressure tuning was established for start of each test:

1. Initially the flow bypass valve was kept fully opened.
2. The opening of the test valve was monitored and the amplitude was increased until full valve opening was achieved.
3. The targeted transvalvular pressure was adjusted by closing the bypass valve.
4. If opening was excessive, amplitude was reduced and the bypass valve was readjusted for targeted transvalvular pressure.
5. If opening was insufficient, amplitude was increased and the bypass valve was adjusted for targeted transvalvular pressure.

6. The inflow pressure of the RWT was independent of the number of test specimens used.

### **7.6.5 Summary**

In summary, the pressure waveforms helped to characterise the RWT and set it up to work correctly. It was essential to maintain physiological pressures during the testing. To achieve this it was important to understand or establish a pressure tuning technique in the RWT, which was discussed in Section 7.6.4. Selecting appropriate specimens for the method development was paramount. The method development should start with the minimum number of specimens to keep the procedure simple. The RWT was designed to test a maximum of six specimens, therefore it was essential to determine the impact of varying test specimens, which was discussed in Section 7.6.3.

## **7.7 Method Development Approach for Testing Biological Heart Valve Roots**

Before beginning the method development for biological heart valve roots, four initial questions were asked and addressed as described in Table 7.2.

**Table 7.2 Specifications for Initial Method Development**

Question	Answer
What will be the intended outcome of the method?	A robust method to assess fatigue and durability of biological heart valve roots under physiological test conditions
What types and sizes of the biological heart valve roots will be used for method development?	Cellular and fixed porcine aortic heart valve roots with valve size $21 \pm 2$ mm
How many test specimens will be used for method development?	Minimum three test specimens
What will be the intended test conditions?	Frequency: 1, 2, 3.3 Hz Transvalvular pressure across the valve: $100 \pm 20$ mmHg - should be maintained for 95% or more of the test cycles Pressure in the aorta: $70 \pm 20$ mmHg Temperature: Ambient temperature Valve dynamics: Valve open fully and closed completely

### **7.8 Method Development: Real Time Fatigue Testing of Biological Heart Valve Roots**

When received from the manufacturer, the RWT had holders to mount frame mounted valves only, but these frame mounted bioprosthetic or mechanical valves differ significantly from that of biological heart valve roots. As the main intention was to test biological heart valve roots in the RWT, it was essential to design a new holder or modify the existing holders. It was decided to use fixed aortic heart valve roots during the initial method development stage to understand any potential confounding factors that may occur during biological heart valve root testing. The fixed heart valve roots were chosen due to longer and easy handling characteristics and thus, the valve holder design could be more easily examined.



### **7.8.1 Design Specification for Heart Valve Root Holder**

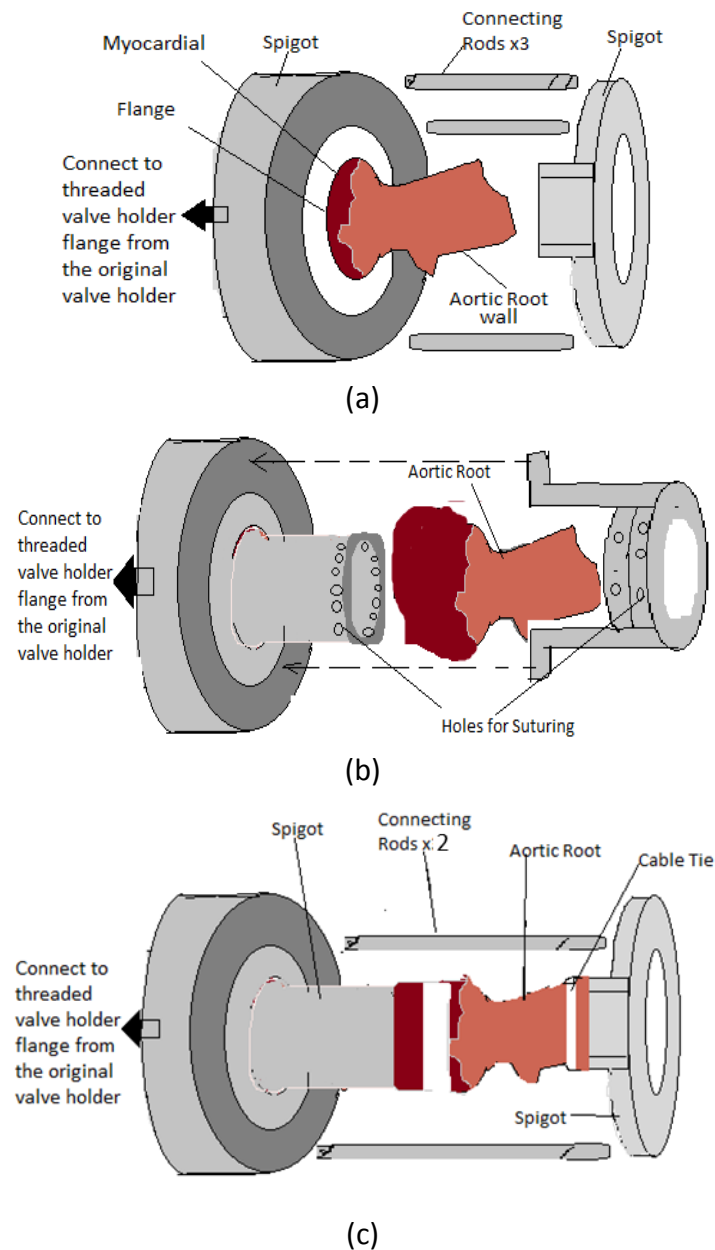
In order for the tester to be used with biological heart valve roots, valve holders had to be designed and manufactured that would fit into the test space provided and that would also accommodate the root wall and myocardial muscles along with the leaflets and annulus. Before designing the holders for the heart valve roots, a number of important parameters were acquired from the characterisation work, validation tests with mechanical valve (Section 7.6) and the literature part of the thesis (Chapter 1). These parameters, together with additional factors considered necessary to design the holder for the heart valve root, have been described in the design specification in Table 7.3.

**Table 7.3 Heart Valve Root Holder Design Specification**

<b>Criteria</b>	<b>Essential= E Desirable=D</b>	<b>Target</b>
<b><u>Design</u></b>		
Robust	E	Should work with heart rate 60-200 bpm
	E	Should work with maximum 37 °C temperature
	E	Can be used with test solution (0.9 % w/v saline, 0.04 % sodium azide solution)
Modular	D	Easy aortic heart valve root mounting (maximum mounting time 5 min, one user able to complete without assistance)
	E	Simple design
	E	Ease of use
Simplicity	D	Maximum number of parts 5
	D	Easy to manufacture
Enable valve visualisation	E	High speed video will be used to assess leaflet dynamics
Easy to clean	E	Less bacterial growth, sterilisable
Attributes	E	Light weight and low cost
<b><u>Performance</u></b>		
Pressure	E	Transvalvular pressure: $100 \pm 20$ mmHg Pressure in the aorta: $70 \pm 10$ mmHg
size	E	$22 \pm 2$ mm diameter of valve with aorta with maximum length 70 mm
Movement	D	Axial and circumferential heart valve root wall maximum movement to 10 mm
<b><u>Measurement Capability</u></b>		
Pressure	E	Inflow and outflow pressure near the test valve

### 7.8.1.1 Conceptual Designs for the Heart Valve Root Holder

The design of the heart valve root holder began with a conceptual design stage in which three conceptual modular designs for the heart valve root holder were generated and are presented in Figure 7.21. The designs varied in heart valve root mounting techniques and suitability for use in RWT but all had the potential to function successfully.



**Figure 7.21 Conceptual Designs for the Heart Valve Root Holder (a) Design involved Sandwiching of Myocardium between the Two Flanges and Attaching Aorta to the Spigot with Cable Tie (b) Design involved Suturing of Myocardium and Aorta onto the Spigots (c) Design involved Attaching Myocardium and Aorta on to the Spigots with Cable Ties**

#### **7.8.1.1.1 Design 1**

Design 1 (Figure 7.21 (a)) used two spigots connected with three connecting rods. The myocardial (muscle) side of the heart valve root could be sandwiched between the two flanges and attached to the spigot. The wall could be attached to the other spigot with cable ties. However, it was thought that problems may arise as a myocardium might get damaged due to the clamping pressure of the two flanges. The design may have a relatively low reliability due to heart valve root damage during the mounting and the number of parts involved.

#### **7.8.1.1.2 Design 2**

This design (Figure 7.21 (b)) was based on suturing of the heart valve root onto the spigots. This design would be relatively robust because of the lack of any axial movement. The reliability of the design would depend largely on the suturing technique to mount the heart valve root on spigots and the type of suture and needle used to make it. Repeated expansion and contraction in a cyclic environment may cause leakage from the suturing line. This design would require a higher level of skill than the previous designs due to the required mounting technique (suturing) of the heart valve root on the spigots. In addition, this design may require a longer time to mount the heart valve root on the spigots.

#### **7.8.1.1.3 Design 3**

This design consisted of two spigots with two connecting rods. The wall and myocardial of the heart valve root was attached to the spigots with cable ties (Figure 7.21 (c)). The wall side spigot was free to slide axially on the connecting rods. This was the simplest of all the conceptual designs.

#### **7.8.1.1.4 Concept Screening**

The proposed concepts were examined, evaluated and filtered with respect to the design objectives, the concept design closest to meeting the design specification was determined prior to proceeding with further optimisation. All the conceptual designs were scored out of 5 for each criteria, compared and ranked on the basis of the features listed in Table 7.4.

**Table 7.4 Concept Screening and Ranking**

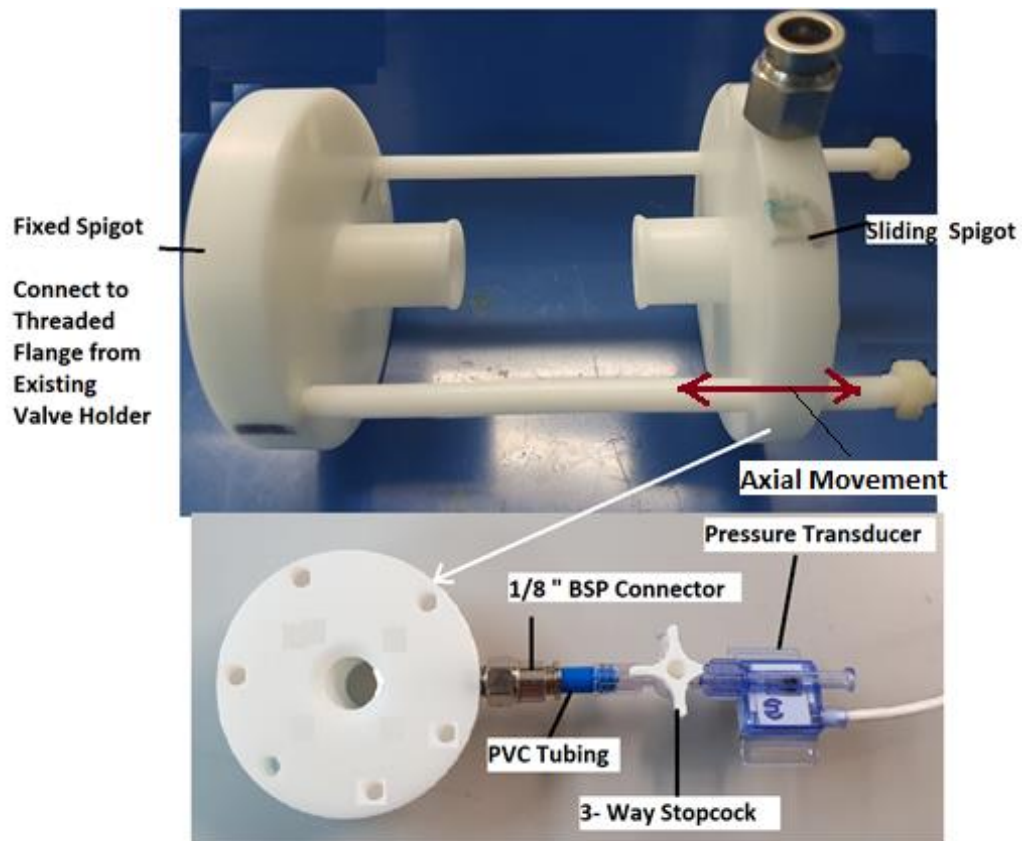
<b>Selection Criteria</b>	<b>Ideal score</b>	<b>Design 1</b>	<b>Design 2</b>	<b>Design 3</b>
Easy heart valve root mounting	5	2	1	5
Simplicity of design	5	2	3	4
Ease of use	5	2	2	5
Number of parts	5	3	4	4
Cost Suitability	5	4	2	4
Easy to manufacture	5	2	4	5
<b>Final Score</b>	<b>30</b>	<b>15</b>	<b>16</b>	<b>27</b>
<b>Rank</b>		<b>3</b>	<b>2</b>	<b>1</b>

The final design selected was design 3. Design 3 ranked highest; hence closest to meet the design specification due to the simplicity in the design and heart valve root mounting. The cable tie heart valve root mounting technique had been used in other experimental techniques (competency testing, pulsatile flow testing, dilation testing) and was a proven reliable concept.

#### **7.8.1.2 Detailed Heart Valve Root Holder Design**

The detailed design and 3D model, based on the conceptual design was created for the heart valve root holder using SolidWorks (Dassault Systèmes, Waltham, MA, USA). The engineering drawings used to manufacture the holder are presented in Appendix C.

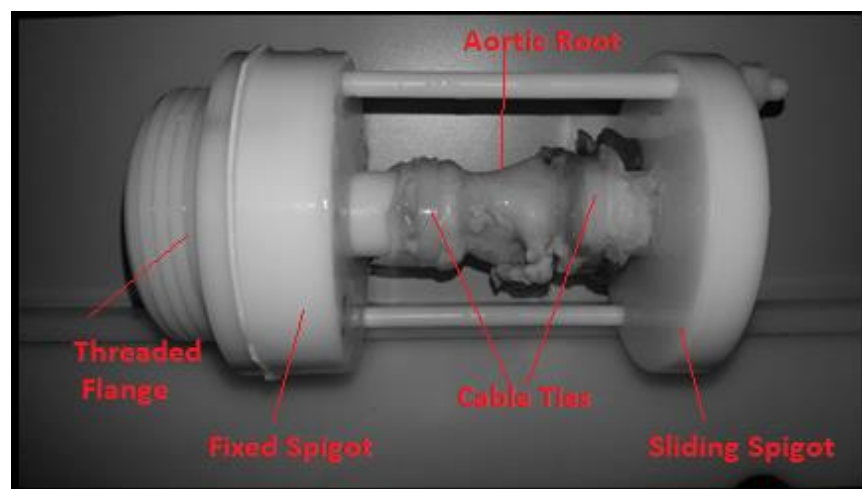
The heart valve root holder design comprised of two spigots, connected and supported by two connecting rods. One spigot was connected with the threaded valve holder flange from the original valve holder, and the other spigot slid axially on the two rods. In order to test the valve performance the inflow and outflow pressure from the heart valve root needed to be measured. For this 1/8" British Standard Pipe (BSP) stainless steel push in fittings were assembled into the sliding spigot and the output pressure transducer was connected as shown in Figure 7.22.



**Figure 7.22 Heart Valve Root Holder for Biological Heart Valve Root with Pressure Measurement Assembly**

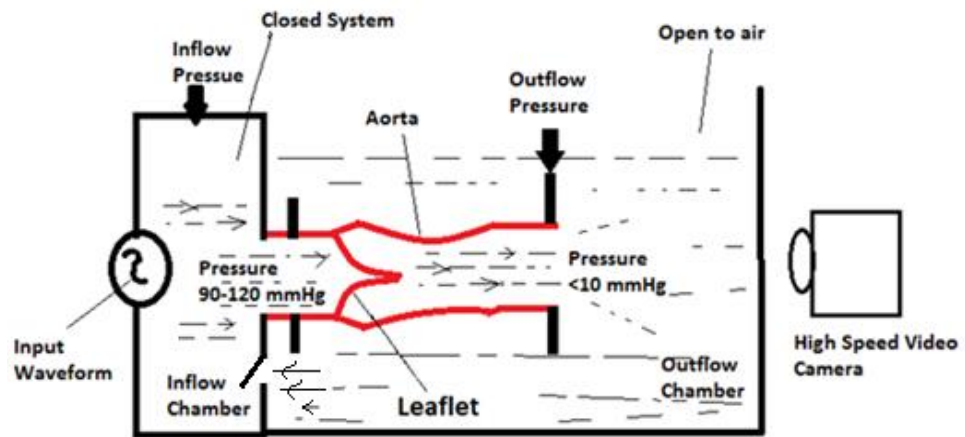
### 7.8.1.3 Heart Valve Root Holder Feasibility Test

The aim of the valve holder feasibility test was to check the design stability and the amount of time required to mount the heart valve root in the holder. A total of 3 porcine aortic roots were fixed in glutaraldehyde as described in Chapter 2. The fixed heart valve roots were mounted on the holder with cable ties as shown in Figure 7.23.

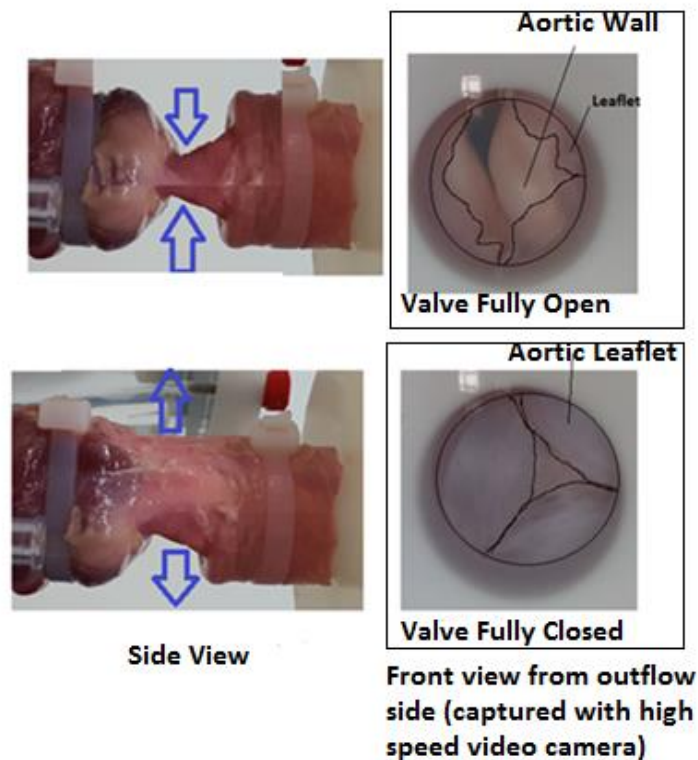


**Figure 7.23 Representative Image of Heart Valve Root Mounting On the RWT**  
Chapter 7

As described in Chapter 2 Section 2.4.7.3, a cable tie gun (part no: STHV, Panduit Europe Ltd) was used to tension and cut the cable ties. The cable ties were sufficiently tight to prevent axial movement along the spigot and stop them being pushed out under pulsatile flow conditions. The RWT was run for 30 min at various possible test conditions to check valve holder and root stability. It was found that the heart valve root holder and heart valve root mounting were appropriate and the valve was closing and opening fully for all the test conditions.



(a)



(b)

**Figure 7.24 (a) Schematic Diagram showing Inflow and Outflow Pressures during the Porcine Aortic Heart Valve Root Testing in the RWT (b) Movement of the Aorta and the Valve Opening and Closing from the Outflow Side**

Following the successful trial with the fixed heart valve roots, 3 cellular porcine aortic heart valve roots were mounted on the same holders with cable ties (Figure 7.23).

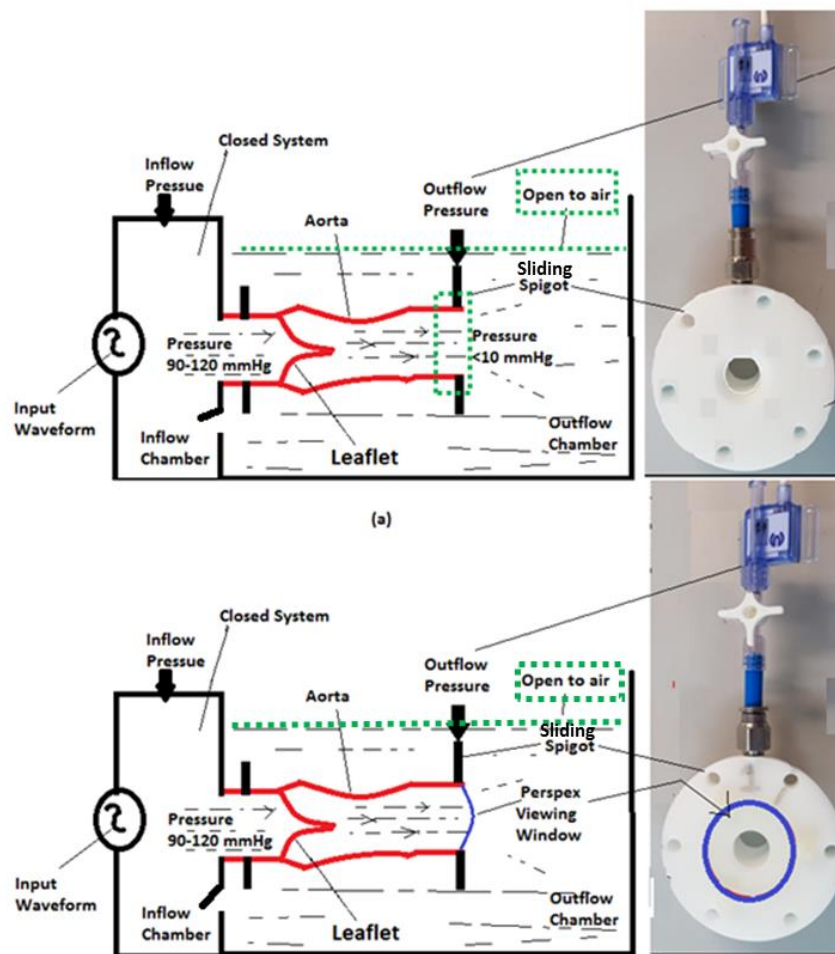
The RWT was run for all possible test frequencies (1, 2 and 3.3 Hz). During this testing, a major issue was identified. The aorta was collapsing and it was difficult to view the valve closing from the outflow side (Figure 7.24). It was identified that the



sliding spigot had an orifice which allowed fluid flow to the outflow chamber, this was open to the air and thus not controlling the aorta pressure (Figure 7.25 (a)). Also the aorta pressure was less than 10 mmHg for all the tested conditions, which was much lower than physiological pressure and not enough to keep the aorta dilated. To resolve this problem, it was necessary to both modify the heart valve root holder design (Section 7.8.1.4) and the RWT itself (Section 7.8.2).

#### 7.8.1.4 Modified Heart Valve Root Holder Design

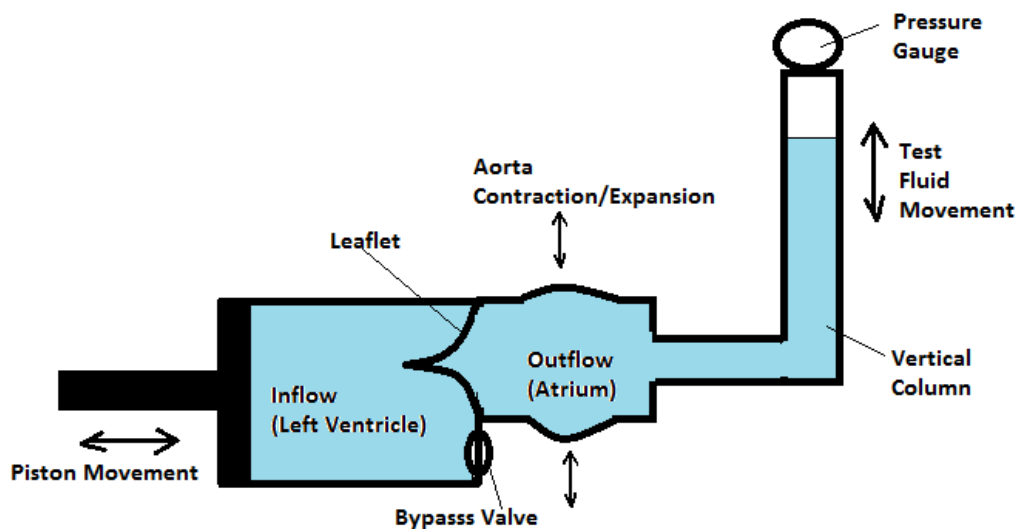
The modification comprised of a viewing window made of Perspex fitted on the outer side to view and record valve dynamics. This also closed the orifice and maintained the pressure. The complete heart valve root holder assembly, including pressure measuring system, Perspex viewing window and spigots is presented in Figure 7.25 (b).



**Figure 7.25 (a) First version of Heart Valve Holder (b) Modified Heart Valve Root Holder for Biological Heart Valve Root Mounted in the RWT with Pressure Measurement Assembly**

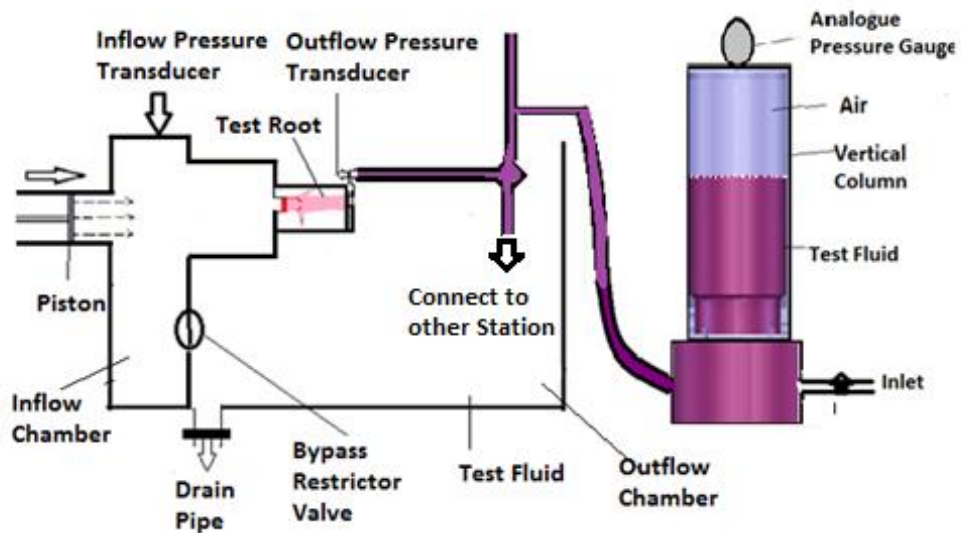
### 7.8.2 Modification of RWT to Control Physiological Pressure of the Aorta during Fatigue Testing of Biological Heart Valve Roots

The complex physiology of the left ventricle involves three-dimensional dynamic myocardial contraction, which cannot be mimicked with the inflow chamber of the RWT, and only involved application of a uniform and simultaneous pressure on the whole ventricle. Similarly, atrial contraction-expansion movement was absent, as the outflow (left atrium) chamber was open to air and not subject to any external load. Even though the heart valve root holder was modified, it was difficult to maintain the physiological test scenario in keeping the aorta dilated. The aorta of the human aortic heart valve root has mean pressure of  $70 \pm 20$  mmHg. To compensate for this, compliance was added to the aorta by means of a vertical column, as shown in Figure 7.26.



**Figure 7.26 Physical Model Illustrating the Application of External Load (Pressure) on the Aorta by Attaching a Vertical Column**

The compliance chamber provided an external load (pressure) to the aorta and also an excess volume area for fluid to move into during the forward stroke or positive part of the cycle.



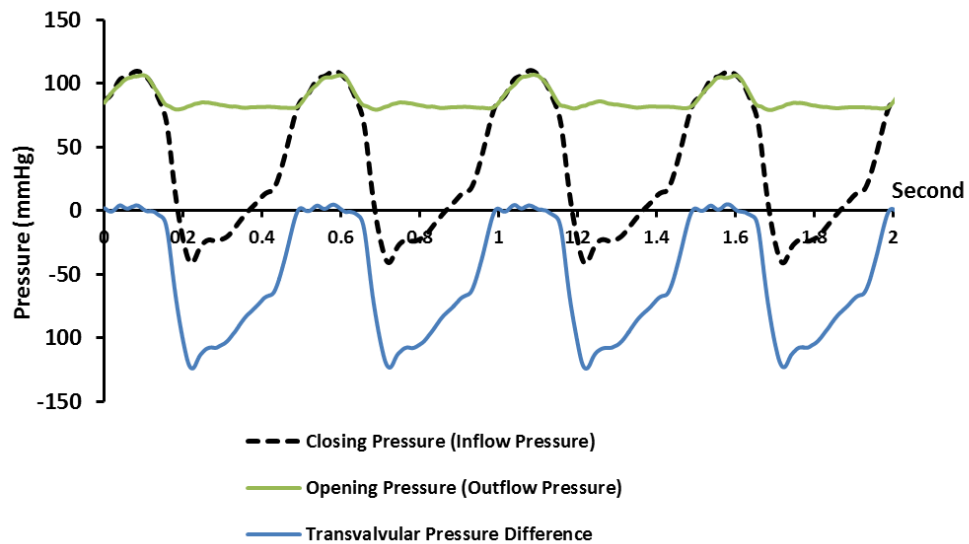
**Figure 7.27 Schematic Diagram of Modified RWT**

All valve holders were connected to the vertical column (compliance chamber) via BSP push-in fittings, 3 way connectors and flexible tubing. The vertical column was filled with 75 % test solution, the top void contained air. A flange mounted analogue pressure gauge was mounted on top of the column. The pressure column of test fluid provided mean pressure to the atrial side of the heart valve root, which was connected to the moving spigot (Figure 7.27).

#### **7.8.2.1 Validation of Modified RWT**

In order to validate the modified RWT design, a test was run with cellular porcine aortic heart valve roots. Three cellular aortic heart valve roots were mounted on three modified heart valve root holders as per the procedure described in the section 7.8.1.3. Upon ensuring the attachment of the heart valve roots to the holders, the whole assembly was secured into the RWT. The holders with heart valve roots were placed in station 1, 3 and 5 (Figure 7.8). The remaining three stations (2, 4, 6) had valve holders with blanking plates (Figure 7.8).

All the holders were connected to the compliance chamber via 1/8" BSP push-in fittings, 3 way connectors and flexible tubing. The RWT's tank was filled with test solution (0.9 % (w/v) saline with 0.04% sodium azide (v/v)). The compliance chamber was filled with 75 % test solution, the top void contained air.



**Figure 7.28 Representative Pressure Waveforms Measured for Cellular Porcine Aortic Heart Valve Roots during Real Time Fatigue and Durability Testing**

The inflow and outflow pressure transducers were mounted as shown in Figure 7.8. Both pressure transducers were calibrated as per the procedure described in Section 7.6.2. The RWT was run for 30 minutes for all possible test frequencies (1, 2 and 3.3 Hz). The pressure tuning was performed as described in the section 7.6.4 to control transvalvular pressure across the valve ( $100 \pm 20$  mmHg) for at least 95 % of the test cycles. The generated pressure due to the addition of the compliance chamber was recorded with an analogue pressure transducer and it was approximately  $75 \pm 5$  mmHg. This set-up enabled the aorta to remain inflated and to attain physiological pressure conditions as described in Table 7.2. The compliance chamber simulated the native compliance of the aorta by allowing it to contract and dilate depending on the fluid volume and without compliance here, the aorta was unnaturally collapsed (Section 7.8.1.3). This meant that the inflow negative pressure generated by the driving mechanisms was sufficiently dampened by the addition of the compliance chamber on the outflow side in the RWT.

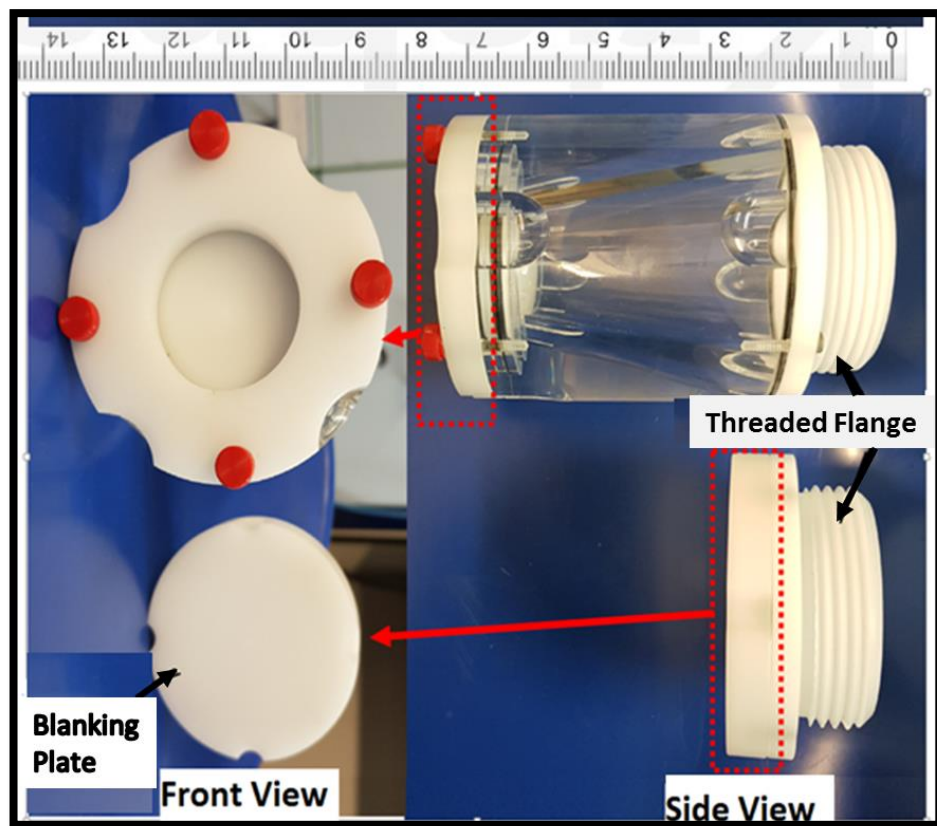
Representative pressure waveforms captured during the testing are displayed in Figure 7.28. Also, valve dynamics were captured using a high speed video camera which showed the valve fully opened and closed for all the applied test conditions.

However, difficulties were encountered during the mounting of the heart valve roots. Due to limited space between two stations, it took an average 10 minutes to

mount each holder with heart valve roots in the RWT. It was also difficult to manipulate the heart valve roots once they were mounted in the RWT. Therefore, it was decided to redesign the blanking plates.

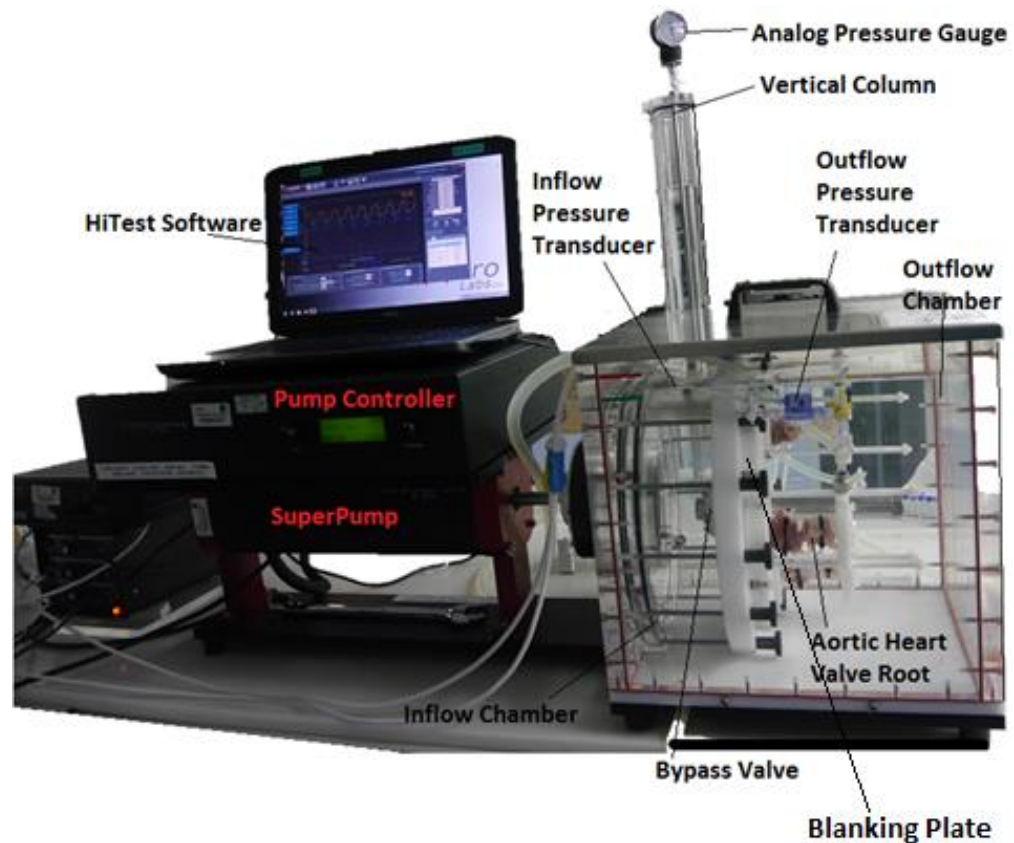
### 7.8.2.2 Modification of Blanking Plates

For easy manipulation of the heart valve roots in the RWT and to create space between two mounted holders in the RWT, the blanking plates (Figure 7.15) were modified. The new design consisted of a blank plate with o-ring seal, connected to the threaded flange from the existing valve holder (Figure 7.29).



**Figure 7.29 Blanking Plate Designs and Assemblies. Top: First Version of the Design. Bottom: Modified Design**

This new blanking plate design was slim, easy to mount and clean. A modified RWT with blanking plates is shown in Figure 7.30.



**Figure 7.30 Modified RWT with Modified Blanking Plates**

### **7.8.3 Summary of the Test Method: Fatigue and Durability Testing of Biological Heart Valve Roots in the RWT**

An *in vitro* real time fatigue and durability testing method for biological heart valve roots has been developed. The methodology included, heart valve root mounting in the RWT, controlling physiological pressure across the test root and associated processes to achieve the physiological valve dynamics. The main features of the method are summarised below.

- The RWT was adapted for any type of biological heart valve roots.
- Pressure and amplitude could be controlled and reproduced in the RWT.
- The amplitude and bypass valve were adjusted in an attempt to set the maximum transvalvular pressure of  $100 \pm 20$  mmHg for 95% or more of the test cycles, and the minimum transvalvular pressure was maintained for at least 5% of each cycle.
- The outflow pressure (aorta pressure) value ( $70 \pm 20$  mmHg) was achieved by adding compliance on the wall side and the amplitude/bypass valve of the RWT was adjusted until the outflow waveform was correct.

- The test resulted in full opening and closing of the valve.
- Compliance of the aorta was essential for modelling the dynamic system. This enabled the system to incorporate and vary the effect of arterial elasticity.

### **7.9 Discussion and Conclusion Following Method Development for Biological Heart Valve Roots**

A RWT was purchased that was originally designed for testing standard frame mounted or mechanical valves. The RWT was validated and characterised in order to understand its behaviour and therefore determine a protocol so that it could be employed to test biological heart valve roots. A heart valve root holder was designed, optimised and manufactured to adapt the RWT for use with biological heart valve roots. The RWT is now understood and can be used for the testing of any type of biological heart valve root.

The aortic valve is located between the left ventricular outflow tract and the ascending aorta in the heart. The complex *in vivo* left ventricular physiology that involves a three-dimensional dynamic myocardial contraction with ventricular twisting cannot be mimicked with the proposed RWT approach. Similarly, atrial contraction was absent, as the outflow side of the heart valve root was not subject to any external load and is only provided with a controlled filling pressure through the vertical column (compliance). Despite such constraints, results were satisfying both in terms of pressure wave morphology and numerical values. The transvalvular pressures and aorta pressures were in agreement with the expected values.

The results demonstrated the proper functioning of the aortic valve with a hydrodynamic behaviour comparable to the *in vivo* conditions. The pressure waveforms were influenced by two main controls, which affected the overall behaviour of the test valve: the presence of the bypass valve between the inflow and outflow chamber, which has introduced local resistances and inertial effects and helped to control reverse (closing) pressure on the test valve.

Due to the pumping mechanism, a large negative closing pressure was experienced by the test heart valve root which caused aorta occlusions. The design of the biological heart valve root holder and addition of compliance with vertical fluid column helped to control physiological pressure across the heart valve root. During a

forward piston stroke or positive part of the input cycle, test fluid was fed back to vertical column which added positive pressure in the aorta (outflow side) and regulated some of the negative inflow pressure.

In summary, the result showed that the RWT can apply physiological test conditions and create forces on the heart valve leaflets, creating a controllable environment that will be necessary in the fatigue testing of biological heart valve roots.

Having developed an *in vitro* real time fatigue method from this study using fixed and cellular porcine aortic heart valve roots, the method was further used for six cellular and six decellularised porcine aortic heart valve roots (Chapter 8).



## **8 *In vitro* Real Time Fatigue Assessment of Cellular and Decellularised Porcine Aortic Heart Valve Roots**

### **8.1 Introduction**

The real time fatigue of cellular and decellularised porcine aortic heart valve roots under physiological cyclic pressures and heart rate conditions was evaluated in the real time wear tester (RWT) using the *in vitro* test methodology developed in Chapter 7. The real time fatigue of porcine aortic heart valve root leaflets was assessed by high speed camera imaging of the leaflet dynamics and through qualitative visual assessment at the end of fatigue assessment in the RWT. For a quantitative assessment of the fatigue of the cellular and decellularised porcine aortic heart valve roots, their hydrodynamic performance was evaluated under pulsatile flow following cyclic conditions in the RWT, and material properties evaluated through tensile testing. In addition, a competency test of heart valve roots was assessed at several intervals (pre-test, mid-test, post-test) to monitor the effect of cyclic loading on the leaflet competency and to eliminate sample to sample variability.

This study comprised of a feasibility study followed by a primary study which fully investigated the effect of decellularisation on the *in vitro* real time fatigue of porcine aortic heart valve roots. The feasibility study was conducted to assess the efficiency and limitations of experimental test methods which included real time fatigue, pulsatile flow and uniaxial tensile tests.

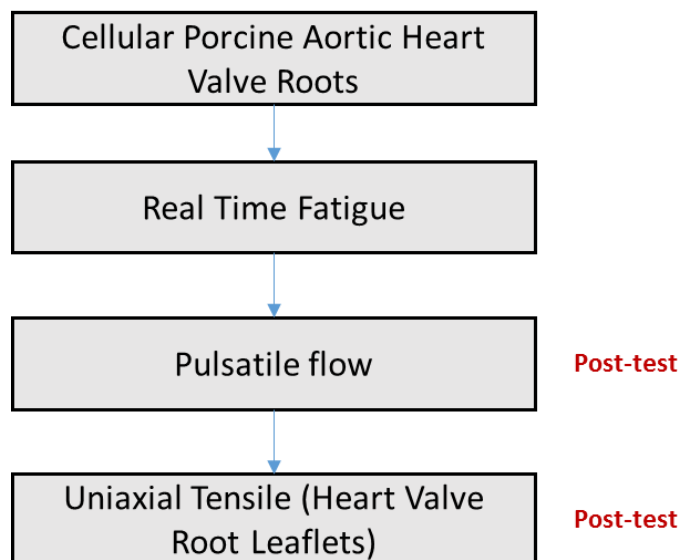
### **8.2 Aim and Objectives**

The aim of the study was to fully investigate *in vitro* real time fatigue of decellularised porcine aortic heart valve roots under physiological cyclic pressures and heart rate conditions and compare it with cellular porcine aortic heart valve roots to derive the effect of decellularisation.

The main objectives were:

1. To determine real time fatigue, pulsatile flow performance and uniaxial tensile properties of the leaflets of cellular porcine aortic heart valve roots within 10 consecutive days to evaluate feasibility and efficiency of the experimental methods and techniques.
2. To determine and compare real time fatigue of the cellular and decellularised porcine aortic heart valve roots under physiological cyclic loading conditions [physiological pressures and heart rate (frequency)] in the RWT.
3. To determine and compare the effect of physiological cyclic loading conditions on competency of the cellular and decellularised porcine aortic heart valve roots.
4. To determine and compare the effect of physiological cyclic loading conditions on pulsatile flow performance of the cellular and decellularised porcine aortic heart valve roots following cyclic fatigue assessment in the RWT.
5. To determine and compare the uniaxial tensile properties of the cellular and decellularised porcine aortic heart valve root leaflets following real time cyclic fatigue and pulsatile flow performance assessment.

### 8.3 Study Experimental Design



**Figure 8.1 Flow Chart Indicating Cellular Porcine Aortic Heart Valve Roots *In Vitro* Performance Assessment Sequence used in the Feasibility Study**

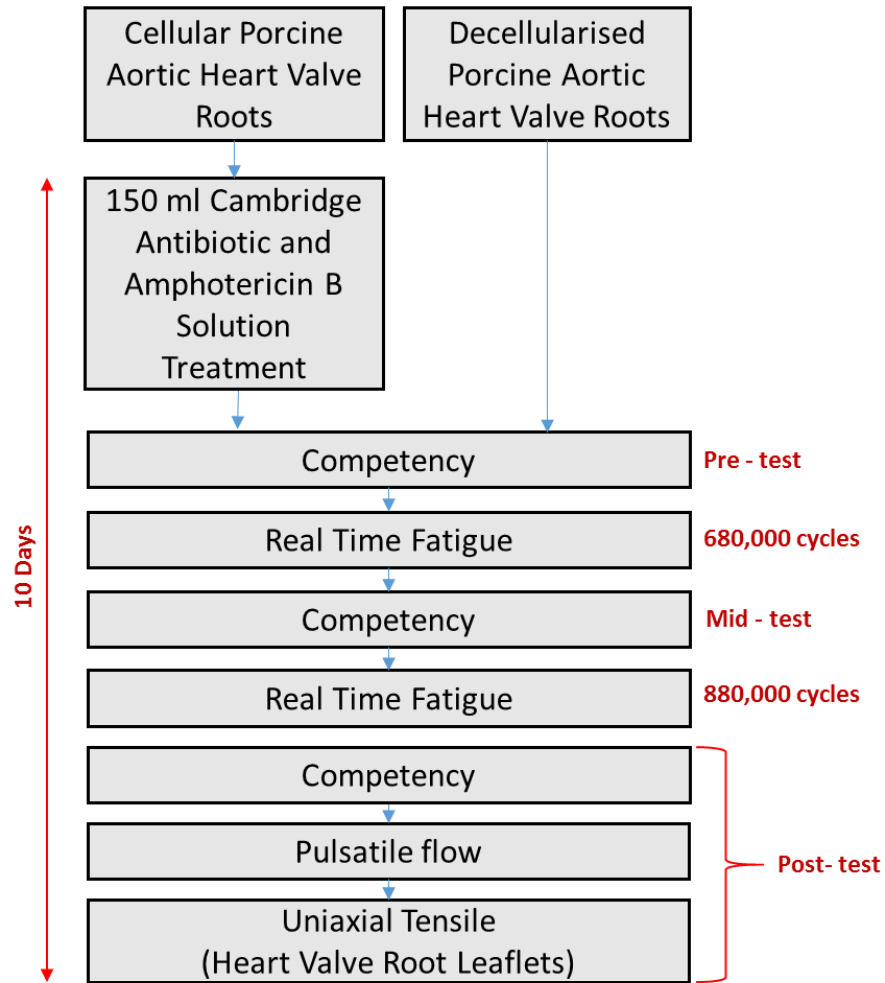
Prior to undertaking a primary study on the decellularised porcine aortic heart valve roots to investigate fatigue under cyclic loading conditions, a feasibility study was conducted to learn about the possibilities and limitations of the experimental

test plan used to derive real time fatigue of cellular and decellularised porcine aortic heart valve roots. In addition, the test plan was used to check the practicability of experimental techniques, for example the stability of the aortic heart valve root for 1.2 million cycles in the RWT, multiple mounting and dismounting of the heart valve root in the RWT and complexity of consecutive test procedures (real time fatigue, pulsatile flow and uniaxial tensile) within 10 consecutive days.

The feasibility study was conducted using three cellular porcine aortic heart valve roots. The heart valve roots were assessed for *in vitro* real time cyclic fatigue, post-test hydrodynamic (pulsatile) and post-test biomechanical (uniaxial tensile properties of leaflets) performance within 10 consecutive days. The test plan for the feasibility study is shown in Figure 8.1. Pulsatile flow performance of the cellular aortic heart valve roots was not assessed prior to the fatigue assessment due to concerns of causing damage to the heart valve roots and also the complexity of the test. In addition, pulsatile flow performance data for the cellular aortic heart valve roots is available in Chapter 3 for comparison.

Following a review of the results and observations from the feasibility study described in the Section 8.6.1., the study plan was optimised and test conditions were refined to assess the effect of decellularisation on the fatigue of the porcine aortic heart valve roots (primary study) within 10 consecutive days.

To minimise growth of contaminating bacteria and fungi during the fatigue assessment in the RWT, the cellular heart valve roots were treated with 150 ml Cambridge antibiotics and amphotericin B solution as per the procedure described in Chapter 2 Section 2.4.3 for the primary study. Also, to eliminate sample variability, a within-sample design (repeated measures) was accepted and competency assessment was added in the primary study test plan, whereby each aortic heart valve root was used as their own control for competency assessment. The competency (pre-test, mid-test and post-test) of the heart valve roots was measured three times to monitor the effect of cyclic loading conditions on the leaflet competency during fatigue assessment in the RWT (Figure 8.2). The advantages of the competency assessment method were being more straightforward and less time consuming than other biomechanical performance measurements.



**Figure 8.2 Flow Chart Indicating Cellular and Decellularised Porcine Aortic Heart Valve Roots Performance Assessment Sequence used in the Primary Study**

The competency (pre-test) of each heart valve root was evaluated before fatigue assessment in the RWT. In sets of three, the heart valve roots were then cycled for 680,000 to 880,000 cycles (mid-test) at 120 bpm heart rate (2 Hz frequency) in the RWT to assess real time fatigue. Following fatigue, the heart valve roots were removed from the RWT for the competency assessment (mid-test). Then following competency, the heart valve roots were mounted straight back in the RWT for further fatigue testing. The fatigue test in the RWT was terminated at 1.2 million cycles and hydrodynamic performance [competency (post-test) and pulsatile flow] of each heart valve root was evaluated. Following evaluation of the hydrodynamic performance, biomechanical performance (uniaxial tensile) of the leaflets (radial and circumferential) from each heart valve root was evaluated.

## **8.4 Materials**

All the cellular porcine aortic heart valve roots were dissected from hearts obtained from M & C Meats, Crossgates, Leeds and John Penny & Sons, Rawdon, Leeds, UK. within 4 hours of slaughter.

The decellularised porcine aortic heart valve roots were prepared by Timothy Munsey and Dr Helen Berry in the Faculty of Biological Sciences (University Of Leeds) using an established low concentration sodium dodecyl sulphate (*SDS*) based decellularisation protocol (Booth et al., 2002, Korossis et al., 2005, Wilcox et al., 2005).

The heart valve root storage and defrosting procedures are described in Chapter 2 Section 2.4.4.

Phosphate buffered saline (PBS) was used to store the heart valve roots in between tests and to keep them hydrated during testing.

### **8.4.1 Feasibility Study**

For the feasibility study, three cellular porcine aortic heart valve roots (A1, A3 and A5) were dissected a day before testing and stored in 150 ml PBS at 4 °C until testing. The sizes (internal diameter) of all the cellular aortic heart valve roots were measured with obturators and they had a mean diameter of  $21 \pm 1$  mm.

The test solution used in the cyclic fatigue test was 0.9 % (w/v) saline.

### **8.4.2 Primary Study**

For the primary fatigue study, all the cellular porcine aortic heart valve roots were treated with 150 ml Cambridge antibiotics and amphotericin B solution as described in Chapter 2 Section 2.4.3 to minimise growth of contaminating bacteria and fungi during the fatigue testing in the RWT.

**Table 8.1 Details of Cellular and Decellularised Porcine Aortic Heart Valve Roots Assessed Including Identification Number and Valve Size**

Cellular Aortic Heart Valve Roots		Decellularised Aortic Heart Valve Roots	
Identification Number	Valve Size (mm)	Identification Number	Valve Size (mm)
Set 1		Set 1	
AC1	23	AD1	21
AC2	23	AD2	20
AC3	24	AD3	22
Set 2		Set 2	
AC4	22	AD4	21
AC5	23	AD5	22
AC6	23	AD6	22

All the cellular porcine aortic heart valve roots were stored in this 150 ml treatment solution and used immediately for testing. Six cellular and six decellularised porcine aortic heart valve roots were used in this study, as before. The sizes (internal diameter) of all the cellular and decellularised heart valve roots were measured with obturators (Table 8.1).

The test solution used in the cyclic fatigue assessment was 0.9 % (w/v) saline with 0.04% sodium azide (v/v) to retard bacterial growth. In the pulsatile flow assessment, 0.9 % (w/v) saline was used.

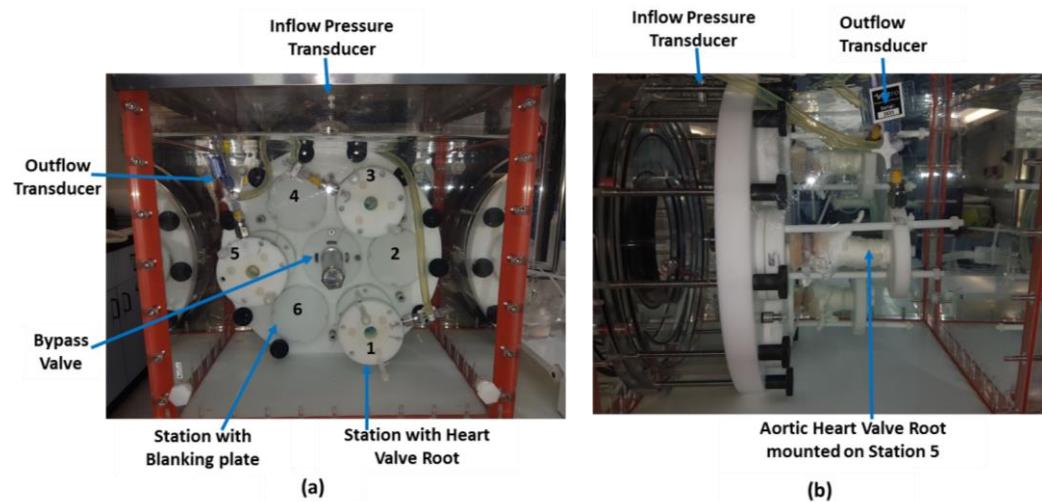
## **8.5 Methods**

### **8.5.1 Methods used in Feasibility Study**

#### **8.5.1.1 Real Time Fatigue**

The real time fatigue of cellular porcine aortic heart valve roots was investigated under physiological cyclic pressures (pressure across the closed valve and aorta pressure) and heart rate conditions. Three porcine cellular aortic heart valve roots were mounted on the heart valve root holders with cable ties as described in the Chapter 7 Section 7.8.1.3. Upon ensuring the attachment of the heart valve root to

the holder, the whole assembly was secured into the RWT. The holders with heart valve roots A1, A3 and A5 were placed in station 1, 3 and 5 respectively; and the remaining stations 2, 4 and 6 were blanked off with blanking plates (Figure 8.3). All the heart valve root holders were connected to the compliance chamber (vertical column) as described in Chapter 7 Section 7.8.2.



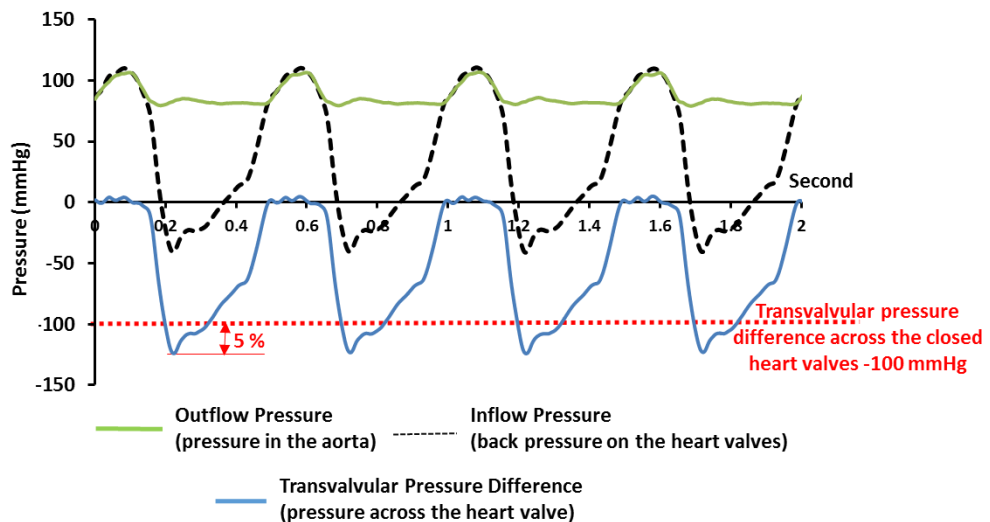
**Figure 8.3 Aortic Heart Valve Root Mounting in the RWT (a) Front View (b) Side View**

The RWT's tank was filled with the test solution (0.9 % (w/v) saline). The vertical column was 75 % filled with test solution and the remaining top void contained air. The inflow and outflow pressure transducers were mounted and calibrated as described in Chapter 7 Section 7.6.2. The outflow transducer was always connected at station 5. The input waveform was a sine wave (S50) with heart rate 120 bpm (2Hz).

The bypass valve and amplitude of the input sine wave were adjusted (pressure tuning process Chapter 7, Section 7.6.3) to achieve full valve closing and opening. The amplitude and bypass valve were adjusted to maintain a target peak transvalvular pressure difference of -100 mmHg over the closed valves for over 95% of the test cycles and to maintain the pressure at -100 mmHg or greater for 5% or more of each cycle duration.

Typical waveforms of the tuned RWT are shown in Figure 8.4, showing a peak transvalvular pressure difference greater than -100 mmHg which was maintained across the closed heart valves for 95% or more of total test cycles, and at least 5% of each cycle. The outflow pressure (aorta pressure) was between 77 to 108 mmHg. The

mean pressure on the top of the vertical column (compliance chamber) was  $92 \pm 15$  mmHg. The RWT was run for a maximum of 1.2 million cycles. During testing, the heart valve roots were checked daily for any artery leakage and alteration of transvalvular pressure difference across the closed valve.



**Figure 8.4 Representative Pressure Waveforms of the Tuned RWT at Heart Rate 120 bpm during Real Time Fatigue Assessment of Cellular Porcine Aortic Heart Valve Roots**

The real time fatigue of cellular porcine aortic heart valve root leaflets was assessed by high speed camera at 500 frames/sec imaging of the leaflet dynamics and through qualitative visual assessment at the end of testing in the RWT.

#### 8.5.1.2 Hydrodynamic Performance under Pulsatile Flow

Following fatigue assessment in the RWT, more detailed examination of the cellular aortic heart valve roots was undertaken under pulsatile flow to assess hydrodynamic performance. The heart valve roots were detached from the RWT holder and mounted in the pulsatile flow simulator.

All the heart valve roots were initially tested at minimum compliance in the pulsatile flow simulator with heart rates of 60, 72, 80 and 100 bpm with corresponding stroke volumes of 60, 70 and 80 ml to determine the peak flow conditions required for testing at maximum compliance, which are detailed in Table 8.2. The detailed test procedure was described in Chapter 2 Section 2.4.7.4.



**Table 8.2 Test Conditions Used in the Pulsatile Flow Performance of Cellular Porcine Aortic Heart Valve Roots (Maximum Compliance Condition)**

Heart Rate (bpm)	Mean Peak Flow (mL .s <sup>-1</sup> )
60	237
72	335
80	370
100	516

The systemic pressure was held between 120 mmHg to 80 mmHg. The hydrodynamic parameters [transvalvular pressure difference during forward flow, the root mean square (RMS) forward flow ( $Q_{RMS}$ ) and effective orifice area (EOA)] were evaluated. The opening and closing of the valve was recorded with a high-speed camera at 500 frames/sec at the maximum compliance condition with heart rate 72 bpm. The EOA is presented as the mean  $\pm$  95% confidence limits.

#### **8.5.1.3 Uniaxial Tensile Properties of the Heart Valve Root Leaflets**

The effect of cyclic loading on the material properties of the leaflets were characterised using uniaxial tensile testing methods in both circumferential and radial directions from each cellular porcine aortic heart valve root, following fatigue and pulsatile flow assessment. The detailed procedure for the uniaxial tensile testing is described in Chapter 2, Section 2.4.8.2.3.1.3. The tensile material parameters [elastin phase slope, collagen phase slope, failure strain and ultimate tensile stress (UTS)] were calculated from the stress-strain graphs. All the data is presented as the mean  $\pm$  95% confidence limits.

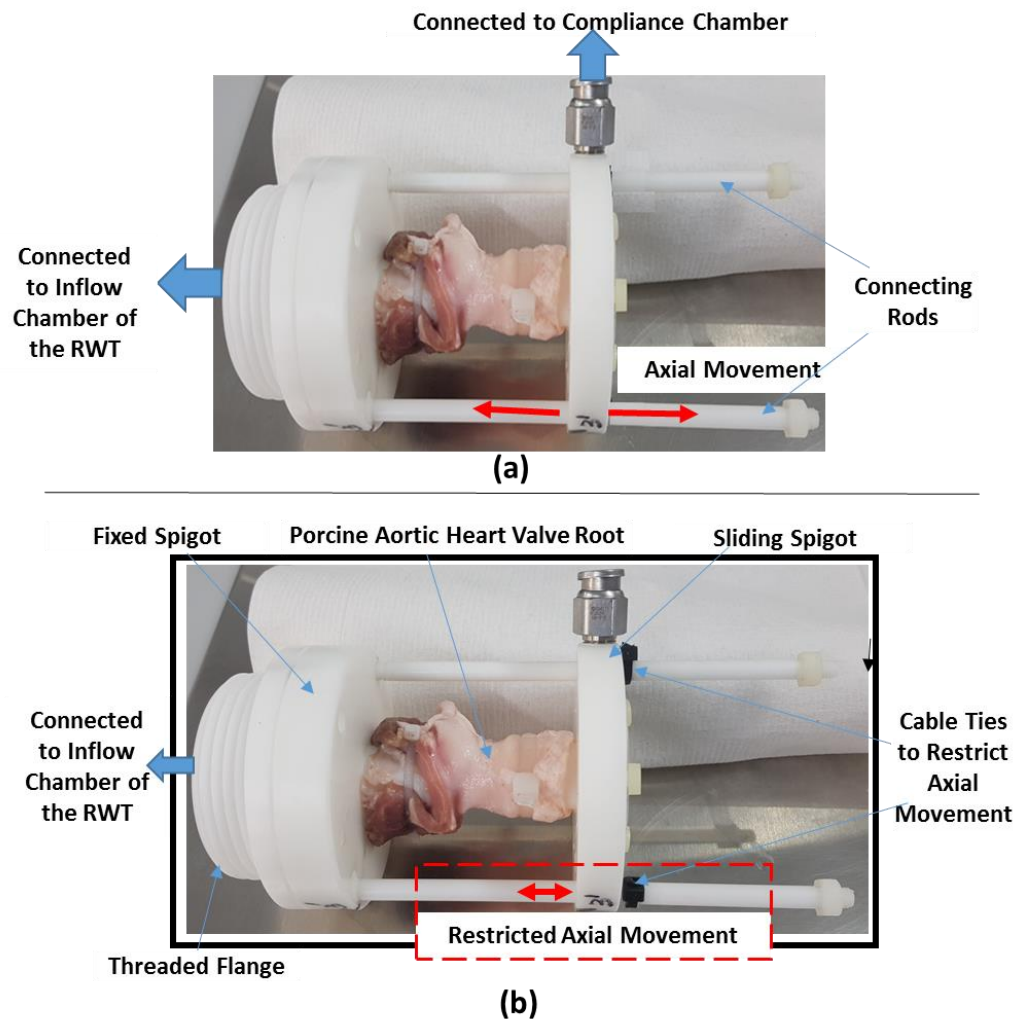
The leaflet from one of the cellular aortic heart valve roots was not tested in the radial direction for uniaxial tensile testing because two of the leaflets had deteriorated during the cyclic fatigue and pulsatile flow test. Hence only two radial and three circumferential cellular aortic leaflet specimens were used.

### **8.5.2 Methods used in Primary Study**

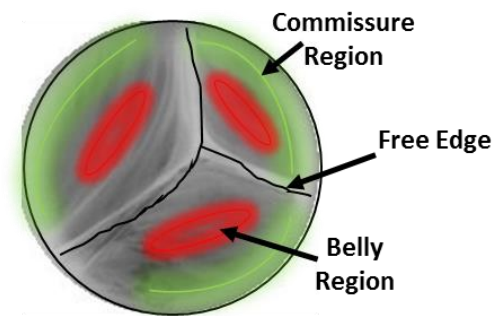
#### **8.5.2.1 Real Time Fatigue**

The real time fatigue of cellular and decellularised porcine aortic heart valve roots was investigated under physiological cyclic pressures and heart rate conditions

following the procedure described in the Section 8.5.1.1. The heart valve roots were tested in sets of 3. Following the results of the feasibility study, the axial movements of all the sliding spigots were restricted by mounting cable ties on the connecting rods for the heart valve root holders as shown in Figure 8.5 (b) to prevent detachment of the heart valve roots from the fixed spigot. The detailed test conditions are described in the Section 8.5.1.1.



**Figure 8.5 Heart Valve Root Mounting (a) with Free Axial Movement of the Sliding Spigot (used in the Feasibility Study) (b) and Restricted Axial Movement of the Sliding Spigot (used in the Primary Study) during the Fatigue Assessment in the RWT**

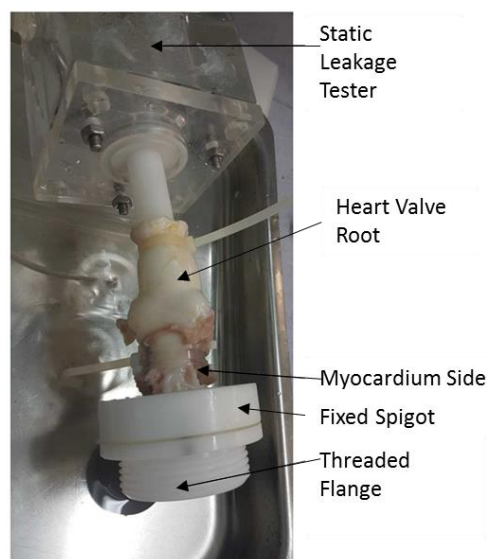


**Figure 8.6 Front View of Valve Closed Phase Showing Belly Region (red), Commissure Region (green) and Free Edge (black)**

The real time fatigue of the aortic cellular and decellularised heart valve root leaflets was assessed by high speed camera at 500 frames/sec imaging of the leaflet dynamics and through qualitative visual assessment at the end of testing in the RWT. Any leaflet damage was identified and reported with respect to three leaflet regions: near the commissures, at the free edge, and in the belly region (Figure 8.6).

#### **8.5.2.2 Hydrodynamic Performance I: Competency (Pre-test, Mid-test, Post-test)**

The competency of each cellular and decellularised porcine heart valve root was measured in terms of leakage flow rate by applying a static back pressure of 120 mmHg. The time taken for the test fluid to drop to 80 mmHg was recorded and leakage flow rate was calculated.



**Figure 8.7 Aortic Heart Valve Root Mounting during Mid-test and Post-test Competency Assessment (Top View)**

During pre-test competency assessment, the myocardium side of the heart valve root was unsupported as described in Chapter 2 Section 2.4.6.1.3. However, during the mid-test and post-test competency assessment, the myocardium of the heart valve root was kept attached to a fixed spigot with the threaded flange from the heart valve root holder for the RWT (Figure 8.7), due to concerns that the heart valve root would deteriorate if removed from the spigot. The wall side of the spigot (sliding) was detached to enable heart valve root attachment to the static leakage tester.

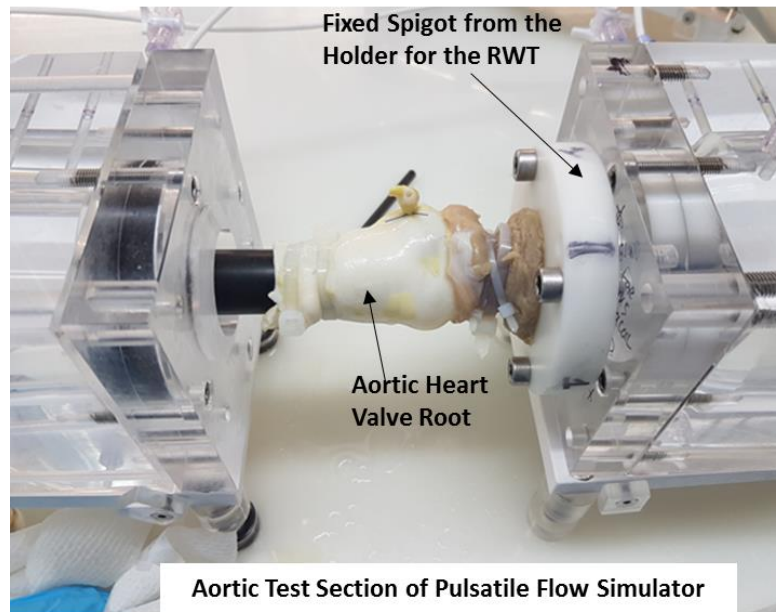
The detailed procedure for competency testing is described in Chapter 2 Section 2.4.6.1.3. The heart valve root was classified as competent if the pressure head had not dropped to 80 mmHg within a cut off time period of 30 min or leakage flow rate  $\leq 0.85 \text{ mL}\cdot\text{s}^{-1}$ .

### **8.5.2.3 Hydrodynamic Performance II: Pulsatile Flow (Post-test)**

Following real time fatigue and post-test competency assessment, more detailed examination of the cellular and decellularised aortic heart valve roots was conducted under pulsatile flow to assess hydrodynamic performance.

After completing post-test competency, the wall side of the heart valve root was detached from the static leakage tester. Before mounting the heart valve root in the pulsatile flow simulator, the threaded flange (Figure 8.7) was removed but the fixed spigot has kept attached. To enable mounting of the heart valve root with the fixed spigot, the pulsatile flow simulator and valve root holder for the RWT was modified (Figure 8.8).

All the heart valve roots were initially tested at minimum compliance in the pulsatile flow simulator with heart rate 60, 72, 80 and 100 bpm with corresponding stroke volumes 60, 70 and 80 ml to determine the peak flow conditions required for the testing at maximum compliance, which are detailed in Table 8.3. The detailed test procedure was described in Chapter 2 Section 2.4.7.4.



**Figure 8.8 Heart Valve Root Mounting with Fixed Spigot attached in the Pulsatile Flow Simulator**

The systemic pressure was held between 120 mmHg to 80 mmHg. The hydrodynamic parameters were evaluated as described in Section 8.5.1.2. The opening and closing of the valve was recorded with a high speed camera at 500 frames/sec at the maximum compliance condition with heart rate 72 bpm.

**Table 8.3 Test Conditions Used in the Pulsatile Flow Performance of Cellular and Decellularised Porcine Aortic Heart Valve Roots (Maximum Compliance Condition)**

Heart Rate (bpm)	Mean Peak Flow (mL.s <sup>-1</sup> )	
	Cellular Aortic Heart Valve Roots	Decellularised Aortic Heart Valve Roots
60	237	260
72	335	352
80	370	401
100	516	577

#### 8.5.2.4 Uniaxial Tensile Properties of the Leaflets (Post-Test)

Following pulsatile flow assessment, the uniaxial tensile properties of leaflets in the circumferential and radial directions from each cellular and decellularised porcine

aortic heart valve root were evaluated. The detailed procedure for uniaxial tensile testing is described in Chapter 2, Section 2.4.8.2.3. The tensile material parameters were calculated from the stress strain graphs.

The leaflets from two of the cellular aortic heart valve roots were not subject to uniaxial tensile testing because the leaflets were torn during the cyclic fatigue and pulsatile flow test and it was difficult to prepare an adequate size of specimen for the uniaxial tensile testing. Hence these samples were omitted and four cellular heart valve roots were used.

### **8.5.3 Statistical Analysis**

All the hydrodynamic and biomechanical performance data for the cellular and decellularised aortic heart valve roots are presented as the mean  $\pm$  95% confidence limits and statistical significance between the cellular and decellularised aortic heart valve roots performance was determined using Student's t-test. A significance level of  $p < 0.05$  was applied. Statistical analyses were performed using SPSS for Windows (version 21.0; SPSS, Inc., USA).

## **8.6 Results**

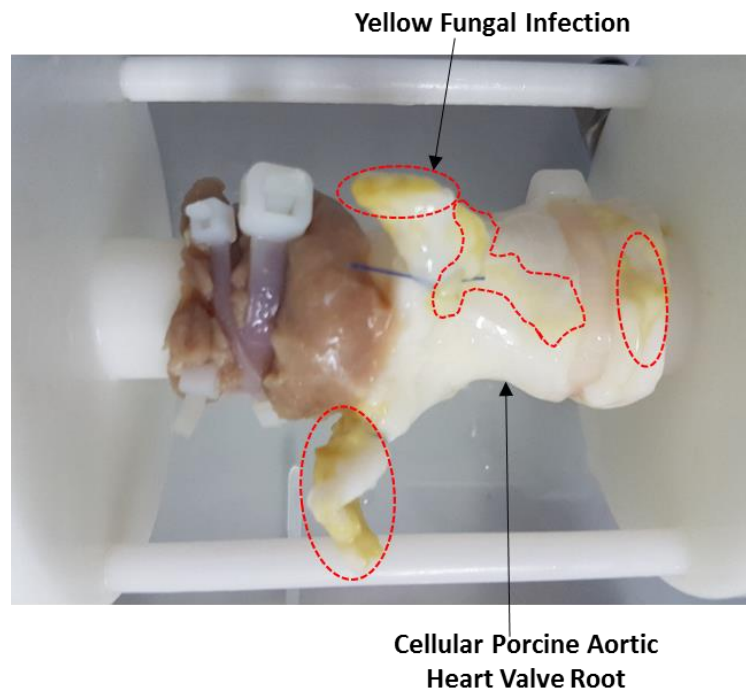
### **8.6.1 Feasibility Study**

#### **8.6.1.1 Real Time Fatigue**

The targeted transvalvular pressure difference (-100 mmHg) across the closed cellular aortic heart valve root was not maintained throughout the experiment due to two of the heart valve roots becoming detached from their spigots. The myocardial side of heart valve root A1 completely detached from the fixed spigot between 345,000 to 432,000 cycles. The RWT was stopped and heart valve root A1 was re-attached to the fixed spigot with cable ties and the fatigue testing continued. After 632,537 cycles, another heart valve root (A5) completely detached again from the myocardial side. Again the RWT was stopped and heart valve root A5 was re-attached and the fatigue testing continued. In both cases the heart valve roots became detached from the spigot between the hours of 5 pm and 9 am the next day, leading to failure in controlling the transvalvular pressure difference across the remaining attached heart valve roots. Due to time limitations, the fatigue assessment was

aborted at 823,053 cycles instead of the planned 1.2 million cycles. Hence, the initial attempt at running the fatigue test for 1.2 million cycles in the RWT with cellular porcine aortic heart valve roots was unsuccessful. At the end of this test, no sign of macroscopic damage was observed in the leaflets of any heart valve roots.

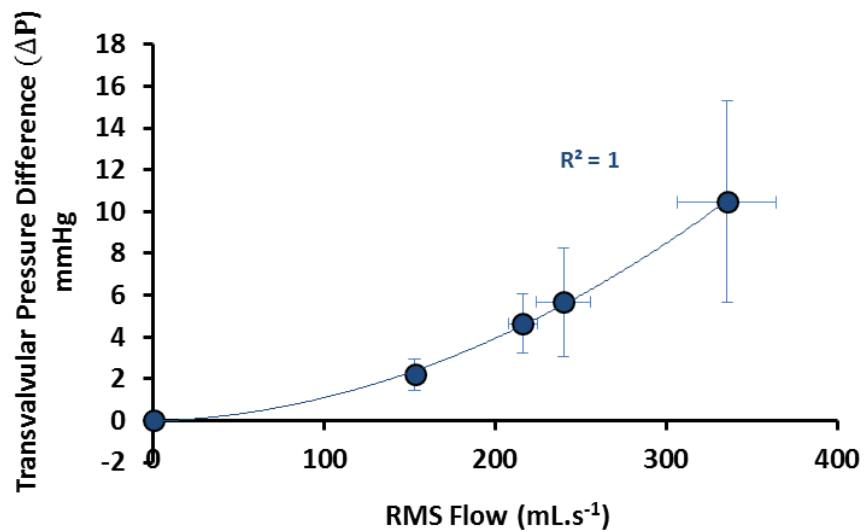
It was observed that within the first hour of fatigue assessment in the RWT the transparent test fluid became grayish in appearance. Also, as the heart valve roots were tested for a longer period of time in the RWT, a problem was identified where a yellow fungal infection (Figure 8.9) in the heart valve roots was observed after approximately 600,000 cycles.



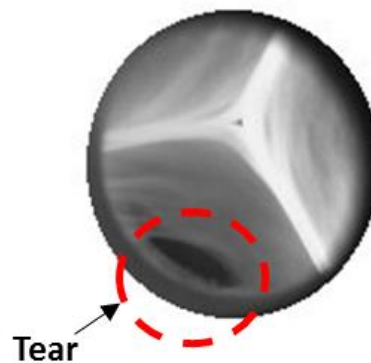
**Figure 8.9 Infected Cellular Porcine Aortic Heart Valve Root during Fatigue Testing in the RWT**

#### **8.6.1.2 Hydrodynamic Performance under Pulsatile Flow**

The mean transvalvular pressure difference versus mean RMS flows for cellular porcine aortic heart valve roots for the heart rates tested is shown in Figure 8.10.



**Figure 8.10 Mean Transvalvular Pressure Difference versus Mean RMS Flow for Cellular (n=3) Porcine Aortic Heart Valve Roots - Data fitted with second order polynomial trend line - The error bars indicate 95 % confidence limits**



**Figure 8.11 Leaflet Tear of the Cellular Porcine Aortic Heart Valve Root A5**

The mean EOA with 95% confidence limits for the cellular porcine aortic heart valve roots at 72 bpm was  $2 \pm 0.21 \text{ cm}^2$ . Complete opening and closing was observed for all the heart valve roots. A tear in the leaflet belly region was observed in one of the heart valve roots (A5; Figure 8.11).

### **8.6.1.3 Uniaxial Tensile Properties of the Cellular Aortic Leaflets**

The mean thickness and tensile parameters of the cellular and decellularised aortic heart valve root leaflets is given in Table 8.4.



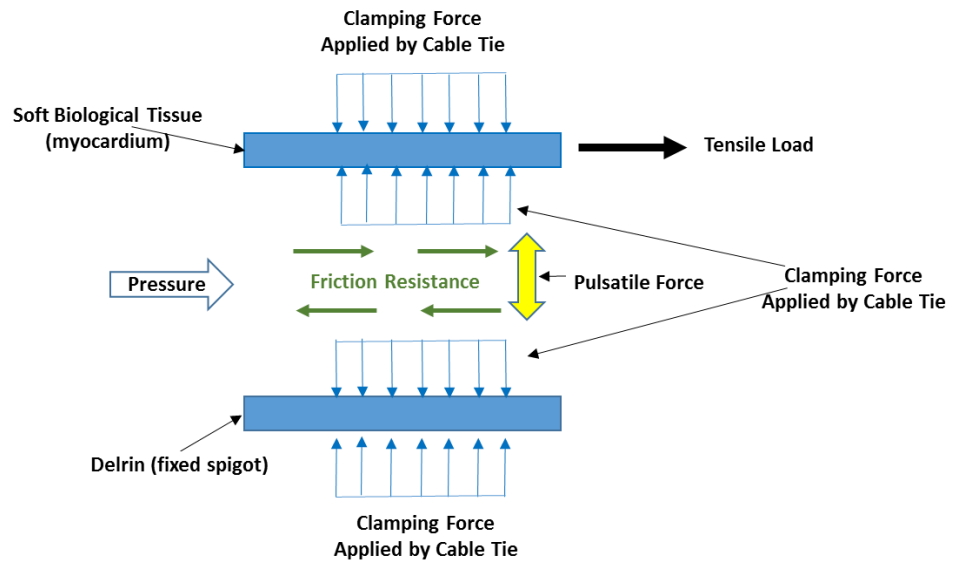
**Table 8.4 Mean Thickness and Mean Tensile Parameters (Collagen Phase Slope  $E_c$ , Elastin Phase Slope  $E_e$ , Ultimate Tensile Stress (UTS), Failure Strain  $\epsilon_f$ )  $\pm$  95 Confidence Limits for the Cellular Porcine Aortic Heart Valve Root Leaflet specimens**

	Radial	Circumferential
Number of Specimens	2	3
Thickness (mm)	$0.38 \pm 0.90$	$0.37 \pm 0.15$
Collagen Phase Slope $E_c$ (MPa)	$1.27 \pm 2.21$	$42.03 \pm 22.02$
Elastin Phase Slope $E_e$ (MPa)	$0.02 \pm 0.03$	$0.04 \pm 0.05$
UTS (MPa)	$0.49 \pm 0.10$	$9.09 \pm 1.42$
Failure Strain $\epsilon_f$	$0.57 \pm 0.27$	$1.03 \pm 0.23$

#### 8.6.1.4 Discussion

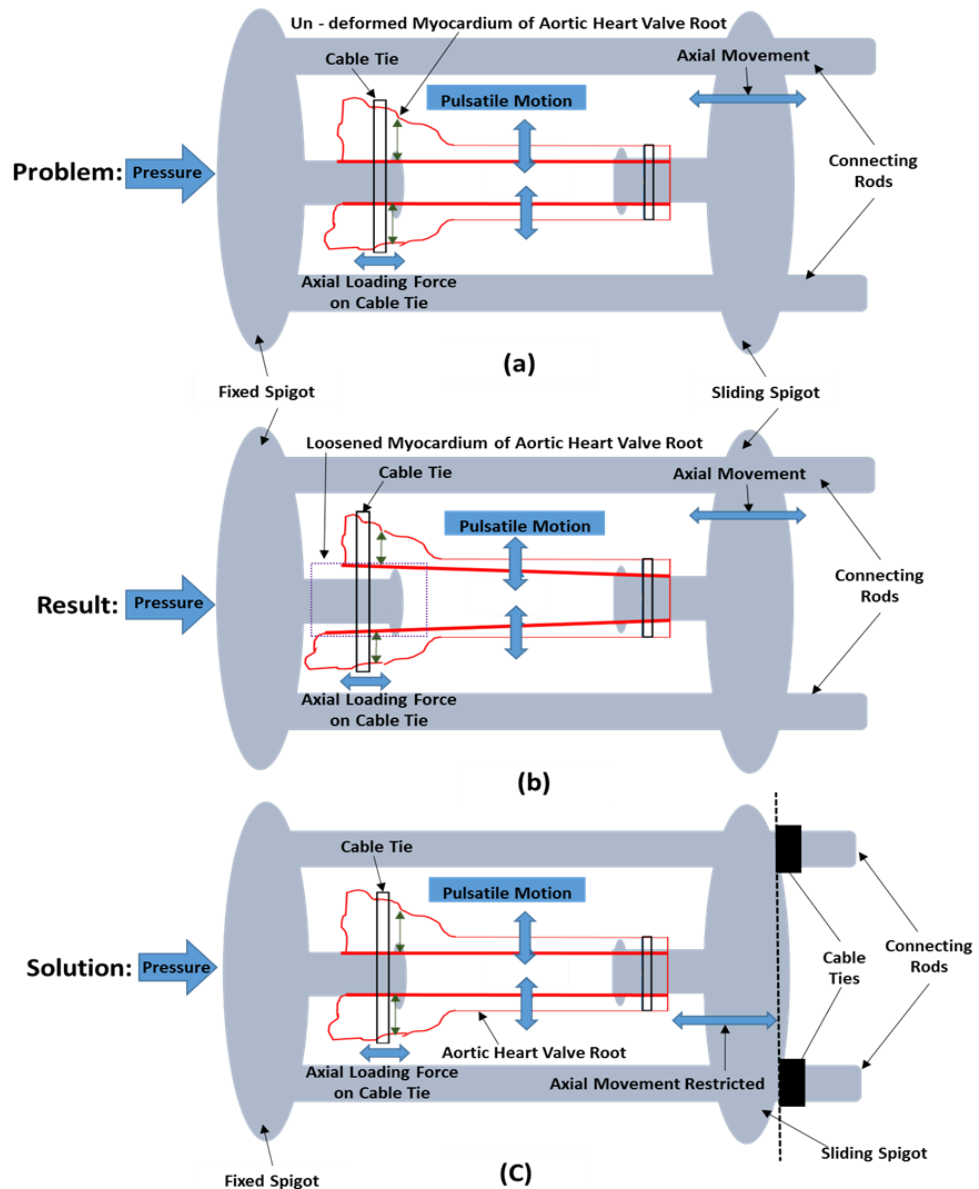
Based on the results and observations from the feasibility study with three cellular porcine aortic heart valve roots, the refinements described below were incorporated into the test plan and test conditions for the primary study.

- To minimise growth of any bacteria and/or fungi during the fatigue testing in the RWT, the cellular heart valve roots were treated with 150 ml Cambridge antibiotic and amphotericin B solution as described in Chapter 2 Section 2.4.3 and 0.04 % sodium azide was added in the test solution (saline) to retard bacterial growth.
- During the fatigue assessment in the RWT, detachment of the heart valve roots on the myocardial side from the fixed spigot was seen twice in two different heart valve roots. Loosening of the heart valve root was attributed to myocardium thinning due to deterioration and simultaneous dynamic pulsatile motion of the wall when dynamically pressurised in the axial direction with respect to the heart valve root clamping [Figure 8.13(b)].



**Figure 8.12 Free Body Diagram of the Clamping of Myocardium of the Heart Valve Root on the Fixed Spigot**

The free body diagram of the myocardium clamping on the fixed spigot is shown in Figure 8.12. When the heart valve root was dynamically pressurised, the heart valve root was under axial tensile load, the tendency of the two surfaces [soft biological tissue (myocardium) and delrin (fixed spigot)] to slip against one another is resisted by the friction between these surfaces. The frictional resistance is equal to the coefficient of friction multiplied by the clamping force between the myocardium and the fixed spigot. After a few days of cyclic testing in the RWT, the heart valve root started to deteriorate which softens and thins the myocardium. Due to myocardium deterioration, the frictional resistance between the two surface decreased and hence the tensile load was exceeded the frictional resistance which made the clamping loose [Figure 8.13 (b)]



**Figure 8.13 Cellular Aortic Heart Valve Roots Mounting (a) Before Fatigue Assessment in the RWT showing Un-deformed Myocardium (b) During Fatigue Assessment in the RWT showing Loosened Myocardium (c) with Restricted Axial Movement of the Sliding Spigot**

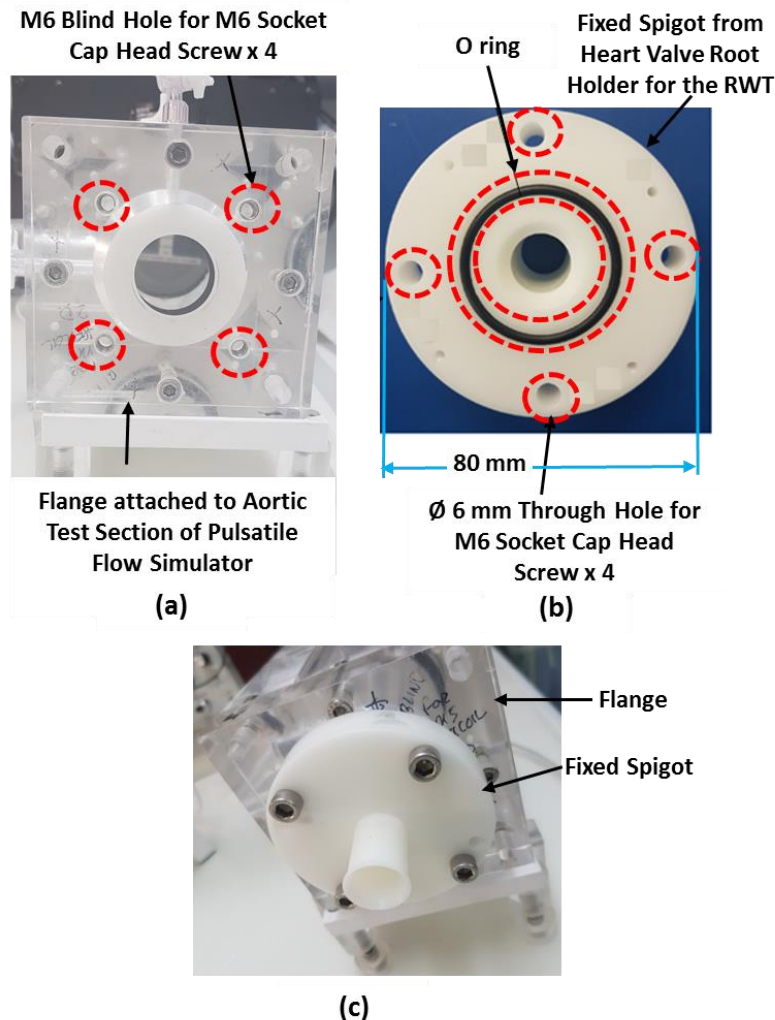
- The test condition was refined, comprising of the restriction of axial movement of the sliding spigot and hence axial movement of the heart valve root during fatigue assessment in the RWT [Figure 8.13 (c)]. A cable tie was tied around the connecting rods and near to the sliding spigot as shown in Figure 8.13 (c), keeping the heart valve root uncompressed. Under the dynamic pressure, part of the tensile load experienced by the heart valve roots was equilibrated by restriction of axial movement of the sliding spigot.

- Fatigue assessment of the heart valve roots was mostly based on the visual inspection or image analysis of high speed videos of the leaflets following RWT cycling. For a quantitative assessment of the heart valve roots performance, the heart valve roots were tested under pulsatile flow conditions, following fatigue assessment. However, due to the complexity, length of the pulsatile flow test and concerns around mounting of the heart valve root in the pulsatile flow simulator, the pulsatile flow performance of the heart valve roots was not evaluated before their fatigue assessment in the RWT and hence it was difficult to clarify whether the fatigue of the heart valve roots directly affected hydrodynamic performance. Therefore, a competency assessment was added to the experimental design at several intervals (pre-test, mid-test, post-test). This also eliminated sample to sample variability.
- A leaflet tear was seen during the pulsatile flow assessment in one of the heart valve roots. The leaflet may have torn due to the application of over pressure during dismantling of the heart valve root from the RWT holder and subsequent mounting of the heart valve root back in the pulsatile flow simulator. Hence, it was decided to keep the myocardium side of the heart valve root attached to the fixed spigot and instead separate the aorta side from the sliding spigot after completing the RWT fatigue assessment.

To enable mounting of the heart valve root still attached to the fixed spigot in the pulsatile flow simulator for further assessment, the fixed spigot and flange for the pulsatile flow simulator were modified. The following modification was involved:

1. The fixed spigot of the RWT was 80 mm in diameter compared to the 40 mm diameter spigot of the pulsatile flow simulator. Therefore to mount the fixed spigot with the heart valve root attached in the pulsatile flow simulator, it was required to modify the mounting flange of the pulsatile flow simulator. Consequently, four equally spaced 6 mm diameter blind holes for M6 socket cap head screw were produced in the flange for the aortic section of the pulsatile flow simulator [Figure 8.14 (a)] to mount the fixed spigot, with the heart valve root attached from the RWT.

2. Four equally spaced through holes were drilled in the fixed spigot to enable its mounting in the pulsatile flow simulator. Also to make the assembly water tight an 'O' ring with an internal diameter of 36 mm was fitted on the back of the fixed spigot [Figure 8.14 (b)].



**Figure 8.14 Modification in the (a) Flange for the Aortic Test Section of the Pulsatile Flow Simulator (Front View) (b) Fixed Spigot from the Heart Valve Root Holder for the RWT (Back View) (C) Mounting of the Fixed Spigot on the Flange (Front View)**

## 8.6.2 Primary Study

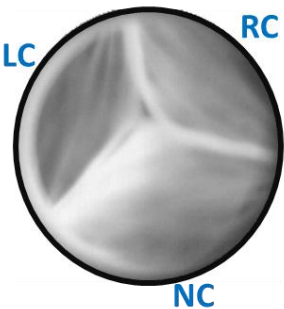
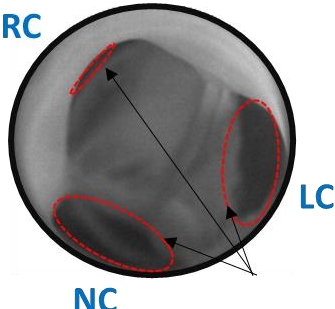
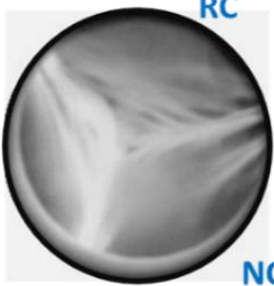
### 8.6.2.1 Real Time Fatigue of Cellular and Decellularised Porcine Aortic Heart

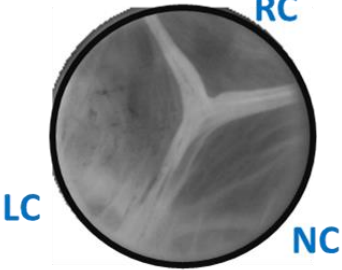
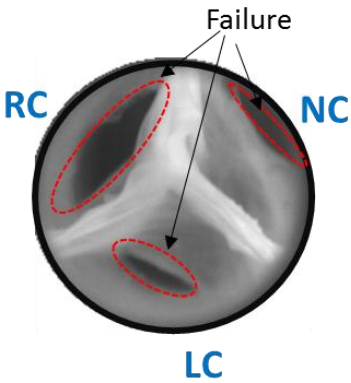
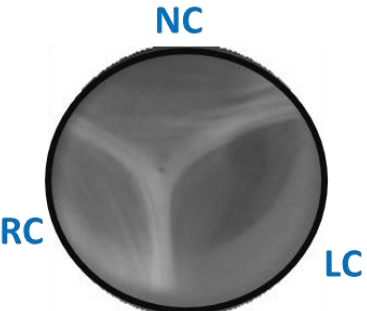
#### Valve Roots

The targeted transvalvular pressure difference (-100 mmHg) across the closed heart valve root was maintained throughout the fatigue testing in the RWT. Once the

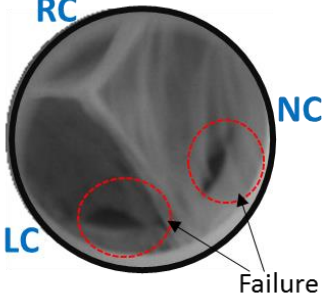
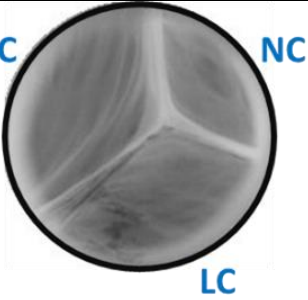
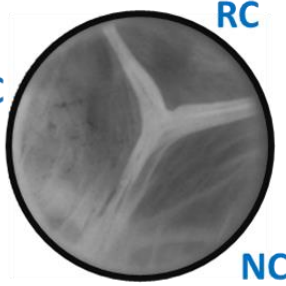
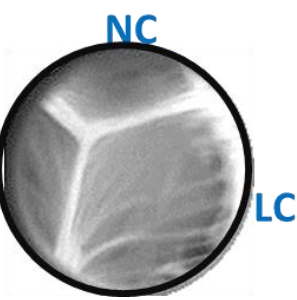
target number of cycles was reached all the heart valve root holders were removed from the RWT with the heart valve roots still attached and visually examined. There was no sign of detachment of the heart valve roots from the spigots. A small amount of yellow staining on the cellular heart valve root walls was observed. Detailed high speed video examination of all the cellular and decellularised porcine aortic heart valve roots at a maximum of 1.2 million cycles are listed in Table 8.5 and Table 8.6 respectively along with the image of each heart valve root in the fully closed phase, captured with a high speed camera.

**Table 8.5 Valve Fully Closed Images (where LC: left coronary leaflet, RC: right coronary leaflet and NC: non-coronary leaflet) and Visual Examinations of the Cellular Porcine Aortic Heart Valve Roots at Maximum 1.2 Million cycles**

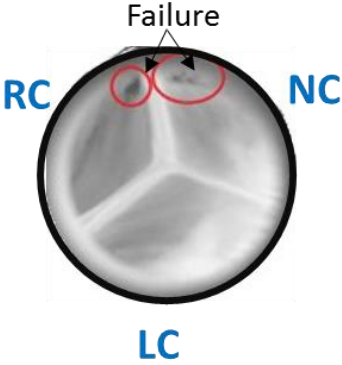
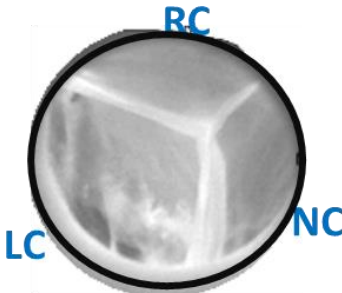
Cellular Porcine Aortic Heart Valve Roots		
Valve ID Number	Valve Fully Closed	Heart Valve Root Visual Examinations
AC1		All leaflets of this heart valve root remained intact with no sign of macroscopic damage.
AC2		All the leaflets of this heart valve root showed signs of macroscopic damage after 889,669 cycles. All leaflets had tear near to leaflet attachment area, although it is not clearly visible for the right coronary leaflet in the image.
AC3		All leaflets of this heart valve root remained intact with no sign of macroscopic damage.

Cellular Porcine Aortic Heart Valve Roots		
Valve ID Number	Valve Fully Closed	Heart Valve Root Visual Examinations
AC4		All leaflets of this heart valve root remained intact with no sign of macroscopic damage.
AC5		All the leaflets of this heart valve root showed signs of macroscopic damage. The right coronary leaflet contained a large tear in the belly region. The non-coronary and left coronary leaflet contained a tear in each near to the leaflet attachment area. The tear in the non-coronary leaflet appeared at approximately 1 million cycles whereas the tears in the other two leaflets were observed at approximately 1.2 million cycles.
AC6		All leaflets of this heart valve root remained intact with no sign of macroscopic damage.

**Table 8.6 Valve Fully Closed Images (where LC: left coronary leaflet, RC: right coronary leaflet and NC: non-coronary leaflet) and Visual Examinations of the Decellularised Porcine Aortic Heart Valve Roots at Maximum 1.2 Million cycles**

Decellularised Porcine Aortic Heart Valve Roots		
Valve ID Number	Valve Fully Closed	Heart Valve Root Examination
AD1		Two leaflets of this heart valve root showed signs of macroscopic damage after 864,712 cycles. The non-coronary and left coronary leaflets contained a tear in each leaflet. These tears were situated near the free edge and in both cases adjacent to the leaflet attachment area.
AD2		
AD3		All leaflets of these heart valve roots remained intact with no sign of macroscopic damage.
AD4		



Decellularised Porcine Aortic Heart Valve Roots		
Valve ID Number	Valve Fully Closed	Heart Valve Root Examination
AD5		Signs of leaflet damage were observed after 861,151 cycles. Two of the leaflets (non-coronary and left coronary) contained a tear in each leaflet. These tears were situated near the free edge and in both cases adjacent to the commissure of the leaflet.
AD6		All leaflets of this heart valve root remained intact with no sign of macroscopic damage.

### 8.6.2.2 Hydrodynamic Performance of Cellular and Decellularised Porcine Aortic Heart Valve Roots

#### 8.6.2.2.1 Hydrodynamic Performance I: Competency

The pre, mid and post-test mean leakage flow rates for the cellular and decellularised aortic heart valve roots are shown in Table 8.7.

All the cellular aortic heart valve roots were fully competent prior to fatigue testing, with mean leakage flow rates of less than  $0.85 \text{ mL}\cdot\text{s}^{-1}$ . The majority of the cellular aortic heart valve roots were competent during the mid-test competency assessment, except cellular heart valve root AC6 (mean leakage flow rate  $16.67 \text{ mL}\cdot\text{s}^{-1}$ ). However, the post-test competency assessment showed that the majority of the cellular aortic heart valve roots were regurgitant. The post-test competency of the cellular aortic heart valve roots AC3 and AC5 could not be measured as the valves were leaking faster than the static pressure applied.

**Table 8.7 Pre, Mid and Post- Test Mean Leakage Flow Rates ( $F_L$ ) of Each Cellular and Decellularised Porcine Aortic Heart Valve Roots**

Cellular Aortic Heart Valve Roots				Decellularised Aortic Heart Valve Roots			
Valve ID Number	Leakage Flow Rate ( $\text{mL}\cdot\text{s}^{-1}$ )			Valve ID Number	Leakage Flow Rate ( $\text{mL}\cdot\text{s}^{-1}$ )		
	Pre- test	Mid- test	Post- test		Pre- test	Mid- test	Post- test
<b>AC1</b>	<0.85	<0.85	4.36	<b>AD1</b>	2.05	xxx	xxx
<b>AC2</b>	<0.85	<0.85	1.53	<b>AD2</b>	0.88	0.99	<0.85
<b>AC3</b>	<0.85	<0.85	xxx	<b>AD3</b>	1.61	4.73	6.02
<b>AC4</b>	<0.85	<0.85	1.19	<b>AD4</b>	<0.85	<0.85	<0.85
<b>AC5</b>	<0.85	<0.85	xxx	<b>AD5</b>	2.24	21.31	1.23
<b>AC6</b>	<0.85	16.67	9.96	<b>AD6</b>	1.64	1.23	1.66

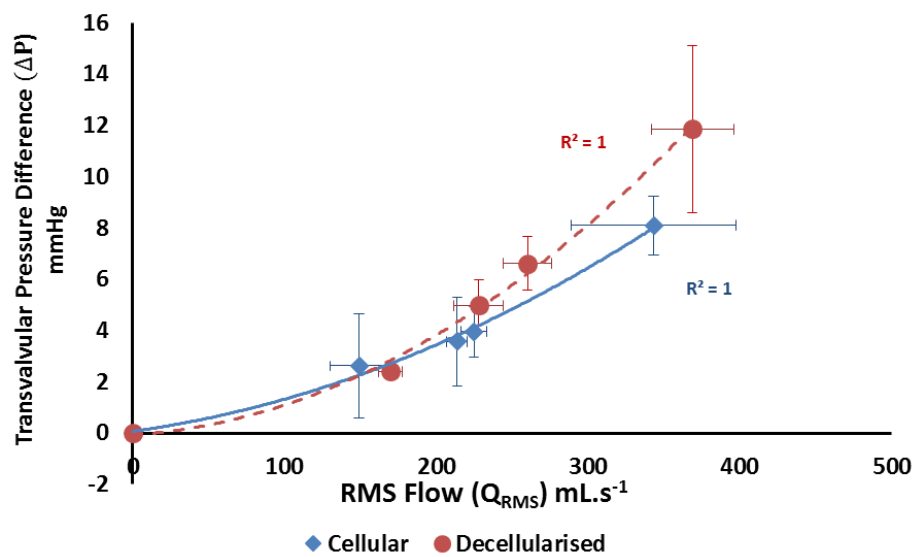
xxx - not measured

The majority of decellularised aortic heart valve roots were regurgitant (with mean leakage flow rate  $> 0.88 \text{ mL}\cdot\text{s}^{-1}$ ) during pre and mid - test competency assessment. The decellularised heart valve root AD5 had the highest mean leakage flow rate  $21.31 \text{ mL}\cdot\text{s}^{-1}$  during the mid-test competency assessment, however, this was reduced to  $1.23 \text{ mL}\cdot\text{s}^{-1}$  during the post-test competency assessment. It was not possible to measure the mid-test and the post-test leakage flow rates for the decellularised aortic heart valve root AD1 as the valve was leaking faster than the static pressure applied. Four out of the six decellularised aortic heart valve roots were regurgitant during post-test competency assessment.

#### **8.6.2.2.2 Hydrodynamic Performance II: Pulsatile Flow**

The mean transvalvular pressure difference versus mean RMS flow for the cellular and decellularised porcine aortic heart valve roots under the tested heart rates is shown in Figure 8.15.

The pulsatile flow performance of the cellular porcine aortic heart valve roots AC2 and AC5 could not be determined as all the leaflets were too damaged for testing to be completed.



**Figure 8.15 Mean Transvalvular Pressure Difference versus Mean RMS Flow for Cellular (n=4) and Decellularised (n=6) Porcine Aortic Heart Valve Roots - Data fitted with second order polynomial trend line - The error bars indicate 95 % confidence limits**

The pulsatile flow performance of the cellular porcine aortic heart valve roots AC1 and AC6 could not be determined at the heart rate of 100 bpm as the myocardium side of the heart valve root detached from the spigot when this condition was applied.

The EOA averaged over the four heart rate conditions for all the cellular and decellularised porcine aortic heart valve roots is shown in Table 8.8.

**Table 8.8 Effective Orifice Area for Each Cellular and Decellularised Porcine Aortic Heart Valve Root Averaged over 4 Heart Rate conditions**

Cellular Aortic Heart Valve Roots		Decellularised Aortic Heart Valve Roots	
Valve ID Number	Effective Orifice Area (EOA) cm <sup>2</sup>	Valve ID Number	Effective Orifice Area (EOA) cm <sup>2</sup>
AC1	1.88	AD1	1.88
AC2	xxx	AD2	2.10
AC3	1.88	AD3	2.16
AC4	2.22	AD4	2.11
AC5	xxx	AD5	1.91
AC6	2.68	AD6	2.18

xxx – not measured

The mean EOA for the decellularised porcine aortic valve heart valve roots ( $2.06 \pm 0.11 \text{ cm}^2$ ) was not significantly different to the cellular porcine aortic heart valve roots ( $2.23 \pm 0.21 \text{ cm}^2$ ) ( $P=0.08$ , Student's t-test).

Fully opened and fully closed Images of all the tested porcine cellular and decellularised aortic heart valve roots are shown in Figure 8.16 and Figure 8.17 respectively.

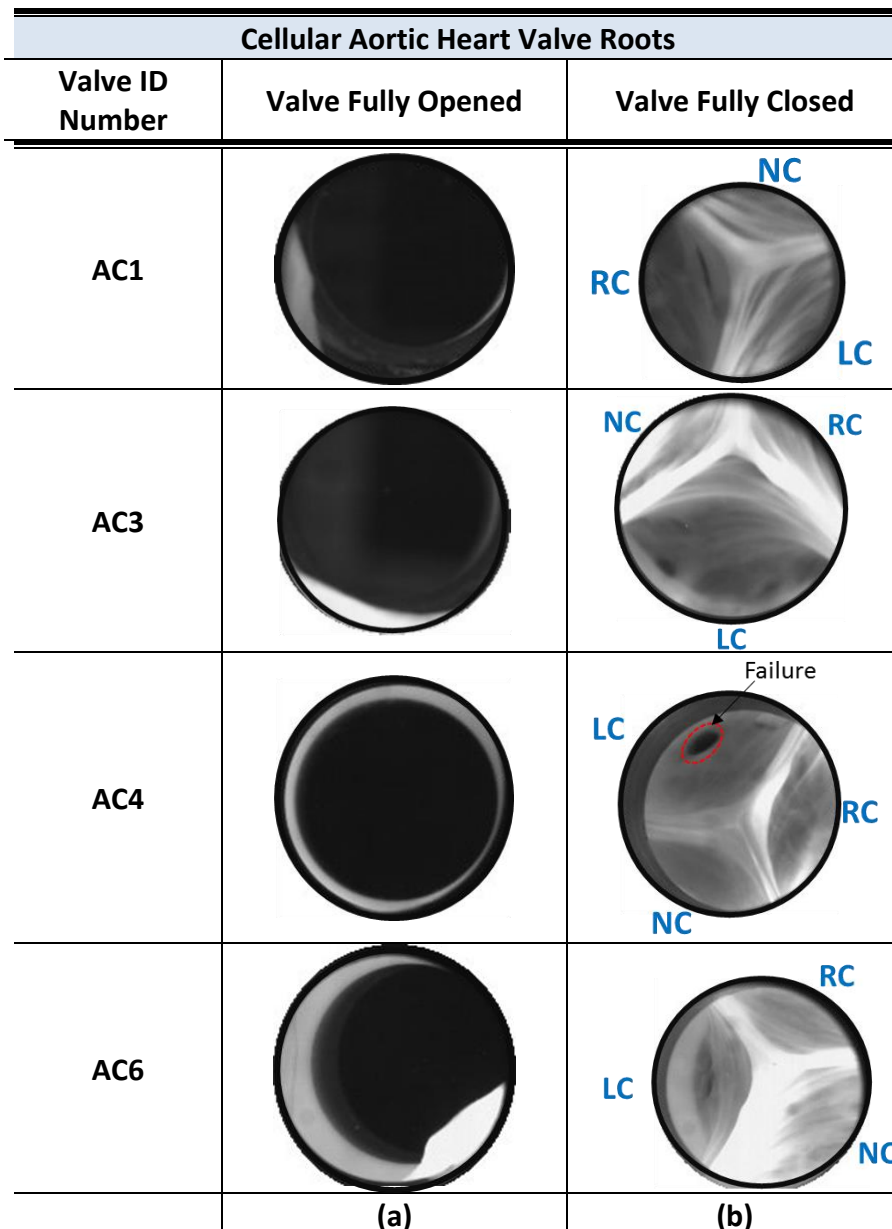


Figure 8.16 (a) Valve Fully Opened and (b) Valve Fully Closed Images of Cellular Porcine Aortic Heart Valve Roots at Heart Rate 72 bpm, captured from the Front View by a High-Speed Camera with a Leaflet Tear in AC4 Highlighted


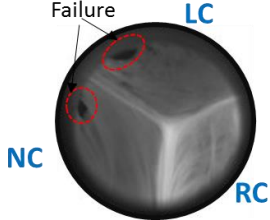

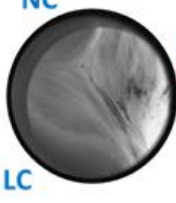

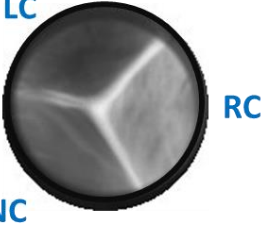

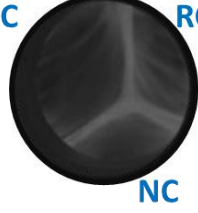

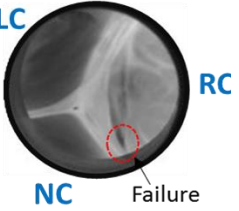

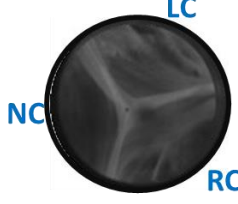
Decellularised Aortic Heart Valve Roots		
Valve ID Number	Valve Fully Opened	Valve Fully Closed
AD1		
AD2		
AD3		
AD4		
AD5		
AD6		
	(a)	(b)

Figure 8.17 (a) Valve Fully Opened and (b) Valve Fully Closed Images of Decellularised Porcine Aortic Heart Valve Roots at Heart Rate 72 bpm, captured from the Front View by a High-Speed Camera with a Leaflet Tears Highlighted in AD1 and AD5

The majority of the cellular porcine aortic heart valve roots showed synchronous leaflet opening and closing characteristics. The fully open leaflet configuration was circular in shape [Figure 8.16(a)]. The non-coronary leaflet in cellular heart valve root AC6 did not open completely. During the closing phase, all the valves were observed to close completely with no visible leakage orifice [Figure 8.16 (b)]. A large tear was detected near the leaflet attachment area of the left coronary leaflet of the cellular heart valve root AC4 which was not seen in the post-test fatigue assessment in the RWT.

The majority of the decellularised porcine aortic heart valve roots showed synchronous leaflet opening and closing characteristics. The right coronary leaflet in decellularised heart valve root AD5 did not open completely [Figure 8.17(a)]. The decellularised heart valve roots AD1, AD2, AD3 and AD4 showed excellent closed leaflet configuration, with perfect coaption at the free edge of the leaflets [Figure 8.17(b)]. However, the decellularised aortic heart valve root AD5 and AD6 had minor central leakage orifices. The majority of the cellular and decellularised aortic heart valve roots had a fully opened leaflet configuration, except cellular heart valve root AC6 and decellularised heart valve root AD5.

### 8.6.2.3 Uniaxial Tensile Properties of the Cellular and Decellularised Aortic Leaflets

The mean thickness  $\pm$  95 % confidence limits and mean tensile parameters with  $\pm$  95 % confidence limits for the cellular and decellularised porcine aortic heart valve root leaflet specimens are shown in Table 8.9 and Table 8.10 respectively.

**Table 8.9 Mean Thickness  $\pm$  95 % confidence limits for the Cellular and Decellularised Porcine Aortic Heart Valve Root Leaflet Radial and Circumferential specimens – p (<0.05) value shows significant difference between cellular and decellularised aortic heart valve roots**

	Specimen Direction	Average Thickness (mm)		p Value
		Cellular	Decellularised	
Number of Specimens		4	6	
Aortic Heart Valve Root Leaflet	Radial	0.57 $\pm$ 0.23	0.28 $\pm$ 0.05	0.002
	Circumferential	0.74 $\pm$ 0.26	0.32 $\pm$ 0.06	0.01

Student's t-test showed significant difference in thickness of the cellular and decellularised leaflet specimens in the radial ( $p=0.002$ ) and circumferential ( $p=0.01$ ) directions.

The initial linear region of the stress-strain curve was used to derive the elastin phase modulus and it was not distinct for one decellularised radial and one decellularised circumferential leaflet specimen. Hence these samples were omitted and five decellularised samples were used for the mean elastin phase slope calculation.

The tensile leaflet parameters (collagen phase slope, elastin phase slope, UTS and failure strain) for the decellularised aortic heart valve roots were significantly different to the cellular aortic heart valve roots in the circumferential direction ( $p<0.05$ , Student's t-test). However, in the radial direction, all the leaflet tensile parameters for the decellularised aortic heart valve roots were similar to the cellular aortic heart valve roots ( $p>0.05$ , Student's t-test).

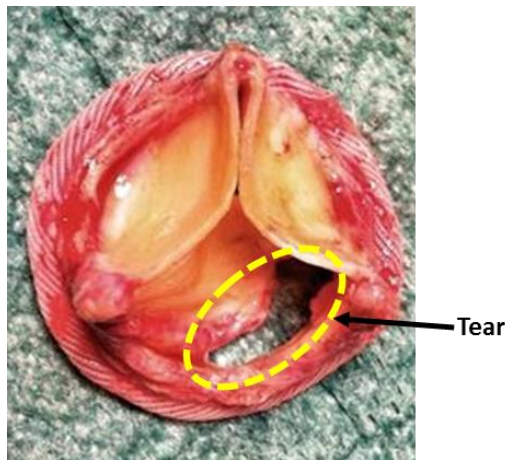
**Table 8.10 Tensile Parameters (Collagen Phase Slope  $E_c$ , Elastin Phase Slope  $E_e$ , Ultimate Tensile Stress  $\sigma_{UTS}$ , Failure Strain  $\epsilon_{failure}$ )  $\pm$  95 % Confidence Limits for Cellular and Decellularised Radial (R) and Circumferential (C) Aortic Leaflet Specimens and Number of Test Specimens (N) \*-Statistical significant difference ( $p<0.05$ ) for decellularised versus cellular aortic heart valve roots.**

Porcine Aortic Heart Valve Roots					
Tensile Parameters for Leaflets	Cellular		Decellularised		p value
	N		N		
<b>Radial</b>					
$E_c$ (MPa)	4	$0.93 \pm 0.98$	6	$2.47 \pm 1.60$	0.10
$E_e$ (MPa)	4	$0.02 \pm 0.01$	5	$0.03 \pm 0.01$	0.07
$\sigma_{UTS}$ (MPa)	4	$0.46 \pm 0.36$	6	$1.06 \pm 0.68$	0.11
$\epsilon_{failure}$	4	$1.03 \pm 0.38$	6	$1.04 \pm 0.17$	0.92
<b>Circumferential</b>					
$E_c$ (MPa)	4	$8.59 \pm 7.92$	6	$53.44 \pm 8.99^*$	0.00001
$E_e$ (MPa)	4	$0.02 \pm 0.01$	5	$0.31 \pm 0.25^*$	0.02
$\sigma_{UTS}$ (MPa)	4	$2.48 \pm 0.66$	6	$9.31 \pm 1.64^*$	0.00003
$\epsilon_{failure}$	4	$0.60 \pm 0.25$	6	$0.27 \pm 0.07^*$	0.002

### 8.6.3 Discussion

The function of the decellularised porcine aortic heart valve roots was similar to the function of cellular porcine aortic heart valve roots throughout the cyclic

testing in the RWT. No detachment of the cellular or decellularised heart valve roots from any of the spigots was detected, indicating that the restriction of axial movement was appropriate. The aorta of the cellular and decellularised heart valve roots maintained its integrity under cyclic pressures in the RWT for 1.2 million cycles. The high speed video analysis showed that the regions of leaflet failures in the cellular porcine aortic heart valve roots were near the commissure and belly region, whereas in the decellularised porcine aortic heart valve roots the leaflet failures were near the commissure region only. It was also observed that in the cellular heart valve roots the leaflet damage progressed towards the free edge and resulted in a large tear compared to the decellularised heart valve roots. Interestingly the regions of leaflets failure observed in both cellular and decellularised were consistent with *in vivo* (Ishihara et al., 1981, Hilbert et al., 1992, Wells and Sacks, 2002, Piñón et al., 2015) and *in vitro* accelerated (Sacks and Smith, 1998, Smith et al., 1999) fatigue induced leaflet tears seen in bioprosthetic porcine heart valves.

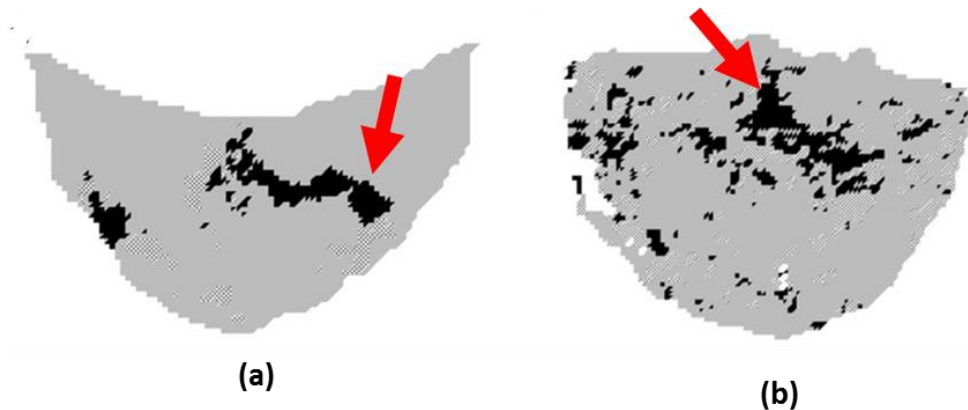


**Figure 8.18 Tear in Explanted Bovine Pericardial Trifecta Heart Valve (Piñón et al., 2015)**

A study by Piñón et al. (2015) showed that a glutaraldehyde treated bovine pericardial Trifecta heart valve (21-mm, St Jude Medical, Inc) had failed in 71-year old female after 3 years of implantation in the aortic position due to a large tear in the non-coronary leaflet as shown in Figure 8.18. However, the Trifecta valve did not show any sign of fatigue at 200 million cycles (equivalent of 5 years) in accelerated wear testing.



The *in vitro* accelerated fatigue and *in vivo* studies reported by Sacks and colleagues (Sacks and Smith, 1998, Sacks and Schoen, 2002) indicated significant changes in porcine bioprosthetic heart valves collagen fiber architecture due to shearing of the fibers. These studies also showed similarity in tissue damage location in the bioprosthetic heart valve leaflet between *in vitro* Figure 8.19 (a) and *in vivo* Figure 8.19 (b) studies.



**Figure 8.19 The Structural Damage (indicated with arrow) in Porcine Bioprosthetic Heart Valve leaflet (a) Subjected to *in vitro* Accelerated Fatigue (b) Explanted from Patient**

Leaflet tear was the main cause of early structural valve deterioration in pericardial bioprosthetic heart valves. The Ionescu-Shiley bovine pericardial valve (Shiley, Inc, Irvine, CA, USA) and the Hancock pericardial xenograft valve (Medtronic, Minneapolis, MN) failed *in vivo* and the causes were early leaflet wear and tear near the commissural regions where the leaflets were sewn to the supporting frame (Ishihara et al., 1981, Hilbert et al., 1992). The “wear and tear” phenomenon leading to valve failure has been reported in another study by (Mohammadi et al., 2006). The freestyle stentless bioprosthetic aortic heart valve roots were explanted in 10 patients after  $10.9 \pm 3.9$  years of implantation due to leaflet tears, located at the leaflet base ( $n = 4$ ) or in the vicinity of the commissure region of leaflets ( $n = 6$ ) (Mohammadi et al., 2006).

All these studies highlight the importance of mechanical stress as one of the main instigators of valve deterioration. In particular, the frequent bending and shear stress in the leaflets during valve opening and closing were thought to be responsible for the development of tears in the bioprosthetic heart valves (Ishihara et al., 1981).

In this study the leaflet structural deterioration was likely due to either leaflet impingement with the heart valve root mounting spigot or to fatigue induced deterioration. In addition, the lack of physiological dilation of the aorta may be an additional cause of the failures in the leaflet belly due to excessive flexion. The *in vitro* RWT setup accelerated cellular death (necrosis) within a few hours of testing in the cellular aortic heart valve roots due to (toxic) sodium azide in the test solution [0.9 % (w/v) saline with 0.04% sodium azide (v/v)] and the lack of oxygen supply (hypoxia); therefore, only the matrix material was tested in the RWT. Necrosis is appended by the release of enzymes (proteinases and matrix metalloproteinases), that are stored by lysosomes, which are capable of digesting cell components or the entire cell itself (Merrick, 2002). Excessive amounts of these enzymes could damage extracellular matrix proteins (collagen) surrounding the cells which form a highly organised fibrous structure in the cellular heart valve root leaflets. In addition, cell membranes in cellular heart valve roots may have been damaged soon after harvesting due to handling and processing (Kitagawa et al., 2001). Hence the tears in the cellular heart valve root leaflets after fatigue testing in the RWT may have been the result of cell necrosis. The decellularised porcine aortic roots tested in the RWT were devoid of cells and exhibited similar fatigue damage (tears in the leaflets). This might be expected since neither type of porcine aortic heart valve root (cellular and decellularised) had any living cells present to help "repair" the damaged collagen that would occur under normal conditions *in vivo* in the heart. Once the decellularised heart valve root is implanted into the human body for use as a replacement heart valve, it is believed that leaflet fatigue will not be permanent due to leaflet regeneration and repair. *In vivo*, it is anticipated based on evidence from a study (Paniagua Gutierrez et al., 2015) on decellularised porcine aortic valve roots implanted in sheep that host cells will populate the leaflets and remodel the matrix.

All six cellular aortic heart valve roots were competent (leakage rate  $<0.85 \text{ mL}\cdot\text{s}^{-1}$ ) before the fatigue testing. After these heart valve roots were cycled for 680,000 to 880,000 cycles in the RWT, the competency (mid-test) of one of the cellular heart valve roots (AC6) was altered. Cellular heart valve root AC6 demonstrated severe regurgitation with a leakage rate of  $16.67 \text{ mL}\cdot\text{s}^{-1}$  whilst the

remaining five heart valve roots were competent having a leakage rate  $<0.85 \text{ mL}\cdot\text{s}^{-1}$ . After 1.2 million cycles of cyclic testing in the RWT, all the cellular aortic heart valve roots were regurgitant and the mean leakage flow rate was  $4.26 \text{ mL}\cdot\text{s}^{-1}$  for four of the heart valve roots whilst two of the heart valve roots leaked faster than the static pressure applied. It was not possible to apply static pressure on these two cellular heart valve roots because the leaflets had deteriorated following cyclic loading in the RWT. A similar phenomenon was observed with the decellularised heart valve roots. During pre-test and mid-test competency assessment five out of six decellularised heart valve roots were not considered competent (having a leakage flow rate  $> 0.85 \text{ mL}\cdot\text{s}^{-1}$ ); however the mean leakage flow rates were  $1.68 \text{ mL}\cdot\text{s}^{-1}$  (mid-test) and  $2.32 \text{ mL}\cdot\text{s}^{-1}$  (post-test). After 1.2 million cycle cyclic testing in the RWT, the heart valve root AD2 appeared to be competent, although this was not case in the pre-test and mid-test competency assessment. Two out of the six decellularised aortic heart valve roots were competent following 1.2 million cycles of testing, whereas three roots were regurgitant with a mean leakage rate of  $2.97 \text{ mL}\cdot\text{s}^{-1}$ . Decellularised heart valve roots AD1 and AD5 had the highest regurgitant flow rates at the point mid-test. This data agreed well with the high speed image analysis from the cyclic testing in the RWT as the tears in the leaflets of decellularised heart valve roots AD1 and AD5 could be seen.

It was not possible to investigate the cellular aortic heart valve roots AC2 and AC5 under pulsatile flow conditions as the leaflets were severely damaged due to the cyclic loading. During the pulsatile flow assessment of cellular aortic heart valve root AC4, a tear near the leaflet attachment region of the leaflet was seen. On the other hand, it was possible to determine the pulsatile flow performance of all the decellularised aortic heart valve roots, including the heart valve roots AD1 and AD5 which had damaged leaflets due to cyclic loading in the RWT. The decellularised porcine aortic heart valve roots showed comparative functionality to the cellular heart valve roots under *in vitro* pulsatile flow conditions in terms of effective orifice area and valve opening and closing behaviour. The pressure/ flow characteristics of the cellular and decellularised aortic heart valve roots showed that at low flow rates the transvalvular pressure difference was very similar, but at higher flow rates the

cellular heart valve roots performed better. However, at higher flow rates, only two of the cellular heart valve roots (AC3 and AC4) were tested for pulsatile flow performance. The pulsatile flow performance of the remaining two cellular heart valve roots AC1 and AC6 could not be obtained at the higher flow rate conditions as the clamping of the heart valve root onto the spigot failed.

The mean thickness of the cellular aortic leaflet specimens was  $0.57 \pm 0.28$  mm in the radial direction and  $0.74 \pm 0.26$  mm in the circumferential direction, which were greater (leaflet thickness in radial direction:  $0.52 \pm 0.11$  mm and in circumferential direction:  $0.63 \pm 0.013$  mm) when it was compared with the control data derived in this study (Chapter 3). The thickness of decellularised aortic leaflet specimens was significantly lower than the thickness of the cellular leaflet specimens in the radial and circumferential directions ( $p < 0.05$ , Student's t-test). This possibly occurred due to leaflet swelling of the cellular aortic heart valve roots. In the cellular aortic valve leaflet, the spongiosa layer contains a high concentration of glycosaminoglycans (GAGs). These GAGs contain a large number of negative charged groups which attract more positively charged ions cations (i.e. sodium ions) (Setton et al., 1998) from the test fluid (saline + 0.04 % sodium azide) into the leaflets, producing an imbalance of the total mobile ion concentration between the inside and the outside of the leaflets. The resultant imbalance of ions between inside and outside-tissue fluid would likely have given rise to an osmotic pressure which caused the tissue to swell. All cellular leaflets likely underwent swelling compared to decellularised leaflets due to exposure to the test solution. However, only minimal leaflet swelling occurred when decellularised leaflets were exposed to the same test solution, this may have been due to the significantly lower GAG content in the decellularised leaflets since SDS was used as a detergent during decellularisation. SDS has been reported to remove GAG's from tissue (Vafaei et al., 2016).

The decellularised aortic leaflets were significantly stronger and stiffer in the circumferential direction compared to the cellular aortic leaflets. The cellular heart valve roots may be degenerating during fatigue assessment in the RWT due to loss of cellular viability. The degeneration is both a molecular event (breaking of molecular chains) and a tissue level event (loss of strength and integrity). Thus, uniaxial tensile

testing (e.g., loss of strength) was used to assess degeneration of the cellular and decellularised aortic leaflets after cyclic fatigue in the RWT. The degeneration of the cellular aortic leaflets was clearly seen from the tensile parameters in this study which were lower than the tensile parameters derived in Chapter 3 (control data) for the fresh cellular aortic leaflets (Table 8.11).

**Table 8.11 Tensile Parameters (Collagen Phase Slope  $E_c$ , Elastin Phase Slope  $E_e$ , Ultimate Tensile Stress  $\sigma_{UTS}$ )  $\pm$  95 % Confidence Limits for the Cellular Aortic Leaflets Following Cyclic Testing in the RWT and for the Fresh Cellular Aortic Leaflets (Chapter 3)**

<b>Tensile Leaflet Parameters for the Porcine Aortic Heart Valve Roots</b>		
	<b>Following Cyclic Testing in the RWT (Current Study)</b>	<b>Fresh Cellular Leaflets (Control Data; Chapter 2)</b>
<b>Radial</b>		
<b><math>E_c</math> (MPa)</b>	0.93 $\pm$ 0.98	1.42 $\pm$ 0.52
<b><math>E_e</math> (MPa)</b>	0.02 $\pm$ 0.01	0.03 $\pm$ 0.01
<b><math>\sigma_{UTS}</math> (MPa)</b>	0.46 $\pm$ 0.36	0.70 $\pm$ 0.26
<b>Circumferential</b>		
<b><math>E_c</math> (MPa)</b>	8.59 $\pm$ 7.92	22.07 $\pm$ 6.44
<b><math>E_e</math> (MPa)</b>	0.02 $\pm$ 0.01	0.81 $\pm$ 0.82
<b><math>\sigma_{UTS}</math> (MPa)</b>	2.48 $\pm$ 0.66	4.17 $\pm$ 0.85

However, this was not a case for the decellularised aortic leaflets. The collagen phase slopes (radial: 2.47  $\pm$  1.60 MPa, circumferential: 53.44  $\pm$  8.99 MPa) and elastin phase slopes (radial: 0.03  $\pm$  0.01 MPa, circumferential: 0.31  $\pm$  0.25 MPa) determined in this study for decellularised aortic leaflets were higher than the collagen phase slopes (radial: 1.5 MPa, circumferential: 42.9 MPa) and elastin phase slopes (radial: 0.002, circumferential: 0.003 MPa) reported in a previous study by Korossis et al. (2002) on porcine aortic heart valve roots decellularised with a similar protocol that had not been tested in the RWT. This showed that the decellularised aortic leaflets maintained their integrity.

Structural valve degeneration due to calcification was not considered in this study. Therefore direct comparison of fatigue in the RWT with *in vivo* clinical data may be inappropriate.

### 8.6.3.1 Limitations and Recommendations

The following limitations and recommendations could be drawn from the real time fatigue testing of cellular and decellularised heart valve roots in the RWT:

- The cellular and decellularised heart valve roots were degenerating during fatigue testing, possibly due to the absence of growth factors and the absence of the biological environment. Therefore, further studies are recommended by simulating the biological environment during fatigue testing of cellular and decellularised heart valve roots.
- The *in vitro* RWT setup accelerated cellular death during testing of cellular aortic heart valve roots due to the presence of toxic sodium azide in the test solution and the lack of oxygen supply.
- Structural morphology of cellular and decellularised leaflets could be assessed after fatigue testing in the RWT by histochemical analysis to determine the microstructural damages due to cyclic loading.
- The heart valve roots could be cycled in fluids with physiological viscosity to assess the effect of shear stress on the wall and leaflets.
- Further long term studies are warranted to understand effect of decellularisation on the valve function for at least 200 million cycles as described by the ISO 5840 (2015).

## 8.7 Conclusion

A real time *in vitro* fatigue assessment along with hydrodynamic performance and uniaxial tensile performance (leaflets) of the cellular and decellularised porcine aortic heart valve roots was performed for the first time in this study. Four cellular and four decellularised aortic heart valve roots showed no mechanical sign of damage, whereas two cellular and two decellularised aortic heart valve roots exhibited signs of macroscopic failure. The site of the fatigue on the decellularised porcine aortic leaflets was identical to the cellular porcine aortic leaflets. The uniaxial tensile results revealed leaflet tissue swelling, loss of stiffness (collagen and elastin phase) and loss of strength in the cellular aortic heart valve roots leaflets compared to the decellularised porcine aortic leaflets in the circumferential direction. Overall,

the results from this study suggested that the SDS decellularised porcine aortic heart valve roots showed fatigue similar to cellular porcine aortic heart valve roots and further long-term fatigue evaluation of the decellularised porcine aortic heart valve roots is warranted.

## 9 Discussion, Conclusions and Future Work

### 9.1 General Discussion

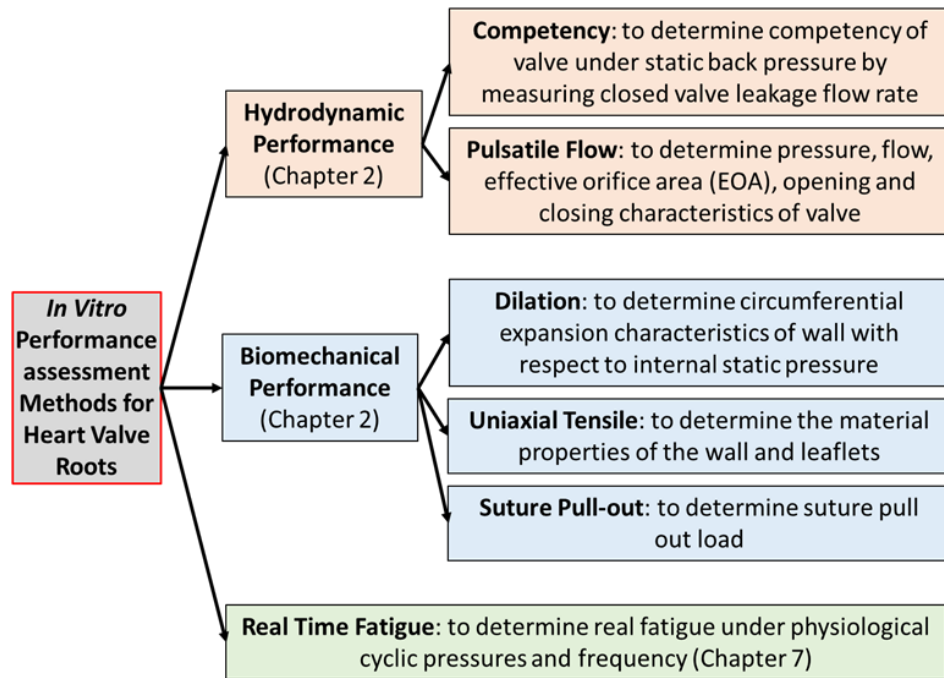
Worldwide, heart valve disease affects more than 100 million people of all ages (Dangas et al., 2016) and is treated by repair or replacement valve surgery. Currently heart valve replacements comprise of mechanical prostheses, bioprostheses, cryopreserved allografts (human donor) and the pulmonary autograft in the aortic position (Ross procedure); and have many disadvantages such as the lack of ability to grow, repair and remodel and therefore no lifetime solution exists for the young patient (Pibarot and Dumesnil, 2009). Tissue engineered (including decellularised) heart valve roots have the potential to overcome many of the drawbacks associated with existing valve replacements. Favourable initial results from the implantation of decellularised porcine and human heart valves have been shown in various studies (Lichtenberg et al., 2006, Costa et al., 2005, Dohmen, 2012, Elkins et al., 2001), however, other studies have been less successful and have led to death of several patients (Ruffer et al., 2010, Simon et al., 2003). Malfunctioning of the valve and incomplete decellularisation of the porcine tissue were identified as contributory factors to their failure (Simon et al., 2003, Ruffer et al., 2010). These studies emphasised the need for complete decellularisation of the porcine tissue and for quantitative pre-clinical evidence of the porcine heart valve roots to evaluate its function and understand its structural properties prior to implantation.

Previous studies (Korossis et al., 2002, Vafaei et al., 2016, 2014) have developed a decellularisation protocol for porcine and human heart valve roots with a view to manufacturing and supplying decellularised allograft heart valve roots and decellularised porcine heart valve roots for clinical use, replacing severely damaged heart valves. The decellularised allograft heart valve roots were developed to minimise the immune response to cryopreserved allograft heart valves and hence overcome the limitations of degeneration over time. However, decellularised allograft heart valve roots suffer from limitations of availability in sizes suitable for young patients. To address this problem, “off the shelf” decellularised porcine heart valve replacements in a range of sizes have been developed. The decellularisation



process involves repeated cycles of low concentration sodium dodecyl sulphate (SDS) in the presence of proteinase inhibitors and hypotonic buffer wash cycles. The decellularised human and porcine heart valve roots were developed on the basis of the hypothesis that removal of the major cellular immunogenic components had been achieved without adverse effects on the extracellular matrix (ECM). To determine whether the ECM had been affected as a result of the low concentration SDS decellularisation treatment, it was essential to assess the *in vitro* functional performance of decellularised heart valve roots. The hydrodynamic and biomechanical performance of low concentration SDS decellularised porcine aortic (Wilcox et al., 2005, Korossis et al., 2002) and pulmonary (2011) heart valve roots have been previously evaluated, however *in vitro* functional performance of low concentration SDS decellularised human aortic and pulmonary heart valve root has not been evaluated before.

All prosthetic heart valves have to conform to ISO 5840 (2015) and FDA (2010) standards, extensively evaluating *in vitro* functional performance prior to clinical implantation. However, the ISO 5840 (2015) and FDA (2010) standards were established based on mechanical and bioprosthetic heart valves and their suitability as test methods for biological heart valve roots is questionable. Biological heart valve roots such as allografts and decellularised heart valve roots exhibit highly time dependent viscoelastic behaviour. Therefore, standard test methods described by ISO 5840 (2015) and FDA (2010), more specifically an accelerated fatigue test method is not appropriate and a real time fatigue test method is required. The evaluation of *in vitro* functional performance of the decellularised heart valve roots is advisable before moving to *in vivo* clinical trial. Therefore, a portfolio of robust *in vitro* test methods (Chapter 2 and 7) was developed, optimised, and applied to investigate biomechanical, hydrodynamic and real time fatigue performance of the decellularised heart valve roots to predict their mechanical safety and reliability before they can be used in clinical studies (Figure 9.1).



**Figure 9.1 *In Vitro* Test Methods Developed to Assess Performance of Biological (Decellularised) Heart Valve Roots**

The hydrodynamic performance of the heart valve roots was characterised in terms of competency under static back pressure and pulsatile flow parameters. To measure competency of the aortic and pulmonary heart valve roots under static back pressure, a static leakage test rig (Jennings, 2001) was modified, where the vertical cylindrical Perspex column was replaced with a longer vertical Perspex column which was able to apply a maximum pressure of 120 mmHg. An evaluation study using porcine pulmonary heart valve roots indicated that the competency assessment method lacked physiological boundary conditions (specifically a lack of annulus support) (Chapter 3). To address this problem, the competency assessment method was modified for decellularised and cellular human pulmonary heart valve roots by adding a delrin ring for annulus support (Chapter 5). To assess hydrodynamic performance of heart valve roots under pulsatile flow, the pulsatile flow simulator used in previous studies (Fisher et al., 1986, Jennings, 2001, 2014) was optimised. The optimised pulsatile flow simulator was capable of mounting cellular and decellularised human pulmonary and aortic heart valve roots.

The biomechanical performance was characterised in terms of root circumferential expansion (dilation); uniaxial tensile parameters for wall and leaflets;

and suture pull-out load for the wall and myocardium. The uniaxial tensile testing method was used to determine wall and leaflet material properties of the heart valve roots rather than the biaxial tensile testing method, due to it being a relatively straightforward method. Circumferential expansion (dilation) was chosen as the indicator of wall stiffness due to its direct representation of the overall arterial compliance. Cylindrical Perspex tubes of different sizes were designed for the dilation test set up to accommodate heart valve root sizes with diameters ranging from 20 mm to 32 mm. This test set up enabled the measurement of circumferential expansion of the human decellularised and cellular aortic and pulmonary heart valve roots in terms of percentage dilation with respect to internal static pressure. The material properties of each of the heart valve root components (wall and leaflets) were evaluated using uniaxial tensile tests to assess how the component material properties affect the function of the valve as a whole. The material testing of heart valve roots is often confounded by local complexities introduced at sample-grip interfaces (i.e., bending, preloading, cross-section area measurement, stress concentrations, tearing). This study developed a suture technique to clamp the tissue specimen with specially designed titanium grips in order to avoid excessive accumulation of stress near the clamp during uniaxial tensile testing. This produced satisfactory results, avoiding specimen rupture close to the grips. Also heart valve root specimens are compressible and hence they change their thickness depending on the vertical force applied on them during thickness measurement. A repeatable and accurate thickness measurement technique was developed for heart valve tissue specimens.

Currently *in vitro* fatigue and durability of replacement heart valves is evaluated in an accelerated fatigue tester according to the ISO 5840 (2015) standard which is not suitable for replacement heart valves with viscoelastic properties. The real time fatigue assessment at physiologic conditions (e.g. heart rates <200 bpm), to cycle counts less than 200 million cycles is recommended by ISO 5840 (2015) for replacement heart valves which have components manufactured from viscoelastic materials. However, the ISO 5840 (2015) standard does not define the test equipment and detail test method for real time fatigue assessment. With the

potential use of decellularised heart valve roots and increased use of biological scaffolds in heart valve tissue engineering, there is a need for a new method to evaluate fatigue and durability of the scaffolds and decellularised heart valve roots. Therefore in this study, a novel *in vitro* real time fatigue assessment method was developed in a real time wear tester (RWT) which replicated physiological transvalvular pressure across the closed valve for at least 95 % of the test cycles. During fatigue assessment, it is essential to regulate physiological transvalvular pressure across the closed valve to attain radial expansion of the leaflets (Lockie et al., 1993). In addition, arterial contraction-expansion movement (dilation) was achieved by producing the physiological mean pressure of  $70 \pm 20$  mmHg within the aorta by modifying the heart valve root holder and adding compliance by a vertical pressure column. Arterial wall dilation is an important property which helps to transmit stress from the leaflets to the wall (Thubrikar, 2018) and thereby reduces fatigue and eventual structural failure of the valve leaflets (Sutton et al., 1995). The validated method was able to evaluate the fatigue of three heart valve roots mounted in the RWT per test for a maximum of 1.2 million cycles (Chapter 8). However, the fatigue assessment method for biological heart valve roots in the RWT requires enhancement due to the lack of flow data through the heart valve root and lack of dilation within the aorta.

The methodologies developed and data derived in this study will provide evidence-based standards of practice and the foundation for further research in the development of the next generation replacement biological heart valve roots such as decellularised heart valve roots. In addition, it would be useful to revise the test protocols described by ISO 5840 (2015) to include a real time fatigue test method for biological heart valve roots or for tissue based scaffolds.

The *in vitro* test methods developed were validated by deriving hydrodynamic and biomechanical performance of cellular porcine aortic and pulmonary heart valve roots (Chapter 3) and then applied to address several research questions in an effort to more fully describe the functional performance of decellularised human aortic and pulmonary heart valve roots prior to clinical studies.

These research questions included:

Chapter 9

### **Effect of decellularisation on human aortic and pulmonary heart valve roots (Chapter 4 and Chapter 5)**

The study showed that neither pulsatile flow parameters nor wall material properties of the human aortic and pulmonary heart valve roots were significantly affected by the low concentration SDS decellularisation treatment. In addition, the circumferential expansion properties of decellularised human aortic heart valve roots were similar to cellular aortic heart valve roots. However, decellularisation significantly altered circumferential expansion properties of human pulmonary heart valve roots. In addition, some of the directional material properties of the aortic and pulmonary leaflets and the hydrodynamic performance under static back pressure of human aortic and pulmonary heart valve roots were altered due to decellularisation. The changes in leaflet material properties after decellularisation may be due to the significant reduction of glycosaminoglycan (GAGs) and removal of cells reported by Vafaei et al. (2016). The loss of GAGs in the decellularised leaflets, may have led to loosening of the fibrous structure, and uncrimping of the circumferentially aligned collagen fibers. This could potentially cause an earlier than normal recruitment and reorientation of the collagen fibers in the direction of applied strain during tensile testing (Williams et al., 2009). Previous research studies on decellularised tissues has shown similar findings in bone tissue (Banse et al., 2002), ligaments (Herbert et al., 2016) and soft tissue (Freed and Doehring, 2005). It is expected that the leaflets of the decellularised roots will recellularise *in vivo* and regain their physiological tensile properties. In addition, the magnitude of changes in decellularised leaflet material properties may not be large enough to influence the performance of the heart valve roots *in vivo*, as these decellularised human and aortic pulmonary heart valves showed excellent hydrodynamic performance under pulsatile flow conditions, compared to cellular pulmonary heart valve roots.

There was a concern that the processing step (scraping) used during decellularisation (2014) may have had an adverse effect, particularly the functional biomechanical performance (dilation and competency) of human pulmonary heart valve roots, as studies have shown that the adventitia layer provides structural support and protects vessels from overstretch (Lu et al., 2004, Laflamme et al., 2006).

Therefore, a subsequent paired comparison of pulmonary heart valve roots with and without decellularisation, and with a physiological competency test model, was performed. The paired comparison showed no significant difference in the functional biomechanical performance of the decellularised and cellular human pulmonary heart valve roots.

In summary, this study has performed for the first time a comparison of *in vitro* biomechanical and hydrodynamic performance of low concentration SDS decellularised cryopreserved aortic and pulmonary human heart valve roots (Vafaei et al., 2016) with conventionally used cryopreserved aortic and pulmonary human heart valve roots and provided valuable pre-clinical data that can support clinical studies of decellularised porcine pulmonary heart valve roots.

#### **Effect of 12 months implantation in sheep on material properties of decellularised porcine pulmonary heart valve roots (Chapter 6)**

Low concentration SDS decellularised porcine pulmonary heart valve roots have been developed (2014) and have been implanted in sheep for 12 months (Berry et al., 2017) with a view to their clinical use as right ventricle outflow tract replacements in the Ross procedure. This study evaluated the material properties of decellularised porcine pulmonary heart valve roots following 12 months implantation in sheep. In addition, the effect of cryopreservation and decellularisation was evaluated on the material properties of cellular porcine pulmonary heart valve roots as the heart valve roots were decellularised and cryopreserved before being implanted in sheep.

The study showed that the material properties of the 12 months explanted decellularised porcine (ExpDCP Porcine) pulmonary heart valve root wall in the axial and circumferential directions were similar to non-implanted decellularised cryopreserved porcine (DecellCP) pulmonary heart valve root wall. However, the tensile leaflet material properties of DecellCP pulmonary heart valve roots appeared to alter following 12 months of implantation in sheep. But the majority of ExpDCP porcine pulmonary root wall and leaflet material parameters (stiffness and strength) showed a decreasing trend which indicated that the ExpDCP porcine pulmonary root wall and leaflets were becoming more like cellular ovine. Indeed, it was observed in the histological and the immunohistochemical analysis that the wall and leaflets of

the decellularised porcine pulmonary heart valve roots were repopulating with ovine cells following 12 months implantation in sheep (Berry et al., 2017). In addition, the low concentration SDS decellularised treatment combined with cryopreservation processing had a minimal effect on porcine pulmonary heart valve roots.

### **Effect of decellularisation on the fatigue of porcine aortic heart valve roots (Chapter 8)**

To derive the effects of low concentration SDS decellularisation on fatigue of porcine aortic heart valve roots, preclinical *in vitro* real fatigue assessment of low concentration SDS decellularised porcine aortic heart valve roots (Wilcox et al., 2005) under physiological cyclic pressures and heart rate conditions for a maximum of 1.2 million cycles was evaluated and compared with cellular porcine aortic heart valve roots for the first time. Results showed that there was no significant difference between the fatigue properties of decellularised and cellular porcine aortic heart valve roots. Four cellular and four decellularised aortic heart valve roots showed no mechanical sign of damage, whereas two cellular and two decellularised aortic heart valve roots exhibited signs of macroscopic fatigue damage (tear). The fatigue damage in all cases was near to the commissure and/or belly region, it may have been due to excessive flexion or due to the lack of physiological dilation of the aorta during testing. *In vivo*, dilation of the aortic heart valve root is assumed to transmit the stress from the leaflets to the wall and thereby reduces fatigue and eventual structural failure of the valve leaflets (Thubrikar, 2018), as detailed in Chapter 1 Section 1.5. Remarkably the regions of leaflet failure observed were consistent with *in vivo* (Ishihara et al., 1981, Hilbert et al., 1992, Wells and Sacks, 2002, Piñón et al., 2015) and *in vitro* accelerated (Smith et al., 1999, Sacks and Smith, 1998) fatigue induced leaflet tears seen in bioprosthetic porcine heart valves. However, in bioprosthetic porcine heart valves (stented and scentless), the dilation of the wall is either limited or eliminated due to the fixation process or presence of stent (Raghavan, 2008). The performance of the decellularised aortic heart valve roots under pulsatile flow following fatigue testing was comparable to cellular aortic heart valve roots. The material properties of the cellular porcine aortic heart valve root leaflets were altered following cyclic fatigue testing and showed a loss of stiffness (in both collagen and

elastin phases) and a loss of strength in the cellular aortic heart valve roots leaflets compared to the decellularised porcine aortic leaflets in the circumferential direction, possibly due to swelling of the cellular aortic heart valve root leaflets. The cellular aortic leaflets consists of the spongiosa layer with highly concentrated negative charged groups in glycosaminoglycans (GAGs) which attract positively charged sodium ions (Setton et al., 1998) from the test fluid (saline + 0.04 % sodium azide) into the leaflets. This produced an imbalance of ions causing the leaflets to swell. Conversely, the leaflet swelling in decellularised leaflets was minimum, though they were exposed to the same test solution due to the fact that GAG content was significantly removed during the decellularisation process (2014, Booth et al., 2002, Gilbert et al., 2006, Vafaei et al., 2016).

Overall, the results from this study suggested that the SDS decellularised porcine aortic heart valve roots showed fatigue similar to cellular porcine aortic heart valve roots.

## **9.2 Limitations and Future Work**

The limitations of this research and considerations for future work are described below.

### **1. Sample size and variability**

The human aortic and pulmonary heart valve roots used in this research came from NHS BT TES, Speke, Liverpool; from elderly donors, and were not suitable for clinical use. In addition, due to the limited availability of human samples, the study was conducted with a relatively low number of samples (n=4) in each group. Sample variability is a common concern when conducting experiments with soft tissue. The heart valve roots from different human donors showed a wide range of variability within the groups (cellular and decellularised) due to their age, size, sex and health condition of the donor. For any future studies assessing the effect of decellularisation on the human heart valve roots it is recommended that a minimum of six samples should be used in each group. It is also recommended to perform a statistical power analysis to verify whether the non-significant differences between the groups are due to lack of relationship between the groups or due to lack of statistical power.



## **2. Test fluid**

The fluid used in the pulsatile flow simulator and RWT was 0.9 % (w/v) saline and 0.9 % (w/v) saline + sodium azide 1 % (w/v) solution. These solutions had lower density and viscosity compared to blood (density of saline: 1.0045 g/mL, viscosity of saline: 0.001 Pa.s; density of blood: 1.060 g/mL, viscosity of blood 0.0035 Pa.s at body temperature), but it was transparent for the benefit of visualisation of leaflet dynamics and ease of cleaning the systems. For future studies in a pulsatile flow simulator and RWT, the use of potential test fluids could be explored which are a closer to a blood analogue.

## **3. Mounting of the heart valve root**

The mounting procedure of the heart valve roots, using the cable tie method in the pulsatile flow simulator and RWT, could be improved to reduce damage to the heart valve root by developing an alternative more robust clamping method.

## **4. *In vitro* real time fatigue assessment method**

The cellular heart valve roots were treated with 150 mL Cambridge antibiotics + 2.5 mL amphotericin B to reduce infection during testing in the RWT. An improved method for treating cellular heart valve roots could be investigated and this would create less opportunity for initial contamination and allow the experiments to run longer with less risk of fungal infection.

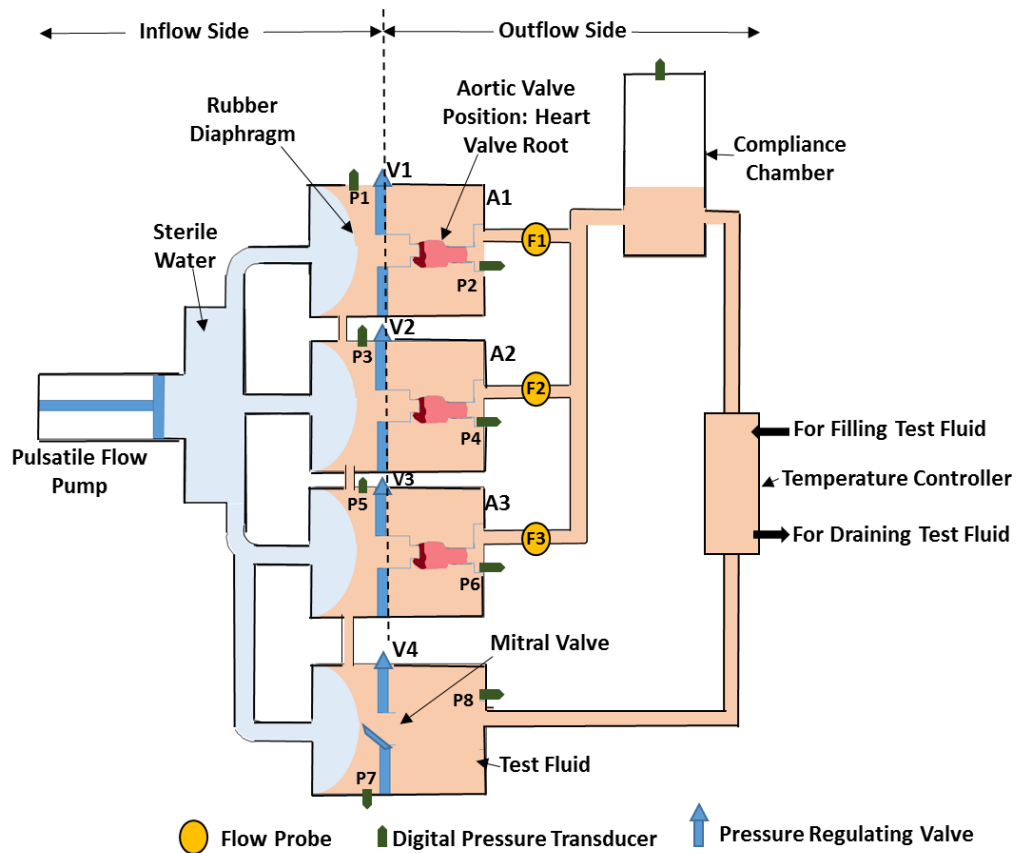
The flow through the heart valve root in the RWT is currently not known. A study involving a flow probe in the flow loop of the RWT would enable more insight into the dynamic environment in which the heart valve roots can be tested.

The *in vitro* fatigue of decellularised porcine aortic heart valve roots was similar to cellular porcine aortic heart valve roots. The fatigue damage (tear) in all cases was near to the leaflet attachment area, it may have been due to excessive flexion or due to the lack of physiological dilation of the aorta during testing. To improve physiological dilation or compliant movement of the aorta during fatigue testing in the RWT, additional compliance could be added. This could be achieved by replacing the existing compliance chamber with an electronically controlled compliance chamber to control the volume of air within the compliance chamber. In addition, to

gain more insight into the effect of cyclic loading and leaflet failure, it is recommended to use histochemical characterisation of the leaflets following fatigue assessment. This will help to investigate, on a microscopic level, what the effect of cyclic loading on collagen and the elastin fibre network in the leaflets is.

An extended duration of fatigue testing could provide more information as to the effects of decellularisation on the heart valve structure. Cellular tissue viability over a longer period of time may be a major hurdle to this proposed future work, therefore this would have to be further evaluated by developing and use of culture medium to retain viability of cellular heart valve roots. Also continuous monitoring of the leaflet dynamics with synchronised pressure measurements would help in the assessment of the leaflet failure mode.

A negative inflow pressure was recorded during the reverse stroke of the pump as a result of the resistance to forward flow through the bypass valve. A possible solution is to use a larger diameter bypass valve or more than one bypass valve. A larger orifice will result in less resistance to the flow and lower negative pressures generated by the suction effect.



**Figure 9.2 Proposed Schematic Diagram of Flow Loop for the RWT**

The heart valve roots under test were not isolated from the inflow side from one another during real fatigue testing which meant it was not possible to control pressure across each closed heart valve individually. To address the limitations with the RWT, the flow loop for the RWT could be redesigned as shown in Figure 9.2.

This proposed flow loop design in Figure 9.2 for the RWT consists of three isolated Perspex valve chambers A1, A2 and A3. The pulsatile flow pump pumps the test fluid through the heart valve roots which are placed in the heart valve chambers A1, A2 and A3. The flow from each heart valve root is monitored by the flow probes F1, F2 and F3, connected to the outflow side of the chambers. The inflow and outflow pressure of the heart valve root can be measured with inflow (P1, P3, P5) and outflow (P2, P4, P6) pressure transducers. The pressure across each heart valve root could be controlled individually with pressure regulating valves (V1, V2 and V3). The other elements of the flow loop are the electronically controlled compliance chamber and temperature controller which are used to add resistance to the circuit and to control

the temperature of test fluid during testing. The fluid flow would pass through the heart valve roots (mounted in the aortic position) by opening the valves during the forward stroke; and during the reverse stroke the fluid flow would pass through the mitral valve and back to the valve chambers.

### 9.3 Conclusion

In summary this thesis has provided important contributions to the field of heart valve replacement:

1. A portfolio of *in vitro* pre-clinical test methods was developed where hydrodynamic and biomechanical performance assessment methods for biological heart valve roots including decellularised heart valve roots were optimised.
2. A novel fatigue assessment method was developed for biological heart valve roots and real time *in vitro* fatigue assessment of the cellular and decellularised porcine aortic heart valve roots was evaluated for the first time in this study, where decellularised porcine aortic heart valve roots showed fatigue similar to cellular porcine aortic heart valve roots.
3. A full functional performance of cryopreserved decellularised human aortic and pulmonary heart valve roots was compared for the first time in a systematic way with conventionally used cryopreserved human aortic and pulmonary heart valve roots, evaluating the effect of decellularisation.
4. The *in vitro* material properties of cryopreserved decellularised porcine pulmonary heart valve roots was evaluated following trans-species implantation of decellularised porcine pulmonary heart valve roots for 12 months.

#### ***Impact of this research:***

These studies provided valuable pre-clinical functional performance data that will contribute to the safety and effectiveness of decellularised human and porcine heart valve roots, which will support clinical translation and commercialisation of SDS decellularised heart valve roots. Following the translation of the decellularisation protocol into a good manufacturing practices-compatible process for donor cryopreserved human heart valve roots in collaboration with NHSBT Tissue & Eye

Services, developed *in vitro* test methods will be applied to assess their functional performance with a view to future clinical use. A sterilisation process will be developed for the decellularised porcine heart valve roots and *in vitro* test methods will be applied to assess functional performance of the decellularised porcine heart valve roots post-sterilisation.

The developed *in vitro* pre-clinical test methods for biological heart valve roots will help in the refinement of *in vivo* large animal studies and improve translation outcome of large animal studies. In addition, the methods and the data from this research has the potential to help in the revision of ISO 5840 (2015) by including such testing for decellularised heart valve roots.

## 10 References

- ALSOUFI, B., AL-HALEES, Z., MANLHIOT, C., MCCRINDLE, B. W., AL-AHMADI, M., SALLEHUDDIN, A., CANVER, C. C., BULBUL, Z., JOUFAN, M. & FADEL, B. 2009. Mechanical valves versus the Ross procedure for aortic valve replacement in children: Propensity-adjusted comparison of long-term outcomes. *Journal of Thoracic and Cardiovascular Surgery*, 137, 362-370.
- ANSSARI-BENAM, A., BADER, D. L. & SCREEN, H. R. C. 2011. A combined experimental and modelling approach to aortic valve viscoelasticity in tensile deformation. *Journal of Materials Science-Materials in Medicine*, 22, 253-262.
- APPLEGATE, P. M., BOYD, W. D., APPLEGATE II, R. L. & LIU, H. 2017. Is it the time to reconsider the choice of valves for cardiac surgery: mechanical or bioprosthetic? *Journal of biomedical research*, 31, 373-376.
- AROKIARAJ, M. C., CENTENO, A., PESQUERA, A. & ZURUTUZA, A. 2016. Novel graphene-coated mechanical bi-leaflet valves after accelerated wear test of 40M test cycles in saline. *Acta Cardiologica*, 71, 331-347.
- ASHOUR, Z. A., SHAWKY, H. A. & HASSAN HUSSEIN, M. 2000. Outcome of pregnancy in women with mechanical valves. *Texas Heart Institute journal*, 27, 240-245.
- BADER, A., SCHILLING, T., TEEBKEN, O. E., BRANDES, G., HERDEN, T., STEINHOFF, G. & HAVERICH, A. 1998. Tissue engineering of heart valves - human endothelial cell seeding of detergent acellularized porcine valves. *European Journal of Cardio-Thoracic Surgery*, 14, 279-284.
- BANSE, X., SIMS, T. J. & BAILEY, A. J. 2002. Mechanical properties of adult vertebral cancellous bone: Correlation with collagen intermolecular cross-links. *Journal of Bone and Mineral Research*, 17, 1621-1628.
- BARAKI, H., TUDORACHE, I., BRAUN, M., HÖFFLER, K., GÖRLER, A., LICHTENBERG, A., BARA, C., CALISTRU, A., BRANDES, G., HEWICKER-TRAUTWEIN, M., HILFIKER, A., HAVERICH, A. & CEBOTARI, S. 2009. Orthotopic replacement of the aortic valve with decellularized allograft in a sheep model. *Biomaterials*, 30, 6240-6246.
- BATEMAN, M. G., QUILL, J. L., HILL, A. J. & IAIZZO, P. A. 2013. The Anatomy and Function of the Semilunar Valves. In: IAIZZO, P. A., BIANCO, R. W., HILL, A. J. & ST. LOUIS, J. D. (eds.) *Heart Valves: From Design to Clinical Implantation*. Boston, MA: Springer US.
- BAZAN, O. & ORTIZ, J. P. 2016. Experimental Validation of a Cardiac Simulator for *in vitro* Evaluation of Prosthetic Heart Valves. *Braz J Cardiovasc Surg*, 31, 151-157.
- BECHTEL, J. F., STIERLE, U. & SIEVERS, H. H. 2008. Fifty-two months' mean follow up of decellularized SynerGraft-treated pulmonary valve allografts. *J Heart Valve Dis*, 17, 98-104; discussion 104.
- BECHTEL, J. F. M., GELLISSEN, J., ERASMI, A. W., PETERSEN, M., HIOB, A., STIERLE, U. & SIEVERS, H.-H. 2005. Mid-term findings on echocardiography and computed tomography after RVOT-reconstruction: comparison of decellularized (SynerGraft)

and conventional allografts☆. *European Journal of Cardio-Thoracic Surgery*, 27, 410-415.

- BERRY, H., T., V., F., W., A., D., LM., J., JG., R., C., C., F., D. D. C., J., F. & E., I. 2007. Temporal Evaluation of Decellularised Porcine Pulmonary Root Performance and Regeneration in a Juvenile Sheep Model. The Heart Valve Society Annual Meeting, 2017 Monaco.
- BEZUIDENHOUT, D., WILLIAMS, D. F. & ZILLA, P. 2015. Polymeric heart valves for surgical implantation, catheter-based technologies and heart assist devices. *Biomaterials*, 36, 6-25.
- BIBEVSKI, S., RUZMETOV, M., FORTUNA, R. S., TURRENTINE, M. W., BROWN, J. W. & OHYE, R. G. 2017. Performance of SynerGraft Decellularized Pulmonary Allografts Compared With Standard Cryopreserved Allografts: Results From Multiinstitutional Data. *The Annals of Thoracic Surgery*, 103, 869-874.
- BILLIAR, K. L. & SACKS, M. S. 2000. Biaxial mechanical properties of the natural and glutaraldehyde treated aortic valve cusp--Part I: Experimental results. *J Biomech Eng*, 122, 23-30.
- BLOT WILLIAM, J., IBRAHIM MICHEL, A., IVEY TOM, D., ACHESON DONALD, E., BROOKMEYER, R., WEYMAN, A., DEFAUW, J., SMITH, J. K. & HARRISON, D. 2005. Twenty-Five-Year Experience With the Björk-Shiley Convexoconcave Heart Valve. *Circulation*, 111, 2850-2857.
- BODNAR, E. 1996. The Medtronic Parallel valve and the lessons learned. *J Heart Valve Dis*, 5, 572-3.
- BOOTH C, F. J., INGHAM E. 2001. *Decellularisation of matrices* 10/478,198
- BOOTH, C., KOROSSIS, S. A., WILCOX, H. E., WATTERSON, K. G., KEARNEY, J. N., FISHER, J. & INGHAM, E. 2002. Tissue engineering of cardiac valve prostheses I: Development and histological characterization of an acellular porcine scaffold. *Journal of Heart Valve Disease*, 11, 457-462.
- BORTOLOTTI, U., MILANO, A., GUERRA, F., MAZZUCCO, A., MOSSUTO, E., THIENE, G. & GALLUCCI, V. 1991. Failure of Hancock pericardial xenografts: Is prophylactic bioprosthetic replacement justified? *The Annals of Thoracic Surgery*, 51, 430-437.
- BOTTIO, T., CASAROTTO, D., THIENE, G., CAPRILI, L., ANGELINI, A. & GEROSA, G. 2003. Leaflet escape in a new bileaflet mechanical valve: TRI technologies. *Circulation*, 107, 2303-6.
- BOTTIO, T., TARZIA, V., DAL LIN, C., BURATTO, E., RIZZOLI, G., SPINA, M., GANDAGLIA, A., NASO, F. & GEROSA, G. 2010. The changing hydrodynamic performance of the decellularized intact porcine aortic root: considerations on in-vitro testing. *J Heart Valve Dis*, 19, 485-91.
- BOUDOULAS, K. D., BORER, J. S. & BOUDOULAS, H. 2013. Etiology of valvular heart disease in the 21st century. *Cardiology*, 126, 139-52.

- BOURGUIGNON, T., BOUQUIAUX-STABLO, A. L., CANDOLFI, P., MIRZA, A., LOARDI, C., MAY, M. A., EL-KHOURY, R., MARCHAND, M. & AUPART, M. 2015. Very long-term outcomes of the Carpentier-Edwards Perimount valve in aortic position. *Ann Thorac Surg*, 99, 831-7.
- BROOM, N. D. 1977. The stress/strain and fatigue behaviour of glutaraldehyde preserved heart-valve tissue. *J Biomech*, 10, 707-24.
- BROWN, J. W., ELKINS, R. C., CLARKE, D. R., TWEDDELL, J. S., HUDDLESTON, C. B., DOTY, J. R., FEHRENBACHER, J. W. & TAKKENBERG, J. J. M. 2010. Performance of the CryoValve\* SG human decellularized pulmonary valve in 342 patients relative to the conventional CryoValve at a mean follow-up of four years. *The Journal of Thoracic and Cardiovascular Surgery*, 139, 339-348.
- BROWN, J. W., RUZMETOV, M., ELTAYEB, O., RODEFELD, M. D. & TURRENTINE, M. W. 2011. Performance of SynerGraft Decellularized Pulmonary Homograft in Patients Undergoing a Ross Procedure. *Annals of Thoracic Surgery*, 91, 416-422.
- BURCH, P. T., KAZA, A. K., LAMBERT, L. M., HOLUBKOV, R., SHADDY, R. E. & HAWKINS, J. A. 2010. Clinical Performance of Decellularized Cryopreserved Valved Allografts Compared With Standard Allografts in the Right Ventricular Outflow Tract. *Annals of Thoracic Surgery*, 90, 1301-1305.
- BUSE, E. E., HILBERT, S. L., HOPKINS, R. A. & CONVERSE, G. L. 2016. Pulse Duplicator Hydrodynamic Testing of Bioengineered Biological Heart Valves. *Cardiovasc Eng Technol*, 7, 352-362.
- BUTTERFIELD, M. & FISHER, J. 2000. Fatigue analysis of clinical bioprosthetic heart valves manufactured using photooxidized bovine pericardium. *J Heart Valve Dis*, Jan;9(1):161-6.
- BUTTERFIELD, M., FISHER, J., DAVIES, G. A. & KEARNEY, J. M. 1991. Leaflet geometry and function in porcine bioprostheses. *Eur J Cardiothorac Surg*, 5, 27-32; discussion 33.
- CAMPO-DEAÑO, L., DULLENS, R. P. A., AARTS, D. G. A. L., PINHO, F. T. & OLIVEIRA, M. S. N. 2013. Viscoelasticity of blood and viscoelastic blood analogues for use in polydimethylsiloxane in vitro models of the circulatory system. *Biomicrofluidics*, 7, 34102-34102.
- CARAPETIS, J. R., STEER, A. C., MULHOLLAND, E. K. & WEBER, M. 2005. The global burden of group A streptococcal diseases. *The Lancet Infectious Diseases*, 5, 685-694.
- CAREW, E. O., BARBER, J. E. & VESELY, I. 2000. Role of preconditioning and recovery time in repeated testing of aortic valve tissues: validation through quasilinear viscoelastic theory. *Ann Biomed Eng*, 28, 1093-100.
- CAREW, E. O., GARG, A., BARBER, J. E. & VESELY, I. 2004. Stress Relaxation Preconditioning of Porcine Aortic Valves. *Annals of Biomedical Engineering*, 32, 563-572.
- CARR-WHITE, G. S., KILNER, P. J., HON, J. K., RUTLEDGE, T., EDWARDS, S., BURMAN, E. D., PENNELL, D. J. & YACOUB, M. H. 2001. Incidence, location, pathology, and



significance of pulmonary homograft stenosis after the Ross operation. *Circulation*, 104, 116-20.

- CASADO, J. A., DIEGO, S., FERRENO, D., RUIZ, E., CARRASCAL, I., MENDEZ, D., REVUELTA, J. M., PONTON, A., ICARDO, J. M. & GUTIERREZ-SOLANA, F. 2012. Determination of the mechanical properties of normal and calcified human mitral chordae tendineae. *J Mech Behav Biomed Mater*, 13, 1-13.
- CASCONE, M. G., BARBANI, N., CRISTALLINI, C., GIUSTI, P., CIARDELLI, G. & LAZZERI, L. 2001. Bioartificial polymeric materials based on polysaccharides. *Journal of Biomaterials Science, Polymer Edition*, 12, 267-281.
- CEBOTARI, S., LICHTENBERG, A., TUDORACHE, I., HILFIKER, A., MERTSCHING, H., LEYH, R., BREYMANN, T., KALLENBACH, K., MANIUC, L., BATRINAC, A., REPIN, O., MALIGA, O., CIUBOTARU, A. & HAVERICH, A. 2006. Clinical application of tissue engineered human heart valves using autologous progenitor cells. *Circulation*, 114, 1132-7.
- CEBOTARI, S., MERTSCHING, H., KALLENBACH, K., KOSTIN, S., REPIN, O., BATRINAC, A., KLECZKA, C., CIUBOTARU, A. & HAVERICH, A. 2002. Construction of autologous human heart valves based on an acellular allograft matrix. *Circulation*, 106, 163-168.
- CEBOTARI, S., TUDORACHE, I., CIUBOTARU, A., BOETHIG, D., SARIKOUCH, S., GOERLER, A., LICHTENBERG, A., CHEPTANARU, E., BARNACIUC, S., CAZACU, A., MALIGA, O., REPIN, O., MANIUC, L., BREYMANN, T. & HAVERICH, A. 2011. Use of Fresh Decellularized Allografts for Pulmonary Valve Replacement May Reduce the Reoperation Rate in Children and Young Adults Early Report. *Circulation*, 124, S115-S123.
- CHANDRAN, K. B., RITTGERS, S. E. & YOGANATHAN, A. P. 2012. *Biofluid Mechanics: The Human Circulation, Second Edition*, Taylor & Francis.
- CHEN, J. H. & SIMMONS, C. A. 2011. Cell-matrix interactions in the pathobiology of calcific aortic valve disease: critical roles for matricellular, matricrine, and matrix mechanics cues. *Circ Res*, 108, 1510-24.
- CHESTER, A. H., EL-HAMAMSY, I., BUTCHER, J. T., LATIF, N., BERTAZZO, S. & YACOUB, M. H. 2014. The living aortic valve: From molecules to function. *Global cardiology science & practice*, 2014, 52-77.
- CHEUNG, D. Y., DUAN, B. & BUTCHER, J. T. 2015. Current progress in tissue engineering of heart valves: multiscale problems, multiscale solutions. *Expert opinion on biological therapy*, 15, 1155-1172.
- CHIRAKANPHAISARN, N., THONGKANLUANG, T. & CHIWPREECHAR, Y. 2018. Heart rate measurement and electrical pulse signal analysis for subjects span of 20–80 years. *Journal of Electrical Systems and Information Technology*, 5, 112-120.
- CHOE, J. A., JANA, S., TEFFT, B. J., HENNESSY, R. S., GO, J., MORSE, D., LERMAN, A. & YOUNG, M. D. 2018. Biomaterial characterization of off-the-shelf decellularized porcine pericardial tissue for use in prosthetic valvular applications. *Journal of Tissue Engineering and Regenerative Medicine*, 12, 1608-1620.

- CHRISTIE, G. W. 1992. Anatomy of aortic heart valve leaflets: the influence of glutaraldehyde fixation on function. *Eur J Cardiothorac Surg*, 6 Suppl 1, S25-32; discussion S33.
- CICHA, I., RUFFER, A., CESNJEVAR, R., GLOCKLER, M., AGAIMY, A., DANIEL, W. G., GARLICH, C. D. & DITTRICH, S. 2011. Early obstruction of decellularized xenogenic valves in pediatric patients: involvement of inflammatory and fibroproliferative processes. *Cardiovasc Pathol*, 20, 222-31.
- CLARK, R. E. 1973. STRESS-STRAIN CHARACTERISTICS OF FRESH AND FROZEN HUMAN AORTIC AND MITRAL LEAFLETS AND CHORDAE TENDINEAE - IMPLICATIONS FOR CLINICAL USE. *Journal of Thoracic and Cardiovascular Surgery*, 66, 202-208.
- CLARK, R. E. & FINKE, E. H. 1974. Scanning and light microscopy of human aortic leaflets in stressed and relaxed states. *J Thorac Cardiovasc Surg*, 67, 792-804.
- CONTI, C. A., VOTTA, E., DELLA CORTE, A., DEL VISCOVO, L., BANCONE, C., COTRUFO, M. & REDAELLI, A. 2010. Dynamic finite element analysis of the aortic root from MRI-derived parameters. *Med Eng Phys*, 32, 212-21.
- CONVERSE, G. L., ARMSTRONG, M., QUINN, R. W., BUSE, E. E., CROMWELL, M. L., MORIARTY, S. J., LOFLAND, G. K., HILBERT, S. L. & HOPKINS, R. A. 2012. Effects of cryopreservation, decellularization and novel extracellular matrix conditioning on the quasi-static and time-dependent properties of the pulmonary valve leaflet. *Acta Biomaterialia*, 8, 2722-2729.
- COSTA, J. N. L., POMERANTZEFF, P. M. A., BRAILE, D. M., RAMIREZ, V. A., GOISSIS, G. & STOLF, N. A. G. 2005. Comparação entre o pericárdio bovino decelularizado e o pericárdio bovino convencional utilizado na confecção de biopróteses valvares cardíacas. *Brazilian Journal of Cardiovascular Surgery*, 20, 14-22.
- COSTA, M. T. B. A. D., DA COSTA, F., D.A., NAZARENO, L. C. F. D., DOMCHOSKI, J., PERUZZO, Â. M., COLATUSO, C., GOMES, C. H. G. & COSTA, I. A. D. 2005. Análise das atividades dos oito anos iniciais do Banco de Valvas Cardíacas Humanas do Hospital de Caridade da Irmandade da Santa Casa de Misericórdia de Curitiba. *Brazilian Journal of Cardiovascular Surgery*, 20, 398-407.
- COX, M. A. J., DRIESSEN, N. J. B., BOUTEN, C. V. C. & BAALJENS, F. P. T. 2006. Mechanical characterization of anisotropic planar biological soft tissues using large indentation: A computational feasibility study. *Journal of Biomechanical Engineering-Transactions of the Asme*, 128, 428-436.
- CRAPO, P. M., GILBERT, T. W. & BADYLAK, S. F. 2011. An overview of tissue and whole organ decellularization processes. *Biomaterials*, 32, 3233-3243.
- D'SOUZA, S. S., BUTTERFIELD, M. & FISHER, J. 2003. Kinematics of synthetic flexible leaflet heart valves during accelerated testing. *J Heart Valve Dis*, 12, 110-9; discussion 119-20.
- DA COSTA, F. D., SANTOS, L. R., COLLATUSO, C., MATSUDA, C. N., LOPES, S. A., CAUDURO, S., RODERJAN, J. G. & INGHAM, E. 2009. Thirteen years' experience with the Ross Operation. *J Heart Valve Dis*, 18, 84-94.

- DA COSTA, F. D. A., COSTA, A., PRESTES, R., DOMANSKI, A. C., BALBI, E. M., FERREIRA, A. D. A. & LOPES, S. V. 2010. The Early and Midterm Function of Decellularized Aortic Valve Allografts. *Annals of Thoracic Surgery*, 90, 1854-1861.
- DA COSTA, F. D. A., DOHMEN, P. M., DUARTE, D., VON GLENN, C., LOPES, S. V., HAGGI, H., DA COSTA, M. B. A. & KONERTZ, W. 2005. Immunological and echocardiographic evaluation of decellularized versus cryopreserved allografts. during the Ross operation. *European Journal of Cardio-Thoracic Surgery*, 27, 572-577.
- DA COSTA, F. D. A., ETNEL, J. R. G., CHARITOS, E. I., SIEVERS, H.-H., STIERLE, U., FORNAZARI, D., TAKKENBERG, J. J. M., BOGERS, A. J. J. C. & MOKHLES, M. M. 2018. Decellularized Versus Standard Pulmonary Allografts in the Ross Procedure: Propensity-Matched Analysis. *The Annals of Thoracic Surgery*, 105, 1205-1213.
- DA COSTA, F. D. A., TAKKENBERG, J. J. M., FORNAZARI, D., BALBI, E. M., COLATUSO, C., MOKHLES, M. M., DA COSTA, A., SAGRADO, A. G., FERREIRA, A. D. D., FERNANDES, T. & LOPES, S. V. 2014. Long-term results of the Ross operation: an 18-year single institutional experience. *European Journal of Cardio-Thoracic Surgery*, 46, 415-422.
- DAGUM, P., GREEN, G. R., NISTAL, F. J., DAUGHTERS, G. T., TIMEK, T. A., FOPPIANO, L. E., BOLGER, A. F., INGELS, N. B., JR. & MILLER, D. C. 1999. Deformational dynamics of the aortic root: modes and physiologic determinants. *Circulation*, 100, 1154-62.
- DANGAS, G. D., WEITZ, J. I., GIUSTINO, G., MAKAR, R. & MEHRAN, R. 2016. Prosthetic Heart Valve Thrombosis. *Journal of the American College of Cardiology*, 68, 2670-2689.
- DASI, L. P., SUCOSKY, P., DE ZELICOURT, D., SUNDARESWARAN, K., JIMENEZ, J. & YOGANATHAN, A. P. 2009. Advances in cardiovascular fluid mechanics: bench to bedside. *Ann N Y Acad Sci*, 1161, 1-25.
- DAVID, H., BOUGHNER, D. R., VESELY, I. & GEROSA, G. 1994. The pulmonary valve. Is it mechanically suitable for use as an aortic valve replacement? *ASAIO J*, 40, 206-12.
- DAVID, T. E., ARMSTRONG, S. & MAGANTI, M. 2010. Hancock II bioprosthesis for aortic valve replacement: the gold standard of bioprosthetic valves durability? *Ann Thorac Surg*, 90, 775-81.
- DAVID, T. E., OMRAN, A., IVANOV, J., ARMSTRONG, S., DE SA, M. P. L., SONNENBERG, B. & WEBB, G. 2000. Dilation of the pulmonary autograft after the ross procedure. *The Journal of Thoracic and Cardiovascular Surgery*, 119, 210-220.
- DAWIDOWSKA, K. 2016. *Aortic Valve Geometry Modeling – Review*.
- DELMO WALTER, E. M., DE BY, T. M. M. H., MEYER, R. & HETZER, R. 2012. The future of heart valve banking and of homografts: perspective from the Deutsches Herzzentrum Berlin. *HSR proceedings in intensive care & cardiovascular anaesthesia*, 4, 97-108.
- DIGNAN, R., O'BRIEN, M., HOGAN, P., THORNTON, A., FOWLER, K., BYRNE, D., STEPHENS, F. & HARROCKS, S. 2003. Aortic valve allograft structural deterioration is associated

with a subset of antibodies to human leukocyte antigens. *Journal of Heart Valve Disease*, 12, 382-391.

- DOHMEN, P. M. 2012. Clinical results of implanted tissue engineered heart valves. *HSR proceedings in intensive care & cardiovascular anesthesia*, 4, 225-31.
- DOHMEN, P. M., LEMBCKE, A., HOLINSKI, S., KIVELITZ, D., BRAUN, J. P., PRUSS, A. & KONERTZ, W. 2007. Mid-term clinical results using a tissue-engineered pulmonary valve to reconstruct the right ventricular outflow tract during the ross procedure. *Annals of Thoracic Surgery*, 84, 729-736.
- DOHMEN, P. M., LEMBCKE, A., HOTZ, H., KIVELITZ, D. & KONERTZ, W. F. 2002. Ross operation with a tissue-engineered heart valve. *Ann Thorac Surg*, 74, 1438-42.
- DOHMEN, P. M., OZAKI, S., NITSCH, R., YPERMAN, J., FLAMENG, W. & KONERTZ, W. 2003. A tissue engineered heart valve implanted in a juvenile sheep model. *Med Sci Monit*, 9, BR97-BR104.
- DOHMEN, P. M., SCHECKEL, M., STEIN-KONERTZ, M., ERDBRUEGGER, W., AFFELD, K. & KONERTZ, W. 2002. In vitro hydrodynamics of a decellularized pulmonary porcine valve, compared with a glutaraldehyde and polyurethane heart valve. *Int J Artif Organs*, 25, 1089-94.
- DONOVAN, F. M., JR. 1975. Design of a hydraulic analog of the circulatory system for evaluating artificial hearts. *Biomater Med Devices Artif Organs*, 3, 439-49.
- DUNCAN, A. C., BOUGHNER, D. & VESELY, I. 1997. Viscoelasticity of dynamically fixed bioprosthetic valves. II. Effect of glutaraldehyde concentration. *The Journal of Thoracic and Cardiovascular Surgery*, 113, 302-310.
- DUPREY, A., KHANAFER, K., SCHLICHT, M., AVRIL, S., WILLIAMS, D. & BERGUER, R. 2010. In Vitro Characterisation of Physiological and Maximum Elastic Modulus of Ascending Thoracic Aortic Aneurysms Using Uniaxial Tensile Testing. *European Journal of Vascular and Endovascular Surgery*, 39, 700-707.
- EDWARDS, M. B., DRAPER, E. R. C., HAND, J. W., TAYLOR, K. M. & YOUNG, I. R. 2005. Mechanical testing of human cardiac tissue: some implications for MRI safety. *Journal of Cardiovascular Magnetic Resonance*, 7, 835-840.
- ELENES, E. Y. & HUNTER, S. A. 2014. *Soft-Tissue Allografts Terminally Sterilized with an Electron Beam Are Biomechanically Equivalent to Aseptic, Nonsterilized Tendons*.
- ELKINS, R. C., DAWSON, P. E., GOLDSTEIN, S., WALSH, S. P. & BLACK, K. S. 2001. Decellularized human valve allografts. *Annals of Thoracic Surgery*, 71, S428-S432.
- ELKINS, R. C., GOLDSTEIN, S., HEWITT, C. W., WALSH, S. P., DAWSON, P. E., OLLERENSHAW, J. D., BLACK, K. S., CLARKE, D. R. & O'BRIEN M, F. 2001. Recellularization of heart valve grafts by a process of adaptive remodeling. *Semin Thorac Cardiovasc Surg*, 13, 87-92.

- ENGELMAYR, G. C., RABKIN, E., SUTHERLAND, F. W. H., SCHOEN, F. J., MAYER, J. E. & SACKS, M. S. 2005. The independent role of cyclic flexure in the early in vitro development of an engineered heart valve tissue. *Biomaterials*, 26, 175-187.
- ERICSSON, A., LINDBLOM, D., SEMB, G., HUYSMANS, H. A., THULIN, L. I., SCULLY, H. E., BENNETT, J. G., OSTERMEYER, J. & GRUNKEMEIER, G. L. 1992. Strut fracture with Bjork-Shiley 70 degrees convexo-concave valve. An international multi-institutional follow-up study. *Eur J Cardiothorac Surg*, 6, 339-46.
- FDA 2010. U.S. Food and Drug Administration . Draft guidance for industry and FDA staff: heart valves - investigational device exemption (IDE) and premarket approval (PMA) Applications. Silver Spring: U.S. Department of Health and Human Services, FDA; 2010. 49p
- FISHER, J. 1986. Design development and evaluation of an improved pericardial bioprosthetic heart valve. *PhD thesis, University of Glasgow*
- FISHER, J., JACK, G. R. & WHEATLEY, D. J. 1986. DESIGN OF A FUNCTION-TEST APPARATUS FOR PROSTHETIC HEART-VALVES - INITIAL RESULTS IN THE MITRAL POSITION. *Clinical Physics and Physiological Measurement*, 7, 63-73.
- FITZPATRICK, J. C., CLARK, P. M. & CAPALDI, F. M. 2010. Effect of decellularization protocol on the mechanical behavior of porcine descending aorta. *Int J Biomater*, 2010.
- FRANK, C., MCDONALD, D., WILSON, J., EYRE, D. & SHRIVE, N. 1995. RABBIT MEDIAL COLLATERAL LIGAMENT SCAR WEAKNESS IS ASSOCIATED WITH DECREASED COLLAGEN PYRIDINOLINE CROSS-LINK DENSITY. *Journal of Orthopaedic Research*, 13, 157-165.
- FREED, A. D. & DOEHRING, T. C. 2005. Elastic model for crimped collagen fibrils. *Journal of Biomechanical Engineering-Transactions of the Asme*, 127, 587-593.
- FUKUSHIMA, S., TESAR, P. J., PEARSE, B., JALALI, H., SPARKS, L., FRASER, J. F. & POHLNER, P. G. 2014. Long-term clinical outcomes after aortic valve replacement using cryopreserved aortic allograft. *J Thorac Cardiovasc Surg*, 148, 65-72 e2.
- GABBAY, S., BORTOLOTTI, U., WASSERMAN, F., FACTOR, S., STROM, J. & FRATER, R. W. 1984. Fatigue-induced failure of the Ionescu-Shiley pericardial xenograft in the mitral position. In vivo and in vitro correlation and a proposed classification. *J Thorac Cardiovasc Surg*, 87, 836-44.
- GABBAY, S., MCQUEEN, D. M., YELLIN, E. L., BECKER, R. M. & FRATER, R. W. 1978. In vitro hydrodynamic comparison of mitral valve prostheses at high flow rates. *J Thorac Cardiovasc Surg*, 76, 771-87.
- GALLAGHER, A. J., NI ANNIADH, A., BRUYERE-GARNIER, K., OTTENIO, M., XIE, H. & GILCHRIST, M. D. 2012. Dynamic tensile properties of human skin. *Proceedings of the International Research Council on the Biomechanics of Injury conference*, 40, 494-502.

- GALLO, I., NISTAL, F., REVUELTA, J. M., GARCIA-SATUE, E., ARTINANO, E. & DURAN, C. G. 1985. Incidence of primary tissue valve failure with the Ionescu-Shiley pericardial valve. Preliminary results. *J Thorac Cardiovasc Surg*, 90, 278-80.
- GAO, G., WU, Y., GRUNKEMEIER, G. L., FURNARY, A. P. & STARR, A. 2004. Durability of pericardial versus porcine aortic valves. *Journal of the American College of Cardiology*, 44, 384-388.
- GARCIA-HERRERA, C. M., ATIENZA, J. M., ROJO, F. J., CLAES, E., GUINEA, G. V., CELENTANO, D. J., GARCIA-MONTERO, C. & BURGOS, R. L. 2012. Mechanical behaviour and rupture of normal and pathological human ascending aortic wall. *Med Biol Eng Comput*, 50, 559-66.
- GILBERT, T. W. 2012. Strategies for tissue and organ decellularization. *J Cell Biochem*, 113, 2217-22.
- GILBERT, T. W., SELLARO, T. L. & BADYLAK, S. F. 2006. Decellularization of tissues and organs. *Biomaterials*, 27, 3675-3683.
- GOECKE, T., THEODORIDIS, K., TUDORACHE, I., CIUBOTARU, A., CEBOTARI, S., RAMM, R., HÖFFLER, K., SARIKOUCH, S., VÁSQUEZ RIVERA, A., HAVERICH, A., WOLKERS, W. F. & HILFIKER, A. 2018. In vivo performance of freeze-dried decellularized pulmonary heart valve allo- and xenografts orthotopically implanted into juvenile sheep. *Acta Biomaterialia*, 68, 41-52.
- GOLDSTEIN, S., CLARKE, D. R., WALSH, S. P., BLACK, K. S. & O'BRIEN, M. F. 2000. Transpecies heart valve transplant: advanced studies of a bioengineered xeno-autograft. *The Annals of Thoracic Surgery*, 70, 1962-1969.
- GOLOMB, G., SCHOEN, F. J., SMITH, M. S., LINDEN, J., DIXON, M. & LEVY, R. J. 1987. The role of glutaraldehyde-induced cross-links in calcification of bovine pericardium used in cardiac valve bioprostheses. *The American Journal of Pathology*, 127, 122-130.
- GORLIN, R. & GORLIN, S. G. 1951. Hydraulic formula for calculation of the area of the stenotic mitral valve, other cardiac valves, and central circulatory shunts. I. *American Heart Journal*, 41, 1-29.
- GOTT, V. L., ALEJO, D. E. & CAMERON, D. E. 2003. Mechanical heart valves: 50 years of evolution. *Ann Thorac Surg*, 76, S2230-9.
- GRAUSS, R. W., HAZEKAMP, M. G., OPPENHUIZEN, F., VAN MUNSTEREN, C. J., GITTEBERGER-DE GROOT, A. C. & DERUITER, M. C. 2005. Histological evaluation of decellularised porcine aortic valves: matrix changes due to different decellularisation methods☆. *European Journal of Cardio-Thoracic Surgery*, 27, 566-571.
- GUEDES, R., A. SILVA, J., VIRIATO, N. & PINTO, V. 2018. *Ligaments' clamping: a novel solution to prevent soft tissue slippage*.
- GUYTON, A. C. & HALL, J. E. 2006. *Textbook of Medical Physiology*, Elsevier Saunders.

- HANSEN, B., MENKIS, A. H. & VESELY, I. 1995. Longitudinal and radial distensibility of the porcine aortic root. *Ann Thorac Surg*, 60, S384-90.
- HARRISON, D. C., IBRAHIM, M. A., WEYMAN, A. E., KULLER, L. H., BLOT, W. J. & MILLER, D. E. 2013. The Bjork-Shiley convexo-concave heart valve experience from the perspective of the supervisory panel. *Am J Cardiol*, 112, 1921-31.
- HASAN, A., RAGAERT, K., SWIESZKOWSKI, W., SELIMOVIC, S., PAUL, A., CAMCI-UNAL, G., MOFRAD, M. R. K. & KHADEMHOSEINI, A. 2014. Biomechanical properties of native and tissue engineered heart valve constructs. *Journal of Biomechanics*, 47, 1949-1963.
- HEILIGER, R., LAMBERTZ, H., GEKS, J. & MITTERMAYER, C. 1987. [Comparative study of mechanical heart valves for implantation in mitral position]. *Herz*, 12, 405-12.
- HELDER, M. R. K., HENNESSY, R. S., SPOON, D. B., TEFFT, B. J., WITT, T. A., MARLER, R. J., PISLARU, S. V., SIMARI, R. D., STULAK, J. M. & LERMAN, A. 2016. Low-Dose Gamma Irradiation of Decellularized Heart Valves Results in Tissue Injury In Vitro and In Vivo. *The Annals of thoracic surgery*, 101, 667-674.
- HELDER, M. R. K., KOUCHOUKOS, N. T., ZEHR, K., DEARANI, J. A., MALESZEWSKI, J. J., LEDUC, C., HEINS, C. N. & SCHAFF, H. V. 2016. Late durability of decellularized allografts for aortic valve replacement: A word of caution. *The Journal of Thoracic and Cardiovascular Surgery*, 152, 1197-1199.
- HEMMER, W. B., DOSS, M., HANNEKUM, A. & KAPFER, X. 2000. Leaflet escape in a TEKNA and an original duromedics bileaflet valve. *Ann Thorac Surg*, 69, 942-4.
- HERBERT, A., BROWN, C., ROONEY, P., KEARNEY, J., INGHAM, E. & FISHER, J. 2016. Bi-linear mechanical property determination of acellular human patellar tendon grafts for use in anterior cruciate ligament replacement. *Journal of Biomechanics*, 49, 1607-1612.
- HILBERT, S. L., FERRANS, V. J., MCALLISTER, H. A. & COOLEY, D. A. 1992. Ionescu-Shiley bovine pericardial bioprostheses. Histologic and ultrastructural studies. *The American Journal of Pathology*, 140, 1195-1204.
- HO, S. Y. 2009. Structure and anatomy of the aortic root. *European Journal of Echocardiography*, 10, i3-i10.
- HOEKSTRA, F., KNOOP, C., VAESSEN, L., WASSENAAR, C., JUTTE, N., BOS, E., BOGERS, A. & WEIMAR, W. 1996. Donor-specific cellular immune response against human cardiac valve allografts. *Journal of Thoracic and Cardiovascular Surgery*, 112, 281-286.
- HOERSTRUP, S. P., SODIAN, R., DAEBRITZ, S., WANG, J., BACHA, E. A., MARTIN, D. P., MORAN, A. M., GULESERIAN, K. J., SPERLING, J. S., KAUSHAL, S., VACANTI, J. P., SCHOEN, F. J. & MAYER, J. E. 2000. Functional Living Trileaflet Heart Valves Grown In Vitro. *Circulation*, 102, lii-44-iii-49.
- HOFFMAN, J. I. 2013. The global burden of congenital heart disease. *Cardiovascular journal of Africa*, 24, 141-145.

- HOKKEN, R. B., BOGERS, A. J., TAAMS, M. A., SCHIKS-BERGHOURT, M. B., VAN HERWERDEN, L. A., ROELANDT, J. R. & BOS, E. 1997. Does the pulmonary autograft in the aortic position in adults increase in diameter? An echocardiographic study. *J Thorac Cardiovasc Surg*, 113, 667-74.
- HOLZAPFEL, G. A., SOMMER, G., GASSER, C. T. & REGITNIG, P. 2005. Determination of layer-specific mechanical properties of human coronary arteries with nonatherosclerotic intimal thickening and related constitutive modeling. *Am J Physiol Heart Circ Physiol*, 289, H2048-58.
- HOMANN, M., HAEHNEL, J. C., MENDLER, N., PAEK, S. U., HOLPER, K., MEISNER, H. & LANGE, R. 2000. Reconstruction of the RVOT with valved biological conduits: 25 years experience with allografts and xenografts☆. *European Journal of Cardio-Thoracic Surgery*, 17, 624-630.
- HONG, H., DONG, N., SHI, J., CHEN, S., GUO, C., HU, P. & QI, H. 2009. Fabrication of a novel hybrid scaffold for tissue engineered heart valve. *J Huazhong Univ Sci Technolog Med Sci*, 29, 599-603.
- HOPKINS, R. A. 2003. Aortic valve leaflet sparing and salvage surgery: evolution of techniques for aortic root reconstruction. *European Journal of Cardio-Thoracic Surgery*, 24, 886-897.
- HUTMACHER, D. W. 2001. Scaffold design and fabrication technologies for engineering tissues — state of the art and future perspectives. *Journal of Biomaterials Science, Polymer Edition*, 12, 107-124.
- ISHIHARA, T., FERRANS, V. J., BOYCE, S. W., JONES, M. & ROBERTS, W. C. 1981. Structure and classification of cuspal tears and perforations in porcine bioprosthetic cardiac valves implanted in patients. *American Journal of Cardiology*, 48, 665-678.
- ISO 5840 2015. 5840-1:2015: Cardiovascular implants -- Cardiac valve prostheses -- Part 1: General requirements; 5840-2:2015: Cardiovascular implants -- Cardiac valve prostheses -- Part 2: Surgically implanted heart valve substitutes. *Geneva: ISO Copyright Office; 2015. 55p.*
- ISO 7198 2016. Cardiovascular implants and extracorporeal systems -- Vascular prostheses - - Tubular vascular grafts and vascular patches.
- ISO 10993-13 2009. Biological evaluation of medical devices -- Part 1: Evaluation and testing within a risk management process.
- ISO 13485 2016. ISO 13485; Medical devices -- Quality management systems -- Requirements for regulatory purposes.
- IWASAKI, K., UMEZU, M., IJIMA, K. & IMACHI, K. 2002. Implications for the Establishment of Accelerated Fatigue Test Protocols for Prosthetic Heart Valves. *Artif Organs*, 26, 420-429.
- JENNINGS, L. M. 2001. *The Pulmonary Bioprosthetic valve*. Doctoral Thesis, University Of Leeds, UK.



- JENNINGS, L. M., BUTTERFIELD, M., BOOTH, C., WATTERSON, K. G. & FISHER, J. 2002. The pulmonary bioprosthesis heart valve: Its unsuitability for use as an aortic valve replacement. *Journal of Heart Valve Disease*, 11, 668-678.
- JENNINGS, L. M., BUTTERFIELD, M., WALKER, P. G., WATTERSON, K. G. & FISHER, J. 2001. The influence of ventricular input impedance on the hydrodynamic performance of bioprosthesis aortic roots in vitro. *Journal of Heart Valve Disease*, 10, 269-275.
- JIAO, T., CLIFTON, R. J., CONVERSE, G. L. & HOPKINS, R. A. 2011. Measurements of the Effects of Decellularization on Viscoelastic Properties of Tissues in Ovine, Baboon, and Human Heart Valves. *Tissue Engineering Part A*, 18, 423-431.
- KALEJS, M., STRADINS, P., LACIS, R., OZOLANTA, I., PAVARS, J. & KASYANOV, V. 2009. St Jude Epic heart valve bioprosthesis versus native human and porcine aortic valves - comparison of mechanical properties. *Interact Cardiovasc Thorac Surg*, 8, 553-6.
- KARCK, M. & HAVERICH, A. 2005. Aortic Valve Reimplantation According to the David Type I Technique. *Operative Techniques in Thoracic and Cardiovascular Surgery*, 10, 246-258.
- KASIMIR, M. T., RIEDER, E., SEEBACHER, G., SILBERHUMER, G., WOLNER, E., WEIGEL, G. & SIMON, P. 2003. Comparison of different decellularization procedures of porcine heart valves. *Int J Artif Organs*, 26, 421-7.
- KITAGAWA, T., MASUDA, Y., TOMINAGA, T. & KANO, M. 2001. Cellular biology of cryopreserved allograft valves. *J Med Invest*, 48, 123-32.
- KLABUNDE, R. 2011. *Cardiovascular Physiology Concepts*, Wolters Kluwer Health.
- KLABUNDE, R. E. 2005. *Cardiovascular physiology concepts*, Philadelphia, Pa. [u.a.], Lippincott Williams & Wilkins.
- KLUIN, J., TALACUA, H., SMITS, A. I. P. M., EMMERT, M. Y., BRUGMANS, M. C. P., FIORETTA, E. S., DIJKMAN, P. E., SÖNTJENS, S. H. M., DUIJVELSHOFF, R., DEKKER, S., JANSSEN-VAN DEN BROEK, M. W. J. T., LINTAS, V., VINK, A., HOERSTRUP, S. P., JANSSEN, H. M., DANKERS, P. Y. W., BAAIJENS, F. P. T. & BOUTEN, C. V. C. 2017. In situ heart valve tissue engineering using a bioresorbable elastomeric implant – From material design to 12 months follow-up in sheep. *Biomaterials*, 125, 101-117.
- KNEIB, C., VON GLEHN, C. Q. C., COSTA, F. D. A., COSTA, M. T. B. A. & SUSIN, M. F. 2012. Evaluation of humoral immune response to donor HLA after implantation of cellularized versus decellularized human heart valve allografts. *Tissue Antigens*, 80, 165-174.
- KNIGHT, R. L., BOOTH, C., WILCOX, H. E., FISHER, J. & INGHAM, E. 2005. Tissue engineering of cardiac valves: re-seeding of acellular porcine aortic valve matrices with human mesenchymal progenitor cells. *J Heart Valve Dis*, 14, 806-13.
- KODALI, S. K., VELAGAPUDI, P., HAHN, R. T., ABBOTT, D. & LEON, M. B. 2018. Valvular Heart Disease in Patients  $\geq 80$  Years of Age. *Journal of the American College of Cardiology*, 71, 2058-2072.

- KONUMA, T., DEVANEY, E. J., BOVE, E. L., GELEHRTER, S., HIRSCH, J. C., TAVAKKOL, Z. & OHYE, R. G. 2009. Performance of CryoValve SG Decellularized Pulmonary Allografts Compared With Standard Cryopreserved Allografts. *Annals of Thoracic Surgery*, 88, 849-855.
- KOOLBERGEN, D. R., HAZEKAMP, M. G., DE HEER, E., VAN HOORN, F., HUYSMANS, H. A., BRUIJN, J. A. & DION, R. A. E. 2002. Structural degeneration of pulmonary homografts used as aortic valve substitute underlines early graft failure. *European Journal of Cardio-Thoracic Surgery*, 22, 802-807.
- KORNBERG, A., WILDHIRT, S. M., SCHULZE, C. & KREUZER, E. 1999. Leaflet escape in Omnicarbon monoleaflet valve. *Eur J Cardiothorac Surg*, 15, 867-9.
- KOROSSIS, S. A., BOOTH, C., WILCOX, H. E., WATTERSON, K. G., KEARNEY, J. N., FISHER, J. & INGHAM, E. 2002. Tissue engineering of cardiac valve prostheses II: Biomechanical characterization of decellularized porcine aortic heart valves. *Journal of Heart Valve Disease*, 11, 463-471.
- KOROSSIS, S. A., WILCOX, H. E., WATTERSON, K. G., KEARNEY, J. N., INGHAM, E. & FISHER, J. 2005. In-vitro assessment of the functional performance of the decellularized intact porcine aortic root. *Journal of Heart Valve Disease*, 14, 408-421.
- KRUCINSKI, S., VESELY, I., DOKAINISH, M. A. & CAMPBELL, G. 1993. Numerical simulation of leaflet flexure in bioprosthetic valves mounted on rigid and expansile stents. *Journal of Biomechanics*, 26, 929-943.
- KUNZELMAN, K. S. & COCHRAN, R. P. 1992. Stress/strain characteristics of porcine mitral valve tissue: parallel versus perpendicular collagen orientation. *J Card Surg*, 7, 71-8.
- LAFLAMME, K., ROBERGE, C. J., GRENIER, G., REMY-ZOLGHADRI, M., POULIOT, S., BAKER, K., LABBE, R., D'ORLEANS-JUSTE, P., AUGER, F. A. & GERMAIN, L. 2006. Adventitia contribution in vascular tone: insights from adventitia-derived cells in a tissue-engineered human blood vessel. *FASEB J*, 20, 1245-7.
- LANGERAK, S. E., GROENINK, M., VAN DER WALL, E. E., WASSENAAR, C., VANBAVEL, E., VAN BAAL, M. C. & SPAAN, J. A. 2001. Impact of current cryopreservation procedures on mechanical and functional properties of human aortic homografts. *Transpl Int*, 14, 248-55.
- LEE, J. M., COURTMAN, D. W. & BOUGHNER, D. R. 1984. The glutaraldehyde-stabilized porcine aortic valve xenograft. I. Tensile viscoelastic properties of the fresh leaflet material. *J Biomed Mater Res*, 18, 61-77.
- LEE, J. M. & LANGDON, S. E. 1996. Thickness measurement of soft tissue biomaterials: a comparison of five methods. *J Biomech*, 29, 829-32.
- LEESON-DIETRICH, J., BOUGHNER, D. & VESELY, I. 1995. Porcine pulmonary and aortic valves: a comparison of their tensile viscoelastic properties at physiological strain rates. *J Heart Valve Dis*, 4, 88-94.

- LEI, Y., JIN, W., LUO, R., LI, G., GUO, G. & WANG, Y. 2018. Bioprosthetic heart valves' structural integrity improvement through exogenous amino donor treatments. *Journal of Materials Research*, 33, 2576-2585.
- LONDON, C. L., DAVIES, M. J., RICHARDSON, P. D. & BORN, G. V. R. 1993. Testing of small connective tissue specimens for the determination of the mechanical behaviour of atherosclerotic plaques. *Journal of Biomedical Engineering*, 15, 27-33.
- LEO, H. L., SIMON, H. A., DAS, L. P. & YOGANATHAN, A. P. 2006. Effect of hinge gap width on the microflow structures in 27-mm bileaflet mechanical heart valves. *J Heart Valve Dis*, 15, 800-8.
- LI, J., LUO, X. Y. & KUANG, Z. B. 2001. A nonlinear anisotropic model for porcine aortic heart valves. *Journal of Biomechanics*, 34, 1279-1289.
- LIAO, J., JOYCE, E. M. & SACKS, M. S. 2008. Effects of decellularization on the mechanical and structural properties of the porcine aortic valve leaflet. *Biomaterials*, 29, 1065-74.
- LICHTENBERG, A., TUDORACHE, I., CEBOTARI, S., RINGES-LICHTENBERG, S., STURZ, G., HOEFFLER, K., HURSCHELER, C., BRANDES, G., HILFIKER, A. & HAVERICH, A. 2006. In vitro re-endothelialization of detergent decellularized heart valves under simulated physiological dynamic conditions. *Biomaterials*, 27, 4221-4229.
- LIM, H.-G., KIM, G. B., JEONG, S. & KIM, Y. J. 2015. Development of a next-generation tissue valve using a glutaraldehyde-fixed porcine aortic valve treated with decellularization,  $\alpha$ -galactosidase, space filler, organic solvent and detoxification. *European Journal of Cardio-Thoracic Surgery*, 48, 104-113.
- LINCOLN, J. & YUTZEY, K. E. 2011. Molecular and developmental mechanisms of congenital heart valve disease. *Birth Defects Res A Clin Mol Teratol*, 91, 526-34.
- LIU, Y., ALLAIRE, P., WOOD, H. & OLSEN, D. 2005. Design and initial testing of a mock human circulatory loop for left ventricular assist device performance testing. *Artif Organs*, 29, 341-5.
- LOCKIE, K. J., BUTTERFIELD, M., FISHER, J., JUSTER, N. P., WATTERSON, K. & DAVIES, G. A. 1993. GEOMETRY OF HOMOGRAFT VALVE LEAFLETS - EFFECT OF DILATION OF THE AORTA AND THE AORTIC ROOT. *Annals of Thoracic Surgery*, 56, 125-130.
- LOGER, K., DE MIRANDA, R. L., ENGEL, A., MARCZYNSKI-BÜHLOW, M., LUTTER, G. & QUANDT, E. 2014. Fabrication and Evaluation of Nitinol Thin Film Heart Valves. *Cardiovascular Engineering and Technology*, 5, 308-316.
- LU, X., PANDIT, A. & KASSAB, G. S. 2004. Biaxial incremental homeostatic elastic moduli of coronary artery: two-layer model. *Am J Physiol Heart Circ Physiol*, 287, H1663-9.
- LUCIANI, G. B., LUCCHESI, G., DE RITA, F., PUPPINI, G., FAGGIAN, G. & MAZZUCCO, A. 2012. Reparative surgery of the pulmonary autograft: experience with Ross reoperations. *Eur J Cardiothorac Surg*, 41, 1309-14; discussion 1314-5.

- LUO, J. 2011. *Production and characterisation of acellular porcine pulmonary heart valve conduits*. PhD Thesis, University of Leeds.
- LUO, J., KOROSSIS, S. A., WILSHAW, S. P., JENNINGS, L. M., FISHER, J. & INGHAM, E. 2014. Development and Characterization of Acellular Porcine Pulmonary Valve Scaffolds for Tissue Engineering. *Tissue Engineering Part A*, 20, 2963-2974.
- MAISH, M. S., HOFFMAN-KIM, D., KRUEGER, P. M., SOUZA, J. M., HARPER, J. J., 3RD & HOPKINS, R. A. 2003. Tricuspid valve biopsy: a potential source of cardiac myofibroblast cells for tissue-engineered cardiac valves. *J Heart Valve Dis*, 12, 264-9.
- MALAMED, S. F. 2007. *Medical Emergencies in the Dental Office - E-Book*, Elsevier Health Sciences.
- MAREI, I., CHESTER, A., CARUBELLI, I., PRODROMAKIS, T., TRANTIDOU, T. & YACOUB, M. H. 2015. Assessment of Parylene C Thin Films for Heart Valve Tissue Engineering. *Tissue Eng Part A*, 21, 2504-14.
- MARTIN, C. & SUN, W. 2012. Biomechanical characterization of aortic valve tissue in humans and common animal models. *Journal of biomedical materials research. Part A*, 100, 10.1002/jbm.a.34099.
- MAVRILAS, D. & MISSIRLIS, Y. 1991. An approach to the optimization of preparation of bioprosthetic heart valves. *Journal of Biomechanics*, 24, 331-339.
- MAYER, J. E., JR., SHIN'OKA, T. & SHUM-TIM, D. 1997. Tissue engineering of cardiovascular structures. *Curr Opin Cardiol*, 12, 528-32.
- MAZINE, A., ROCHA, R. V., EL-HAMAMSY, I. & ET AL. 2018. Ross procedure vs mechanical aortic valve replacement in adults: A systematic review and meta-analysis. *JAMA Cardiology*, 3, 978-987.
- MCCLOSKEY, K., PONSONBY, A.-L., CARLIN, J. B., JACHNO, K., CHEUNG, M., SKILTON, M. R., KOLEFF, J., VUILLERMIN, P. & BURGNER, D. 2014. Reproducibility of aortic intima-media thickness in infants using edge-detection software and manual caliper measurements. *Cardiovascular Ultrasound*, 12, 18.
- MCGREGOR, C., BYRNE, G., RAHMANI, B., CHISARI, E., KYRIAKOPOULOU, K. & BURRIESCI, G. 2016. Physical equivalency of wild type and galactose  $\alpha$  1,3 galactose free porcine pericardium; a new source material for bioprosthetic heart valves. *Acta Biomaterialia*, 41, 204-209.
- MENDELSON, K. & SCHOEN, F. J. 2006. Heart valve tissue engineering: concepts, approaches, progress, and challenges. *Ann Biomed Eng*, 34, 1799-819.
- MERRICK, M. A. 2002. Secondary injury after musculoskeletal trauma: a review and update. *Journal of athletic training*, 37, 209-217.
- MEURIS, B. & FLAMENG, W. 2008. Antimineralization Treatment. *Encyclopedia of Biomaterials and Biomedical Engineering, Second Edition (Online Version)*. CRC Press.

- MILNOR, W. R. 1990. *Cardiovascular physiology*, New York, Oxford University Press.
- MIRNAJAFI, A., RAYMER, J. M., MCCLURE, L. R. & SACKS, M. S. 2006. The flexural rigidity of the aortic valve leaflet in the commissural region. *Journal of Biomechanics*, 39, 2966-2973.
- MISFELD, M. & SIEVERS, H. H. 2007. Heart valve macro- and microstructure. *Philos Trans R Soc Lond B Biol Sci*, 362, 1421-36.
- MOHAMMADI, S., BAILLOT, R., VOISINE, P., MATHIEU, P. & DAGENAIS, F. 2006. Structural deterioration of the Freestyle aortic valve: Mode of presentation and mechanisms. *The Journal of Thoracic and Cardiovascular Surgery*, 132, 401-406.
- MOKHLES, M. M., RIZOPOULOS, D., ANDRINOPOULOU, E. R., BEKKERS, J. A., ROOS-HESELINK, J. W., LESAFFRE, E., BOGERS, A. J. & TAKKENBERG, J. J. 2012. Autograft and pulmonary allograft performance in the second post-operative decade after the Ross procedure: insights from the Rotterdam Prospective Cohort Study. *Eur Heart J*, 33, 2213-24.
- MOORADIAN, D. L. 2016. *Extracellular Matrix-derived Implants in Clinical Medicine*, Elsevier Science.
- NAGY, Z. & WATTERSON, K. G. 2008. [Ross procedure versus mechanical aortic valve replacement in young adults]. *Magy Seb*, 61 Suppl, 23-7.
- NAGY, Z. L., FISHER, J., WALKER, P. G. & WATTERSON, K. G. 2000. The in vitro hydrodynamic characteristics of the porcine pulmonary valve and root with regard to the Ross procedure. *The Journal of Thoracic and Cardiovascular Surgery*, 120, 284-289.
- NAKAYAMA, K. H., BATCHELDER, C. A., LEE, C. I. & TARANTAL, A. F. 2010. Decellularized rhesus monkey kidney as a three-dimensional scaffold for renal tissue engineering. *Tissue engineering. Part A*, 16, 2207-2216.
- NARINE, K., ING, E. C., CORNELISSEN, M., DESOMER, F., BEELE, H., VANLANGENHOVE, L., SMET, S. D. & NOOTEN, G. V. 2006. Readily available porcine aortic valve matrices for use in tissue valve engineering. Is cryopreservation an option? *Cryobiology*, 53, 169-81.
- NATALI, A., PAVAN, P., CARNIEL, E., DARIO, P. & IZZO, I. 2008. Characterization of soft tissue mechanics with aging. *Engineering in Medicine and Biology Magazine, IEEE*, 27, 15-22.
- NEUMANN, A., SARIKOUCH, S., BREYMAN, T., CEBOTARI, S., BOETHIG, D., HORKE, A., BEERBAUM, P., WESTHOFF-BLECK, M., BERTRAM, H., ONO, M., TUDORACHE, I., HAVERICH, A. & BEUTEL, G. 2014. Early systemic cellular immune response in children and young adults receiving decellularized fresh allografts for pulmonary valve replacement. *Tissue Eng Part A*, 20, 1003-11.
- NKOMO, V. T., GARDIN, J. M., SKELTON, T. N., GOTTDIENER, J. S., SCOTT, C. G. & ENRIQUEZ-SARANO, M. 2006. Burden of valvular heart diseases: a population-based study. *Lancet*, 368, 1005-11.

- NUMATA, S., FUJISATO, T., NIWAYA, K., ISHIBASHI-UEDA, H., NAKATANI, T. & KITAMURA, S. 2004. Immunological and histological evaluation of decellularized allograft in a pig model: comparison with cryopreserved allograft. *J Heart Valve Dis*, 13, 984-90.
- O'BRIEN, M. F., HARROCKS, S., STAFFORD, E. G., GARDNER, M. A., POHLNER, P. G., TESAR, P. J. & STEPHENS, F. 2001. The homograft aortic valve: a 29-year, 99.3% follow up of 1,022 valve replacements. *J Heart Valve Dis*, 10, 334-44; discussion 335.
- O'BRIEN, M. F., HARROCKS, S., STAFFORD, E. G., GARDNER, M. A. H., POHLNER, P. G., TESAR, P. J. & STEPHENS, F. 2001. The homograft aortic valve: A 29-year, 99.3% follow up of 1,022 valve replacements. *Journal of Heart Valve Disease*, 10, 334-344.
- OEI, F. B., STEGMANN, A. P., VAN DER HAM, F., ZONDERVAN, P. E., VAESSEN, L. M., BAAN, C. C., WEIMAR, W. & BOGERS, A. J. 2002. The presence of immune stimulatory cells in fresh and cryopreserved donor aortic and pulmonary valve allografts. *J Heart Valve Dis*, 11, 315-24; discussion 325.
- OZAWA, H., UENO, T., TAIRA, M., TODA, K., KURATANI, T. & SAWA, Y. 2018. Application of a Fresh Decellularized Pulmonary Allograft for Pulmonary Valve Replacement in Japan. *Circulation Journal*, 82, 1526-1533.
- PAK, O., ALDASHEV, A., WELSH, D. & PEACOCK, A. 2007. The effects of hypoxia on the cells of the pulmonary vasculature. *European Respiratory Journal*, 30, 364-372.
- PANIAGUA GUTIERREZ, J. R., BERRY, H., KOROSSIS, S., MIRSADRAEE, S., LOPES, S. V., DA COSTA, F., KEARNEY, J., WATTERSON, K., FISHER, J. & INGHAM, E. 2015. Regenerative potential of low-concentration SDS-decellularized porcine aortic valved conduits in vivo. *Tissue Eng Part A*, 21, 332-42.
- PARK, S., HWANG, H. Y., KIM, K.-H., KIM, K.-B. & AHN, H. 2012. Midterm Follow-up after Cryopreserved Homograft Replacement in the Aortic Position. *The Korean Journal of Thoracic and Cardiovascular Surgery*, 45, 30-34.
- PATWARDHAN, A. M. & VAIDEESWAR, P. 2004. Stress strain characteristics of glutaraldehyde treated porcine aortic valve tissue following ethanol treatment. *Indian Journal of Thoracic and Cardiovascular Surgery*, 20, 67-71.
- PENTA, A., QURESHI, S., RADLEY-SMITH, R. & YACOUB, M. H. 1984. Patient status 10 or more years after 'fresh' homograft replacement of the aortic valve. *Circulation*, 70, 1182-6.
- PERRI, G., POLITO, A., ESPOSITO, C., ALBANESE, S. B., FRANCALANCI, P., PONGIGLIONE, G. & CAROTTI, A. 2012. Early and late failure of tissue-engineered pulmonary valve conduits used for right ventricular outflow tract reconstruction in patients with congenital heart disease. *Eur J Cardiothorac Surg*, 41, 1320-5.
- PIBAROT, P. & DUMESNIL, J. G. 2009. Prosthetic Heart Valves Selection of the Optimal Prosthesis and Long-Term Management. *Circulation*, 119, 1034-1048.
- PIERCE, E. L., SIEFERT, A. W., PAUL, D. M., WELLS, S. K., BLOODWORTH, C. H. T., TAKEBAYASHI, S., AOKI, C., JENSEN, M. O., GILLESPIE, M. J., GORMAN, R. C., GORMAN, J. H., 3RD & YOGANATHAN, A. P. 2016. How Local Annular Force and

- Collagen Density Govern Mitral Annuloplasty Ring Dehiscence Risk. *Ann Thorac Surg*, 102, 518-26.
- PIÑÓN, M., DURÁN, D., PAZOS, P. & PRADAS, G. 2015. Leaflet tear in a Trifecta aortic bioprosthesis 34 months after implantation. *Interactive CardioVascular and Thoracic Surgery*, 20, 281-282.
- PUPELLO, D. F., N. BESSONE, L., P. HIRO, S., LOPEZ-CUENCA, E., GLATTERER GLATTERER, M. S., C. BROCK, J., W. ANGELL, W. & EBRA, G. 1992. *Bioprosthetic Valve Durability in the Elderly: The Second Decade*.
- QUINN, K. P. & WINKELSTEIN, B. A. 2011. Preconditioning is correlated with altered collagen fiber alignment in ligament. *J Biomech Eng*, 133, 064506.
- QUINN, R. W., HILBERT, S. L., BERT, A. A., DRAKE, B. W., BUSTAMANTE, J. A., FENTON, J. E., MORIARTY, S. J., NEIGHBORS, S. L., LOFLAND, G. K. & HOPKINS, R. A. 2011. Performance and morphology of decellularized pulmonary valves implanted in juvenile sheep. *Ann Thorac Surg*, 92, 131-7.
- QUINN, R. W., L. HILBERT, S., CONVERSE, G., BERT, A., BUSE, E., DRAKE, W., ARMSTRONG, M., J. MORIARTY, S., LOFLAND, G. & HOPKINS, R. 2012. *Enhanced Autologous Re-endothelialization of Decellularized and Extracellular Matrix Conditioned Allografts Implanted Into the Right Ventricular Outflow Tracts of Juvenile Sheep*.
- RAGHAV, V., OKAFOR, I., QUACH, M., DANG, L., MARQUEZ, S. & YOGANATHAN, A. P. 2016. Long-Term Durability of Carpentier-Edwards Magna Ease Valve: A One Billion Cycle In Vitro Study. *Ann Thorac Surg*, 101, 1759-65.
- RAGHAVAN, D. 2008. *ECM STABILIZATION STRATEGIES FOR BIOPROSTHETIC HEART VALVES FOR IMPROVED DURABILITY*.
- RAHMANI, B., TZAMTZIS, S., SHERIDAN, R., MULLEN, M. J., YAP, J., SEIFALIAN, A. M. & BURRIESCI, G. 2017. In Vitro Hydrodynamic Assessment of a New Transcatheter Heart Valve Concept (the TRISKELE). *J Cardiovasc Transl Res*, 10, 104-115.
- REGULATION 2017/745. Regulation (EU) 2017/745 of the European Parliament and of the Council of 5 April 2017 on medical devices, amending Directive 2001/83/EC, Regulation (EC) No 178/2002 and Regulation (EC) No 1223/2009 and repealing Council Directives 90/385/EEC and 93/42/EEC (Text with EEA relevance. ).
- REIMER, J. M., SYEDAIN, Z. H., HAYNIE, B. H. T. & TRANQUILLO, R. T. 2015. Pediatric tubular pulmonary heart valve from decellularized engineered tissue tubes. *Biomaterials*, 62, 88-94.
- RIEDER, E., KASIMIR, M. T., SILBERHUMER, G., SEEBACHER, G., WOLNER, E., SIMON, P. & WEIGEL, G. 2004. Decellularization protocols of porcine heart valves differ importantly in efficiency of cell removal and susceptibility of the matrix to recellularization with human vascular cells. *J Thorac Cardiovasc Surg*, 127, 399-405.
- RIPPEL, R. A., GHANBARI, H. & SEIFALIAN, A. M. 2012. Tissue-engineered heart valve: future of cardiac surgery. *World J Surg*, 36, 1581-91.

- RIZZOLI, G., RUSSO, R., VALENTE, S., MAZZUCCO, A., VALFRE, C., BRUMANA, T., ARU, G., RUBINO, M., ROCCO, F. & GALLUCCI, V. 1984. Dehiscence of aortic valve prostheses: analysis of a ten-year experience. *Int J Cardiol*, 6, 207-21.
- ROACH, M. R. & BURTON, A. C. 1957. THE REASON FOR THE SHAPE OF THE DISTENSIBILITY CURVES OF ARTERIES. *Canadian Journal of Biochemistry and Physiology*, 35, 681-690.
- ROBERTS, M. B. V. & MITCHELMORE, J. 1985. *Biology for CXC*, Walton-on-Thames, Surrey, Eng., Nelson.
- ROBINSON, P. S., JOHNSON, S. L., EVANS, M. C., BAROCAS, V. H. & TRANQUILLO, R. T. 2008. Functional tissue-engineered valves from cell-remodeled fibrin with commissural alignment of cell-produced collagen. *Tissue Eng Part A*, 14, 83-95.
- ROGER, V. L., GO, A. S., LLOYD-JONES, D. M., BENJAMIN, E. J., BERRY, J. D., BORDEN, W. B., BRAVATA, D. M., DAI, S., FORD, E. S., FOX, C. S., FULLERTON, H. J., GILLESPIE, C., HAILPERN, S. M., HEIT, J. A., HOWARD, V. J., KISSELA, B. M., KITTNER, S. J., LACKLAND, D. T., LICHTMAN, J. H., LISABETH, L. D., MAKUC, D. M., MARCUS, G. M., MARELLI, A., MATCHAR, D. B., MOY, C. S., MOZAFFARIAN, D., MUSSOLINO, M. E., NICHOL, G., PAYNTER, N. P., SOLIMAN, E. Z., SORLIE, P. D., SOTOODEHNIA, N., TURAN, T. N., VIRANI, S. S., WONG, N. D., WOO, D. & TURNER, M. B. 2012. Heart disease and stroke statistics--2012 update: a report from the American Heart Association. *Circulation*, 125, e2-e220.
- ROOSENS, A., ASADIAN, M., DE GEYTER, N., SOMERS, P. & CORNELISSEN, R. 2017. Complete Static Repopulation of Decellularized Porcine Tissues for Heart Valve Engineering: An in vitro Study. *Cells Tissues Organs*, 204, 270-282.
- ROSS, D., JACKSON, M. & DAVIES, J. 1991. PULMONARY AUTOGRAFT AORTIC-VALVE REPLACEMENT - LONG-TERM RESULTS. *Journal of Cardiac Surgery*, 6, 529-533.
- ROUSSEAU, E. P. M., SAUREN, A., VANHOUT, M. C. & VANSTEENHOVEN, A. A. 1983. ELASTIC AND VISCOELASTIC MATERIAL BEHAVIOR OF FRESH AND GLUTARALDEHYDE-TREATED PORCINE AORTIC-VALVE TISSUE. *Journal of Biomechanics*, 16, 339-&.
- RUFFER, A., PURBOJO, A., CICHA, I., GLOCKLER, M., POTAPOV, S., DITTRICH, S. & CESNJEVAR, R. A. 2010. Early failure of xenogenous de-cellularised pulmonary valve conduits - a word of caution! *European Journal of Cardio-Thoracic Surgery*, 38, 78-85.
- SABBAH, H. N., HAMID, M. S. & STEIN, P. D. 1986. MECHANICAL STRESSES ON CLOSED CUSPS OF PORCINE BIOPROSTHETIC VALVES - CORRELATION WITH SITES OF CALCIFICATION. *Annals of Thoracic Surgery*, 42, 93-96.
- SACKS, M. 2000. Biaxial Mechanical Evaluation of Planar Biological Materials. *Journal of elasticity and the physical science of solids*, 61, 199-246.
- SACKS, M. S. 2001. The Biomechanical Effects of Fatigue on the Porcine Bioprosthetic Heart Valve. 11, 17.



- SACKS, M. S., MERRYMAN, W. D. & SCHMIDT, D. E. 2009. On the biomechanics of heart valve function. *Journal of Biomechanics*, 42, 1804-1824.
- SACKS, M. S. & SCHOEN, F. J. 2002. Collagen fiber disruption occurs independent of calcification in clinically explanted bioprosthetic heart valves. *J Biomed Mater Res*, 62, 359-71.
- SACKS, M. S., SCHOEN, F. J. & MAYER, J. E. 2009. Bioengineering challenges for heart valve tissue engineering. *Annu Rev Biomed Eng*, 11, 289-313.
- SACKS, M. S. & SMITH, D. B. 1998. Effects of accelerated testing on porcine bioprosthetic heart valve fiber architecture. *Biomaterials*, 19, 1027-36.
- SACKS, M. S. & SUN, W. 2003. Multiaxial mechanical behavior of biological materials. *Annu Rev Biomed Eng*, 5, 251-84.
- SACKS, M. S. & YOGANATHAN, A. P. 2007. Heart valve function: a biomechanical perspective. *Philosophical Transactions of the Royal Society B-Biological Sciences*, 362, 1369-1391.
- SAMPATH KUMAR, A., TALWAR, S., SAXENA, A. & SINGH, R. 2006. Ross procedure in rheumatic aortic valve disease. *Eur J Cardiothorac Surg*, 29, 156-61.
- SANTORO, R., VENKATESWARAN, S., AMADEO, F., ZHANG, R., BRIOSCHI, M., CALLANAN, A., AGRIFOGLIO, M., BANFI, C., BRADLEY, M. & PESCE, M. 2017. Acrylate-based materials for heart valve scaffold engineering. *Biomater Sci*, 6, 154-167.
- SARIKOUCH, S., HORKE, A., TUDORACHE, I., BEERBAUM, P., WESTHOFF-BLECK, M., BOETHIG, D., REPIN, O., MANIUC, L., CIUBOTARU, A., HAVERICH, A. & CEBOTARI, S. 2016. Decellularized fresh homografts for pulmonary valve replacement: a decade of clinical experience. *Eur J Cardiothorac Surg*, 50, 281-90.
- SAUREN, A. A., VAN HOUT, M. C., VAN STEENHOVEN, A. A., VELDPAUS, F. E. & JANSSEN, J. D. 1983. The mechanical properties of porcine aortic valve tissues. *J Biomech*, 16, 327-37.
- SCHENKE-LAYLAND, K., OPITZ, F., GROSS, M., DORING, C., HALBHUBER, K. J., SCHIRRMEISTER, F., WAHLERS, T. & STOCK, U. A. 2003. Complete dynamic repopulation of decellularized heart valves by application of defined physical signals - an in vitro study. *Cardiovascular Research*, 60, 497-509.
- SCHICHL, K. & AFFELD, K. 1993. A computer controlled versatile pulse duplicator for precision testing of artificial heart valves. *Int J Artif Organs*, 16, 722-8.
- SCHMIDT, A., BRIXIUS, K. & BLOCH, W. 2007. Endothelial precursor cell migration during vasculogenesis. *Circ Res*, 101, 125-36.
- SCHOEN, F. J., FERNANDEZ, J., GONZALEZ-LAVIN, L. & CERNAIANU, A. 1987. Causes of failure and pathologic findings in surgically removed Ionescu-Shiley standard bovine pericardial heart valve bioprostheses: emphasis on progressive structural deterioration. *Circulation*, 76, 618-27.

- SCHOEN, F. J. & LEVY, R. J. 1999. Tissue heart valves: Current challenges and future research perspectives. *Journal of Biomedical Materials Research*, 47, 439-465.
- SCHUSTER, A., GRÜNWARD, I., CHIRIBIRI, A., SOUTHWORTH, R., ISHIDA, M., HAY, G., NEUMANN, N., MORTON, G., PERERA, D., SCHAEFFTER, T. & NAGEL, E. 2010. An isolated perfused pig heart model for the development, validation and translation of novel cardiovascular magnetic resonance techniques. *Journal of Cardiovascular Magnetic Resonance*, 12, 53.
- SCHUSTER, P. R. & WAGNER, J. W. 1989. A preliminary durability study of two types of low-profile pericardial bioprosthetic valves through the use of accelerated fatigue testing and flow characterization. *J Biomed Mater Res*, 23, 207-22.
- SEDDON, A. M., CURNOW, P. & BOOTH, P. J. 2004. Membrane proteins, lipids and detergents: not just a soap opera. *Biochimica et Biophysica Acta (BBA) - Biomembranes*, 1666, 105-117.
- SEEBACHER, G., GRASL, C., STOIBER, M., RIEDER, E., KASIMIR, M.-T., DUNKLER, D., SIMON, P., WEIGEL, G. & SCHIMA, H. 2008. Biomechanical Properties of Decellularized Porcine Pulmonary Valve Conduits. *Artif Organs*, 32, 28-35.
- SETTON, L. A., TOHYAMA, H. & MOW, V. C. 1998. Swelling and curling behaviors of articular cartilage. *J Biomech Eng*, 120, 355-61.
- SHADDY, R. E. & HAWKINS, J. A. 2002. Immunology and failure of valved allografts in children. *Annals of Thoracic Surgery*, 74, 1271-1275.
- SIDDIQUI, R. F., ABRAHAM, J. R. & BUTANY, J. 2009. Bioprosthetic heart valves: modes of failure. *Histopathology*, 55, 135-144.
- SIEVERS, H. H., STIERLE, U., SCHMIDTKE, C. & BECHTEL, M. 2003. Decellularized pulmonary homograft (SynerGraft) for reconstruction of the right ventricular outflow tract: first clinical experience. *Z Kardiol*, 92, 53-9.
- SIMON, P., KASIMIR, M. T., SEEBACHER, G., WEIGEL, G., ULLRICH, R., SALZER-MUHAR, U., RIEDER, E. & WOLNER, E. 2003. Early failure of the tissue engineered porcine heart valve SYNERGRAFT (TM) in pediatric patients. *European Journal of Cardio-Thoracic Surgery*, 23, 1002-1006.
- SMITH, D. B., SACKS, M. S., PATTANY, P. M. & SCHROEDER, R. 1999. Fatigue-induced changes in bioprosthetic heart valve three-dimensional geometry and the relation to tissue damage. *J Heart Valve Dis*, 8, 25-33.
- SODIAN, R., SPERLING, J. S., MARTIN, D. P., EGOZY, A., STOCK, U., MAYER, J. E., JR. & VACANTI, J. P. 2000. Fabrication of a trileaflet heart valve scaffold from a polyhydroxyalkanoate biopolyester for use in tissue engineering. *Tissue Eng*, 6, 183-8.
- SOKOLIS, D. P., BOUDOULAS, H. & KARAYANNACOS, P. E. 2002. Assessment of the aortic stress-strain relation in uniaxial tension. *J Biomech*, 35, 1213-23.

- SPINA, M., ORTOLANI, F., MESSLEMANI, A. E., GANDAGLIA, A., BUJAN, J., GARCIA-HONDUVILLA, N., VESELY, I., GEROSA, G., CASAROTTO, D., PETRELLI, L. & MARCHINI, M. 2003. Isolation of intact aortic valve scaffolds for heart-valve bioprostheses: Extracellular matrix structure, prevention from calcification, and cell repopulation features. *Journal of Biomedical Materials Research Part A*, 67A, 1338-1350.
- STAAB, M. E., NISHIMURA, R. A., DEARANI, J. A. & ORSZULAK, T. A. 1998. Aortic valve homografts in adults: a clinical perspective. *Mayo Clin Proc*, 73, 231-8.
- STARR, A., FESSLER, C. L., GRUNKEMEIER, G. & HE, G. W. 2002. Heart valve replacement surgery: past, present and future. *Clin Exp Pharmacol Physiol*, 29, 735-8.
- STEHLE, R. & IORGA, B. 2010. Kinetics of cardiac sarcomeric processes and rate-limiting steps in contraction and relaxation. *J Mol Cell Cardiol*, 48, 843-50.
- STEINHOFF, G., STOCK, U., KARIM, N., MERTSCHING, H., TIMKE, A., MELISS, R. R., PETHIG, K., HAVERICH, A. & BADER, A. 2000. Tissue engineering of pulmonary heart valves on allogenic acellular matrix conduits - In vivo restoration of valve tissue. *Circulation*, 102, 50-55.
- STELLA, J. A., LIAO, J. & SACKS, M. S. 2007. TIME DEPENDENT BIAXIAL MECHANICAL BEHAVIOR OF THE AORTIC HEART VALVE LEAFLET. *Journal of biomechanics*, 40, 3169-3177.
- STOCK, U. A. & MAYER, J. E., JR. 2001. Tissue engineering of cardiac valves on the basis of PGA/PLA Co-polymers. *J Long Term Eff Med Implants*, 11, 249-60.
- STRADINS, P., LACIS, R., OZOLANTA, I., PURINA, B., OSE, V., FELDMANE, L. & KASYANOV, V. 2004. Comparison of biomechanical and structural properties between human aortic and pulmonary valve. *European Journal of Cardio-Thoracic Surgery*, 26, 634-639.
- SUH, Y. J., KIM, Y. J., HONG, Y. J., LEE, H.-J., HUR, J., IM, D. J., KIM, Y. J. & CHOI, B. W. 2015. Measurement of Opening and Closing Angles of Aortic Valve Prostheses In Vivo Using Dual-Source Computed Tomography: Comparison with Those of Manufacturers' in 10 Different Types. *Korean Journal of Radiology*, 16, 1012-1023.
- SUTTON, J. P., 3RD, HO, S. Y. & ANDERSON, R. H. 1995. The forgotten interleaflet triangles: a review of the surgical anatomy of the aortic valve. *Ann Thorac Surg*, 59, 419-27.
- SYEDAIN, Z., REIMER, J., SCHMIDT, J., LAHTI, M., BERRY, J., BIANCO, R. & TRANQUILLO, R. T. 2015. 6-month aortic valve implantation of an off-the-shelf tissue-engineered valve in sheep. *Biomaterials*, 73, 175-84.
- SYEDAIN, Z. H., MEIER, L. A., REIMER, J. M. & TRANQUILLO, R. T. 2013. Tubular heart valves from decellularized engineered tissue. *Annals of biomedical engineering*, 41, 2645-2654.
- TAKKENBERG, J. J., VAN HERWERDEN, L. A., GALEMA, T. W., BEKKERS, J. A., KLEYBURGLINKERS, V. E., EIJKEMANS, M. J. & BOGERS, A. J. 2006. Serial echocardiographic assessment of neo-aortic regurgitation and root dimensions after the modified Ross procedure. *J Heart Valve Dis*, 15, 100-6; discussion 106-7.

- TAVAKKOL, Z., GELEHRTER, S., GOLDBERG, C. S., BOVE, E. L., DEVANEY, E. J. & OHYE, R. G. 2005. Superior durability of SynerGraft pulmonary allografts compared with standard cryopreserved allografts. *Ann Thorac Surg*, 80, 1610-4.
- THEODORIDIS, K., MÜLLER, J., RAMM, R., FINDEISEN, K., ANDRÉE, B., KOROSSIS, S., HAVERICH, A. & HILFIKER, A. 2016. Effects of combined cryopreservation and decellularization on the biomechanical, structural and biochemical properties of porcine pulmonary heart valves. *Acta Biomaterialia*, 43, 71-77.
- THUBRIKAR, M. J. 2018. *The Aortic Valve*, CRC Press.
- THUBRIKAR, M. J., DECK, J. D., AOUAD, J. & NOLAN, S. P. 1983. Role of mechanical stress in calcification of aortic bioprosthetic valves. *J Thorac Cardiovasc Surg*, 86, 115-25.
- THUBRIKAR, M. J., SKINNER, J. R., EPPINK, R. T. & NOLAN, S. P. 1982. Stress analysis of porcine bioprosthetic heart valves in vivo. *J Biomed Mater Res*, 16, 811-26.
- TORPY, J. M., BURKE, A. E. & GLASS, R. M. 2007. Heart valve infections. *JAMA*, 297, 1396-1396.
- TOZZI, P., AL-DARWEESH, A., VOGT, P. & STUMPE, F. 2001. Silver-coated prosthetic heart valve: a double-bladed weapon. *European Journal of Cardio-Thoracic Surgery*, 19, 729-731.
- TSAMIS, A., KRAWIEC, J. T. & VORP, D. A. 2013. Elastin and collagen fibre microstructure of the human aorta in ageing and disease: a review. *Journal of The Royal Society Interface*, 10.
- TSENG, H., KIM, E. J., CONNELL, P. S., AYOUB, S., SHAH, J. V. & GRANDE-ALLEN, K. J. 2013. The Tensile and Viscoelastic Properties of Aortic Valve Leaflets Treated with a Hyaluronidase Gradient. *Cardiovascular Engineering and Technology*, 4, 151-160.
- TUDORACHE, I., CEBOTARI, S., STURZ, G., KIRSCH, L., HURSCHLER, C., HILFIKER, A., HAVERICH, A. & LICHTENBERG, A. 2007. Tissue engineering of heart valves: Biomechanical and morphological properties of decellularized heart valves. *Journal of Heart Valve Disease*, 16, 567-573.
- TUDORACHE, I., HORKE, A., CEBOTARI, S., SARIKOUCH, S., BOETHIG, D., BREYMAN, T., BEERBAUM, P., BERTRAM, H., WESTHOFF-BLECK, M., THEODORIDIS, K., BOBYLEV, D., CHEPTANARU, E., CIUBOTARU, A. & HAVERICH, A. 2016. Decellularized aortic homografts for aortic valve and aorta ascendens replacement. *European Journal of Cardio-Thoracic Surgery*, 50, 89-97.
- VAFAGEE, T., THOMAS, D., DESAI, A., JENNINGS, L. M., BERRY, H., ROONEY, P., KEARNEY, J., FISHER, J. & INGHAM, E. 2016. Decellularization of human donor aortic and pulmonary valved conduits using low concentration sodium dodecyl sulfate. *J Tissue Eng Regen Med*.
- VAN SOLDT, B. J., DANIELSEN, C. C. & WANG, T. 2015. The mechanical properties of the systemic and pulmonary arteries of Python regius correlate with blood pressures. *J Morphol*, 276, 1412-21.

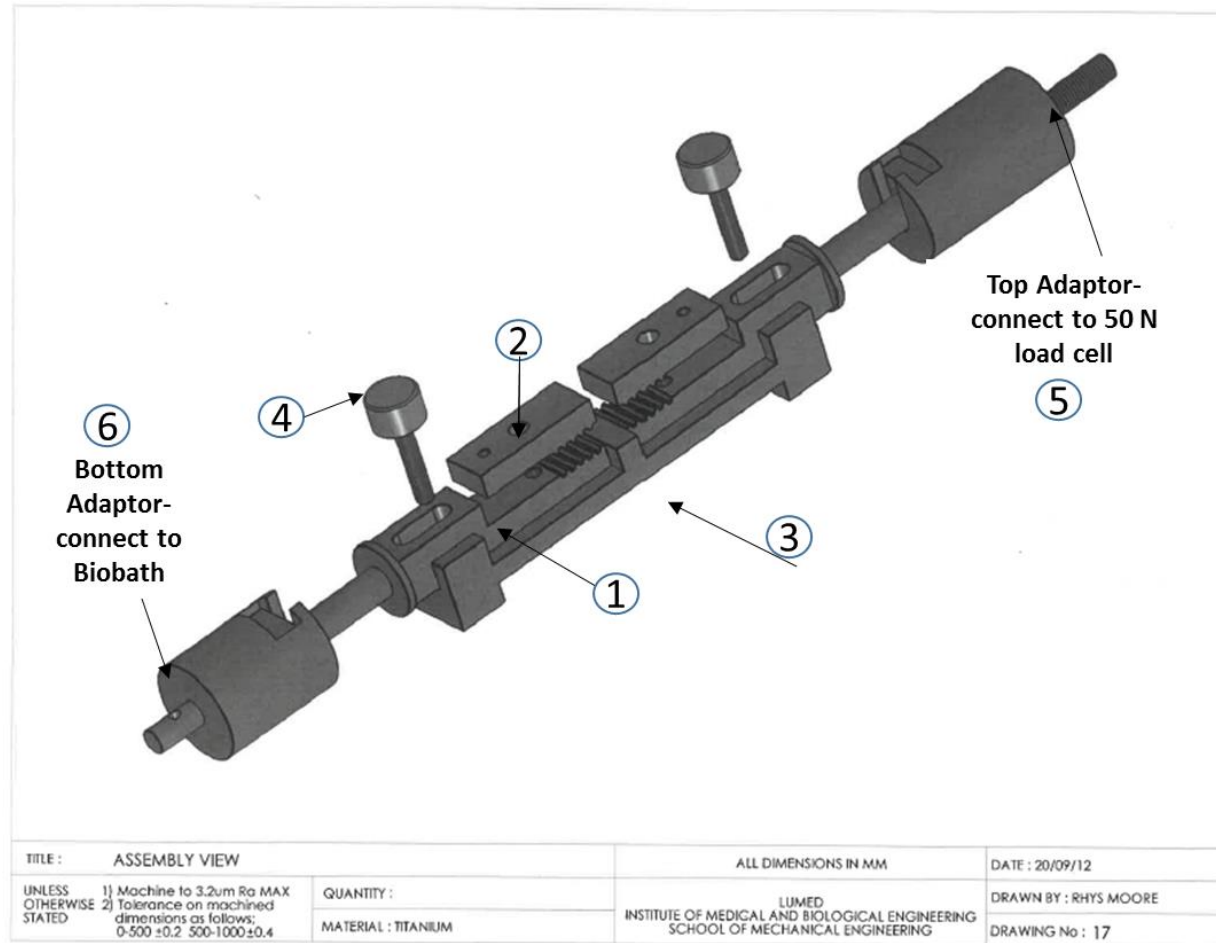
- VESELY, I. 1995. Bioprosthetic valve tissue viscoelasticity: implications on accelerated pulse duplicator testing. *Ann Thorac Surg.*, Aug;60(2 Suppl):S379-82.
- VESELY, I. 1998. The role of elastin in aortic valve mechanics. *J Biomech*, 31, 115-23.
- VESELY, I., BARBER, J. E. & RATLIFF, N. B. 2001. Tissue damage and calcification may be independent mechanisms of bioprosthetic heart valve failure. *J Heart Valve Dis*, 10, 471-7.
- VESELY, I. & BOUGHNER, D. 1989. Analysis of the bending behaviour of porcine xenograft leaflets and of natural aortic valve material: bending stiffness, neutral axis and shear measurements. *J Biomech*, 22, 655-71.
- VESELY, I., BOUGHNER, D. & SONG, T. 1988. Tissue Buckling as a Mechanism of Bioprosthetic Valve Failure. *The Annals of Thoracic Surgery*, 46, 302-308.
- VESELY, I., BOUGHNER, D. R. & LEESON-DIETRICH, J. 1995. Bioprosthetic valve tissue viscoelasticity: implications on accelerated pulse duplicator testing. *Ann Thorac Surg*, 60, S379-82; discussion S383.
- VESELY, I., MENKIS, A. H., RUTT, B. & CAMPBELL, G. 1991. Aortic valve/root interactions in porcine hearts: implications for bioprosthetic valve sizing. *J Card Surg*, 6, 482-9.
- VESELY, I. & NOSEWORTHY, R. 1992. Micromechanics of the fibrosa and the ventricularis in aortic valve leaflets. *J Biomech*, 25, 101-13.
- WALKER, P. G. & YOGANATHAN, A. P. 1992. In vitro pulsatile flow hemodynamics of five mechanical aortic heart valve prostheses. *European Journal of Cardio-Thoracic Surgery*, 6, S113-S123.
- WALRAEVENS, J., WILLAERT, B., DE WIN, G., RANFTL, A., DE SCHUTTER, J. & SLOTEN, J. V. 2008. Correlation between compression, tensile and tearing tests on healthy and calcified aortic tissues. *Medical Engineering & Physics*, 30, 1098-1104.
- WARNOCK, J. N., GAMEZ, C. A., METZLER, S. A., CHEN, J., ELDER, S. H. & LIAO, J. 2010. Vasoactive agents alter the biomechanical properties of aortic heart valve leaflets in a time-dependent manner. *J Heart Valve Dis*, 19, 86-95.
- WELLS, S. M. & SACKS, M. S. 2002. Effects of fixation pressure on the biaxial mechanical behavior of porcine bioprosthetic heart valves with long-term cyclic loading. *Biomaterials*, 23, 2389-2399.
- WHEATLEY, D. J., FISHER, J., REECE, I. J., SPYT, T. & BREEZE, P. 1987. Primary tissue failure in pericardial heart valves. *J Thorac Cardiovasc Surg*, 94, 367-74.
- WILCOX, H. E., KOROSSIS, S. A., BOOTH, C., WATTERSON, K. G., KEARNEY, J. N., FISHER, J. & INGHAM, E. 2005. Biocompatibility and recellularization potential of an acellular porcine heart valve matrix. *Journal of Heart Valve Disease*, 14, 228-237.
- WILCZEK, P., PAULINA, G., KAROLINA, J., MARTYNA, M., GRAZYNA, W., ROMAN, M., ALDONA, M., ANNA, S. & ANETA, S. 2018. Biomechanical and morphological stability of acellular scaffolds for tissue-engineered heart valves depends on different storage conditions. *J Mater Sci Mater Med*, 29, 106.

- WILLIAMS, C., LIAO, J., JOYCE, E. M., WANG, B., LEACH, J. B., SACKS, M. S. & WONG, J. Y. 2009. Altered structural and mechanical properties in decellularized rabbit carotid arteries. *Acta Biomaterialia*, 5, 993-1005.
- WOLLMANN, L. C. F. D. N., LAURINDO, C. A. H., COSTA, F. D. A. D. & MORENO, A. N. 2011. Efeito da criopreservação e/ou da descelularização na matriz extracelular de condutos valvados porcinos. *Brazilian Journal of Cardiovascular Surgery*, 26, 490-496.
- YACOB, M. H., KLIEVERIK, L. M. A., MELINA, G., EDWARDS, S. E. R., SARATHCHANDRA, P., BOGERS, A., SQUARCIA, U., SANI, G., VAN HERWERDEN, L. A. & TAKKENBERG, J. J. M. 2006. An evaluation of the ross operation in adults. *Journal of Heart Valve Disease*, 15, 531-539.
- YADAVA, O. P. 2013. *Follow-up after Cardiovascular Surgery - ECAB*, Elsevier Health Sciences.
- YANKAH, C. A., WENG, Y. G. & HETZER, R. 2010. *Aortic Root Surgery: The Biological Solution*, Steinkopff.
- YOGANATHAN, A. 1989. Flow characteristics of prosthetic heart valves. *The International Journal of Cardiac Imaging*, 4, 5-8.
- YOGANATHAN, A. P., HE, Z. & CASEY JONES, S. 2004. Fluid mechanics of heart valves. *Annu Rev Biomed Eng*, 6, 331-62.
- ZEHR, K. J., YAGUBYAN, M., CONNOLLY, H. M., NELSON, S. M. & SCHAFF, H. V. 2005. Aortic root replacement with a novel decellularized cryopreserved aortic homograft: Postoperative immunoreactivity and early results. *Journal of Thoracic and Cardiovascular Surgery*, 130, 1010-1015.
- ZHANG, X., XU, B., PUPERI, D. S., WU, Y., WEST, J. L. & GRANDE-ALLEN, K. J. 2015. Application of hydrogels in heart valve tissue engineering. *J Long Term Eff Med Implants*, 25, 105-34.
- ZHOU, J., QUINTERO, L. J., HELMUS, M. N., LEE, C. & KAFESJIAN, R. 1997. Porcine aortic wall flexibility. Fresh vs Denacol fixed vs glutaraldehyde fixed. *ASAIO J*, 43, M470-5.
- ZUCKERMAN, D. M., BROWN, P. & NISSEN, S. E. 2011. Medical device recalls and the FDA approval process. *Arch Intern Med*, 171, 1006-11.

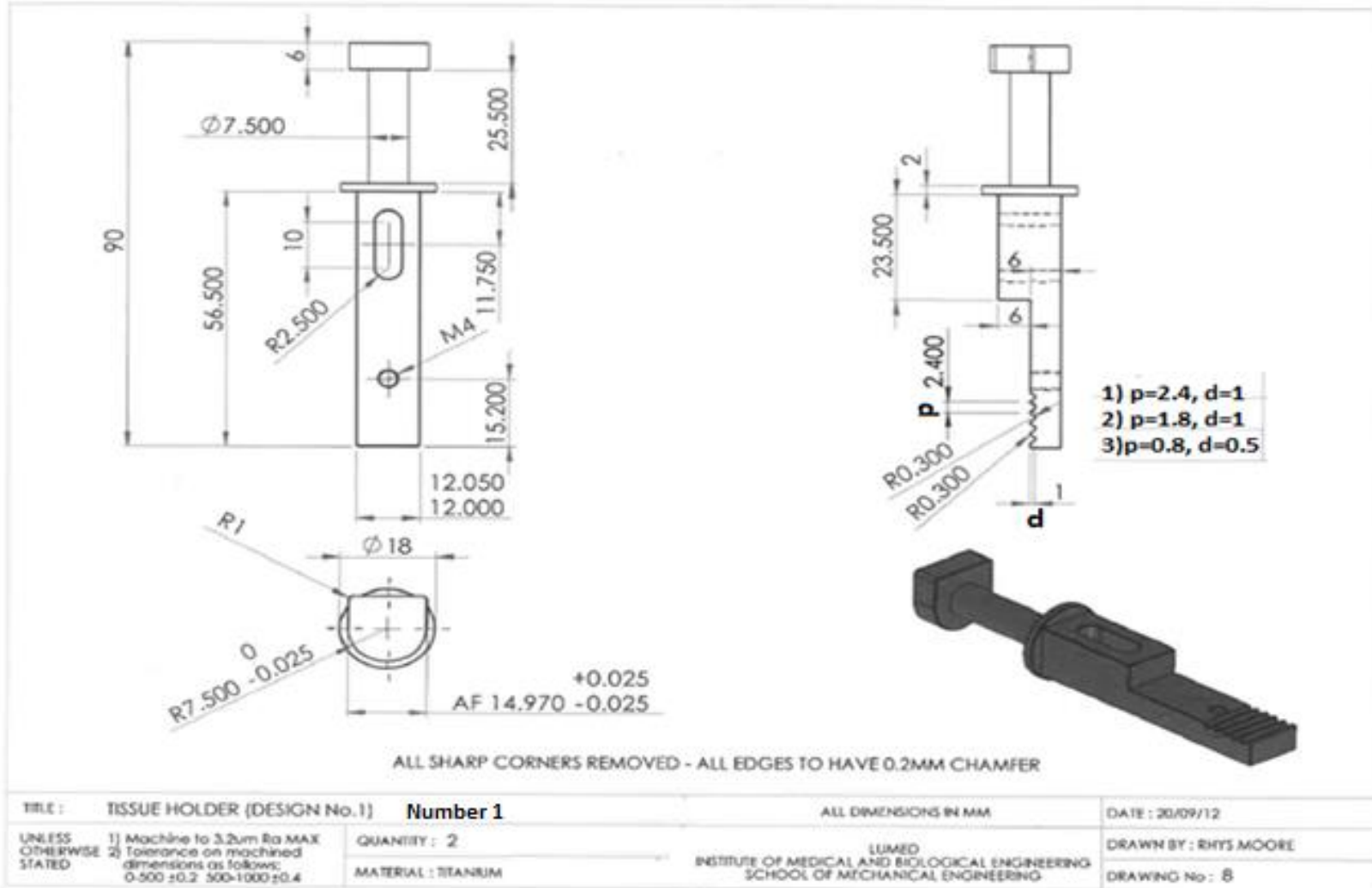
## 11 Appendix A: Journal Publications

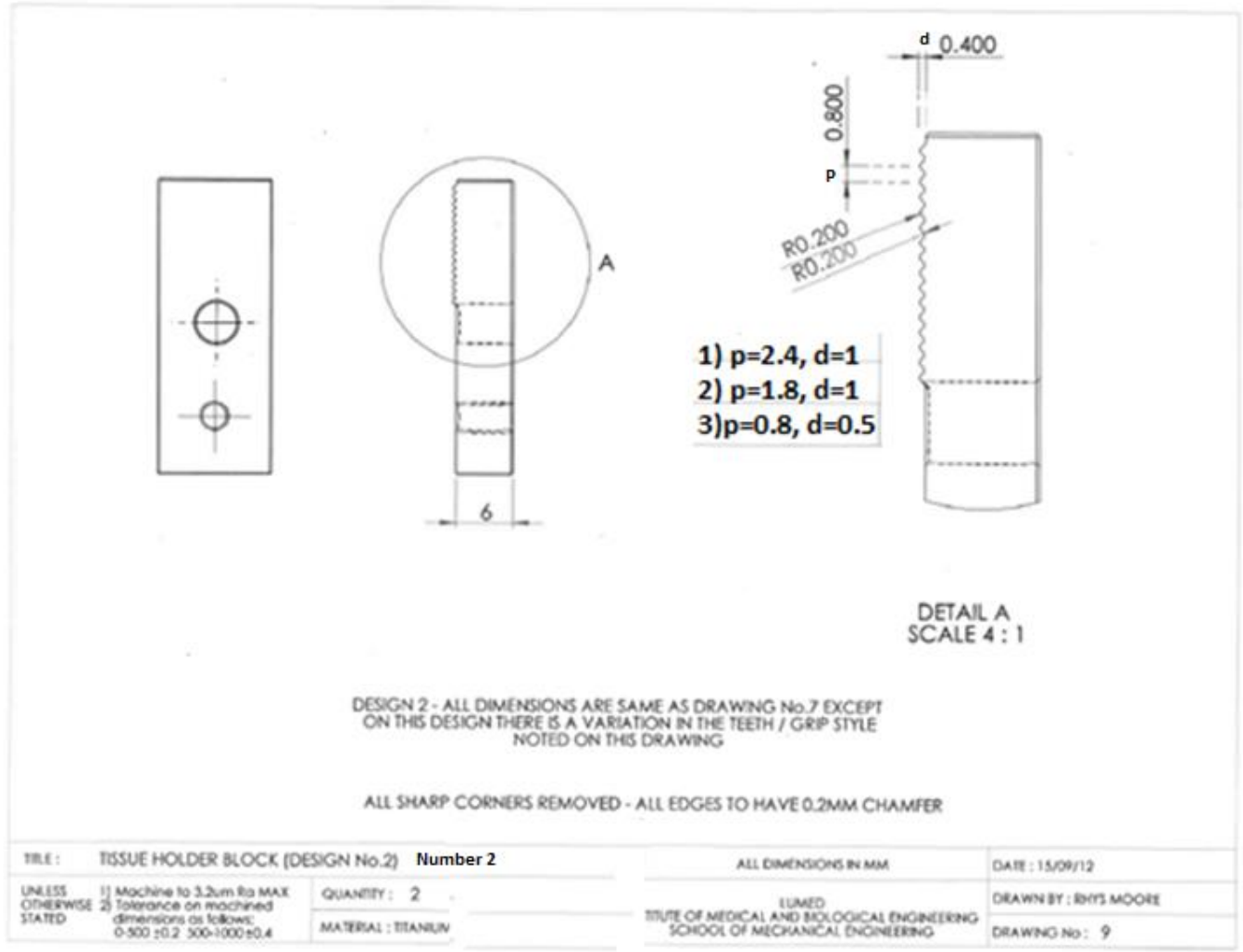
1. **Amisha Desai**, Tayyebah Vafaee, Paul Rooney, John Kearney, Helen Berry, Eileen Ingham, John Fisher, Louise M Jennings (2018). In vitro biomechanical and hydrodynamic characterisation of decellularised human pulmonary and aortic roots; *Journal of the Mechanical Behavior of Biomedical Materials*, 79. pp. 53-63. ISSN 1751
2. Tayyebah Vafaee, Daniel Thomas, **Amisha Desai**, Louise M Jennings, Helen Berry, Paul Rooney, John Kearney, John Fisher, and Eileen Ingham (2018) Decellularization of human donor aortic and pulmonary valved conduits using low concentration sodium dodecyl sulfate; *Journal of Tissue Engineering Regenerative Medicine* Feb; 12(2): e841–e853.

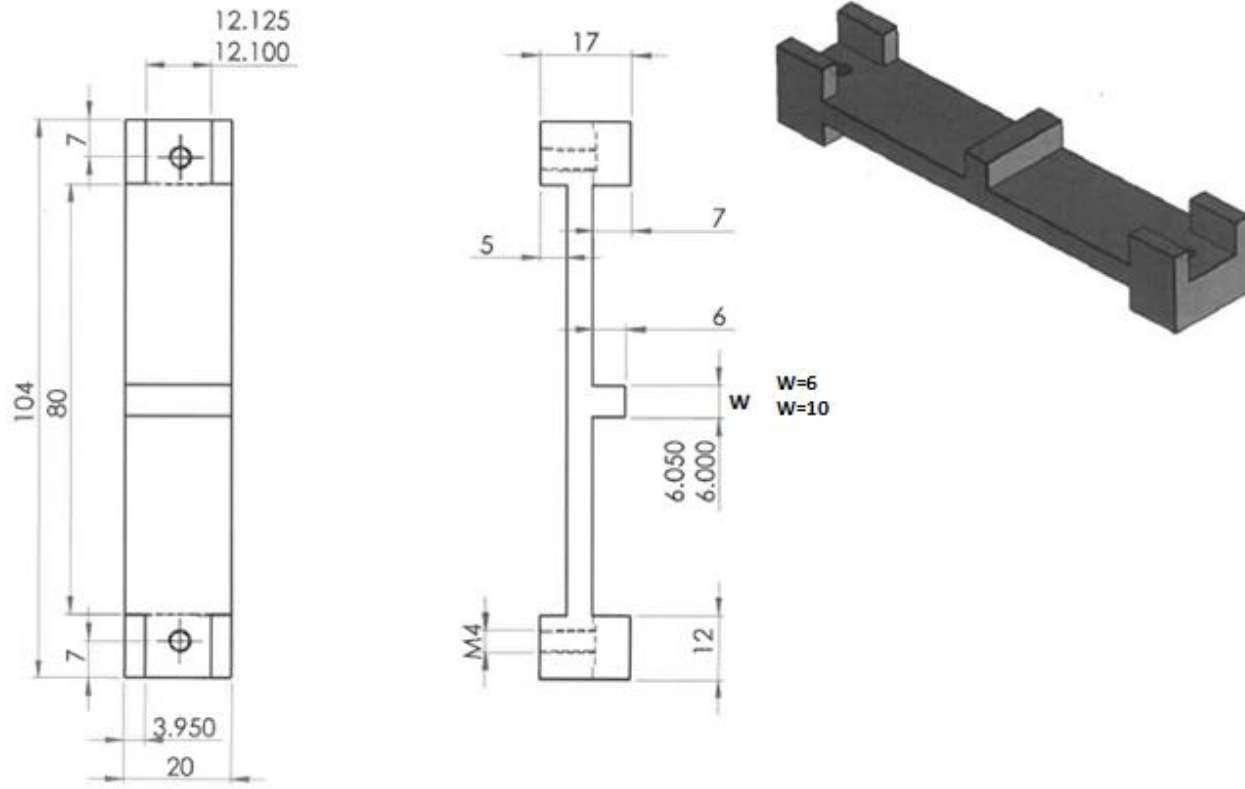
## 12 Appendix B: Engineering Drawings for Tissue Specimen Holder and Adaptors for the Uniaxial Tensile Tester





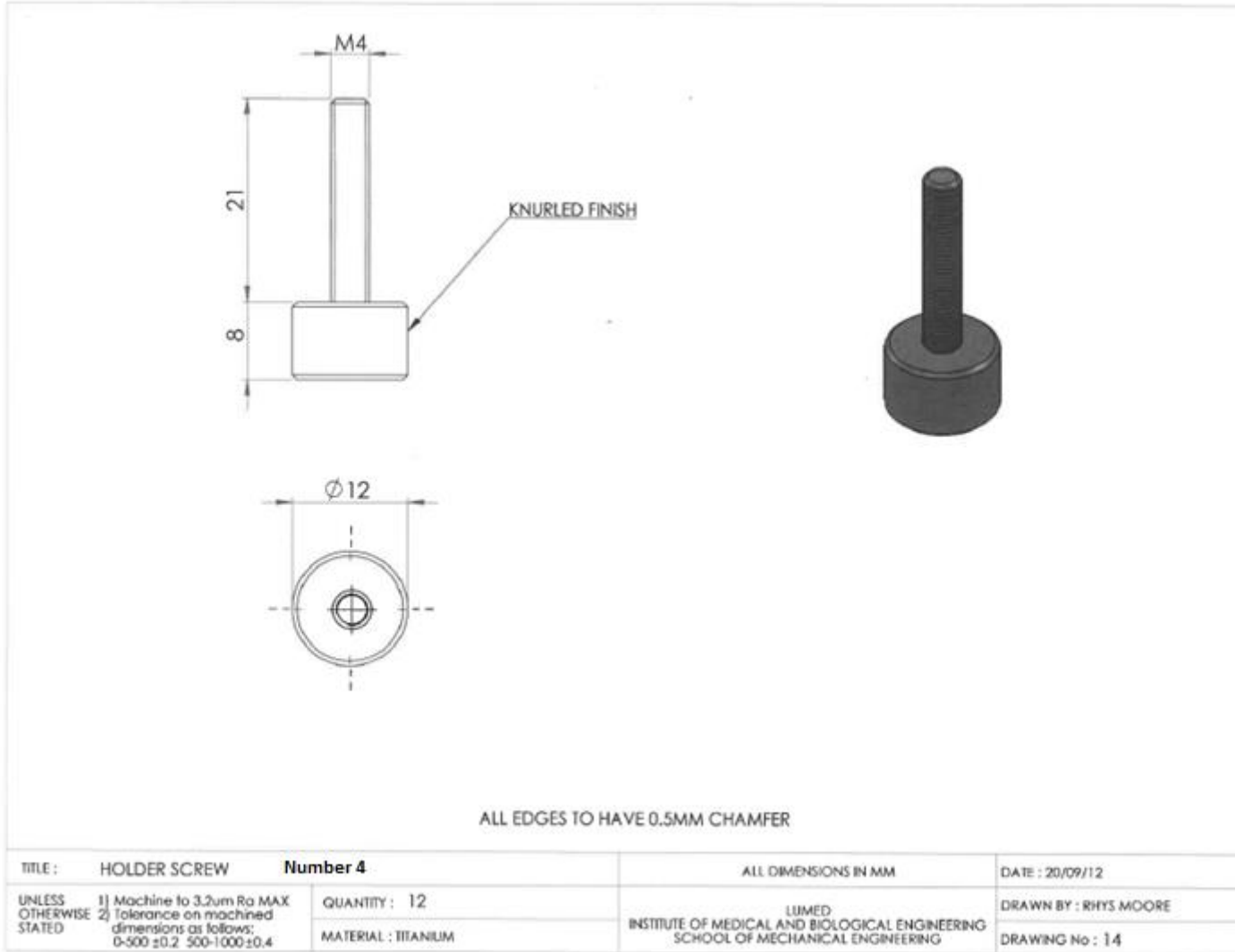


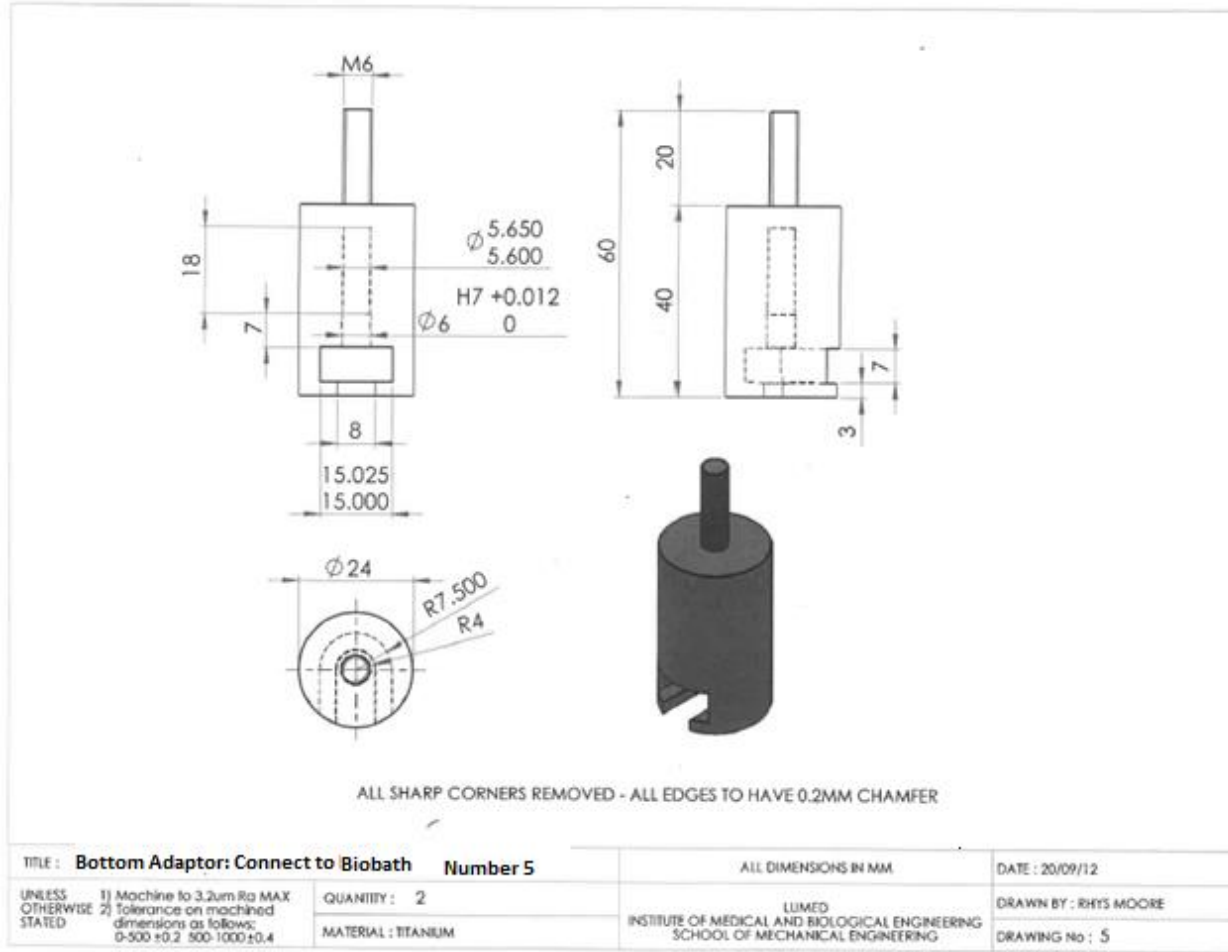


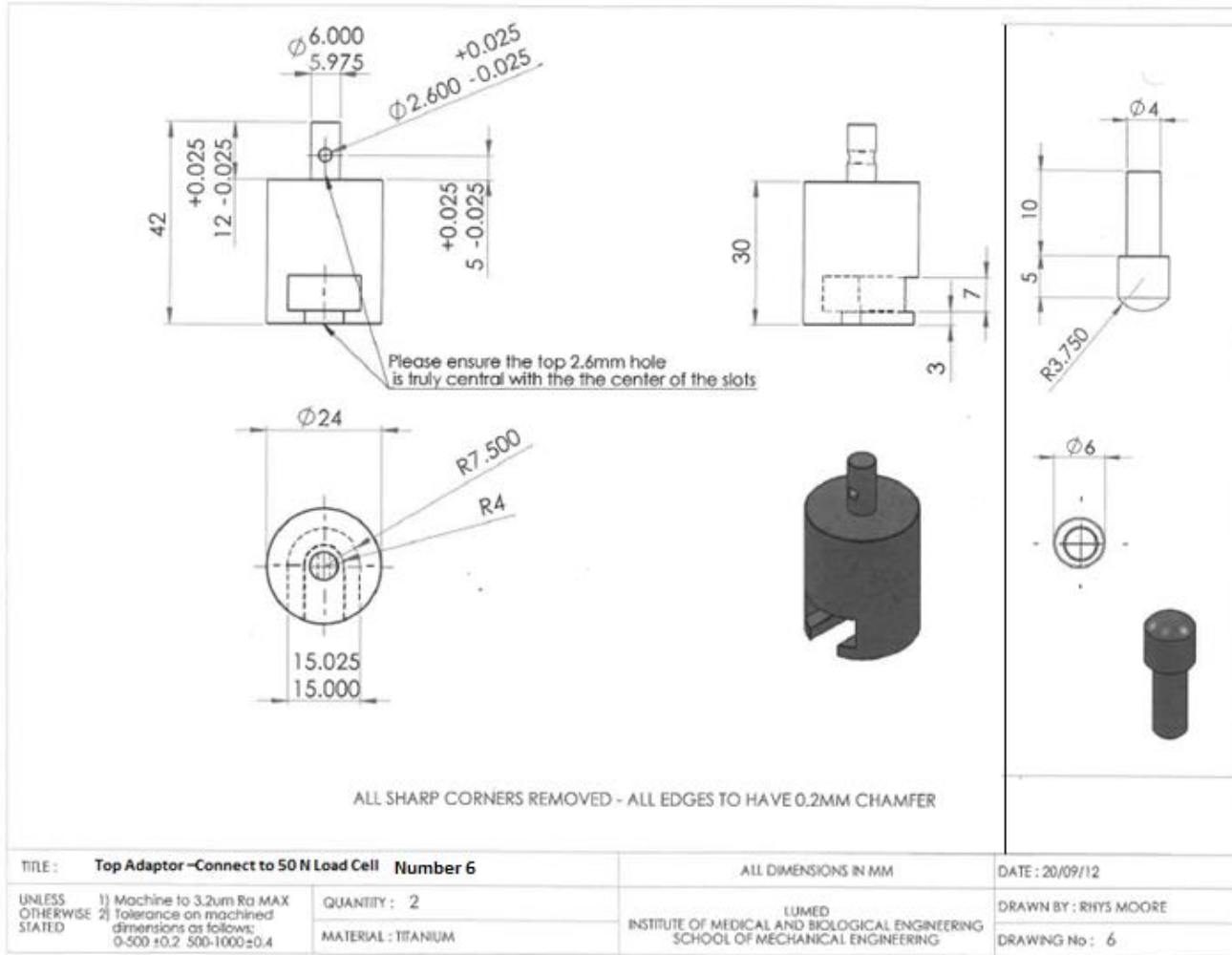


ALL SHARP CORNERS REMOVED - ALL EDGES TO HAVE 0.2MM CHAMFER

TITLE : <b>BASE PLATE (6GAUGE) Number 3</b>		ALL DIMENSIONS IN MM	DATE : 20/09/12
UNLESS OTHERWISE STATED	1) Machine to 3.2um Ra MAX	QUANTITY : 1	DRAWN BY : RHYS MOORE
	2) Tolerance on machined dimensions as follows: 0-500 ±0.2 500-1000 ±0.4	MATERIAL : TITANIUM	DRAWING No : 2
		LUMED INSTITUTE OF MEDICAL AND BIOLOGICAL ENGINEERING SCHOOL OF MECHANICAL ENGINEERING	







### 13 Appendix C: Engineering Drawing for Heart Valve Root Holder for the RWT

